UNIVERSITY OF CYPRUS

DEPARTMENT OF CHEMISTRY

COMPUTATIONAL STUDY OF IONIC EFFECTS ON THE CONFORMATIONAL STABILITY AND THE HELIX/COIL EQUILIBRIUM OF MODEL OLIGOPEPTIDES

DOCTORAL DISSERTATION

FILIPPOS IOANNOU

2013

DEPARTMENT OF CHEMISTRY

COMPUTATIONAL STUDY OF IONIC EFFECTS ON THE CONFORMATIONAL STABILITY AND THE HELIX/COIL EQUILIBRIUM OF MODEL OLIGOPEPTIDES

FILIPPOS IOANNOU

A Dissertation
Submitted in Partial Fulfillment of the
Requirements for the Degree of
Doctor of Philosophy
at the University of Cyprus

January 2013

APPROVAL PAGE

Doctoral Candidate: Filippos Ioannou

Dissertation Title: COMPUTATIONAL STUDY OF IONIC EFFECTS ON THE CONFORMATIONAL STABILITY AND THE HELIX/COIL EQUILIBRIUM OF MODEL OLIGOPEPTIDES

The present Doctorate Dissertation was submitted in partial fulfillment of the requirements for the Degree of Doctor of Philosophy in the ***Department of Chemistry****, and was approved on* ***14 January, 2013*** *by the members of the* ***Examination Committee:***

Research Supervisor: Epameinondas Leontidis, Professor

Committee Member: Sophia C. Hayes, Assistant Professor

Committee Member: Nico van der Vegt, Professor

Committee Member: Costas S. Patrickios, Professor

Committee Member: Spiros Skourtis, Associate Professor

This Thesis is co-advised by Georgios Archontis, Associate Professor (Department of Physics, University of Cyprus)

Dedicated to my parents Dimitris and Maria,
to my wife Stella and daughter Maria

ΕΥΧΑΡΙΣΤΙΕΣ

Φτάνοντας στο τέλος ενός μεγάλου στόχου, και με την ολοκλήρωση μίας μακρινής και δύσκολης πορείας, νιώθω την ανάγκη να αφιερώσω λίγες γραμμές ευχαριστώντας ανθρώπους με τους οποίους συνεργάστηκα και συνυπήρξα όλο αυτό το χρονικό διάστημα.

Αρχικά, θα ήθελα να ευχαριστήσω τους επιβλέποντες καθηγητές μου Δρ. Γεώργιο Αρχοντή, Αναπληρωτή Καθηγητή του Τμήματος Φυσικής Πανεπιστημίου Κύπρου και Δρ. Επαμεινώνδα Λεοντίδη, Καθηγητή του Τμήματος Χημείας Πανεπιστημίου Κύπρου. Τους ευχαριστώ για την εμπιστοσύνη που έδειξαν στο πρόσωπό μου όλα αυτά τα χρόνια, την επιστημονική καθοδήγηση, τη θερμή υποστήριξη και αμέριστη συμπαράστασή τους, αλλά και για το αμείωτο ενδιαφέρον τους, καθ' όλη τη διάρκεια της εκπόνησης και συγγραφής της διατριβής αυτής. Η συμβολή τους στην υλοποίηση της Διατριβής, από την ανάθεση του θέματος μέχρι την ολοκλήρωση της, υπήρξε καθοριστική. Θα ήθελα να τους ευχαριστήσω για τη δυνατότητα εκπόνησης διδακτορικής διατριβής που μου έδωσαν και για όλες τις ευκαιρίες που μου προσέφεραν απλόχερα στη συνέχεια, μέσω των οποίων έλαβα τόσο γνώσεις αλλά και εμπειρίες ζωής που θα με συνοδεύουν για πάντα.

Επίσης, θα ήθελα να ευχαριστήσω θερμά την Επίκουρη Καθηγήτρια Δρ. Σοφία Χαραλάμπους-Hayes και τον Καθηγητή Κώστα Πατρίκιο, του Τμήματος Χημείας του Πανεπιστημίου Κύπρου, για τη συμμετοχή τους στις επιτροπές αξιολόγησης της ερευνητικής μου εργασίας και για τις πολύτιμες παρατηρήσεις / υποδείξεις τους για τη βελτίωση της εργασίας αυτής. Επιπρόσθετα, θα ήθελα να ευχαριστήσω τον Αναπληρωτή Καθηγητή στο Τμήμα Φυσίκης του Πανεπιστημίου Κύπρου Δρ. Σπύρο Σκούρτη και τον Καθηγητή Nico van der Vegt του "Κέντρου Ευφυών Διεπιφανειών» του Πολυτεχνείου Darmstadt της Γερμανίας (Center for Smart Interfaces, Technical University of Darmstadt, Germany) για την ευγενή αποδοχή τους να συμμετάσχουν στην εξεταστική μου επιτροπή, καθώς και για τις υποδείξεις τους στην επιμέλεια του τελικού κειμένου της διατριβής.

Θα ήταν παράλειψή μου να μην ευχαριστήσω το Πανεπιστήμιο Κύπρου και το Ίδρυμα Προώθησης Έρευνας για τη χρηματοδότησή μου κατά τη διάρκεια εκπόνησης της Διδακτορικής μου Διατριβής.

Τέλος, ένα μεγάλο ευχαριστώ οφείλω στους δικούς μου ανθρώπους που πάντα ήταν εκεί να με στηρίζουν και να με εμψυχώνουν για να συνεχίσω το δύσκολο αυτό αγώνα.

Θα ήθελα να εκφράσω ένα μεγάλο ευχαριστώ στη γυναίκα μου Στέλλα Αντωνίου, για τη συνεχή ενθάρρυνση, την υπομονή και τη βοήθεια της όλα αυτά τα χρόνια. Σε ευχαριστώ που ήσουν και είσαι πάντα δίπλα μου. Σε ευχαριστώ για όλα…

Το πιο μεγάλο ευχαριστώ από όλα το αφιερώνω στους γονείς μου Δημήτρη και Μαρούλα που ήταν πάντα δίπλα μου όλο αυτό το χρονικό διάστημα. Είμαι ευγνώμων για όσα μου έχουν προσφέρει όλα αυτά τα χρόνια και σίγουρα σε αυτούς χρωστάω τα πάντα.

ABSTRACT

The present Doctoral Thesis is a computational investigation of the effects of salts on the conformational stability and on the helix-coil transition of model oligopeptides, aiming to shed light on the mechanism of specific ion action on the protein folding process, a key problem in biochemistry and biophysics. Current literature contains very limited information on salt effects on protein conformations, although salts are known to affect the stability and solubility of proteins, and have also been found to play a role in protein aggregation phenomena leading to the formation of amyloid fibrils, nanostructures and stimulus-responsive peptide-based systems. We have quantified the salt effects on the helix-coil equilibrium of model peptides by checking the effect of salts on the Ramachandran maps and computing the associated Lifson-Roig and Zimm-Bragg helix-coil transition parameters as a function of salt concentration. Such a computation has never been attempted before in the presence of salts and constitutes the major innovation in the present project.

Because the equilibration times for oligopeptides or ions in solution tend to be quite long, the high-efficiency replica exchange simulation method has been used, which is based on simultaneous simulations of the same system at several temperatures. To our knowledge, this is the first time that this method is applied to a mixed protein-salt solution. In addition to its sampling efficiency, the method has provided insights on the conformational stability and helix/coil equilibrium of the studied peptides at a wide range of temperatures.

The present study is divided in three parts. In the first part studies of ionic effects on the stability of the conformation of the protein backbone are reported. These results were obtained by performing simulations of the simplest possible oligopeptides: the properly blocked alanine dipeptide (Ac-Ala-NMe) and alanine tetrapeptide (Ac-Ala_3-NMe). In our investigation of salt effects on the conformations of an alanine dipeptide, we found that the "intrinsic" conformational states of the backbone, as described by Ramachandran maps, are not greatly affected even by large concentrations of NaCl and NaI. In the case of an alanine tetrapeptide, however, the Ramachandran maps show an increased tendency for more compact conformations in the presence of salts, with NaI being more effective. Our finding that compact conformations are enhanced by salts was associated with a concomitant increase in the formation probabilities of the α-helical hydrogen bond (i/i+4), and other hydrogen bonds (i/i+3, i/i+2). We were able to show that the enhancement is not

due to stronger ion-peptide interaction, or to a difference in the hydration of the peptide in the presence of ions. We also verified that Cl^- ions prefer to stay away from the peptides, while I^- ions have a preferential interaction with the hydrophobic methyl groups, as was also observed in previous oligopeptide simulations.

In the second part of the thesis studies of ionic effects on the stability of the α-helix secondary-structural motif and the helix/coil equilibrium have been carried out. Here we have simulated the model peptide Ace-$(AAQAA)_3$-NMe (AQ) in aqueous electrolyte solutions. The use of this neutral peptide in which charge-charge electrostatic effects on helix stability are absent, allows focusing on the salting-in and salting-out interactions of the solution ions with the nonpolar and other peptide groups. From the simulations of this peptide it was also possible to extract the parameters of the Zimm-Bragg and Lifson-Roig statistical-mechanical models of the helix-coil transition and the average peptide helicity as a function of electrolyte type, concentration and temperature. Our simulations show a net stabilization of α-helical structures in the presence of high concentrations of NaCl, and a net destabilization in the presence of high-concentrations of NaI. An important conclusion of the analysis of these simulations is that the net impact of salt on the stability of helical conformations is best understood by considering separately its influence on the helix nucleation and propagation steps.

The third part of the thesis deals with the effects of ions on the strength of interactions between solvent-exposed, charged side-chains in α-helix-forming peptides and the impact of solvent-exposed salt-bridge formation on the α-helix/coil equilibrium. We simulated the model peptides Ace-AAQAA-EAQKA-AAQAA-NMe (EK+3), Ace-AAQAA-EAQAK-AAQAA-NMe (EK+4) and Ace-AAQAA-EAQAA-KAQAA-NMe (EK+5), which differ from peptide AQ in that they contain oppositely charged amino acids (E, K) in positions *i*/*i*+3, *i*/*i*+4 and *i*/*i*+5. Sequences EK+4 and EK+5 were found to have reduced helicities relative to AQ; while, sequence EK+3 has increased helicity, which is highly correlated with the formation of the intramolecular E – K salt bridges.

As a general conclusion the present study shows that the addition of electrolytes affects the helix/coil equilibrium of model peptides in several different ways and that separate consideration of each factor can assist in the understanding of the net salt impact on helicity.

ΣΥΝΟΨΗ

Η παρούσα διδακτορική διατριβή είναι μια υπολογιστική μελέτη της επίδρασης των αλάτων στη στερεοδιαταξική σταθερότητα και την ισορροπία έλικας/τυχαίου σπειρώματος ολιγοπεπτιδίων, με στόχο τη διαφώτιση του μηχανισμού της ιοντικής δράσης στην διαδικασία της πρωτεϊνικής αναδίπλωσης, που είναι ένα θεμελιώδες πρόβλημα στη βιοχημεία και τη βιοφυσική. Η τρέχουσα βιβλιογραφία περιέχει πολύ περιορισμένες πληροφορίες για την επίδραση των αλάτων στις διαμορφώσεις των πρωτεϊνών, αν και τα άλατα είναι γνωστό ότι έχουν επιπτώσεις στη σταθερότητα και τη διαλυτότητα των πρωτεϊνών, και έχει βρεθεί επίσης ότι διαδραματίζουν ρόλο σε φαινόμενα συσσωμάτωσης πρωτεϊνών που οδηγούν στο σχηματισμό αμυλοειδών ινιδίων, νανοδομών και συστημάτων που βαζίζονται σε πεπτίδια και ανταποκρίνονται σε περιβαλλοντικές διεγέρσεις (stimulus-responsive peptide-based systems). Έχουμε προσδιορίσει την επίδραση των αλάτων στην ισορροπία έλικας/τυχαίου σπειρώματος ολιγοπεπτιδίων μελετώντας την επίδραση των αλάτων στους χάρτες Ramachandran και υπολογίζοντας τις παραμέτρους μετάπτωσης έλικας/τυχαίου σπειρώματος Lifson-Roig και Zimm-Bragg συναρτήσει της συγκέντρωσης αλάτων. Ένας τέτοιος υπολογισμός δεν έχει διεξαχθεί ποτέ προηγουμένως στην παρουσία αλάτων και αποτελεί τη σημαντικότερη καινοτομία της παρούσας διατριβής.

Επειδή οι χρόνοι εξισορρόπησης της μοριακής δυναμικής των ολιγοπεπτιδίων ή των ιόντων σε διαλύματα τείνουν να είναι αρκετά μεγάλοι, έχει χρησιμοποιηθεί στη διατριβή αυτή η υψηλής απόδοσης μέθοδος προσομοίωσης replica exchange, η οποία είναι βασισμένη στις ταυτόχρονες προσομοιώσεις του ίδιου συστήματος σε διάφορες θερμοκρασίες. Από ό,τι γνωρίζουμε, αυτή είναι η πρώτη φορά που η μέθοδος εφαρμόζεται σε ένα μείγμα πεπτιδίων με ιόντα. Εκτός από τη σημαντική επιτάχυνση της εξισορρόπησης των προσομοιώσεων, η μέθοδος έχει παράσχει λεπτομέρειες για τη στερεοδιαταξική σταθερότητα και την ισορροπία έλικας/τυχαίου σπειρώματος ολιγοπεπτιδίων των υπό μελέτη πεπτιδίων για ένα ευρύ φάσμα θερμοκρασιών.

Η παρούσα μελέτη διαχωρίζεται σε τρία μέρη. Το πρώτο μέρος αναφέρεται στη μελέτη της επίδρασης των ιόντων στη στερεοδιαταξική σταθερότητα της κύριας αλυσίδας των πεπτιδίων. Η μελέτη αυτή βασίστηκε σε προσομοιώσεις των απλούστερων δυνατών πεπτιδίων: του διπεπτιδίου Αλανίνης (Ac-Ala-NMe) και του τετραπεπτιδίου Αλανίνης (Ac-Ala_3-NMe) με τα κατάλληλα τερματικά άκρα. Από τη μελέτη της επίδρασης των

ιόντων στις διαμορφώσεις του διπεπτιδίου της αλανίνης βρέθηκε ότι οι διαμορφώσεις της κύριας αλυσίδας, όπως περιγράφονται από τους χάρτες Ramachandran, δεν επηρεάζονται ακόμα και από υψηλές συγκεντρώσεις NaCl και NaI. Αντίθετα, στην περίπτωση του τετραπεπτιδίου Αλανίνης, οι χάρτες Ramachandran υποδεικνύουν αυξητική τάση για πιο συμπαγείς διαμορφώσεις στην παρουσία αλάτων, με το NaI να έχει τη μεγαλύτερη επίδραση. Η παρατήρηση αυτή, ότι οι συμπαγείς διαμορφώσεις αυξάνονται παρουσία αλάτων, συσχετίζεται με συνακόλουθη αύξηση της πιθανότητας σχηματισμού δεσμών υδρογόνου «τύπου» α-έλικας (*i*/*i*+4), και άλλων δεσμών υδρογόνου (*i*/*i*+3, *i*/*i*+2). Κατορθώσαμε να δείξουμε ότι η αύξηση δεν οφείλεται στις ισχυρές αλληλεπιδράσεις ιόντων-πεπτιδίου, ή στη διαφορά εφυδάτωσης του πεπτιδίου στην παρουσία ιόντων. Επίσης επιβεβαιώσαμε ότι τα ιόντα Cl^- προτιμούν να παραμένουν μακριά από τα πεπτίδια, ενώ τα ιόντα I^- έχουν τάση να αλληλεπιδρούν με τις υδρόφοβες μεθυλομάδες, όπως έχει παρατηρηθεί σε προηγούμενες προσομοιώσεις ολιγοπεπτιδίων.

Το δεύτερο μέρος της διατριβής μελετά την επίδραση των ιόντων στη στερεοδιαταξική σταθερότητα της δευτεροταγούς δομής της α-έλικας και στην ισορροπία έλικας/τυχαίου σπειρώματος ολιγοπεπτιδίων. Εδώ έχουμε προσομοιώσει το πεπτίδιο Ace-$(AAQAA)_3$-NMe (AQ) σε υδατικά διαλύματα ηλεκτρολυτών. Η χρήση αυτού του ουδέτερου πεπτιδίου στο οποίο απουσιάζουν οι άμεσες ηλεκτροστατικές συνεισφορές φορτίου-φορτίου στη σταθερότητα της έλικας, επιτρέπουν να εστιάσουμε στις αλληλεπιδράσεις salting-in (εναλάτωσης) και salting-out (εξαλάτωσης) των ιόντων με τις μη πολικές και τις υπόλοιπες πεπτιδικές ομάδες. Από τις προσομοιώσεις αυτού του πεπτιδίου ήταν δυνατή η εξαγωγή των παραμέτρων των στατιστικών μοντέλων της ισορροπίας έλικας/τυχαίου σπειρώματος Zimm-Bragg και Lifson-Roig και ο υπολογισμός της μέσης ελικότητας συναρτήσει του τύπου του ηλεκτρολύτη, της συγκέντρωσης και της θερμοκρασίας. Οι προσομοιώσεις μας έδειξαν ξεκάθαρη σταθεροποίηση των δομών της α-έλικας στην παρουσία υψηλών συγκεντρώσεων NaCl, και ξεκάθαρη αποσταθεροποίηση στην παρουσία υψηλών συγκεντρώσεων NaI. Ένα σημαντικό συμπέρασμα από την ανάλυση αυτών των προσομοιώσεων είναι ότι η επίδραση των αλάτων στη σταθερότητα των ελικοειδών διαμορφώσεων γίνεται καλύτερα κατανοητή εξετάζοντας ξεχωριστά την επιρροή τους στην έναρξη και διάδοση της έλικας.

Το τρίτο μέρος της διατριβής μελετά την επίδραση των ιόντων στην ισχύ των αλληλεπιδράσεων μεταξύ εκτεθειμένων στο διαλύτη, φορτισμένων πλευρικών αλυσίδων

πεπτιδίων που σχηματίζουν α-έλικα. Μελετά επίσης την επιρροή των αλάτων στο σχηματισμό γεφυρών αλάτων μεταξύ τέτοιων πλευρικών ομάδων. Προσομοιώσαμε τα πεπτίδια Ace-AAQAA-EAQKA-AAQAA-NMe (EK+3), Ace-AAQAA-EAQAK-AAQAA-NMe (EK+4) και Ace-AAQAA-EAQAA-KAQAA-NMe (EK+5), τα οποία διαφέρουν από το πεπτίδιο AQ στο ότι περιέχουν αντίθετα φορτισμένα αμινοξέα (E, K) στις θέσεις *i*/*i*+3, *i*/*i*+4 and *i*/*i*+5. Οι ακολουθίες EK+4 και EK+5 βρέθηκαν να έχουν ελαττωμένη ελικότητα σε σχέση με το AQ, ενώ η ακολουθία EK+3 έχει αυξημένη ελικότητα, που σχετίζεται άμεσα με το σχηματισμό ενδομοριακών γεφυρών αλάτος E – K.

Σαν γενικό συμπέρασμα η παρούσα εργασία έδειξε ότι η προσθήκη ηλεκτρολύτη επηρεάζει την ισορροπία έλικας/ τυχαίου σπειρώματος πεπτιδίων με πολλούς διαφορετικούς τρόπους και ότι η ξεχωριστή εκτίμηση του κάθε παράγοντα μπορεί να βοηθήσει στη βαθύτερη κατανόηση της συνολικής επίδρασης των αλάτων στην ελικότητα.

TABLE OF CONTENTS

LIST OF FIGURES

LIST OF TABLES

LIST OF SCHEMES

1. Introduction

The identification of the mechanism of protein folding, a process by which a linear chain of amino acids comes together to form a three-dimensional structure, is still an unsolved problem in biophysics. Protein folding phenomena play a major role in life processes. The understanding of the mechanism of secondary structure formation is thought to shed light on the protein folding problem, as one of the most elementary processes in protein folding dynamics is the formation of α-helices. The number of theoretical investigations of the helix-coil transition is vast, either with focus on the stability and structure [Scholtz and Baldwin, 1992; Chakrabartty and Baldwin, 1995; Vila et al., 2000; Garcia and Sanbonmatsu, 2002] or on folding kinetics [Hummer et al., 2000; Monticelli et al., 2005].

Because salts and other electrolytes are always present in high concentrations in biological systems, understanding their effects on protein behavior at the molecular level is important to quantify their interactions in a biological context.

More than 100 years ago, Hofmeister [Hofmeister, 1888] and Lewith [Lewith, 1888] published experimental results showing the specific effect of various salts on the aqueous solubility of proteins. By specific effects we mean those that do not depend on the magnitude of the ionic charge alone. They are manifested when ions of the same charge produce a different effect in a particular system. Since then, numerous experimental studies have shown the importance of specific ion effects in a multitude of biological and physicochemical phenomena [Collins and Washabaugh, 1985; Cacace, 1997; Kunz, 2010]. On the basis of the magnitude of their specific effects, ions have been ordered into sequences (one for anions and one for cations), which are called the Hofmeister series. Anions, based on their increasing salting-in potency for proteins, can be ordered in the following way:

$$SO_4^{2-}, HPO_4^{2-}, OH^-, F^-, HCOO^-, CH_3COO^-, Cl^-, Br^-, NO_3^-, I^-, SCN^-, ClO_4^-$$

Although the Hofmeister series plays a significant role in a broad range of phenomena, its understanding was slow in coming. Only in the last few years a clearer understanding of specific ion action has started to emerge. Even today, with our much improved understanding, we can still find several different ideas about the nature of specific salt

effects, many of which have been proposed a long time ago; for example, a favorite explanation of specific salt effects for a long time was that ions modify the structure and properties of water. The character of water as a solvent for biomolecules would change in specific ways in the presence of electrolytes, for example its local dielectric or microscopic (cavity) surface tension might change. Based on such ideas it has become standard practice to call ions on the left of Cl^- in the anionic Hofmeister series ‘‘cosmotropes’’ or ‘‘structure makers’’, whereas ions on the right of Cl^- are called ‘‘chaotropes’’ or ‘‘structure breakers’’.

The effect of salts on the helix-coil transition of peptides has been studied rather little experimentally [Marqusee and Baldwin, 1987; Scholtz et al., 1991; Smith and Scholtz, 1998] and only very recently by MD simulations [Fedorov et al., 2007; Dzubiella, 2008, Asciutto, 2010], although salts are known to affect the stability and solubility of proteins, and have also been found to play a role in protein aggregation phenomena leading to the formation of amyloid fibrils and nanostructures [Hamada et al., 2009; Klement et al., 2007; Raman et al., 2005].

At high concentrations ($c > 1$ M) salt effects on proteins and polypeptides are pronounced, highly sequence and salt-type specific, and typically lead to changes in protein solubility, stability, and/or denaturation [Baldwin, 1996]. Although an order of magnitude higher than the typical physiological conditions ($c \sim 0.1 - 0.3$ M), high salt concentrations play an important biochemical role in the field of protein crystallization [Dumetz et al., 2007], in food industry as fermentation additives [Dyer, 1951], and for the function and stability of biotechnologically interesting halophilic (salt-loving) enzymes [Lanyi, 1974]. Additionally the study of protein structures in high salinity solvents is instructive, as salt-specific effects are amplified. From a computational perspective, salt effects can be examined more efficiently in molecular dynamics (MD) simulations at high salt concentrations. Numerous theoretical studies have focused on short oligoalanine peptides, which serve as models for the study of peptide conformation dynamics and helix formation [Graf, 2007; Dzubiella, 2008; Dzubiella, 2009; Mu, 2003; Ohkubo, 2003; Feig, 2008]

In the past few years, research on specific salt effects has been reinvigorated by the advent of powerful new experimental and computational methodologies. Regarding computations, new ideas about salt effects have been tested when improved additive or polarizable force

fields became available [Anisimov et al., 2005; Borodin, 2009; Horinek et al., 2009]. A large increase of scientific work on the origin of specific ion action at aqueous interfaces has resulted in new and significant insights [Kunz, 2010; Jungwirth and Tobias, 2006; Gopalakrishnan et al., 2006]. In particular, the contribution of porizability to the attraction of loosely hydrated ions to the free water surface, hydrophobic or hydrophilic self-assembled monolayers, or lipid bilayers has been thoroughly investigated [Jungwirth and Tobias, 2006; Jungwirth and Tobias, 2002; Dang and Chang, 2002; Archontis et al., 2005; Archontis et al., 2006; Scwierz et al., 2010; Vacha et al., 2010].

Despite these recent advances, much less progress has been made in understanding salt effects on protein stability and solubility. It is indeed surprising that this scientific area, which initially triggered the research on ionic specificity [Hofmeister 1888], is currently the least advanced. Current research in this area follows two main directions: There are workers who try to understand the specific interactions of ions with protein surfaces [Pegram and Record, 2008; Lund et al., 2008], (either direct or water-mediated [Shimizu et al., 2008; Shulgin and Ruckenstein 2005]) or the salt-mediated protein-protein interactions and the second virial coefficients of protein solutions [Bostrom et al., 2006]. These works address the problem of protein solubility and crystallization from solution, and the surface-mediated mechanisms of salting-in and salting-out. A different line of investigation, originally carried out experimentally [Scholtz et al., 1991; Smith and Scholtz, 1998; Maison et al., 2001; Graf et al., 2007; Xiong et al., 2009], but more recently and to a larger extent computationally [Fedorov et al., 2007; Fedorov et al., 2009; Dzubiella, 2008; Dzubiella, 2009; Asciutto et al., 2010; Heyda et al., 2010; Von Hansen et al., 2010], is the use of specially designed oligopeptides and other related model compounds [Heyda et al., 2010; Yu et al., 2010] in the effort to assess the specific ionic interactions with the peptide backbone or with individual side chains, and the effects of ions on the secondary structure of the peptides. These works address more directly the issue of protein stability and conformation.

The work in this thesis falls in the second group of investigations. We have carried out a computational investigation of the effect of salts on the helix-coil transition of model oligopeptides, aiming to shed some light on the mechanism of specific ion action on the general protein folding process. We hope that the new results in the present thesis may open some new possibilities for the computational study of specific salt effects on protein

conformations in solutions, including eventually the stability of halotolerant proteins, the control of salt-responsive peptide solutions and the salt-dependence of fibril formation by proteins associated with neurodegenerative diseases.

We have addressed several aspects of the impact of ions on the structural properties and stability of oligopeptides. More specifically, we have studied ionic effects on:

1) The stability of the conformation of the peptide backbone.
2) The stability of the α-helix secondary-structural motif and the helix/coil equilibrium.
3) The strength of interactions between solvent-exposed, charged side-chains in α-helix-forming peptide.
4) The impact of solvent-exposed salt-bridge formation on the α-helix/coil equilibrium.

To investigate question (1) we used the simplest possible oligopeptides: the properly blocked alanine dipeptide (Ac-Ala-NMe) [Rossky and Karplus, 1979; Mezei et al., 1985; Tobias and Brooks, 1992; Ishizuka et al., 2010] and alanine tetrapeptide (Ac-Ala_3-NMe) [Tobias and Brooks, 1991]. The alanine dipeptide serves as a model of the protein backbone. It has a single pair of backbone dihedral angles (φ,ψ) and two peptide groups, which can form an intramolecular hydrogen bond. It allows checking the specific ion effects on the Ramachandran plot of di-alanine and the relative interaction of the ions with the backbone peptide groups and the methyl side chain and blocking groups [Rossky and Karplus, 1979; Mezei et al., 1985; Tobias and Brooks, 1992; Ishizuka et al., 2010].

The alanine tetrapeptide introduces additional dimensions [Tobias and Brooks, 1991]. With the particular choice of N-terminal and C-terminal blocking groups adoped (see Chaper 4.2), it has three complete pairs of backbone torsional angles (φ_i, ψ_i) and four peptide groups. Thus, it can form a variety of hydrogen-bonding interactions, including two i, i+3 hydrogen bonds encountered in protein β-turns (C_YO_Y-N_3H_{N3}, C_1O_1-N_TH_{NT}) and one i, i +4 hydrogen bond encountered in α-helices (C_YO_Y-N_TH_{NT}). Thus, closed, "quasi-helical" conformations are possible in this system, and the conformational space is greatly extended with respect to the dipeptide. Even though no large scale secondary structure can be formed by the tertrapeptide, an increase of "closed" conformations would immediately signify that the presence of salts stabilizes the initial helix-formation step in this type of oligopeptides, and vice versa.

To investigate question (2), we have simulated the model peptide Ac-$(AAQAA)_3$-NMe in aqueous electrolyte solutions. Experimental studies have shown that this peptide adopts an α-helical conformation in NaCl solutions, with stability (average helicity) that depends on the ionic strength of the solution [Scholtz et al, 1991; Shalongo et al, 1994; Smith and Scholz, 1998]. The peptide has been employed in several computational studies of the helix/coil equilibrium in implicit and explicit solvent, but not in the presence of salts [Shirley and Brooks, 1997; Ferrara et al, 2000; Gnanakaran and Garcia, 2005]. The use of this neutral peptide in which charge-charge electrostatic effects on helix stability are absent, allows to focus on the salting-in and salting-out interactions of the solution ions with the peptide groups and nonpolar groups. From the simulations of this peptide it is also possible to extract the parameters of the Zimm-Bragg and Lifson-Roig statistical-mechanical models of the helix-coil transition and the average peptide helicity as a function of electrolyte concentration and temperature.

For questions (3) and (4), we have simulated the model peptides Ac-AAQAA-EAQKA-AAQAA-NMe, Ac-AAQAA-EAQAK-AAQAA-NMe and Ac-AAQAA-EAQAA-KAQAA-NMe, which differ from the peptide of question (2) in that they contain oppositely charged amino acids (E, K) in positions *i*/*i*+3, *i*/*i*+4 and *i*/*i*+5. Experimental studies with the same systems have shown that the electrostatic interactions are not completely screened even at 2.5 M NaCl [Smith and Scholtz, 1998]. The major objective of the simulations is to determine the extent of these electrostatic interactions in the range of concentrations and temperatures considered, and their impact on the stability of the helix. Furthermore, the simulations of these charged model peptides can provide insights on the interaction between the charged side chains and the distribution of ions around the nonpolar, polar and charged groups.

To keep the systems simple, we have only used sodium chloride (NaCl) and sodium iodide (NaI) as electrolytes. NaCl is generally expected not to give strong specific salt effects in most systems [Collins and Washabaugh, 1985; Cacace et al., 1997; Kunz, 2010; Leontidis and Aroti, 2009] while iodide is definitely a chaotropic anion and can be used to illustrate potential side-chain or backbone interactions of the more hydrophobic ions [Fedorov et al., 2007; Fedorov et al., 2009; Dzubiella, 2008; Dzubiella, 2009]. We have used a range of

electrolyte concentrations (0 – 3 M) to investigate concentration effects on the oligopeptide structures.

The accurate sampling of electrolyte solutions requires long simulation times. To accelerate sampling, we have used the powerful replica exchange simulation method, which simultaneously propagates several replicas of the system at various temperatures and allows the controlled exchange of conformations between different temperatures (details in chapter 2.8) [Sanbonmatsu and Garcia, 2002; Buchete and Hummer, 2008].

1.1 Project Goals and Innovation

Protein folding is usually discussed theoretically in terms of (a) independent amino acid residue conformations, described by two-dimensional (φ, ψ) maps of torsion angles, and (b) phenomenological parameters describing the thermodynamics of α-helix formation. So far the influence of electrolytes on the torsion maps and the helix-formation parameters has never been assessed, although electrolytes are always present in polypeptide solutions and affect protein conformation, stability and solubility (salting-in and salting-out phenomena). In this work we have set the following scientific goals:

(a) To examine the effect of sodium salts (NaCl and NaI) on the torsion angle maps of alanine dipeptide, a model test solute.
(b) To examine the effect of sodium salts (NaCl and NaI) on the preference of alanine tetrapeptide for "special" conformations.
(c) To investigate the effects of the same salts on longer alanine-based peptides, with known folding propensities towards α-helices. The formation of α-helices is usually described by two parameters for helix nucleation and propagation. These parameters are computed by the proposed simulations as a function of temperature and salt concentration and type.
(d) To link the observed salt effects to actual local interactions, through examination of pair correlation functions, hydrogen bonding patterns and other data available from the simulations.
(e) To explain experimental data on α-helix formation by the same oligopeptides in the presence of salts.

(f) To quantify the strength of electrostatic interactions between solvent-exposed charged side chains in a helix and the impact of these interactions on helix stability in the presence of ions.

Several aspects of this work are innovative:

(a) For the first time the effect of electrolytes on Ramachandran plots of the alanine dipeptide have been examined. Even for this simple model peptide such information is nonexistent.
(b) The Lifson-Roig parameters for helix formation have seldom been obtained from simulation. In the present work they have been computed for a range of salt concentrations and temperatures and for a number of oligopeptides of increasing length and complexity.
(c) This is the first Molecular Dynamics study of model oligopeptides which have a pair of oppositely charged amino acids at different spacing.
(d) Because both the peptides and the ions in solution take a very long time to sample the available phase space, the replica-exchange method with parallel temperatures has been used. This has been used successfully in the past for peptides [Sanbonmatsu and Garcia, 2002; Buchete and Hummer, 2008], but not extensively for electrolyte solutions and certainly not for the combination of the peptides and salts in the same solution.
(e) A large number of different criteria have been used in the data analysis to quantify the interactions between ions and specific polypeptide groups. Apart from computing all relevant radial distribution functions, we have carried out careful analysis of local ion excesses and local hydrogen bonding between ions and peptide groups. We have tried to link this information to the effects of electrolytes on the Lifson-Roig helix-coil parameters. Such a systematic attempt to link phenomenological thermodynamics to local interactions has not been attempted so far.
(f) For the first time there is a very systematic sequential work on model peptides, in which we add new interactions with each new model, using what has already been learned from the previous models.

2. Basic Theoretical Background

2.1 Specific Ion Effects and the Hofmeister Series

The effect of electrolytes in aqueous solutions on different biological and physicochemical phenomena has been the subject of numerous studies since the late 19th century. The two first influential works, which defined the area of specific salt effects, belong to Lewith [Lewith, 1888] and Hofmeister [Hofmeister, 1888]. These authors examined systematically for the first time the effects of salt solutions on the solubility of proteins. They found that (a) the log(solubility) of many proteins in electrolyte solutions depends linearly on electrolyte concentration, and that (b) a different log(solubility) vs. salt concentration curve is obtained for each electrolyte irrespectively of the charge of the ions. Following this pioneering work, a large number of experimental studies have shown the importance of specific ion effects in all kinds of biological and physicochemical phenomena; ions in aqueous solutions have been found to affect polymer cloud points [Schott et al., 1984], the critical micelle concentration of surfactant molecules [Ray et al., 1971; Zhang et al., 1996], pH measurements [Camoes et al., 1997; Boström et al., 2001, Boström et al, 2003], zeta and surface potentials of lipid membranes [McLaughlin et al., 1975; Tatulian, 1983; Clarke et al., 1999; Franks, 2002], the surface tension of electrolytes [Jarvis et al., 1968; Weissenborn and Pugh, 1996], the enzymatic activity of biomolecules [Wright and Diamond, 1977; Hochachka and Somero, 1984; Hall and Darke, 1995] etc. The two older reviews that were published on the topic of specific salt effects and are still heavily cited [Collins and Washabaugh, 1985; Cacace et al., 1997] contain more than 900 references to the extensive experimental work carried out in the 20th century. Depending on the strength of their effects in several phenomena, ions have been ordered into sequences, which are called the Hofmeister series or the lyotropic series. Typical Hofmeister series for cations and anions are as follows:

$$Cs^+ > Rb^+ > NH_4^+ > K^+ > Na^+ > Li^+ > Ba^{2+} > Sr^{2+} > Ca^{2+} > Mg^{2+}$$

$$SO_4^{2-} > HPO_4^{2-} > OH^- > F^- > CH_3COO^- > Cl^- > Br^- > NO_3^- > I^- > BF_4^- \approx ClO_4^- > SCN^-$$

In the above sequences, ions are ordered mostly according to their ability to salt-out proteins; the strongest salting-out ions are placed by convention on the left side of the sequences. Anions were found to have much stronger impact than cations in several phenomena. To return back to the protein solubility problem, anions that are located to the left of Cl^- decrease protein solubility and therefore are called salting-out ions. Anions to the right of Cl^- often (but not always!) have the opposite effect and thus they are called salting-in ions. The Cl^- ion is said to be an indifferent ion and the direction of many specific anion effects is found to change around the Cl^- ion.

For almost 100 years the precise origin of specific salt effects was very poorly understood. Thanks to a strong revival of interest in the topic and the strong and persistent efforts of many research groups, considerable progress in this area has been made in recent years. The following discussion of existing theoretical ideas will focus mostly on anions, since the systematic trends in the case of cations are less well-defined and the effects are often weaker.

Different ideas about the nature of specific salt effects have been proposed: The main older idea was that since ions interact with water very strongly they modify the structure of water, especially regarding the populations of H-bonded clusters [Chaplin, 1999]. For this reason anions to the left of Cl^- in the Hofmeister series have been called cosmotropes, following the idea that they enhance water structuring (structure makers), while anions to the right of Cl^- are called chaotropes or structure breakers. For ions with the same charge, the other most important property is their size, quantified by their Pauling radius [Leontidis, 2002]. Generally, cosmotropic ions have small Pauling radii, because of their higher electric fields they are strongly hydrated, losing their water of hydration with difficulty. The opposite holds for chaotropic ions, which are more weakly hydrated. Another fundamental property of ions is their polarizability, which is the ability of their electronic shells to undergo deformation in an electric field. Although, the polarizability of an anion is related to its size and internal structure, it is often considered as a propery that can dictate ionic behavior independently. In general, cosmostropic ions have small polarizabilities and chaotropic ions large polarizabilities, although marked exceptions exist (SO_4^{2-} is a cosmotropic ion with high polarizability).

To explain specific salt effects Collins and Washabaugh [Collins and Washabaugh, 1985] have developed a molecular model, based on the idea that the water surrounding an ion can be divided into three layers. The first layer is adjacent to the ion, and is equivalent to the well-known first solvation shell. The third layer represents the water in the bulk solution and the second layer has properties determined by the other two layers (it could be described as a second hydration shell). The main default of this model is its complexity (involving the interactions between the three hydration shells) and inability to provide solid quantitative information. Following the same idea regarding the water structure around ions, and also some experimental insights, many biologists [Chaplin, 1999] consider low-density and high-density water close to biological interfaces and examine the way the two water regions are affected by ions.

Ninham and Yaminski [Ninham and Yaminski, 1997] suggested in an important paper that the origin of the Hofmeister series could be due to the existence of dispersion interactions between ions and surfaces, and ions and water molecules. Due to the fact that the classical Gouy-Chapman theory of electrical double layers cannot explain the mechanism of action of Hofmeister ions, they claimed that an ionic dispersion potential acting between ions and any interface must be included in the theory of electrostatic effects. The new extended model can be used to explain the results of several experiments, as long as the ions do not form chemical bonds with surfaces. Boström et al., [Boström et al., 2001] explained the surface tension of electrolytes using the concept of dispersion forces. They added ion specificity into their electrostatic calculations using a dispersion potential and retaining the main picture of Onsager and Samaras [Onsager and Samaras, 1934], which assumes the existence of a layer free of ions close to the water surface. The results in their highly-cited paper do not agree however with recent molecular simulations of electrolyte solution surfaces, which demonstrate that anions have a higher affinity (higher concentration) for the free water surface than cations of the same charge [Jungwirth et al., 2000] while large, polarizable anions exhibit strong concentration peaks close to the water surface [Jungwirth et al., 2002; Archontis and Leontidis, 2006]. It should be denoted that these simulations used a polarizable model for water and ions.

Another qualitative model suggests that ion specificity arises as the result of a fine balance between ion-water and water-water interactions [Collins, 1997]. Recent computer simulations studies using Monte-Carlo and Molecular dynamics giving emphasis to

hydration interactions support this idea while focusing on electrolyte effects on the hydrogen-bonding network of water [Karlström et al., 2002; Hribar et al., 2002].

Kim D. Collins published another significant study in 2004 [Collins, 2004]. We quote here his main idea that he summarized in the following rule: *The law of matching water affinities: oppositely charged ions in free solution form inner sphere ion pairs spontaneously only when they have equal water affinities.* Making use of different techniques (Sephadex G-10 gel sieving chromatography, Jones-Dole viscosity B coefficients, and solution neutron and X-ray diffraction) he showed that small ions of high charge density (e.g., sulfate, phosphate, the carboxylate, sodium, and fluoride) are strongly hydrated (cosmotropes) whereas large monovalent ions of low charge density (e.g., ammonium, chloride, potassium, and the positively charged amino acid side chains) are weakly hydrated (chaotropes). When the ions are small (hard or cosmotropic) the surrounding water molecules are tightly bound to the ion, while when the ions are big (soft or chaotropic) the hydration shell is loosely bound. The discrimination between these two types is based on the relative strength of ion-water interactions compared to water-water interactions. The horizontal line illustrated in Figure 2.1 between Na^+ and K^+ for cations and Cl^- and F^- for anions is roughly defined by the strength of water-water interactions (ideal behavior, no preferential interactions). Water is here considered to be a zwitterion with a cationic portion of the (interpolated) ideal cation size and an anionic portion of the (interpolated) ideal anion size at the horizontal line, also illustrated in Figure 2.1. The strongly hydrated ions above the line in Figure 2.1 are referred to as “small”, the weakly hydrated ions below the line as “large” and water (at the line) as a “medium-size” zwitterion. Two strongly hydrated small ions of opposite charge experience a very strong reciprocal attraction. They can therefore attach to each other forming direct ion pairs and expelling the hydration spheres between them. Although the electrostatic attraction between the weakly hydrated large ions is much smaller, their hydration spheres are so loosely bound that the chaotropic ions can also form direct ion pairs expelling hydration water between them. In contrast, when we consider one small and one large oppositely charged large ion the attraction of the large ion is not strong enough to force the small ion to lose its hydration shell. As a consequence, a couple of a large and small ion cannot form strong ion pairs; it forms by necessity only water-separated ion pairs. This explanation of ‘like seeks like’ is illustrated in Figure 2.2.

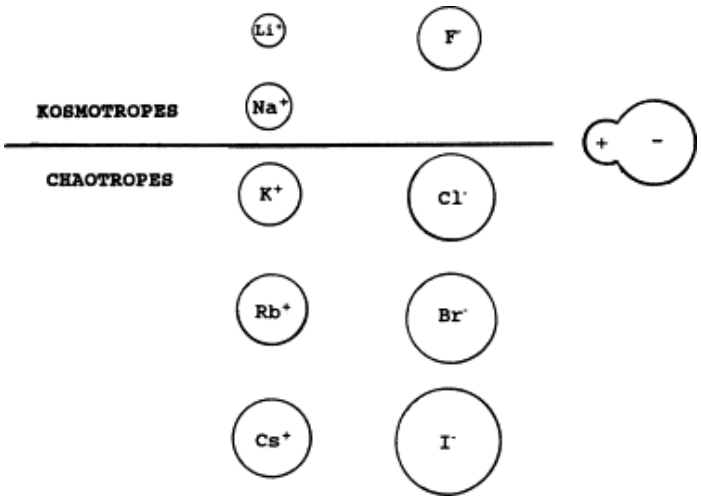

Figure 2.1: *Division of the group IA cations and the VIIA halide anions into [strongly hydrated] cosmotropes (water structure makers) and [weakly hydrated] chaotropes (water structure breakers). The ions are drawn approximately to scale. A water molecule is represented as a zwitterion of radius 1.78 Å for the anionic portion and 1.06 Å for the cationic portion [Collins, 2004].*

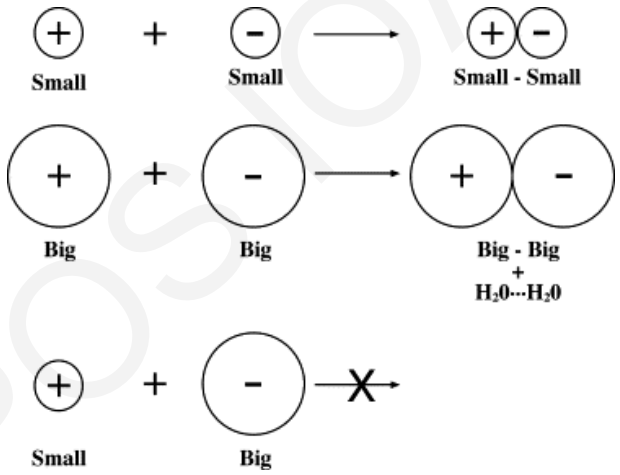

Figure 2.2: *Ion size controls the tendency of oppositely charged ions to form inner sphere (contact) ion pairs. Small ions of opposite sign spontaneously form contact ion pairs in aqueous solution; and large ions as well; mismatched ions of opposite sign do not spontaneously form contact ion pairs in aqueous solution. A large monovalent cation in this picture has a radius larger than 1.06 Å; a large monovalent anion has a radius larger than 1.78 Å [Collins, 2004].*

The idea of Collins [Collins, 2004] is fruitful, even if it is an oversimplification. For example, as an ion approaches an interface, ion-interface and water interface interactions must also be considered besides ion-water and water-water interactions.

Vlachy et al. proposed a Hofmeister-like ordering of charged headgroups of surfactant-like molecules and combined the proposed headgroup ordering with the law of matching water affinities [Vlachy et al, 2009]. The following Figure 2.3 shows the results. Of all the considered anionic headgroups, carboxylate turns out to be the hardest, whereas sulfate and sulfonate are soft headgroups. Their *charge density* and the resulting strength of the ion-water interaction compared with water-water interactions is the single parameter that determines their behavior. The detailed geometry of the headgroups, the resulting water geometry and ion polarizabilities are other properties that may also have an impact. However, Collins's law of matching water affinities coupled to the headgroup charge densities may qualitatively explain many experimental findings, especially those concerning micelles, polyelectrolytes and vesicles.

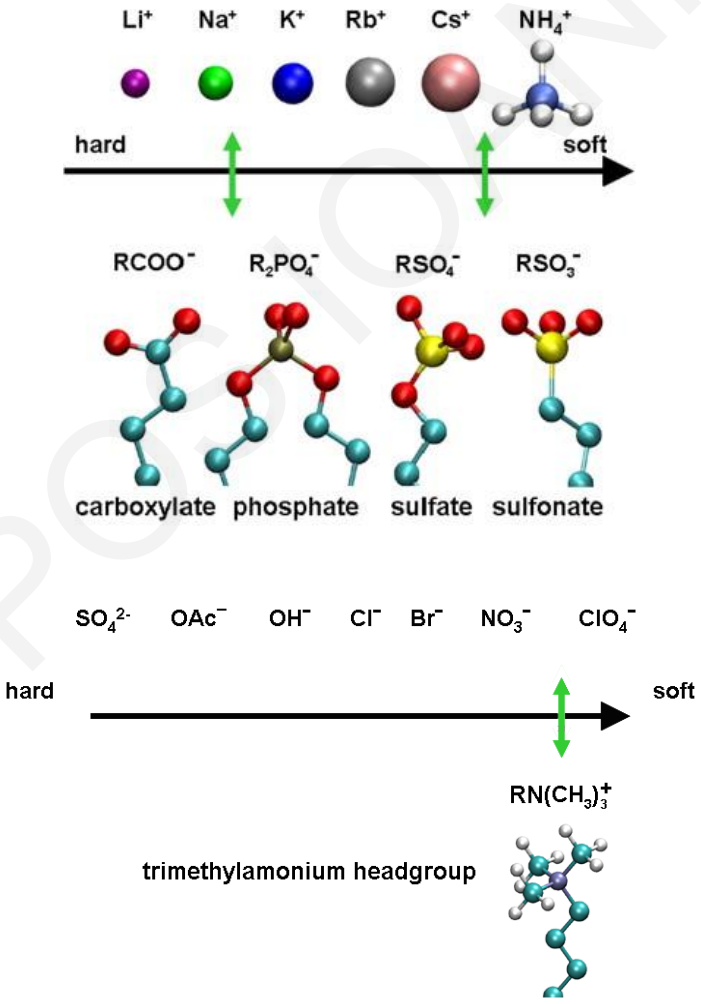

Figure 2.3: *(a) Ordering of anionic surfactant headgroups and the respective counterions regarding their capabilities to form contact pairs. The green arrows mean strong interactions (close ion pairs). (b) Ordering of anionic counterions with respect to their affinity for the trimethylammonium headgroup [Vlachy et al., 2009].*

The observations that surface potential varies widely for different salts of the same valence provided evidence for differential partitioning of salt cations and anions at the air-water interface [Frumkin, 1924; Randles, 1957]. Within the past 15 years, MD simulations, surface spectroscopic measurements, and electrospray ionization mass spectrometry have provided additional evidence on the idea that the cation and anion of a salt partition differently between the surface and the bulk solution; in fact it is now believed that some anions actually accumulate at the surface [Petersen and Saykally, 2006; Jungwirth and Tobias, 2006; Archontis et al., 2005; Archontis and Leontidis, 2006]. Pegram and Record [Pegram and Record, 2007] developed a solute-partitioning model for individual ions between bulk solution and the air-water interface and used it to analyze the available surface tension data [Kumar, 2001; Washburn, 2003] by determining partition coefficients of Hofmeister anions and cations between the bulk solution and the air-water interface. They demonstrated that the relative rankings of the cation and anion partition coefficients generally agree qualitatively with the Hofmeister series obtained from ion effects on biopolymer processes. Figure 2.4 contains the comparison that they created. The left column in this graph contains ion partitioning coefficients between air-water surface and bulk electrolyte solution. The right column provides the qualitative ranking of the ions, provided by von-Hippel from examination of the interactions of protein surfaces from water [von Hippel et al, 1964]. Figure 2.4 shows that the anion partition coefficients derived from surface tension increments (STI $d\gamma/dm_2$) are correlated (both in rank order and approximate magnitude) to the Hofmeister series of anions. In this study, anions range from almost complete exclusion from the air-water surface to moderate surface accumulation. Relative to the sulfate anion (which was taken to be completely excluded), CO_3^{2-} is also almost completely excluded while F^- and HO^- are more weakly excluded from the air-water surface. For Br^-, NO_3^- and I^- there appears to be an approximately uniform distribution while for ClO_3^-, SCN^- and ClO_4^- a moderate surface accumulation is predicted. For cations, Figure 2.4 reveals a significant shift in magnitude of partition coefficients. Alkali metal cations and GuH^+ are widely separated in both series, but the Li^+, Na^+, K^+, and Cs^+ cations are almost completely excluded from the air-water surface. The overall good agreement of the series obtained from surface tension with the Hofmeister rankings, suggests that a dominant factor for ion specificity must be the partial dehydration of the ions. The Pegram and Record analysis [Pegram and Record, 2007] predicts that Na^+ is completely excluded and Cl^- is only moderately excluded from the surface, in agreement qualitatively with MD calculations [Jungwirth and Tobias, 2001]. The large shift between

cation STI-derived partition coefficients and inferred placements in the biopolymer Hofmeister series (as shown in Figure 2.4) suggests that cations interact relatively better than anions with protein surfaces rather than with the air-water surface. These two observations lead to the conclusion that the thermodynamics of transferring cations and anions from the bulk to a surface are dominated by different interactions.

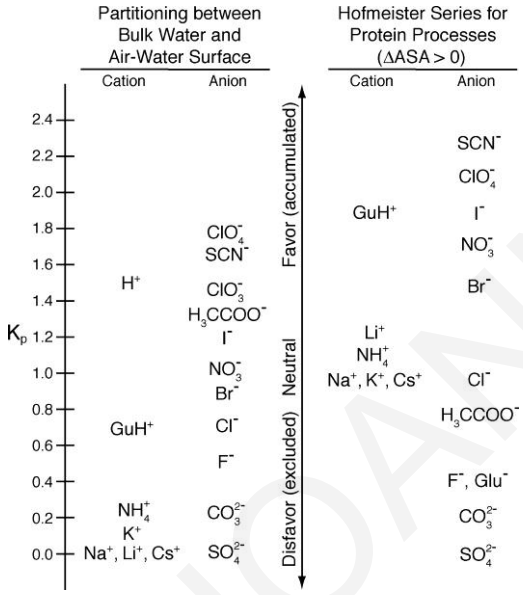

Figure 2.4: *Comparison of single-ion partition coefficients $K_{p,I}$ for partitioning of ions between bulk water and the air-water surface with relative Hofmeister rankings of anions and cations for processes which expose protein surface to water (e.g., unfolding) [Pegram and Record,2007].*

More useful models must not be based on the air-water surface, which is devoid of ion-surface interactions. A more complex "partitioning" model, accounting for both sodium complexation with liquid head groups and anion partitioning within lipid monolayers is described by Leontidis [Leontidis and Aroti, 2009]. The partitioning parameters suggested by such a comprehensive model correlate well with several measures of ion specificity, such as ionic volume, von Hippel chromatographic parameters, or viscosity *B*-coefficients. The competition of cavity and ion hydration terms formed the basis of the model for the partitioning chemical potentials. The model leads to a very good correlation of the partitioning chemical potentials with a function of the ionic radius, showing that specific anion effects on zwitterionic lipid monolayers mostly depend on ionic size. Thiocyanate and acetate ions are two notable exceptions from this correlation. Their charged distribution is not spherically symmetric; therefore they are expected to have orientation-dependent interactions with the water-lipid interface.

It is obvious from the above broad spectrum of alternative explanations that it is still not clear in all situations whether ions act through precisely defined, specific, local interactions, or through more delocalized collective interactions. Elucidation of the mechanism of action of the Hofmeister ions in a particular experimental situation or molecular dynamics simulation often gives a better understanding on numerous ion-specific phenomena, and has a strong impact on biology and chemistry.

2.2 Solvation

2.2.1 Water

Water is a special liquid both from a physical and from a chemical point of view. The extensive hydrogen bonding between water molecules leads to a high boiling point and unique solvating abilities. The water molecule is dipolar with a dipole moment of 1.86 D [Clough et al., 1973] in the gas phase and 2.6 D in the liquid phase [Silvestrelli and Parrinello, 1999]. The significant dipole moment results from the relatively electron-poor hydrogen atoms and the electron-rich oxygen atoms. The oxygen atom of a water molecule can form hydrogen bonds with electron-accepting hydrogen atoms of other molecules. Hydrogen-bonds are formed when the two lone electron pairs of the oxygen atom partly donate their electron density to the hydrogen atoms of neighboring molecules. The energy content of a hydrogen bond between water molecules is roughly 5.6 kcal/mol [Suresh and Naik, 2000]. Ideally, every water molecule could donate and accept two hydrogen bonds, as depicted schematically in Figure 2.5. This happens for all water molecules in ice I, which has a crystal structure built up from tetrahedrally coordinated water molecules [Bernal and Fowler, 1933]. Even in the liquid phase, the water tetrahedrons created by extensive hydrogen-bonding are a prominent feature of the liquid structure. A snapshot of a typical pure liquid water simulation at 300 K is shown in Figure 2.6. Several tetrahedrally surrounded water molecules are found in this structure, along with a large number of water molecules that are only partly coordinated.

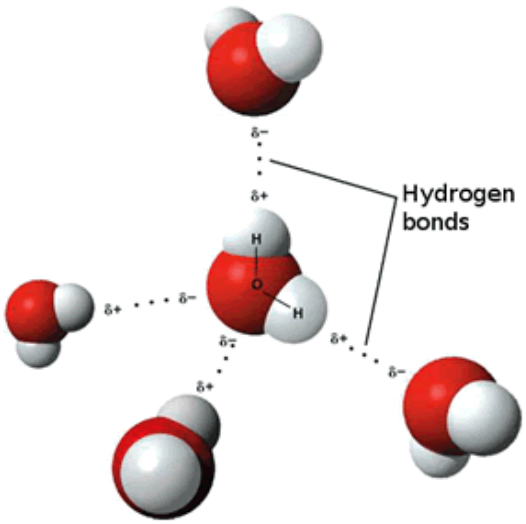

Figure 2.5: *Representation of hydrogen bonds (dotted lines) between water molecules [I_1].*

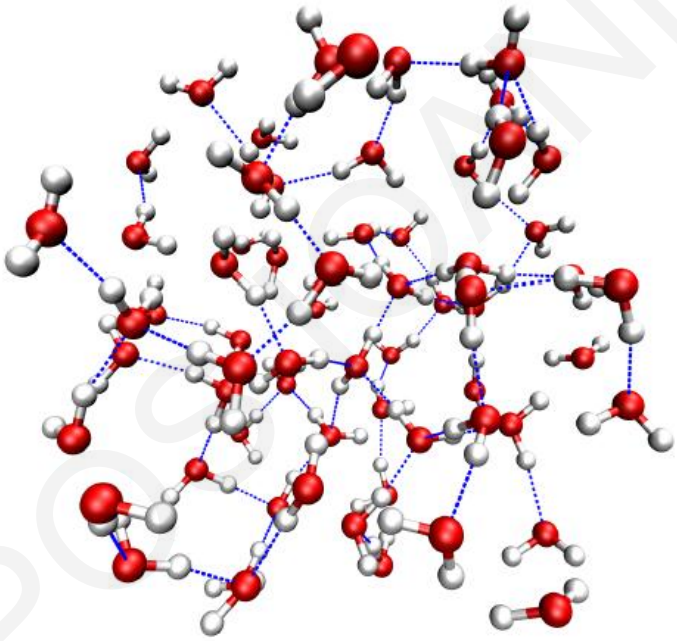

Figure 2.6: *Snapshot of liquid water. Hydrogen bonds are represented by the dotted blue lines [Heuft, 2006].*

A quantitative way to examine the structure of a liquid is to use radial distribution functions (RDF). The RDFs for pure liquid water at 300 K are shown in Figure 2.7. The structured nature of the liquid is made clear by the sharp and well-defined peaks in the RDFs. The first O–H peak is at 1.8 Å and represents the hydrogen-bonded O–H pairs. The normalized integral of the peak corresponds to exactly 1 oxygen atom and 2 hydrogen atoms, in complete agreement with an average tetrahedral coordination of the water molecules.

Since the hydrogen bond interactions dominate the structure of liquid water, it follows that they also affect the dynamical properties of water in many ways. For example, the diffusion coefficient of water molecules is rather small for such a small molecule. However it should always be remembered that the hydrogen bond network is highly dynamic with hydrogen bond continuously breaking and forming. This dynamic behavior must be taken into account in the analysis of the behavior of aqueous solvation shells around ions.

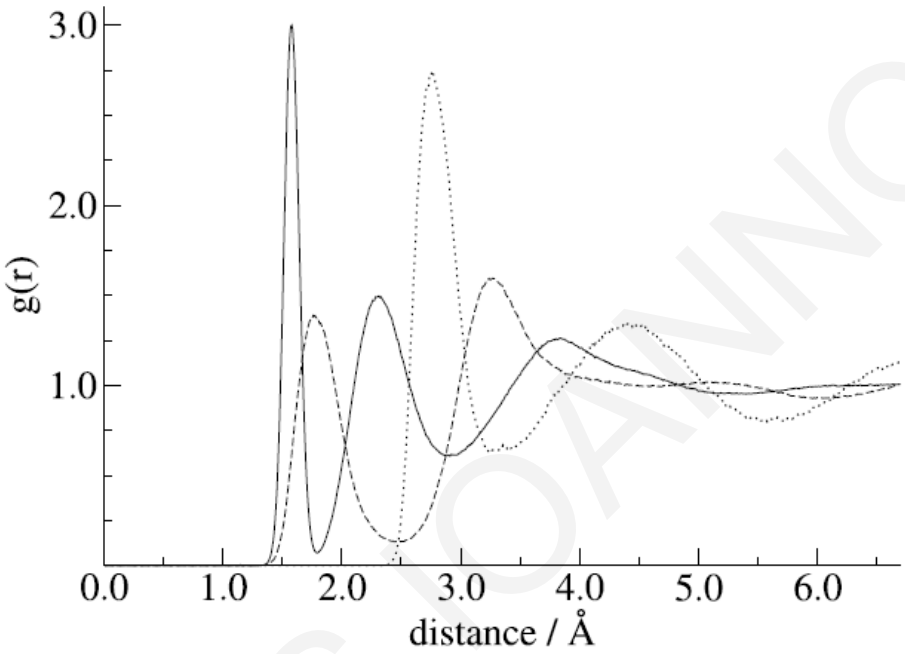

Figure 2.7: *Rdf of pure liquid water, O–H (dashed line), O–O (dotted line) and H–H (solid line) [Heuft, 2006].*

2.2.2 Ions in Water

A disruption of the hydrogen bond network is caused when ions are introducted into liquid water. The water molecules rearrange in the presence of the ions, and for this reason the hydrogen bonds between water molecules are broken increasing the energy of the system. Ions however interact quite strongly with water through formation of hydrogen-bonds but also through ion-dipole interactions. These ion-water interactions compensate for the loss of water-water hydrogen bonds and result in a negative free energy of solvation. The strength of ion-water interactions depends on the size and the charge of the ion. According to Ninham's idea the polarizability of the ions also plays a significant role [Ninham et al., 1997]. In addition, there is a marked difference in the way that the anions and cations interact with water. The first solvation shell of anions is more compatible with the natural structure of liquid water, hence the free energy of solvation of anions is more negative than

that of cations of the same size [Grossfield, 2005]. Figures 2.8 and 2.9 present typical pictures of the first solvation shells of water molecules around positive and negative ions. These images do not provide the whole story however, especially when considering large ions. The local water network is extensively disrupted by large ions, beyond the first solvation shell. Thus the solvation of large ions is more complex, with conflicting interactions contributing. It is, often found that large ions have smaller free energy of solvation than small ions.

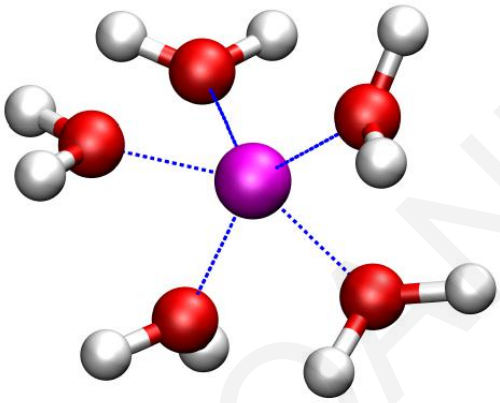

Figure 2.8: *A cation surrounded by water molecules [Heuft, 2006].*

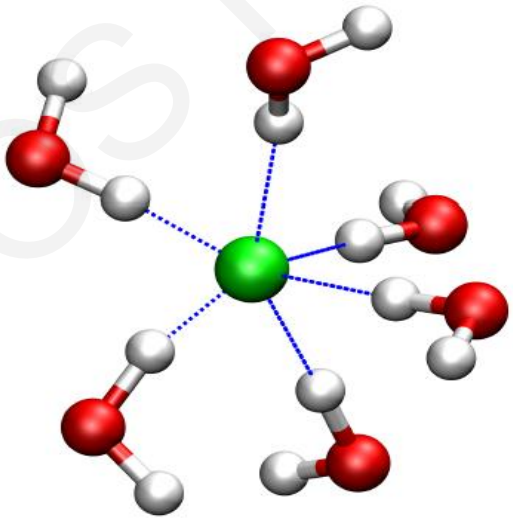

Figure 2.9: *An anion surrounded by water molecules [Heuft, 2006].*

The four halide ions, F^-, Cl^-, Br^- and I^-, often serve as prototype solutes to study ion-water interactions in detail. The total charge and outer electron configuration of halide ions are identical, but there are considerable differences in the ionic sizes and masses. In order to understand the relative strength of anion-water interactions, in this series the $X^-(H_2O)$ (X =

F, Cl, Br, I), we tabulate enthalpies of the hydrogen-bonds between these anions and water in Table 2.1, together with the radii of the ions [Weast CRC Press, 1975].

Table 2.1: *Ionic radii of the common halide ions and hydrogen bond energies for $X^-(H_2O)$. a.[Weast CRC Press, 1975] , b. [Weis et al., 1999] and c. [Hiraoka et al., 1988].*

ion	ionic radius/Å[a]	ΔH^0/kcal/mol
fluoride	1.33	-26.2 ± 0.8[b]
chloride	1.81	-14.7 ± 0.6[c]
bromide	1.96	-11.7 ± 0.4[c]
iodide	2.20	-10.3 ± 0.3[c]

Ions are often classified either as a 'structure-maker' or a 'structure-breaker' depending on their overall influence on the structure of bulk water. This is a quite old idea that still permeates physical chemistry and biology text books [Dill, 2002]. However recent studies [Grossfield, 2005; Omta et al., 2003] have revealed that the structure making or breaking effect of ions is only limited to the first or second solvation shell.

The hydration number (number of coordinating water molecules and the geometry of the coordination sphere) can be obtained from X-ray and neutron diffraction experiments. These techniques are too slow, however to yield information on the dynamics of ionic solvation. Dynamics can be probed with Fourier Transform Infrared (FTIR) spectroscopy. In this method however the signal of the coordinating water molecules tends to be obscured by that of the bulk water molecules. Nonlinear pump-probe spectroscopy has provided significant insights into the dynamics of ionic solvation. In this method, water molecules in the first hydration shells of the ions are selectively excited using a pump laser pulse, and their dynamic response is probed by a second, probe laser pulse [Kropman and Bakker, 2001]. The time resolution of pump-probe experiments is currently in the range of femtoseconds, so they can provide properties such as the residence time and the rotational reorientation time of water molecules in the first solvation shells. This powerful method still cannot be generally applied to all ions.

In the last 30 – 40 years, computational research has also provided much useful information about aqueous ion solvation. With molecular dynamics (MD) one can follow the motion of atoms with a temporal resolution of femtoseconds. Hence, MD provides a direct way to investigate certain properties that cannot be studied in experiments or can be studied only indirectly.

The precise computational method and the ion-ion and ion-water interaction parameters play a critical role in the accurate computational investigation of aqueous electrolyte solutions [Brodsky, 1996]. Numerous methods, ranging from simple forcefields [Jorgensen, 1983] to advanced *ab initio* simulations [Laasonen et al., 1993] have been applied in the study of pure liquid water. The introduction of an ion to the system complicates the models used considerably. The problem of aqueous ion solvation has been found to be sensitive to the polarizability of both the water molecules and the ions [Stuart and Berne, 1996], the geometrical constraints on the water model (if water bonds are held rigid or are flexible), many-body effects, and other subtle effects. In the case that any of these are not implemented correctly in the algorithm there could be consequences for both structural and dynamical features of the system. Efforts to implement all or most of these effects using advanced forcefield models or *ab initio* type techniques, results in large increases of the required computer power. The availability and power of computer clusters and supercomputers, in recent years has enhanced the capabilities of computational methods tremendously, and has allowed the investigation of progressively more complicated models.

2.3 Ion Binding to Biomolecules

The stability of protein conformations in electrolyte solutions depends on a number of factors, such as the macromolecular net charge, and salt type, concentration and valency [Baldwin, 1996]. Effects of the specific chemical nature of the salts that go beyond the valency are usually classified as Hofmeister or ion-specific effects. Hofmeister originally [Hofmeister, 1888] arranged ions based on to their ability to precipitate or 'salt-out' egg white proteins. The effects of cations on protein structures are generally less pronounced than those of anions. The Hofmeister ordering was found not to be entirely fixed however. It is affected by the solution pH and the protein iso-electric point (pI). For example, in second virial coefficient measurements of lysozyme, (with a pI in the range of 10 to 11) it was found that protein association is induced by anions such as iodide and thiocyanate [Piazza and Pierno, 2000] which are supposed to be "salting-in" ions. A "reverse" Hofmeister series was in fact observed in these measurements. A systematic SAXS study revealed that a Hofmeister reversal for pH < pI is observed for several small proteins, such as α-crystallins, γ-crystallins, ATCase and Brome Mosaic Virus [Finet et al., 2004].

A number of recent investigations examine ion specificity of protein association as largely depending on interactions between salt ions and the macromolecular surface [Zhang and Cremer, 2006]. For pH < pI, anionic adsorption reduces the total macro ion charge thus reducing the repulsion between the cationic biomolecules. It thus assists complexation. The opposite effect can be observed for negatively charged proteins (pH > pI).

The Hofmeister reversal can be obtained by combining the Poisson-Boltzmann continuum electrostatics with ion-specific dispersion forces between small ions in solution and macro-ions [Boström et al., 2005]. According to their polarizabilities, larger ions such as iodide and thiocyanate have stronger dispersion forces with the macromolecular surface than do smaller ions, such as chloride and bromide. While dispersion is indeed ion specific, additional important mechanisms are also ion specific and may be dominant in certain circumstances. Protein surfaces are not uniform. They are formed by polar and nonpolar groups to which salt ions have very different affinities. For example, large anions are attracted to hydrophobic patches on surfaces via surface-modified solvation and polarization [Jungwirth and Tobias, 2006; Lund et al., 2008]. Direct ion-pairing [Bjerrum, 1926; Jagoda-Cwiklik et al., 2007] between ions and charged surface groups may exist under several circumstances. It is also highly ion-specific [Vrbka et al., 2006].

Simulation work on proteins, oligopeptides, and amino acid residues has shown that sodium and potassium bind differently to biomolecules [Vrbka et al., 2006; Dzubiella, 2008]. In general, it has been observed that the affinity of sodium to protein surfaces is more than twice that of potassium. The cationic attraction stems mainly from pairing with acidic carboxyl groups on glutamate and aspartate, and with backbone carbonyl groups. The same simulations have also shown that hydrophilic anions (e.g. F^- or SO_4^{2-}), although strongly repelled from hydrophobic domains, can bind to specific groups of the protein surface.

2.4 α-Helix Structure

Proteins contain regular regions of the polypeptide chain, folded in specific conformations called secondary structure. The first such secondary structure that was theoretically proposed and experimentally confirmed was the α-helical structure. The scientific community has been captivated by the elegant simplicity of the α-helical structure. It is stabilized by hydrogen bonding between the backbone carbonyl oxygen and the peptide amide four residues away.

Pauling, Corey and Branson were the first to theoretically describe the α-helix in 1951 [Pauling et al., 1951]. Their ingenuous model was supported by X-ray analysis of haemoglobin [Perutz, 1951]. The first protein crystal structure that was analyzed was that of myoglobin, in which most secondary structure is helical [Kendrew et al., 1960]. Since then α-helical domains have been found in most globular proteins. The α-helix is the most usual secondary structure in proteins, with ~30% of residues found in α-helices [Barlow et al., 1988]. The α-helix motif is obtained by a combination of an orthogonal circular rotation and a linear translation of the protein backbone. More specifically, the α-helix is formed by a linear translation of 5.4 Å per turn and a circular rotation of 3.6 residues per turn. The i to $i + 4$ hydrogen bonds between backbone carbonyl and amide groups are the major driving forces for the stability. The carbonyls in the α-helix serve as hydrogen bond acceptors for the peptide N-H donors four residues away. Such a hydrogen-bonding pattern can be best satisfied if the backbone dihedral angles φ and ψ are constrained to a narrow range of values around -60^{o} and -45^{o}, respectively. When the α-helix is viewed with the N-terminus at the bottom and the C-terminus at the top (as shown in Figure 2.10), all the carbonyls point up and all the N-H groups point down. The interior of an α-helix is tightly packed by the backbone atoms $-C_aCONH-$, while the side chains point away from the helix axis. Therefore, the side chains spaced "i, $i + 3$", "i, $i + 4$" and "i, $i + 7$" are close in space and interactions between them affect helix stability. On the other hand, the side chain pairs are on opposite faces of the helix when the spacing is "i, $i + 2$", "i, $i + 5$" and "i, $i + 6$", and thus do not interact in significant ways.

The backbone dihedral angles φ and ψ can describe the conformation of polypeptides. Most theoretical φ, ψ combinations are sterically excluded, allowing only the broad β region and narrower α region in the (φ, ψ) map. The succession of the sterically allowed φ,

ψ angles naturally positions the backbone NH and CO groups towards each other for hydrogen bond formation. Hence, strong hydrogen bonds are created in the most stable conformations.

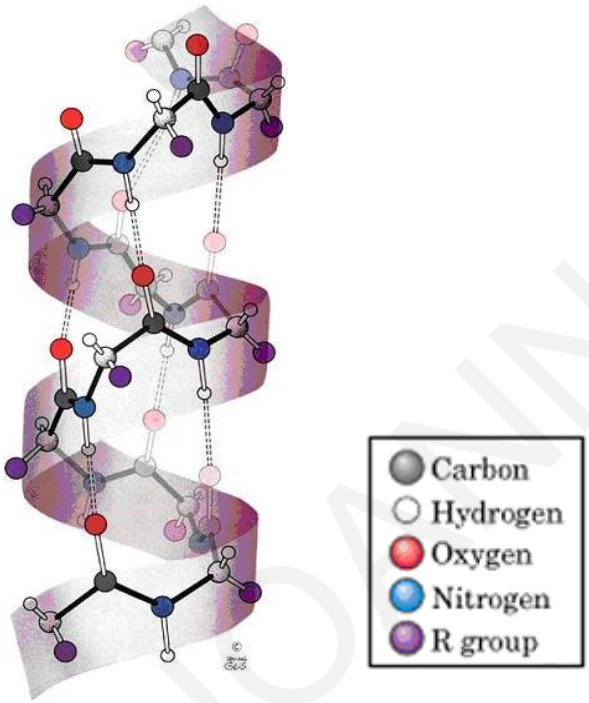

Figure 2.10: *The right-handed α-helix [Cantor and Schimmel, 1980].*

2.4.1 Ramachandran Plots

Each residue in a polypeptide chain has two bonds about which restricted rotation is allowed. Depending on the values of the angles of rotation, defined as φ and ψ, different structures may be formed (Figure 2.11). Consequently, the configuration of a protein backbone may be described with the specification of these two angles for each residue. With these conventions, the backbone conformation any single residue in a protein can be described by a point on a diagram with coordinates φ and ψ. When all residues of a protein are found in a particular secondary structure (an α-helix, for example), their points on (φ, ψ) space would overlap. Thus, a single point on a (φ, ψ) diagram also describes a given secondary structure. Such diagrams are called Ramachandran plots, after the biochemist who first made extensive use of them. A major advantage of the Ramachandran plots is that they allow to immediately distinguish the sterically allowed structures from those that are not allowed. A Ramachandran plot for poly-alanine contains three different possible

regions (Figure 2.12). In the top-left region the (φ, ψ) values correspond to parallel and antiparallel β sheets and the collagen helix. The other major observed region corresponds to right-handed α helices and a smaller third region to left-handed α helices. Although we see the left-handed α-helix in Figure 2.12, this region is not usually as favored energetically as the region of the right-handed form and is therefore not observed experimentally.

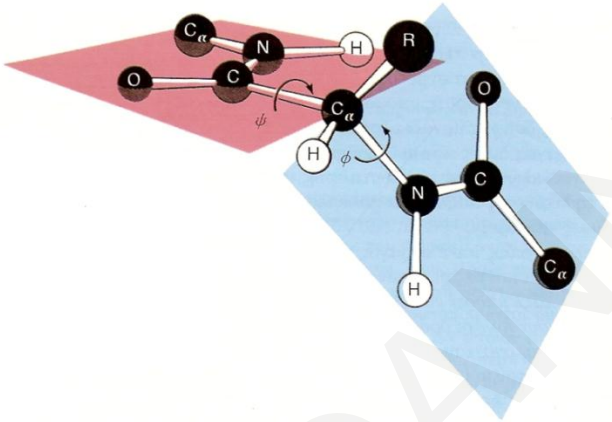

Figure 2.11: *Rotation around bonds in a polypeptide chain. Rotation is allowed only about the C_α – N and C - C_α bonds. The angles of rotation about these bonds are defined as φ and ψ. The extended conformation of the chain shown here corresponds to $\varphi = 180^o$, $\psi = 180^o$ [C. Levinthal, 1966].*

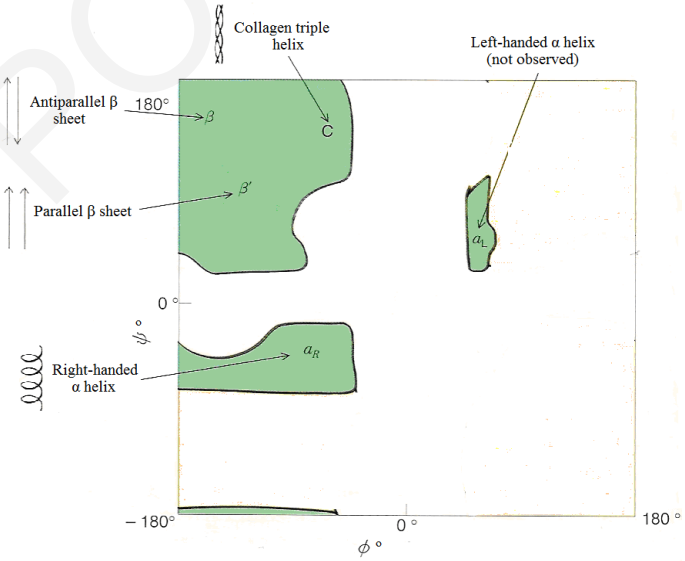

Figure 2.12: *Ramachandran plot which shows allowed values of φ and ψ for L-alanine [Stryer, 1997].*

2.4.2 Thermodynamics of α-Helix Formation

Pauling assumed that hydrogen bonding is the main source of stability of the α-helix [Pauling et al., 1951]. However it was soon found that such a description of the mechanism of the stabilization of α-helices is not sufficient. The complexity of the mechanism of helix stabilization was addressed in the second half of the 20th century by John Schellman from a thermodynamic point of view [Schellman, 1955]. Even though considerable work has been done in this area there are some details of the thermodynamics of the helix-coil transition which still need elucidation [Scholtz et al., 1992; Chakrabartty et al., 1995; Rohl and Baldwin, 1998]. From the structure of an α-helix, it is clear that the arrangement of the *i* to *i* + 4 hydrogen-bonding pattern by the peptide backbone is enthalpically the driving force for helix formation [Schellman, 1955]. There is also no doubt that the helix formation limits the configurational freedom of the side chain, thus leading to an entropy reduction [Padmanabhan et al., 1990; O'Neil and Degrado, 1990; Creamer and Rose, 1992; Blaber et al., 1994]. In fact, residues with smaller side chains (such as alanine) suffer a small loss in the configurational entropy, while for large side chains the opposite occurs (see e.g. the valine case [Creamer and Rose, 1992]). The loss in configurational entropy is so important, that it was proposed as the major factor that defines the helix-forming propensities of different amino acids [Creamer and Rose, 1994]. Blaber et al. [Blaber et al., 1994] examined the validity of this idea, by calculating the loss of side-chain configurational entropy for all residues. The computed $\Delta\Delta S$ values for nonpolar residues were found similar to the ones computed by Creamer and Rose [Creamer and Rose, 1992]; however, Blaber et al. found little correlation between helix propensity ($\Delta\Delta G$) and entropy loss ($\Delta\Delta$S) when considering both polar and nonpolar residues. Luo and Baldwin [Luo and Baldwin, 1999] noted that despite the good correlation between $\Delta\Delta G$ and $\Delta\Delta$S, entropy can explain only a 50–70% of the difference in $\Delta\Delta G$ even for nonpolar residues. The lack of correlation between $\Delta\Delta G$ and $\Delta\Delta S$ for all residues, and the smaller than unity slope of the $\Delta\Delta G$ versus T.$\Delta\Delta$S plot (Figure 2.13) for nonpolar residues implies that different amino acid residues contribute in different ways to the enthalpy of the helix-coil transition.

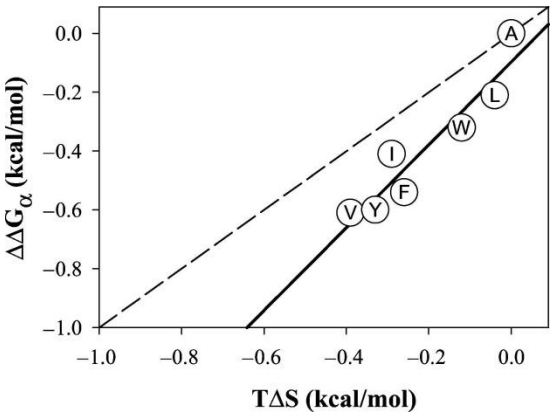

Figure 2.13: *Correlation between the configurational entropy (T.ΔS) change upon the helix–coil transition for nonpolar side chains according to Creamer and Rose [Creamer and Rose, 1992] and the universal helix propensity scale of Pace and Scholtz [Pace and Scholtz, 1998] ($\Delta\Delta G_a$). The solid line is a linear fit $\Delta\Delta G_a$ = 1.41.T.ΔS-0.1 (r = 0.94). The dashed line has a slope of 1 and is drawn for comparison [Makhatadze, 2006].*

2.4.3 The Quest for Enthalpy of the Helix-Coil Transition

A direct calorimetric measurement of the enthalpy of helix-coil transition is difficult to make. ΔH is generally quite difficult to measure accurately. In addition there do not exist good simple model systems [Scholtz et al., 1991; Richardson and Makhatadze, 2004]. A major source of uncertainty in the DSC measurements is the fact that the helix-coil transition is not sharp, but rather occurs over a broad range of temperatures. Isothermal titration calorimetry (ITC) can measure the enthalpy of a transition when it is triggered by changing some system variable at a fixed temperature. It is not possible to use denaturants such as urea or guanidinium hydrochloride in ITC experiments, because their dissolution and dilution in water contribute large enthalpy changes and tend to mask the helix-coil transition itself [Makhatadze and Privalov, 1990]. However, it is possible to trigger the helix-coil transition by the specific binding of a metal ion to a high-affinity site. Metal ions also have considerable dilution heats, but the situation is easiear to manage. Bierzynski and co-workers [Siedlecka et al., 1999] were the first to introduce such a model system, using a peptide sequence cut from the Ca(II)-binding loop of calmodulin, which forms a helical structure in the C-terminal part of the molecule when a metal atom binds to its N-terminal. The enthalpy of the helix coil transition is obtained in this case by measuring heats of metal binding to sequences of increasing length. The combination of CD measurements with ITC has proved that the enthalpy of the helix-coil transition does not depend of the peptide length [Lopez et al., 2002; Goch et al., 2003].

A considerable advance was achieved by using a particular peptide sequence as a host for 12 different amino acid residues (see Table 2.2) which are placed at a fixed guest position in the sequence [Richardson et al., 2005]. The guest residues were selected to probe differences in size, shape, hydrophobicity and hydrogen-bonding potential. They included the natural amino acids alanine (A), glycine (G), valine (V), leucine (L), isoleucine (I), phenylalanine (F), asparagine (N), glutamine (Q), serine (S), and threonine (T), and also the nonnatural amino acids norvaline (J) and 2-aminobutyric acid (B).

Table 2.2: *Abbreviations for Different Peptide Sequences in ITC Experiments [Richardson et al., 2005]*[a].

Peptide name	Peptide sequence	Δh_a kcal/mol
P2A	Ac-DKDGYISAAEAAAQ-NH_2	0.89 ± 0.08
P2B	Ac-DKDGYISAAEABAQ-NH_2	0.91 ± 0.09
P2F	Ac-DKDGYISAAEAFAQ-NH_2	0.86 ± 0.10
P2G	Ac-DKDGYISAAEAGAQ-NH_2	0.40 ± 0.08
P2I	Ac-DKDGYISAAEAIAQ-NH_2	0.74 ± 0.11
P2J	Ac-DKDGYISAAEAJAQ-NH_2	0.89 ± 0.10
P2L	Ac-DKDGYISAAEALAQ-NH_2	0.95 ± 0.10
P2N	Ac-DKDGYISAAEANAQ-NH_2	0.56 ± 0.10
P2Q	Ac-DKDGYISAAEAQAQ-NH_2	0.53 ± 0.10
P2S	Ac-DKDGYISAAEASAQ-NH_2	0.67 ± 0.13
P2T	Ac-DKDGYISAAEATAQ-NH_2	0.61 ± 0.11
P2V	Ac-DKDGYISAAEAVAQ-NH_2	0.60 ± 0.10

[a]*In addition to the standard single-letter abbreviations for naturally occurring amino acid residues, the following abbreviations were used for nonnatural amino acid residues: norvaline, J; a-aminobutyric acid, B.*

Differences in the enthalpy of the helix-coil transition between different amino acid residues (Figure 2.14) were measured in this work. Alanine has an enthalpy of helix-coil transition of 0.9 ± 0.1 kcal/mol. This is a small, positive value, shared with other amino acid residues, which are nonpolar but not β-branched side chains, such as Leu, Phe, as well as with nonnatural amino acid residues norvaline (J) and amino butyric acid (B). Amino acid residues with β-branched or polar side chains have an even lower enthalpy of helix-coil transition at ~0.6 kcal/mol. Gly, which does not have a side chain, has the lowest enthalpy of helix-coil transition at 0.4 kcal/mol. Since there is no side chain, glycine can sample the largest φ/ψ space on the Ramachandran plot among all amino acid residues. This flexibility affects the backbone accessibility of this residue, which is the largest. Moreover, glycine lacks the favorable van der Waals interactions that add a significant enthalpic component [Loladze et al., 2002; Makhatadze and Privalov, 1995]. The addition

of the side chain and of the C_b atom adds favorable van der Waals interactions but also creates steric hindrances, thus decreasing the solvent accessibility to the backbone. This is further decreased if a side chain is β-branched, as in Val or Thr. A decrease in solvent accessibility in the helical state results in the exposure of more polar backbone with negative enthalpy of hydration upon the helix–coil transition [Avbelj and Baldwin, 2002; Baldwin, 2002; Makhatadze and Privalov, 1995]. This in turn results in a lower enthalpy of ΔH_a for β-branched side chains. It is not easy to understand why amino acid residues with polar side chains such as Ser, Asn, and Gln have lower enthalpy.

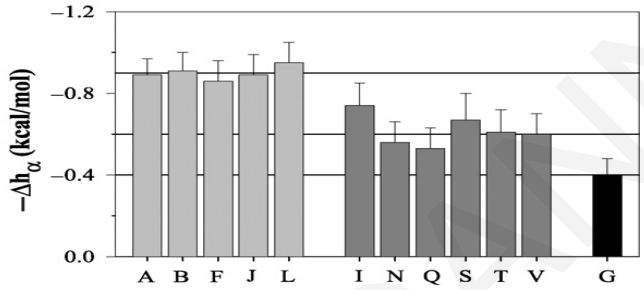

Figure 2.14: *Comparison of the enthalpy of helix formation Δh_α obtained for different amino acid side chains [Richardson et al., 2005]. Horizontal lines are drawn at -0.9, -0.6, and -0.4 kcal/mol [Makhatadze, 2006].*

The difference in the enthalpies of the helix-coil transition for different amino acids residues helps rationalize the observed thermodynamic propensity scales in enthalpic and entropic terms. In Figure 2.15 one sees a comparison of the thermodynamic propensity scales made by Pace and Scholtz [Pace and Scholtz, 1998], $\Delta\Delta G_{P\&S}$, with the entropy changes upon the helix–coil transition, $T.\Delta\Delta S$, as reported by Blaber et al. [Blaber et al., 1994] and Creamer and Rose [Creamer and Rose, 1994]. A sum of $T.\Delta\Delta S$ and $\Delta\Delta h_\alpha$ is also reported in the table for a direct comparison with $\Delta\Delta G$. The observed thermodynamic propensity is better described by the $T.\Delta\Delta S + \Delta\Delta h_\alpha$. It is evident that both enthalpic and entropic components define the thermodynamic helix propensity scale. For some amino acid residues (such as Q and S), the decrease in enthalpy is a decisive factor, while for others (such as F or J) entropy is the major determinant in agreement with the earlier conclusions of Creamer and Rose [Creamer and Rose, 1992]. Finally, there exist amino acid residues for which both enthalpic and entropic contributions are equally important.

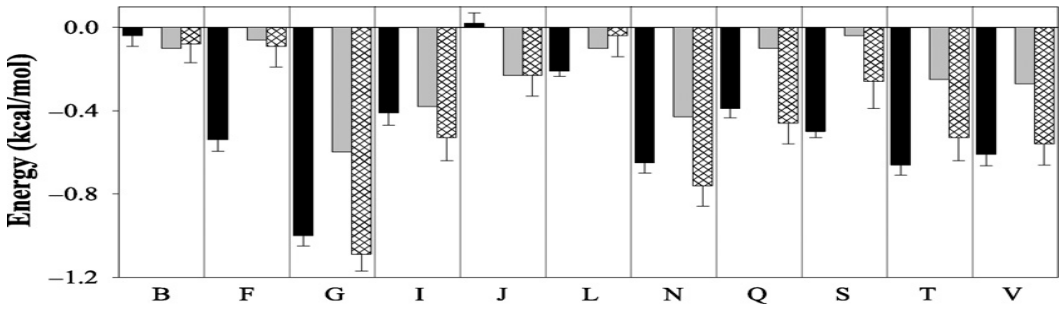

Figure 2.15: *Comparison of helical propensity scale, $\Delta\Delta G_{P\&S}$ – [Pace and Scholtz, 1998] black bars with the change in configurational entropy upon the helix–coil transition $T.\Delta\Delta S$ only, gray bars, or with the sum of $T.\Delta\Delta S$ and the enthalpy of helix formation $\Delta\Delta h_a$, patterned bars.Configurational entropy changes upon the helix–coil transition are taken from Blaber et al. (1994) with the exception of those for nonnatural amino acids B and J, which were taken from Creamer and Rose (1992). The enthalpy changes are from Richardson et al. (2005). All parameters are calculated relative to alanine [Makhatadze, 2006].*

2.5 Helix-Coil Transition Theories

Peptide conformations are described mostly by using bond lengths, bond angles, and torsional angles rather than atomic coordinates. Conformational properties vary most strongly with torsional angles, which are consequently used to classify local conformations. The three main-chain torsional angles φ**,** ψ, and ω (see Figure 2.16) define the conformation of the polypeptide backbone, hence its secondary structure [Edsall et al., 1966]. Excluding proline residues, ω is almost always close to 180^o. With this convention a sequential list of values of (φ_i,ψ_i) for all residues *i* specifies uniquely the conformation of a polypeptide.

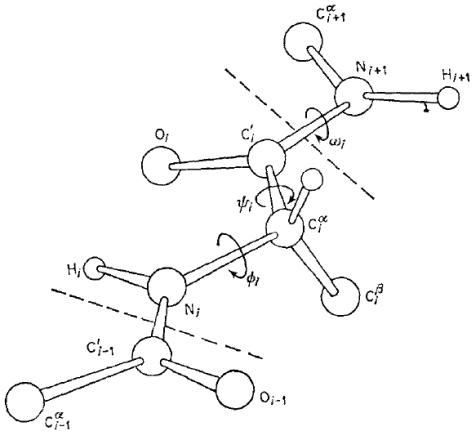

Figure 2.16: *Perspective drawing of a section of a polypeptide chain representing two peptide units. The limits of a residue are indicated by dashed lines. The recommended notation for the backbone atoms and for bond rotations is shown [Edsall et al, 1966]*

Using molecular models it can be proved that the polypeptide chain can be represented as a sequence of "isolated" pairs of conformational angles. The two angles φ_i and ψ_i in each pair are strongly interdependent, but they are very weakly dependent on the conformational angles of neighboring residues [Brant, 1965]. (The *x*-proline sequence is an exception [Schimmel, 1968]). The successful virtual-bond model for the polypeptide chain is based on this assumed separation into independent residue conformations [Flory, 1969]. Two-dimensional energy maps which explore the stability of protein and peptide conformations are also based on this idea.

In this molecular model and energy-based picture, solvent molecules are typically ignored. Conformational probabilities do depend on the solvent; however, so it is proper to deduce them from free energy maps (i.e., the potential of average force or of average torque, [Lifson and Oppenheim, 1960]), and not from steric or energy considerations.

Despite the fact that solvent molecules may affect chain conformational probabilities, it is mostly assumed in helix-coil theories that the independence of residues persists for the random coil also on a free energy basis. It is obvious however that the formation of helices or other secondary structures introduces longer-range interactions and results in interdependent local conformations.

In the following discussion we will adopt the notation of Qian and Schellman [Qian and Schellman, 1992]. During α-helix formation the carbonyl of peptide group *i* is hydrogen-bonded to the NH of peptide group *i + 4*. This is a basic assumption in the thermodynamics of helix formation. Formation of a helical hydrogen bond fixes four consecutive peptide units, which means that the φ and ψ angles of the three intervening residues must acquire specific values. Adding a peptide unit to an existing helix involves a free energy, ΔG_s, which is composed of the free energy associated with H-bond formation, the negative entropy of fixing the main-chain conformation, and the change in free energy of the side chains. The latter includes interactions with the helix and the entropic losses due to conformational restrictions. Side chain - side chain interactions are usually not included and must be added a posteriori. As a proper free energy ΔG_s is associated with a “local” equilibrium constant *s*, called the helix-propagation constant. ΔG_s and *s* obviously depend on the nature of the side chain of the residue added to the helix. The formation of the first H-bond must be handled in a different way. ΔG for the first H-bond is written as ΔG_{nuc} +

ΔG_s, where ΔG_{nuc} is the excess free energy associated with fixing the first two residues in a specific conformation without the compensation of H-bond formation. With this assumption the free energy of a helix with n_h H-bond is $\Delta G = \Delta G_{nuc} + n_h \Delta G_s = \Delta G_{nuc} + (n_r - 2)\Delta G_s$, where n_r, is the number of consecutive helical residues. The equilibrium constant for the complete formation of a helix is then:

$$K = e^{\left(-\frac{\Delta G}{R.T}\right)} = e^{\left(-\frac{\Delta G_{nuc}}{R.T}\right)}.e^{\left(-\frac{(n_r-2)\Delta G_s}{R.T}\right)} = \sigma.s^{n_r-2}$$

ΔG_{nuc} is supposed to be purely entropic so that σ is temperature independent.

The helix-coil model thus treats helix formation as a two-stage process, separating the nucleation and propagation steps. The nucleation parameter governs the nucleation step, and is usually considered independent of temperature as well as of the nature of the amino acids involved. The propagation process is described by the growth propagation parameter which considers the 1-4 H-bond interaction between peptide groups, the entropy loss that occurs because the residue is fixed in the helix and side chain-helix interactions.

Two types of theories of the helix-coil transition exist: (1) Theories which count hydrogen bonds [Schellman, 1955; Peller, 1959; Gibbs and DiMarzio, 1959; Zimm and Bragg, 1959]. These are thermodynamic theories in the sense that the nature of the interactions leading to nucleation and growth are not specified. (2) Theories based on residues and conformational integrals [Lifson, 1960; Nagai, 1960] which are true statistical mechanical theories. Both types of theories approach the helix-coil problem in a valid way, although they are very different. The following sections refer extensively to the work of Qian and Schellman [Qian and Schellman, 1992], who compared some of the details of the helix-coil models.

2.5.1 The Lifson-Roig Theory

In the Lifson-Roig (LR) model the residue is the conformational unit of the polypeptide chain, which centers about the α-carbon atom of the amino acid. The residue conformation determines the φ and ψ angles of the backbone, and the conformational angles of the side chain. The length of the polypeptide chain is the number (N_r,) of C_α, atoms. The number of

residues in an α-helix (n_r,) is the number of consecutive residues with angles (φ, ψ) that are consistent with the α-helical conformation.

The LR theory categorizes the states of a residue by its (φ,ψ) values. If the (φ,ψ) values of a residue lie in the narrow area consistent with α-helix formation, then this residue is taken to be helical and assigned the symbol h. In this representation h refers to the helical conformation of the residue and does not mean that it is necessarily part of a helix. Residues that are nonhelical, according to this classification are represented with the symbol c. Based on these rules, the instantaneous conformation of a polypeptide chain can be designated with a sequence such as cchhchccchhc, which specifies the state of each residue. The sequence just written would be a random coil sequence, because we need three or more consecutive residues to be in the h conformation in order to form a helix.

The statistical weight of residue *i*, when it is in the coil state, is defined as the integral of its Boltzmann factor over all nonhelical states (the notation of Qian and Schellman [Qian and Schellman, 1992] is used in what follows):

$$u_i' = \int_{nonhelical} e^{-W_1(i)/kT}\, d\varphi_i d\psi_i \qquad \text{(Eq. 2.1)}$$

Here $W_l(i)$ is the free energy of the conformation (φ_i,ψ_i); i.e.

$$e^{-W_1(i)/kT} = \langle e^{-U_1(i)/kT} \rangle$$

where U_1 is the energy of the local residue energy and the average is taken over side chain conformations and solvent coordinates. Both u_i' and W_1 (i) depend on the amino acid in the ith position.

The statistical weight of a residue in the helical conformation, independent of whether it is helix or not, is defined as an integral over the helical region of conformational space

$$v_i' = \int_{helical} e^{-W_1(i)/kT}\, d\varphi_i d\psi_i \qquad \text{(Eq. 2.2)}$$

The sum of u_i' and v_i' is the conformational integral over all possible (φ_i,ψ_i) values:

$$z_i = u_i' + \upsilon_i' \qquad \text{(Eq. 2.3)}$$

The subscript *i* is needed when the peptide contains more than one type of amino acid (heteropolymer). In most of the following formulas we shall drop it, however, essentially treating a homopolymer. In a homopolymer, υ'/z gives the probability of the helix conformation and u'/z that of the nonhelical conformation, while υ'/u' is the ratio of the helix to the coil conformation. The LR theory defines the coil state as the reference state, $\upsilon = \upsilon'/u'$ is then the statistical weight of the helical state when a helix is absent and $1 = u'/u'$ (unity) is the statistical weight of the coil state.

With the assumption that individual residue conformations are independent, the conformational integral of the random coil can be calculated as the product of the conformational integrals of individual residues:

$$Z = \prod_1^{N_r} z_i \qquad \text{(Eq. 2.4)}$$

Eq. 2.4 is approximate, because the product in Eq. 2.4 includes all possible conformations of the whole chain. It includes sequences of three or more residues which are found in the helical conformation and should therefore be parts of hydrogen-bonded helices. Equation 2.4 needs to be corrected to prevent strings of helical residues from appearing in random coil sequences. This correction is indeed intrinsic to the LR theory.

Residues are conformationally dependent on each other in the α-helix, since the formation of each H-bond restricts three consecutive residues to the helical conformation. A new statistical weight, w', must be defined for the description of a residue which is both helical and hydrogen-bonded:

$$w_i' = \int_{helical} e^{-W/kT}\, d\varphi_i d\psi_i \qquad \text{(Eq. 2.5)}$$

where $W = W_1(i) + W_3(i\text{-}1, i, i\text{+}1)$. $W_1(i)$ is the same local residue free energy as in Eqs (2.1) or (2.3) while $W_3(i\text{-}1, i, i\text{+}1)$ is a function of three (φ, ψ) pairs and contains the additional

contributions that arise from the longer-range interactions which take place in helix formation.

A sequence of n_r helical units (h-type) has $n_h = n_r - 2$ associated hydrogen bonds. The LR theory assigns the statistical weight υ' to two of these units and the helical weight w' to the remainder, so that the total weight of the sequence is $(\upsilon')(w')^{n_r-2}$. Although there is complete flexibility how to assign the weights, the LR theory assigns the υ' weights to be the two terminal residues of the helix.

In conclusion, in the LR theory a chain is described by its residues and these are given three statistical weights, u', υ' and w'. A c-residue is always given the weight of u'; an h-residue is given a weight of υ', except if it is flanked on both sides by h-residues, when it is given a weight of w'. u', υ' and w' are normalized to 1, υ, and w for practical calculations. υ is the equilibrium constant for the formation of the helical conformation in the random coil. It is considerably less than unity [Brant, 1967] because of the low entropy associated with confinement in the helical region and of the electrostatic repulsions. The same weight is used for the two residues in a helix which are not compensated by H-bond formation. Thus, the nucleation parameter in the LR theory is υ^2.

Using the weights u', υ' and w' we can create a statistical weight matrix, which descripes triplets of residues, regarded as sequential, overlapping pairs. In the rotation of Qian and Schellman [Qian and Schellman, 1992], this matrix is:

$$\mathrm{M} = \begin{array}{c} \\ h\bar{h} \\ h\bar{c} \\ c\bar{h} \\ c\bar{c} \end{array} \begin{array}{c} \begin{array}{cccc} \bar{h}h & \bar{h}c & \bar{c}h & \bar{c}c \end{array} \\ \begin{pmatrix} w' & v' & 0 & 0 \\ 0 & 0 & u' & u' \\ v' & v' & 0 & 0 \\ 0 & 0 & u' & u' \end{pmatrix} \end{array} \qquad \text{(Eq. 2.6a)}$$

The weights in matrix M refer to the residues indicated by upper bars. For example, the (1 1) element refers to a $h\bar{h}h$ triplet configuration, in which the middle h residue is assigned weight w'. The (1 2) element refers to a $h\bar{h}c$ triplet, where the middle residue is assigned weight v'. The (1 3) element refers to a $h\bar{h}$ pair followed by a $\bar{c}h$; this is clearly not possible, hence the weight is zero.

The 4 x 4 matrix is singular and can be reduced to the 3 x 3 matrix in the left of (Eq. 2.6b). Introduction of the renormalized weights *w*, υ, 1 leads to the matrix on the right of (Eq. 2.6b), which is commonly used.

$$M = \begin{matrix} \\ h\bar{h} \\ h\bar{c} \\ c(\bar{h}\cup\bar{c}) \end{matrix} \begin{matrix} \bar{h}h & \bar{h}c & \bar{c}(h\cup c) \end{matrix} \begin{pmatrix} w' & v' & 0 \\ 0 & 0 & u' \\ v' & v' & 0 \end{pmatrix} = \begin{matrix} \\ h\bar{h} \\ h\bar{c} \\ c(\bar{h}\cup\bar{c}) \end{matrix} \begin{matrix} \bar{h}h & \bar{h}c & \bar{c}(h\cup c) \end{matrix} \begin{pmatrix} w & v & 0 \\ 0 & 0 & 1 \\ v & v & 1 \end{pmatrix} \quad \text{(Eq. 2.6b)}$$

Here h ∪ c is the Lifson-Roig notation for the union of the (local) configuration space of h and c [Lifson, 1961]. In the 3 x 3 matrices of (Eq. 2.6b) the third-row label represents either h or c; depending on the first element of the column label. It should be noted that c is always given the statistical weight of *u´* regardless of its neighbors. By standard methods [Poland and Scheraga, 1970] the partition function of the whole chain is given by:

$$Z = \begin{pmatrix} 0 & 0 & 1 \end{pmatrix} M^{N_r} \begin{pmatrix} 0 \\ 1 \\ 1 \end{pmatrix} \quad \text{(Eq. 2.7)}$$

Matrix diagonalization methods provide the partition function; a number of average properties can be calculated from the resulting analytical expression [Poland and Scheraga, 1970; Zimm and Bragg, 1959; Lifson and Roig, 1961]. One of the most interesting chain properties is the average number of helical hydrogen bonds per molecule, which is given by the formula:

$$< n_{\mathrm{h}} >= \partial \ln Z / \partial \ln w \quad \text{(Eq.2.8)}$$

This property, or rather $<n_h>$ $/N_h$, is a good measure of fractional helicity, directly comparable to the results of CD measurements at 222 nm. For chains that contain more than one helix the total average number of helical residues, omitting the trivial single helical residues, is $<n_h> + 2<n_s>$, where $<n_s>$ is the number of helices of at least two units. $<n_s>$ can be determined from the derivative $\partial \ln Z / \partial \ln v_{12}$, where v_{12} is element (1 2) of the LR matrix [Lifson, 1961]. Other quantities that can be calculated from the matrix formulation of chain statistics are the average length of helices ($<n_h>/<n_s>$) and probabilities for individual units in the chain, such as the probability that a residue is in the

first, last, or central position in a helix and the probability that its NH or CO group are hydrogen-bonded to another peptide unit [Qian and Schellman, 1992].

2.5.2 The Zimm-Bragg Theory

Another matrix theory, equivalent to the LR theory but following a different mathematical formulation is the Zimm-Bragg theory (ZB). The units used in the ZB calculation are peptide units classified by hydrogen-bond formation. If the NH group of a particular peptide is involved in an α-helical hydrogen bond, the unit is given the symbol 1; if not, it is given the symbol 0. The first hydrogen bond in a helix starting from the N-, is given weight σs; hydrogen bonds contiguous to a preceding hydrogen bond are given the weight s. All non-H-bonded NH's are weighted by unity. s is the ratio of the probability of helical continuation relative to the probability of termination and plays the role of a propagation equilibrium constant. σ is a weight attached to the first unit and represents the barrier to helix initiation.

The following example demonstrates how to assign statistical weights to a peptide sequence in the ZB model. Suppose we have a molecule which contains 9 peptide units with units 3-7 forming a helix. Figure 2.17 gives us the coding for this sequence. Even though we have five helical peptide units, (five *h* units in LR notation) we have only two hydrogen bonds as indicated for positions 6 and 7, hence, only two entries are equal to 1 in the ZB coding. Due to the structure of the α-helix (Figure 2.17), each "1" must be preceded by at least three consecutive "0"s which are underlined. These are the three peptide units at the N terminal end of the helix which have no NH hydrogen bonds. Making use of the rules of ZB theory, Figure 2.17 shows the weights assigned to the peptide units.

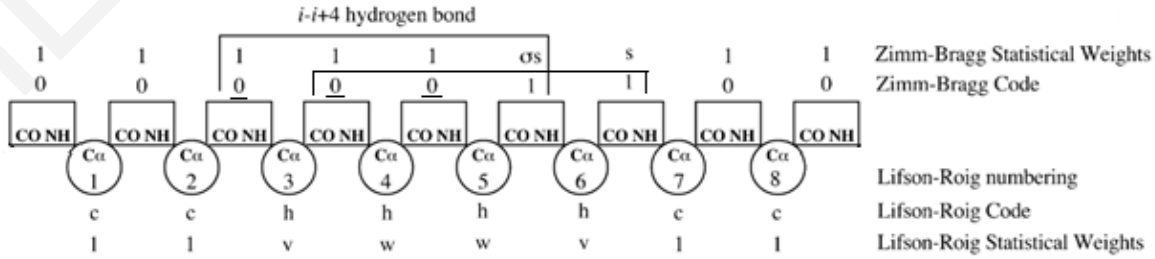

Figure 2.17: *Zimm–Bragg and Lifson–Roig codes and weights for the α-helix [Qian and Schellman, 1992].*

In order to establish all the weights in a sequence, according to ZB theory, we need to know the states of four consecutive peptide units. This means that the bases of the statistical weight matrices are overlapping triplets, so the matrix is of dimension $8 = 2^3$. It can be shown however that, there are only 11 nonvanishing elements of the matrix, and the secular equation is quartic. Based on this observation Poland and Scheraga have demonstrated that the full ZB matrix may be reduced to a 4 x 4 matrix [Poland and Scheraga, 1970]. However, ZB also presented an approximate 2 x 2 matrix solution to the chain conformation problem which provides a good alternative and has been widely used. In a similar spirit, Poland and Scheraga have suggested an alternative 2 x 2 matrix approximation of the LR method [Poland and Scheraga, 1965].

Regarding the ZB model Qian and Schellman note that: (1) The nonhelical "0" units of the ZB model are not the same as the c units of the LR theory. The former represent coil units which may have any allowed conformation (including the helical conformation), whereas the "c" state of the LR theory excludes helical conformations by construction. (2) The helical *"0"* units are given the same weight as the coil '0" units. (3) The *w* and *s* parameters of the two theories are not identical since s is the probability of a hydrogen-bonded unit relative to that of a coil unit (conformational integral *z*, *eq 2*.3); *w* is the probability of a hydrogen-bonded unit relative to a unit which is not in the helical conformation (conformational integral *u΄*, Eq 2.1).

Although the υ and w parameters of the Lifson-Roig theory differ from the σ and s parameters of the Zimm-Bragg theory, σ and s may be computed readily from υ and w by using relations (Eq. 2.9 and 2.10) derived by Qian and Schellman [Qian and Schellman, 1992]

$$s = \frac{w}{1+\upsilon} \qquad \text{(Eq. 2.9)}$$

$$\sigma = \frac{\upsilon^2}{(1+\upsilon)^4} \qquad \text{(Eq. 2.10)}$$

There has been an extensive elaboration on the initial Zimm-Bragg and Lifson-Roig helix-coil theories in order to include additional interactions, such as preferences of specific residues for the N-cap, N1, N2, N3 and C-cap positions, helix dipoles, side chain

interactions and 3_{10}-helix formation [Doig et al., 1994]. Most recent studies rely upon the LR model [Lifson and Roig, 1961]. In the original model, weights are assigned to residues in the centre of hhh triplets (a weight of *w* for propagation) or in the centre of chh or hhc triplets (a weight of *υ* for initiation). Residues in all other triplets have weights of 1. LR-based models have been extended by explicitly assigning weights to additional conformations.

N1 is called the first residue in a helical (*h*) conformation at the N-terminus and N-cap the preceding residue, the last in a non-helical (*c*) conformation before the beginning of the helix. Argos and Palau [Argos and Palau, 1982] were the first to show that N-cap preferences differ from other helical positions. LR theory can include N-capping by assigning a weight of n to the central residue in a cch triplet [Doig et al., 1994]. Similarly, the C-cap is the first residue in a nonhelical conformation (c) at the C-terminus of a helix. C-cap weights (c-values) are assigned to central residues in hcc triplets to include C-capping in the LR theory.

Since helices have 3.6 residues per turn, side chains of helical spaced "i, i + 3" or "i, i + 4" are close in space. Thus, it is possible to observe significant side chain interactions when four or five consecutive residues are in a helix. These interactions can be included in an extended LR model by assigning a weight of w × q to hhhh quartets and w × p to hhhhh quintets (Stapley et al., 1995). The side chain interaction is between the first and last residues in these groups.

Generally, extensions to the basic LR model have been stimulated by the discovery of additional features that affect stability in protein crystal structures. Including them within an enlarged helix-coil theory allowed the assessment of the effect of these features on helix stability.

2.5.3 Lifson-Roig Parameters Calculated

Except from our own recent study [Ioannou et al., 2011], the effect of salts on the Lifson-Roig parameters of oligopeptides chains has never been studied before. The study most relevant to ours concerning the calculation of the Lifson-Roig parameters is a paper by Best and Hummer [Best and Hummer, 2009]. They performed REMD molecular dynamics simulations of the blocked peptide Ac-$(AAQAA)_3$-NH_2 in pure water only and computed

the helicity and the Lifson-Roig parameters of the peptide using many different force fields. Figure 2.18 compares the overall fraction of helix of the peptide determined from the various simulations they performed to that estimated from NMR using chemical shifts [Shalongo et al., 1994]. All simulations, regardless of the force field used, resulted in only a gradual dependence of helical population on temperature, while the experiments suggest a much sharper transition, with all helicity being lost above ≈350 K. A similar weak dependence of helical population on temperature was also observed in a recent simulation study by the Pande group, who used their own modified force field ff99φ [Huang et al., 2008]. Using a Bayesian approach, Best and Hummer determined the optimal LR parameters describing the helix formation for each force field and temperature. The fitted parameters w(T) and υ(T) are plotted as a function of temperature in Figure 2.19. Near 300 K, the fitted w, 1.10 and 1.00 for ff03* and ff99SB*, respectively, are rather small relative to experimental estimates at this temperature (≈1,28) [Rohl and Baldwin, 1997]. The fitted υ, 0.18 and 0.21 for ff03* and ff99SB*, are one order of magnitude larger than the experimental estimates of 0.03 - 0.05 [Rohl et al., 1996; Rohl and Baldwin, 1997]. It was stated by Hummer that although the force fields match the overall helicity fraction in experiment, the higher nucleation parameter (υ) relative to experiment indicated that the helix formation in the simulations is less cooperative than inferred experimentally.

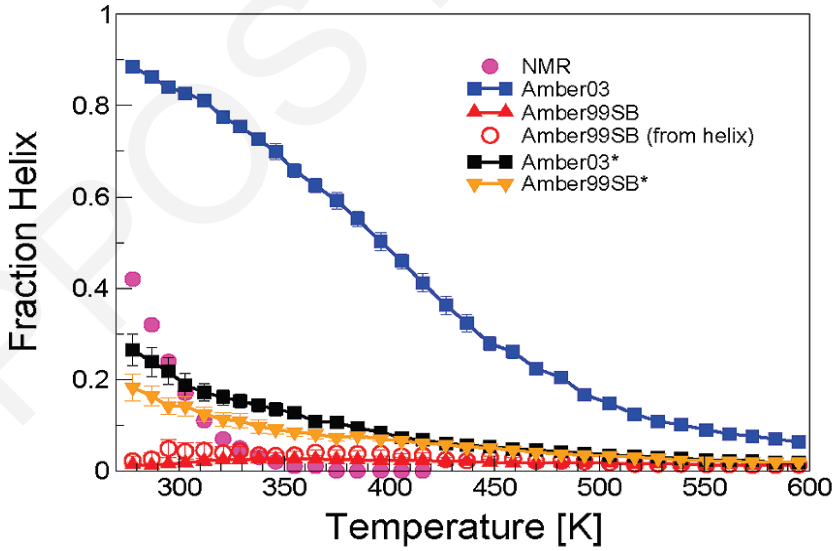

Figure 2.18: *Temperature dependence of helix formation in Ac-(AAQAA)3-NH2. Fraction helix as a function of temperature for ff03 (blue squares) ff99SB (red triangles), and the revised force fields ff03* (black squares) and ff99SB* (orange triangles); experimental estimate from NMR chemical shifts given as magenta circles [Best and Hummer, 2009].*

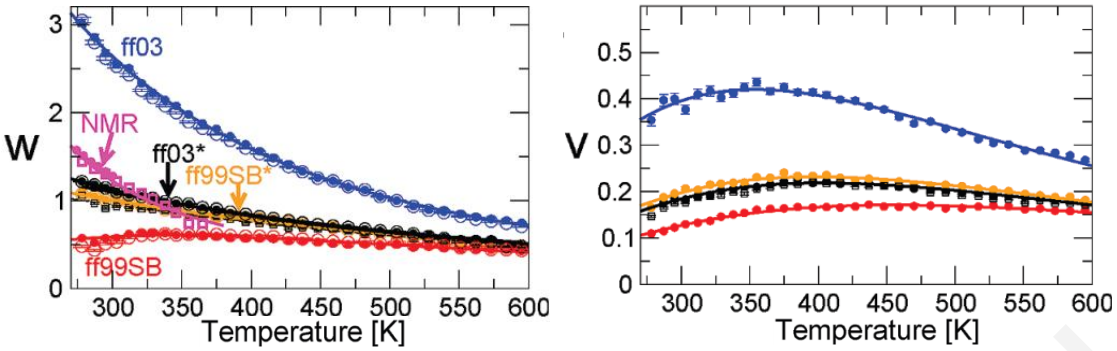

Figure 2.19: *Fitted LR parameters as a function of temperature. (A) The helix extension parameter w. (B) The nucleation parameter factor u. Colors as in Figure 2.18 [Best and Hummer, 2009].*

2.6 Deciphering Rules of Helix Stability in Peptides

Several experimental and computational studies exist with focus on the thermal stability of α-helices [Scholtz and Baldwin, 1992] and on helix nucleation/unfolding kinetics [Huang et al., 2002; Hummer et al., 2000, 2001; Williams et al., 1996]. Extensive studies of de novo designed peptides by Baldwin and co-workers [Marqusee and Baldwin, 1987; Marqusee et al., 1989; Scholtz and Baldwin, 1992] have shown that isolated alanine-based peptides (16–17 residues long), with charged residues (Lys, Glu, or Arg) added to increase solubility, can form stable α-helices in aqueous solution. The reason for the exceptionally high thermal stability of the helices of alanine-based peptides is still not quite understood.

One of the proposed reasons for this stability is the intrinsic ‘‘high helix-forming potential’’ of alanine [Chakrabartty et al., 1994; Marqusee et al., 1989; Spek et al., 1999]. The helical propensities of individual residues are often deduced by introducing natural amino acids as guests into a host matrix [Ingwall et al., 1968], or by fitting statistical-mechanical models of helix-coil transition, such as the Zimm-Bragg [Zimm and Bragg, 1959] or the Lifson-Roig model [Lifson and Roig, 1961], to the observed temperature dependence of helical content. This simplistic approach omits several important aspects of the problem, such as the neighboring residues in the inclusion site, or the effect of tertiary interactions on the helix-forming tendency [Doig et al., 1994; Miller et al., 2002].

In other studies it has been proposed that the stabilization of the helices in alanine-based peptides results from salt-bridge-based interactions of charged side chains (such as Lys, Glu, or Arg) [Marqusee and Baldwin, 1987; Mayne et al., 1998], interactions of charged

residues with the helix dipole [Huyghues-Despointes et al., 1993; Lockhart and Kim, 1993; Shoemaker et al., 1985], or the free energy gained by hydration of charged residues [Vila et al., 1992; Williams et al., 1998]. It has also been recently suggested [Vila et al., 2000] that the high thermal stability of helices of alanine-based peptides containing large charged side-chain substituents results from the shielding of the hydrogen-bonding backbone amide and carbonyl groups from solvent water molecules by the side chains.

The evaluation of this broad range of molecular mechanisms postulated to explain helical stability of peptides is difficult due to the lack of detailed experimental data at the molecular-level. It is for this reason that trajectories from all-atom replica exchange molecular dynamics (REMD) simulations can shed light on the questions of (a) which are the helix-stabilizing factors, and (b) what is their relative importance.

2.6.1 Role of Side Chains in Stability of α-Helix

Garcia and Sanbonmatsu studied atomic models of the thermodynamics of the structural transition of peptides that form α-helices [Garcia and Sanbonmatsu, 2002]. They applied the replica exchange molecular dynamic (REMD) method to the equilibrium folding/unfolding thermodynamics of a 21 residue peptide with a large propensity of forming α-helical structures in water at room temperature. This was an Arg-containing peptide, Ac-A_5 $(AAARA)_3$A-methyl-amide (NMe) (Fs peptide, where Fs stands for "folded short"), which has been experimentally studied quite extensively [Williams et al., 1996; Lockhart and Kim, 1993]. To establish the role of sequence variation in the formation of α-helices, they also simulated a peptide containing only Ala residues, Ac-A_{21}-Nme (A21), which is practically insoluble in water, hence it cannot be studied experimentally, whereas long sequences of Ala flanked by charged amino acids are soluble and have been widely studied [Ingwall et al., 1968; Spek et al., 1999]. Garcia et al. performed REMD simulations of the A21 (42 replicas with annealed α-helical initial configurations) and Fs peptides (46 replicas with annealed α-helical configurations) by using a modified PARM96 force field.

Figure 2.20 shows the helix content profiles as a function of T for the Fs and A21 peptides with this modified force field. The helical content (θ_f) is higher near ambient temperature and a melting transition occurs over a broad range of temperatures for these short peptides.

The modified force field predicted a 50% helical content at 345 K and 90% helical content at 275 K for the Fs peptide. Their results are in agreement with experimental data for Fs [Williams et al., 1996; Lockhart and Kim, 1993]. A21 is much less helical, e.g., a 34% helical content at 275 K was obtained. The Lifson-Roig helix propagation and nucleation parameters for A21 were found to be $w_o = 1.37$ and $v_o = 0.076$ at 273 K, which correspond to $s_o = 1.3$ and $\sigma_o = 0.004$ of the Zimm-Bragg model, in agreement with the CD measurments of Yang et al. ($\sigma_o = 0.004 \pm 0.002$ for assumed values of $s_o = 1.4 - 1.7$) [Yang et al., 1998].

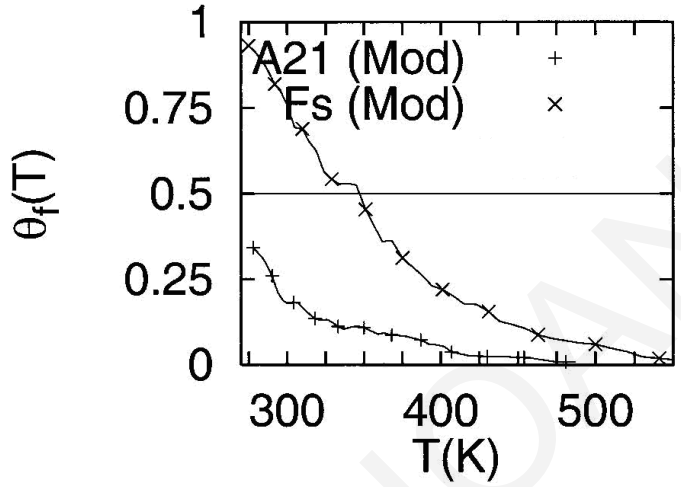

Figure 2.20: *The helical content of A21 and Fs peptides as a function of temperature [Garcia and Sanbonmatsu, 2002].*

From the helical percentages at various temperatures the estimated difference in free energy between A21 and Fs at 350 K is 5.8 kJ/mol. This difference must result from the Arg side chain. To test the hypothesis that chain desolvation might be responsible for this stabilization [Vila et al., 2000], Garcia and Sanbonmatsu also calculated the coordination of water to the peptide backbone. Figure 2.21 shows the water coordination number for the oxygen atoms of the peptide backbone carbonyl groups. Carbonyl oxygen atoms that form helical hydrogen bonds have on average only one coordinated water molecule. End carbonyl oxygen atoms that do not participate in hydrogen bonds with the backbone have two coordinated water molecules. Shielded carbonyl oxygen atoms do not have any water of coordination. The α-helical conformation predominates at low temperature. In contrast, at high temperature, the peptide is in the coil conformation and shows a coordination number between 1.0 and 2.0. The low coordination number of carbonyl oxygens at high temperature (for example, at position 6 of A21 at 456 K, shown in Figure 2.21) stems from intramolecular hydrogen bonds that do not necessarily participate in an α-helical conformation.

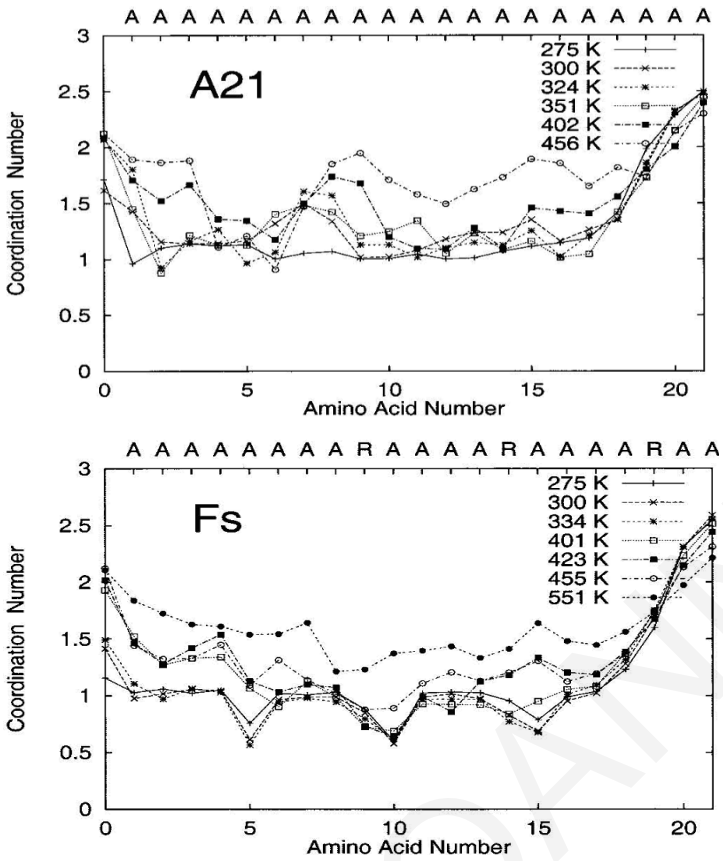

Figure 2.21: *Water coordination to the backbone carbonyl oxygen atoms along the peptide sequence [Garcia and Sanbonmatsu, 2002].*

In the Fs peptide at low temperature there exist three positions along the sequence at which the coordination number adopts a number of 0.5. These particular positions correspond to four carbonyl oxygens before Arg side chains, which are shielded from water by the bulky Arg side chain. A coordination number of 0.5 is obtained in this case as the average of two configurations (see Figure 2.22) which yield coordination numbers of 1 and 0.

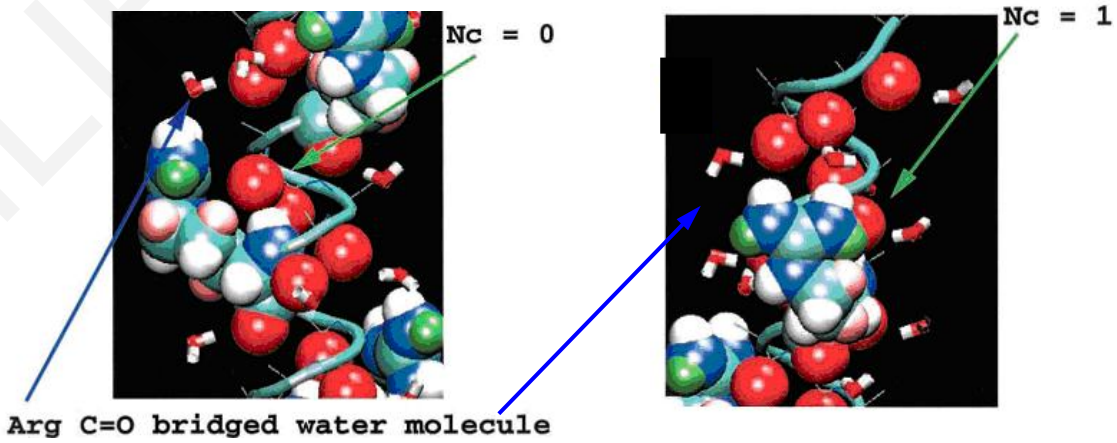

Figure 2.22: *Illustration of the shielding of the backbone carbonyl oxygen atoms by the Arg side chain of Fs [Garcia and Sanbonmatsu, 2002].*

The fact that backbone carbonyl atoms can be "shielded" by the Arg side chains is proved by the examination of hydrogen bond formation probabilities along the peptide chain [Garcia and Sanbonmatsu, 2002]. Figure 2.23 shows the probabilities of participation in an α-helical conformation for all amino acids of the model peptide studied as a function of temperature, for T = 275, 300, 325, 350, and 400 K. The probability increases for entropic reasons toward the center of the chain and decreases toward the C terminus. Again for obvious reasons this behaviour is observed at all temperatures, but at higher temperatures the probability to form a helix is less. For the Fs peptide below 350 K, relatively higher tendency for helical conformations is observed for amino acids 7, 12, and 17. The Arg residues are at positions 9, 14, and 19, and the low-coordination number carbonyl oxygens are at positions 5, 10, and 15. It can therefore be concluded that those residues which show larger relative helical propensities are in position *i* between a shielded carbonyl oxygen at *i - 2*, and the Arg at *i + 2*. The shielded hydrogen bond is between the carbonyl oxygen at *i - 2* and the amino group at *i + 2*.

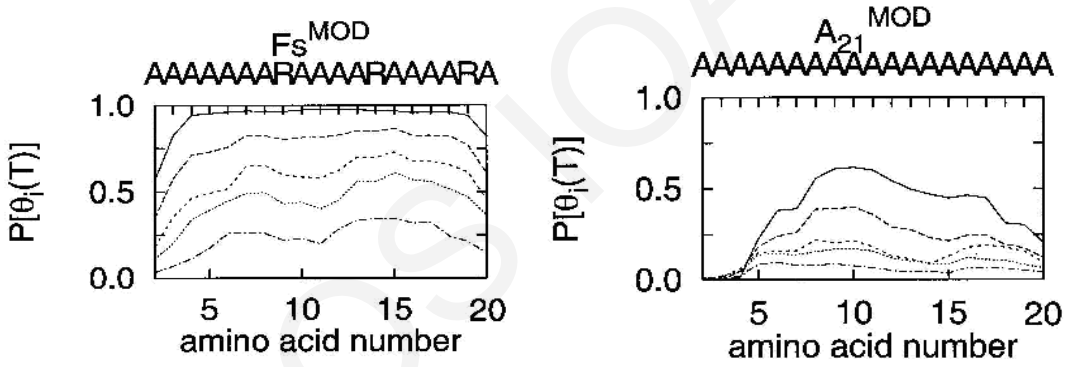

Figure 2.23: *Probability of participation in an α-helical conformation for each amino acid (amino 2-20) in the A21 and Fs peptides, at temperatures 275, 300, 325, 350, and 400 K. At lower T α-helical formation probabilities are larger [Garcia and Sanbonmatsu, 2002].*

Measurements of the number of water molecules coordinating the backbone carbonyl oxygens over a broad T range indicate that the additional stabilization observed for the Fs peptide relative to the A21 peptide may be ascribed to the partial shielding of the backbone hydrogen bonds from water, provided by the Arg side chains. Vila *et al.* [Vila et al., 2000] proposed that α-helical stabilization can be induced by bulky side chains (both polar and nonpolar), which hinder the approach of water molecules to backbone atoms. Garcia's and Sanbonmatsu's simulations verify this claim, and provide a microscopic description of the shielding effect of side-chains. Details of the shielding not described by Vila *et al.* [Vila et

al., 2000] are the shielding by an Arg at site *i* of the carbonyl oxygen at *i – 4*, and the energetically favourable interaction of the charged side chain with the carbonyl oxygen.

2.6.2 Role of Salt-Bridge Formation in Stability of α-Helix

Ghosh et al. assessed the contribution of large side chains to α-helix stability through salt-bridge formation [Ghosh et al., 2003]. In their study they simulated the alanine-rich peptide, Ac-YAEAAKAAEAAKAAEAAKAF-Nme, referred to as the EK peptide, that has three pairs of "*i, i* + 3" glutamic acid (-) and lysine (+) substitutions employing an identical simulation method with Garcia and Sanbonmatsu [Garcia and Sanbonmatsu, 2002]. Results obtained with the EK peptide were compared to those for the A21 and Fs peptides [Garcia and Sanbonmatsu, 2002] and used to evaluate the contribution of salt-bridges to α-helix stability. The helical content of the peptide was calculated using the Lifson-Roig model [Lifson and Roig, 1961]. For the 20-residue EK peptide, the number of residues that can be labelled helical is ≤ 18. Melting profiles were obtained using the temperature-dependent helical content.

The fractional α-helical content in A21, EK and Fs peptides is shown in Figure 2.24 as a function of the temperature of the solution. The EK peptide has ~85% helical content at ambient temperatures, and the melting temperature of ~350 K in agreement with experimental data on EK which give T_m values approximately equal to 320–340 K [Marqusee and Baldwin, 1987; Scholtz et al., 1995].

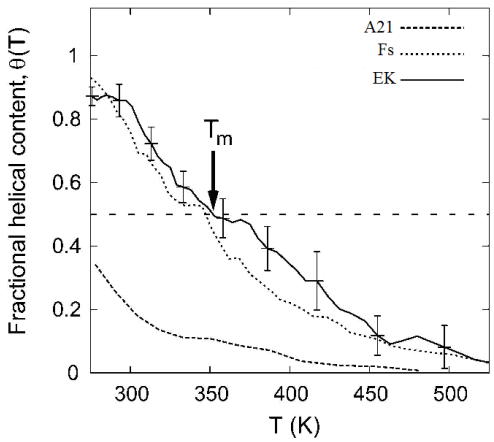

Figure 2.24: *Equilibrium fractional α-helical content, θ(T), for A21, Fs and EK peptides [Ghosh et al., 2003].*

The melting profiles and T_m values shown in Figure 2.24 show that the thermal stabilities of the helical configurations of the EK and Fs peptides are almost equivalent. The helical conformation of these two peptides are pronounced and thermally much more stable than those of A21. This proves that a small number of simple substitutions of alanines by lysine (K) and glutamic acid (E) residues (EK peptide) or by arginine (R) (Fs peptide) leads to a considerable stabilization of the helical conformations of these alanine – based peptides.

E and K residues in the EK peptide have opposite charges. The formation of EK- or KE-type salt-bridges is therefore possible, which could stabilize the helical conformers. Experimental studies of alanine-based peptides containing oppositely charged residues have shown that the charged substituents can influence the helical content and stability of the peptide, especially when salt-bridges can be formed [Marqusee and Baldwin, 1987]. Ghosh et al. monitored the distances between atoms of salt-bridge-forming residues, and found that in fact the formation of the KE-type salt-bridges involves side-chain conformations with unfavourable torsion potentials. KE-type salt-bridges were in fact not observed in their simulations.

Figure 2.25 shows the distribution of distances between the carboxylate carbon and amine nitrogen atoms of E^- and K^+ pairs averaged over the three pairs Glu3–Lys6, Glu9–Lys12, and Glu15–Lys18 at five different temperatures. At 279 K, the distribution of EK ion-pair separations shows two distinct regions. The sharp peak near 4.5 Å corresponds to contact ion-pair formation by EK residues (Figure 2.25), whereas broader peaks near 7 and 10 Å correspond to ion pairs separated by one and two water molecules. Increasing temperature does not affect the height of the contact peak at 4.5Å; in a systematic way however, the population of water-separated conformations becomes broader with increasing temperature, indicating that at higher temperature the peptide samples extended conformations more often.

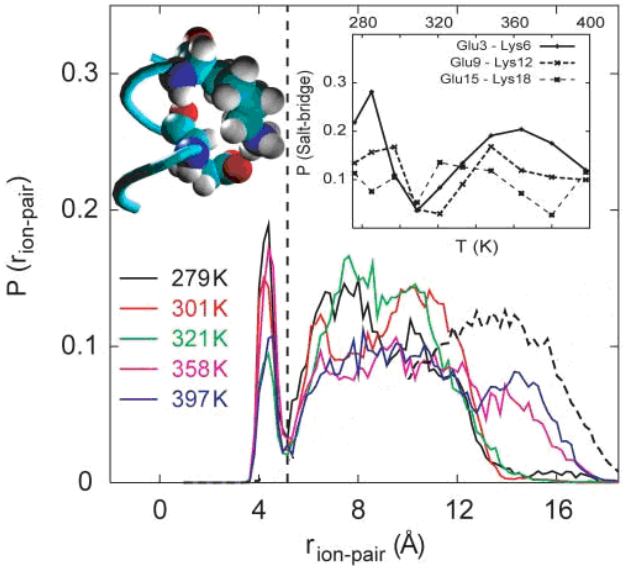

Figure 2.25: *Distribution of distances between the carboxylate carbon atom on Glu and the amine nitrogen atom on Lys, averaged over the three "i, i + 3" (E, K) pairs in the EK peptide. A snapshot of a typical Glu9-Lys12 contact/salt-bridge configuration at T = 279 K is also shown. Inset shows the probability of salt-bridge formation as a function of temperature separately for each of the three "i, i + 3" (E, K) pairs [Ghosh et al., 2003].*

The temperature-dependent probability of formation of a salt-bridge in the EK peptide (obtained from the area under the contact peak) is shown in the inset of Figure 2.25. At temperatures near 300 K this probability is low, ~10–20% for all three possible E^-, K^+ pairs. If each salt-bridge is assumed to make an independent favorable contribution to helix stability, then the sum of such contributions appears relatively insensitive to temperature. The low (~10–20%) overall probability of individual salt-bridge formation and its relative temperature insensitivity indicate that the contribution of salt-bridges to the stability of the EK helix is not a dominant factor. The increased thermal stability of the EK peptide compared to the A21 peptide is not entirely due to salt-bridge formation. This finding supports the hypothesis of Scheraga and coworkers [Vila et al., 2000], who claimed that stabilization of helical conformers can be achieved through shielding of the backbone intrapeptide hydrogen bonds by large side-chain substituents. Indeed, the hydration pattern for the EK peptide backbone obtained from the REMD simulations shows that lysine side chains do not allow water to approach certain backbone H-bond-forming carbonyl (-C=O) and amide (-N-H) groups at low temperatures.

2.7 Replica Exchange Molecular Dynamics (REMD)

Biomolecular systems have a rough energy landscape, which contains many energetic barriers that are considerably larger than thermal energies. These large barriers can easily trap biomolecular systems in local minima. The sampling problem posed by such a difficult phase space can be overcome with a technique called replica exchange molecular dynamics (REMD). The REMD algorithm provides an increased conformational sampling rate sufficient for simulating helix-coil equilibrium [Sugita and Okamoto, 1999; Gnanakaran et al., 2003].

In the replica-exchange method [Nymeyer et al., 2004], a number of identical copies of the system (replicas) are simulated at different temperatures, spanning a predefined temperature range (Tmin, Tmax). The minimum temperature is usually chosen so as to be near the temperature of interest for the biological systems examined. It is of course understood that as the minimum temperature decreases the sampling difficulties and simulation time will increase quickly. The maximum temperature on the other hand must be high enough so that replicas at this temperature quickly cross the largest energetic barriers of the energy landscape and lose memory of their initial condition. In the case of most small biological simulations an appropriate Tmax is more than 500 K or about twice larger in temperature than room temperature. The temperatures of the intermediate replicas are modified accordingly so that each replica executes a random walk in temperature space (i.e., each replica spans the entire range of temperatures throughout the course of the simulation, without being trapped in any temperature interval). A usual rule for accepting temp-changes (subject to testing) is to choose the replica temperatures, so that a uniform exchange-probability (~16%) is obtained between adjacent replicas.

Configuration exchanges are attempted periodically in order to transfer new configurations surpassing barriers from runs at high temperature to those at low temperature. Those exchange attempts are accepted with a Metropolis probability

$$P_{REMD}(i \leftrightarrow j) = \min\{1, \exp[(\beta_j - \beta_i)\,(U_j - U_i)]\} \qquad \text{(Eq. 2.11)}$$

Which ensures detailed balance and maintains the canonical distributions at each temperature [with U_i the potential energy of the i^{th} replica, $\beta_i = 1 / (k_B T_i)$, and k_B the

Boltzmann constant]. After an accepted exchange, the particle velocities are rescaled to the new temperature, or redrawn from Maxwell-Boltzmann distributions valid for the new temperature. From eq. 2.11, it is evident that only replicas with neighbouring target temperatures will have significant exchange probabilities. This fact prompts us to attempt only exchanges between neighbouring (in temperature) replicas. Through a series of exchange attempts, high-temperature conformations are transferred occasionally to low temperature runs, facilitating the exploration of new configuration-space regions.

The REMD method has several advantages: It is based on exchange procedures that are inexpensive and easy to implement, it produces information over a range of temperatures, and it works well even in systems with explicit solvent. A comparison of this algorithm with constant temperature molecular dynamics applied to peptides at room temperature showed that REMD decreased the sampling time by factors of 20 or more [Sanbonmatsu and Garcia, 2002]. To use REMD one must specify the number of replicas, the temperatures of these replicas (i.e., the temperature schedule), and the frequency for attempting temperature exchanges. The effective use of REMD relies heavily upon the choice of these parameters, and this is of course system specific and can only be established with trial and error procedures.

2.8 New Ion Parameters

The role of alkali (Li^+, Na^+, K^+, Rb^+, and Cs^+) and halide (F^-, Cl^-, Br^-, and I^-) ions in many biological phenomena is crucial, since they affect stabilization of biomolecular structures, influence biomolecular dynamics, and influence homeostasis and signaling. An accurate model of the monovalent ions is necessary in order to model ionic interactions in atomistic simulations of biomolecular structure, dynamics and function. Acceptable models should be able to reproduce several properties of ions at the same time. In particular, good models should reproduce the interactions of these ions with each other in the crystal and in solution, and the interactions of ions with other molecules. The current state-of-the art regarding biomolecular modeling employs simple additive, nonpolarizable, pairwise potentials for atomic interactions. Joung and Cheatham have built better models of the monovalent ions within the pairwise interaction framework, Their models are tuned to balance crystal and solution properties in Ewald simulations of well-known water models

[Joung and Cheatham, 2008]. In recent years it has been proven that truly accurate treatments of ions require the inclusion of nonadditivity and polarizability (particularly for the anions). For some ions even a quantum mechanical treatment is in order. Despite all this, Joung and Cheathan merely sought to push the limits of the additive treatments. The starting point of this work were several observations from long simulations with the AMBER force fields of biomolecules in salt solutions, in which salt crystals formed well below their solubility limit. This observation implies that anion-cation attractions in these force fields are too strong, leading to severe inaccuracies in concentrated solutions. To improve the situation Joung and Cheathan reoptimized the parameters of the Lennard-Jones (LJ) potential for alkali and halide ions for specific choices of water models. The test properties, against which they optimized the new parameters, were hydration free energies of the solvated ions and also lattice energies (LE) and lattice constants (LC) of alkali halide salt crystals. The optimization across the entire alkali and halide series avoids systematic deviations. The new ion parameters developed were associated with some of the most commonly used rigid and nonpolarizable water models, uch as TIP3P, TIP4P$_{EW}$, and SPC/E. Besides reproducing solution and crystal properties very well, the new ion parameters also reproduce ion-water binding energies and the radii of the first hydration shells.

Table 2.3: *Final LJ Parameters for the Alkali and Halide Ions with Different Water Models [Joung and Cheatham, 2008]*

	TIP3P		TIP4P$_{EW}$		SPC/E	
	$R_{min}/2$ (Å)	ε (kcal/mol)	$R_{min}/2$ (Å)	ε (kcal/mol)	$R_{min}/2$ (Å)	ε (kcal/mol)
Li^+	1.025	0.0279896	0.808	0.1039884	0.791	0.3367344
Na^+	1.369	0.0874393	1.226	0.1684375	1.212	0.3526418
K^+	1.705	0.1936829	1.590	0.2794651	1.593	0.4297054
Rb^+	1.813	0.3278219	1.709	0.4331494	1.737	0.4451036
Cs^+	1.976	0.4065394	1.888	0.3944318	2.021	0.0898565
F^-	2.303	0.0033640	2.538	0.0015752	2.257	0.0074005
Cl^-	2.513	0.0355910	2.760	0.0116615	2.711	0.0127850
Br^-	2.608	0.0586554	2.768	0.0303773	2.751	0.0269586
I^-	2.860	0.0536816	2.952	0.0417082	2.919	0.0427845

3. Bibliography Examination: Ion specific Action on the Secondary Structure of Proteins and Peptides

In this chapter we examine what is currently known about salt effects on the helix-coil transition of model oligopeptides, especially focusing on existing molecular simulations. Unraveling the mechanisms by which salt (de)stabilizes protein structures is a challenging task, as there exists a subtle balance of nonspecific screening and specific ion - solute and ion - water interactions [Baldwin, 1996; Tobias and Hemminger, 2008; von Hippel and Wong, 1969]. The action of salts on the properties of short ($\leq$ 20 amino acids) helices has been studied very little experimentally [Marqusee and Baldwin, 1987; Scholtz et al., 1991; Scholtz et al., 1993; Smith and Scholtz, 1997]. MD simulations have only appeared very recently, and they concern the trialanine peptide in sodium halide solutions [Fedorov et al., 2007], the helicity of polyglutamic acid (PGA) [Fedorov et al., 2009], the *N*-methylacetamide (NMA) molecule [Heyda et al., 2009], short alanine based "EK", "$(AE)_6$" and "$(AK)_6$"-peptides stabilized by glutamic acid (Glu or E) and lysine (Lys or K) salt bridges [Dzubiella, 2008; Dzubiella, 2009] and the alanine peptide $AAAAA(AAARA)_3A$ (where R arginine) [Asciutto et al., 2010].

Marquesee and Baldwin studied experimentally the helix stabilization of four alanine-based peptides by Glu^- - Lys^+ salt bridges [Marqusee and Baldwin, 1987]. Each peptide had three glutamic acid/lysine residue pairs and the terminal groups were blocked with acetyl and amide groups to avoid the helix-destabilizing interactions of these groups with the helix dipole. In one set of peptides ("*i*+4"), the glutamic acid and lysine residues are spaced 4 residues or 1 residue apart. In another set of peptides ("*i*+3"), the spacing is 3 or 2 residues (Fig. 3.1). Within each of these sets, a pair of peptides was made, in which the positions of the glutamic acid and lysine residues were reversed [Glu, Lys (E,K) vs. Lys, Glu (K,E)] in order to examine the potential effects of the interaction of the charged side chains with the helix dipole. The helicity was determined by measuring the mean residue ellipticity, [θ], using circular dichroism (CD).

(*i*+4) E,K: Ac A E A A A K E A A A K E A A A K NH_2

(*i*+4) K,E: Ac A K A A A E K A A A E K A A A E NH_2

(*i*+3) E,K: Ac A E A A K A E A A K A E A A K A NH_2

(*i*+3) K,E: Ac A K A A E A K A A E A K A A E A NH_2

Figure 3.1: *Sequences of the four peptides designed. Ac, acetyl; A, alanine; E, glutamic acid; K, lysine [Marqusee and Baldwin, 1987].*

At low temperature (1^{o}C) and at pH=7, all peptides showed significant helix content. Table 3.1 lists the extent of helix formation (measured by $-[\theta]_{222}$) for all four peptides at pH=7 and at 0.01 and 1.0 M NaCl. Both glutamic and lysine are ionized at this pH. At this low temperature, the average helical content is clearly different for each peptide: at 0.01 M NaCl, $-[\theta]_{222}$ ranges from 29,000 degree·cm^{2}·dmol^{-1} for (*i*+4)E,K to 8500 for (*i*+3)K,E. Since the peptides are otherwise identical, this measurements confirm the importance of amino acid sequence, and hence side-chain interactions, on discussing the helix stability of such oligopeptides.

Effects caused by reversing the charge sequence (E,K or K,E) are larger in the *i*+3 peptides than in the *i*+4 peptides and are greater at 0.01 M than at 1.0 M NaCl (Table 3.1). For the *i*+3 peptides, the change in $-[\theta]_{222}$ for E,K → K,E is really strong; from 17,600 to 8500 at 0.01 M NaCl and from 17,400 to 12,000 at 1.0 M NaCl. These changes point to the existence of a helix chain-dipole interaction: in the E,K peptides this interaction is expected to stabilize the helix, but in the K,E peptides it should destabilize it. For the *i*+4 peptides, the observed change is much smaller.

A comparison of helix content between peptides with different charge spacings (*i*+4, *i*+3) and the same orientation (E,K or K,E) revealed that particular residue spacing leads to different degrees of stabilization. The data shown in Table 3.1 indicate that the *i*+4 peptides are stabilized by ion pairs or salt bridges more than the *i*+3 peptides. At pH=7 and 0.01 M NaCl, where helix stabilization by salt bridges is maximal, the value of $-[\theta]_{222}$ is by about 11,000 greater in (*i*+4)E,K than in (*i*+3)E,K. Similarly, in the K,E orientation, $-[\theta]_{222}$ of (*i*+4)K,E is by 17,000 greater than that of (*i*+3)K,E. It is not entirely clear why such a difference in stabilization occurs.

Table 3.2: *Helix content (pH 7.0, 1^0C) [Marqusee and Baldwin, 1987]*

$-[\theta]_{222}$, degree·cm^2·dmol^{-1}		
Peptide	0.01 M NaCl	1.0 M NaCl
(*i*+4) E,K	29,000	24,800
(*i*+4) K,E	25,300	25,700
(*i*+3) E,K	17,600	17,400
(*i*+3) K,E	8,500	12,000

Scholtz and his team studied experimentally the effect of ionic strength on the helix-coil equilibrium of a short, alanine-based peptide [Scholtz et al., 1991]. The studied peptide sequence was Ac-$(AAQAA)_3Y(NH_2)$. This choice was made because alanine has a high helix-forming tendency [Marqusee et al., 1989], while the three Gln residues, spaced (*i*,*i*+5), provide the necessary aqueous solubility. The single tyrosine residue allowed accurate measurements of the peptide concentration by tyrosine absorbance. The acetyl and amide blocking groups eliminated the charges on α-NH_3^+ and α-COO^- groups, respectively.

Salts were used that are either helix-stabilizing (Na_2SO_4) or –destabilizing ($CaCl_2$, NaCl) at high ionic strength. The study revealed that there is an increase in α-helix content with ionic strength, at low ionic strength, for all three salts [Figure 3.2.a]. For the neutral AQ peptide the helicity increases up to 1 M NaCl, presumably due to screening of the helix macrodipole. For larger NaCl concentrations the helicity decreases. In Figure 3.2.b, the changes in free energy for helix stability after subtraction of the specific Hofmeister effect for each of the three salts are shown. From this result we realize that ion-helix interactions are helix stabilizing in all concentrations.

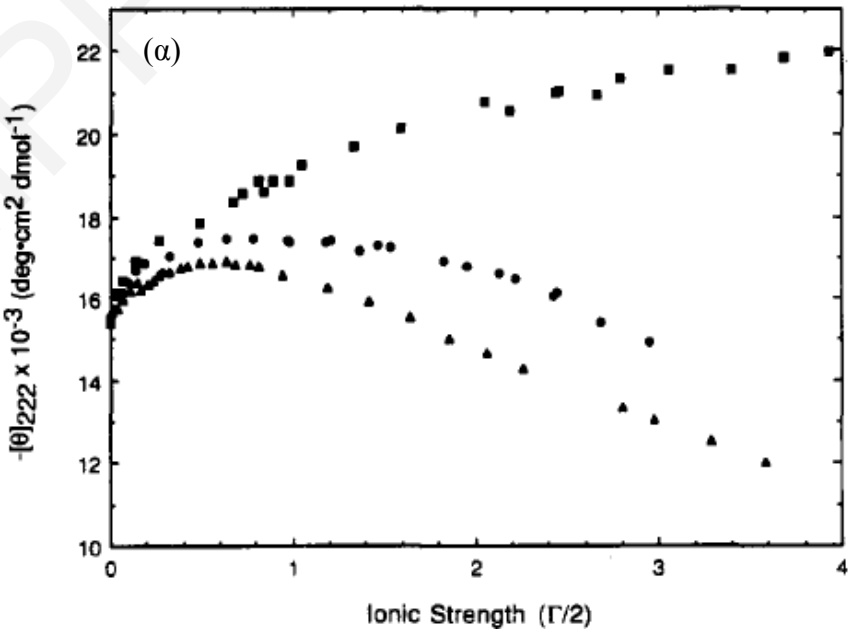

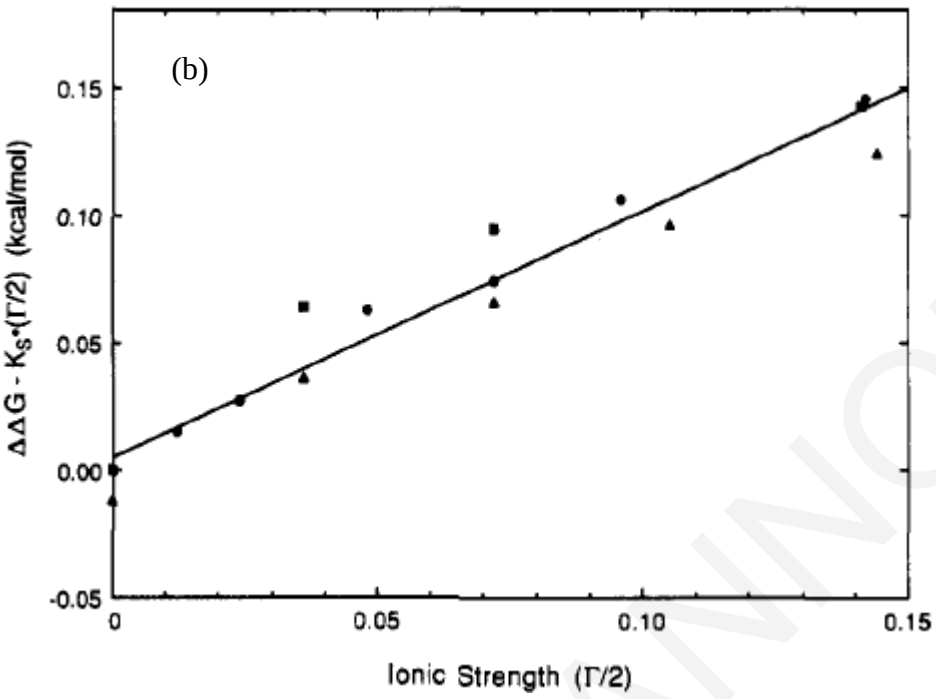

Figure 3.2*(a) Helical content of the peptide as a function of ionic strength for each of the three salts: Na_2SO_4 (■), NaCl (●), and $CaCl_2$ (▲). The helical content was determined by CD at 0 ^oC in 1.0 mM NaH_2PO_4 at pH 7.0. (b) Changes in free energy for helix stability after subtraction of the specific Hofmeister effect for each of the three salts [Scholtz et al., 1991].*

The contribution to helix stability of different Glu – Lys interactions has also been measured by Schlotz circular dichroism (CD) measurements at 0 ^oC [Scholtz et al., 1993]. A single pair of Glu and Lys residues was placed at four different spacings, and in both orientations regarding the terminals, in an otherwise neutral alanine-glutamine peptide helix (Table 3.2).

Table 3.2: *Peptide Sequences [Scholtz et al., 1993]*

Peptide Sequences	
AQ ref	Ac-AAQAA-AAQAA-AAQAA-Y$(NH)_2$
	Glu – Lys series
E5K6	Ac-AAQAE-KAQAA-AAQAA-Y$(NH)_2$
E5K7	Ac-AAQAE-AKQAA-AAQAA-Y$(NH)_2$
E6K9	Ac-AAQAA-EAQKA-AAQAA-Y$(NH)_2$
E6K10	Ac-AAQAA-EAQAK-AAQAA-Y$(NH)_2$
	Lys – Glu series
K6E9	Ac-AAQAA-KAQEA-AAQAA-Y$(NH)_2$
K6E10	Ac-AAQAA-KAQAE-AAQAA-Y$(NH)_2$

The order of helix stabilization by the potential formation of an ion-pair was found to be (i, i+4) > (i, i+3) >> (i, i+2) ≈ (i, i+1). It was shown that the (i, i+3) and (i, i+4) Glu – Lys interactions are helix-stabilizing and are similar in strength to each other, regardless of the orientation of the side chains while no significant hydrogen-bonding interactions were found for the (i, i+1) or (i, i+2) Glu – Lys spacings.

The interactions between the polar side chains of glutamate and lysine have also been examined by Smith and Scholtz [Smith and Scholtz, 1998] using CD measurements at 0 ^{o}C. The peptides employed in their study are derivatives of the neutral Ala - Gln host peptide [Scholtz et al, 1991]. The peptide served as a host, into which they substituted pairs of polar residues (Glu – Lys, Asp – Lys, Glu - His) at positions 6, 9, 10 and 11, to provide (i, i+3), (i, i+4), and (i, i+5) potential interactions. The guest sites were selected so as to place the potential interactions in the center of the peptide, where the average helicity is higher, end effects are minimized, and potential interactions with the Gln residues of the host are avoided [Huyghue-Despointes et al., 1993; Scholtz et al., 1993]. Every peptide with a guest residue was found to be less helical than the host peptide, presumably because of the lower w-values (Table 3.3) between host and guest residues (Table 3.4). The main results from this study were that shorter side chains have larger ΔG_{sc} values, although there are more restrictions on the spacing and intra-helical orientations of residues with shorter side chains. The strength of the interaction between fully-charged ion pairs can be diminished by salt, but the interaction is not completely screened even at 2.5 M NaCl. All the interactions between the polar residues employed in this study stabilize helix formation, suggesting that solvent-exposed ion pairs together with hydrogen bonds can contribute to the conformational stability of proteins and peptides.

Table 3.3: *Lifson-Roig Helix-Coil Parameters for these Peptides [a][Smith and Scholtz, 1998]*

residue	*w*-value(s)
$<AQ>_{favorable}$ [b]	1.35, 1.38, 1.37
$<AQ>_{unfavorable}$ [c]	1.30, 1.36, 1.35
Asp^0	0.40
Asp^-	0.38
Glu^0	0.70
Glu-	0.54
His^0	0.36
His^+	0.22
Lys^+	1.00

[a] Parameters used in the analysis of the data. The Lifson-Roig formalism of helix-coil theory has been used as implemented in the computer program *helix2*, written by Carol Rohl [Rohl et al., 1996]. The data used to determine the parameters for the charged residues are summarized in Rohl et al. [Rohl et al., 1996]. They used a constant nucleation parameter (υ = 0.036) for all residues [Rohl et al., 1996]. [b,c] The Ala-Gln host peptide is treated as a homopolymer. The average $<w_{AQ}>$ is the best-fit parameter for the set of peptides with at least one favorable (unfavorable) charge-dipole interaction. The three $<w_{AQ}>$ values are for the data sets in 0.01, 1.0, and 2.5 M NaCl, respectively. [c] The Ala-Gln host peptide is treated as a homopolymer. The average $<w_{AQ}>$ is the best-fit parameter for the set of peptides with at least one unfavorable charge-dipole interaction. The three $<w_{AQ}>$ values are for the data sets in 0.01, 1.0, and 2.5 M NaCl, respectively.

Table 3.4: *Observed Helicity ($-[\theta]_{222}$ in deg cm^2 $dmol^{-1}$) of each of the peptides at 0 °C[a] [Smith and Scholtz, 1998]*

	0.01 M NaCl			1.0 M NaCl			2.5 M NaCl		
peptide	*i,i*+3	*i,i*+4	*i,i*+5	*i,i*+3	*i,i*+4	*i,i*+5	*i,i*+3	*i,i*+4	*i,i*+5
E^0K^+	10700	12100	9800	12450	14150	11100	12750	13450	10600
E^-K^+	11400	12750	8500	11750	13100	9700	11050	12100	9200
D^0K^+	7700	8500	6900	7900	9500	8000	7500	8700	7600
D^-K^+	8200	9200	7400	8900	10000	8400	8000	8900	8000
E^0H^+	4200	3900	4400	4800	4500	5100	4000	4300	4800
E^-H^+	4500	4100	3600	5000	4400	4300	4400	4000	4000
E^-H^0	5100	4400	4700	5600	5100	5500	4700	4900	5200
AQhost[b]		15580			16580			15250	
K^+E^0	10050	9700	7900	12100	11050	10400	11750	11400	9900
K^+E^-	9000	10350	6900	10350	10700	9100	8650	8650	8700
K^+D^0	7800	8100	5900	9600	10100	7900	8600	8700	7500
K^+D^-	8400	10300	5800	8400	10100	7700	7400	8700	7300
H^+E^0	5100	5400	2700	5700	5900	3900	4500	4500	3700
H^+E^-	4400	5300	2300	5000	5300	3300	4100	4300	3100
H^0E^-	3300	3300	3400	6400	6600	4700	5200	5400	4500

[a] For each orientation and charged state of the polar residues, data are provided for the three different spacings at each of the three NaCl concentrations. The entries for Glu^0 or Asp^0 with Lys^+ were determined at pH=2.5, while those for the full ion pair (Glu^- or Asp^- with Lys^+) are at pH=7.0. The Glu - His data were measured at pH=2.5 (Glu^0 - His^+), pH=5.5 (Glu^- - His^+), or pH=8.5 (Glu^- - His^0). The ionization state on the charged residue is given by a superscript (0/+/-). [b] The host peptide has no guest residues and is arbitrarily listed under the (*i*, *i*+4) column. The peptides listed above the host all contain at least one favorable charge-helix macrodipole interaction and those listed after the host have at least one unfavorable charge-helix macrodipole interaction.

Recent simulations with more complex oligopeptides suggest a complex dependence of helical stability on salt type and concentration in the solution.

Fedorov et al. performed molecular dynamics (MD) simulations of the alanine tripeptide (AA3) in ionic solutions [Fedorov et al., 2007]. To investigate the specific effects of the halide anion series they simulated aqueous solutions of sodium fluoride, chloride, bromide and iodide with different molar concentrations: 0.20, 0.50, 1.00 and 2.00 M. By defining any conformation of AA3 with (φ, ψ) belonging to the region ([-110^o: -20^o)], [-70^o: +50^o]) as a 'compact' conformation, and all other conformations as 'extended', they calculated the percentages of the 'folded' conformations for all investigated systems. As seen in Table 3.5, the percentage of compact conformations varied with ionic type and concentration. Sodium fluoride seems to be the best stabiliser of compact conformations up to its solubility limit (≈1. M).

Table 3.5: *% of compact ('folded') conformations of the alanine tripeptide for different salt concentrations. For comparison, the number for bulk water solution is given (0.0 M salt concentration) [Fedorov et al., 2007].*

Salt	0.0 M	0.20 M	0.50 M	1.00 M	2.00 M
NaF	12.2	21.9	52.6	33.8	15.3[a]
NaCl	12.2	17.1	14.5	9.0	9.0
NaBr	12.2	19.5	16.1	21.2	14.8
NaI	12.2	22.5	15.2	20.2	10.9

[a] *–the 2.0 M concentration is above the maximum solubility of NaF [Fedorov et al., 2007].*

To reveal details of the tripeptide-ion interactions Fedorov et al. calculated the potentials of mean force (PMF) between the tripeptide, water and co-solutes (anions and cations). These PMFs generally exhibit a sequence of minima, which correspond to the maximum density of water sites in the corresponding water shells. Figure 3.3 shows the water oxygen-hydrogen PMF together with selected ion-water and peptide-water PMFs.

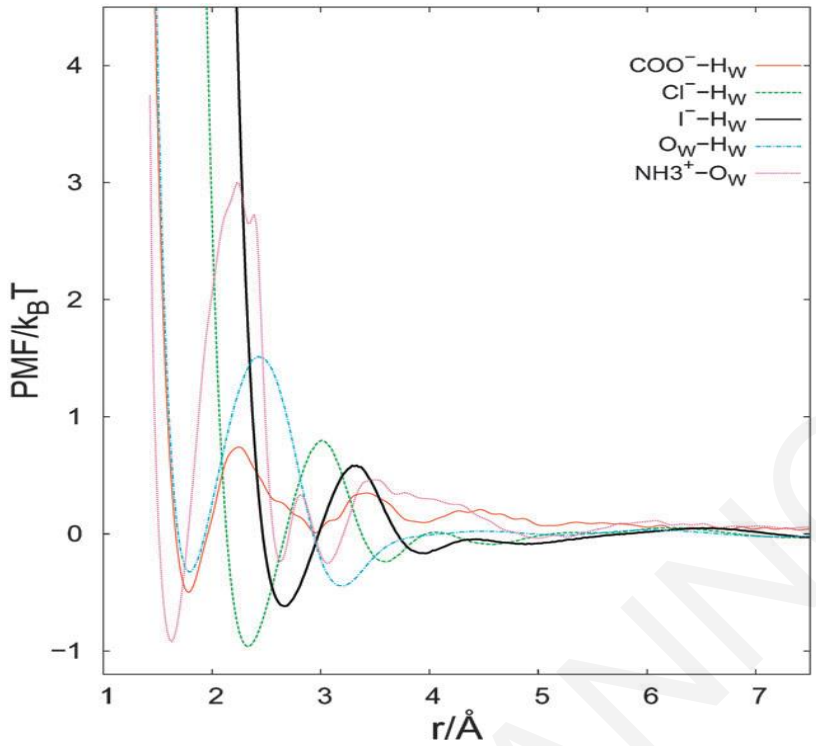

Figure 3.3: *PMFs corresponding to the water-water (oxygen-hydrogen PMF), chloride-water and peptide-water interactions for the charged sites of the alanine tripeptide (NH^+_3 and COO^-) [Fedorov et al., 2007].*

The NH^+_3–ion PMFs are shown in Figure 3.4a. Only Cl^- PMFs have slightly negative values at the position of the first minimum. This means that for bigger anions the direct binding to NH_3^+ is less favourable than shell-shell contacts (secondary minima corresponding to the intersolute distance ≈ 5-6 Å). This is especially true for the I^- ion, which has a large positive difference (> 2 k_BT) between the depths of the first and secondary NH_3^+ - I^- PMF minima. The NH_3^+ group is strongly hydrated as seen from Figure 3.3. It is energetically unfavourable to dehydrate this group. Therefore, in spite of the attractive electrostatic interactions, big anion interactions with the NH_3^+ group are water-mediated. Solvent-separated ion pairs are formed, rather than direct ion-pairs.

The COO^--ion PMFs are shown in Figure 3.4b. Unlike the NH_3^+ group the carboxylate terminus is weakly hydrated (see Figure 3.4b) and the Na^+ cations can easily dehydrate it — this group is surrounded by a cloud of sodium ions which are in direct contact with it, and screen the repulsive COO^--anion interactions. As a consequence, some of the COO^--anion PMFs have noticeable minima around 4 – 5 Å. As the Na^+ ion is strongly hydrated, shell–shell and shell–group interactions take place, giving rise to a number of secondary minima in the corresponding PMFs. In fact, the COO^-–sodium interactions via

intermediate water are less favourable than the direct COO^-–sodium contacts, as can be seen from the large negative difference (~1–2 k_BT) between the depths of the first and secondary minima in the COO^-- Na^+ PMFs.

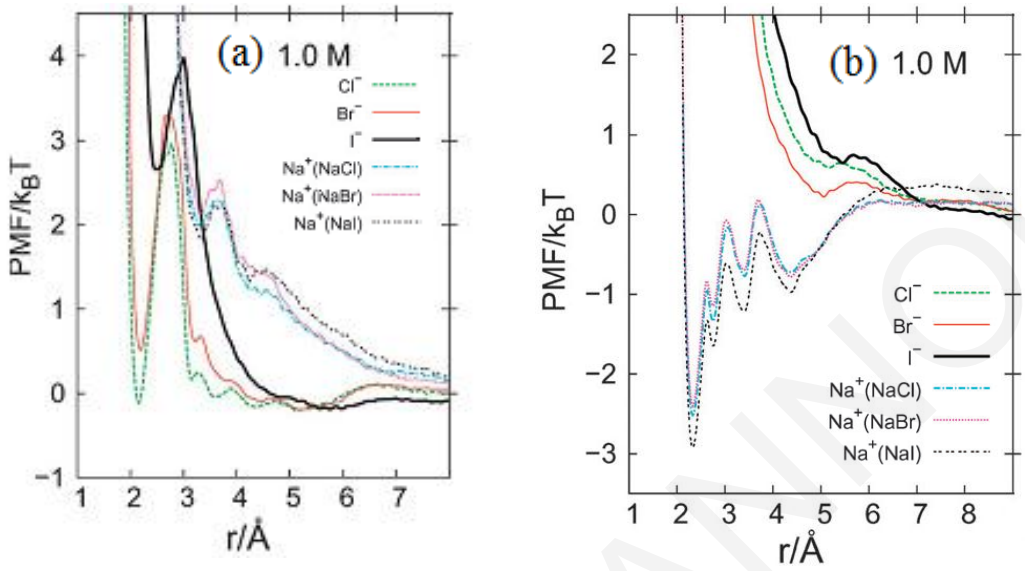

Figure 3.4: *PMFs (a) NH^+_3–ion PMFs and (b) COO^--ion [Fedorov et al., 2007].*

Fedorov's study also revealed that for large ions (Br^-, I^-) the ion-water-peptide contacts are preferred to direct ion-peptide contacts and that these ions tend to be closer to the hydrophobic peptide groups. On the contrary, for ions with small ionic radius (Na^+, F^-), direct ion-peptide contacts are preferred and these ions are attracted to highly charged groups and form contact-ion pairs with them (NH_3^+ and COO^-).

Let us comment more on the fact that in the case of the bigger anions, both anions and cations tend to be closer to the hydrophobic peptide groups. This fact corresponds to the idea of 'quasi-hydrophobic' behaviour of the large halides [Lynden-Bell and Rasaiah, 1997]. (c) The chaotropes (bromide and iodide ions) tend to be close to the hydrophobic groups, but the kosmotropes (fluoride and sodium ions) tend to be close to the hydrophilic groups. The chloride ions are almost 'neutral' in this sense, and their behavior is dictated according to their concentration. Overall a "nonlinear" effect of the anions on the tripeptide conformation is observed which decreases with salt concentration. Another point to make is that the positively charged N-terminus is hydrated more strongly than the negatively charged C-terminus, leading to quite different pictures of counterion interactions with these groups. There is a high energetic cost for moving water molecules away from the NH_3^+

group, and as a consequence, more weakly hydrated anions prefer to interact with that group via an intermediate water shell rather than by the direct contacts.

In 2009 Fedorov published an additional MD study of the effects of aqueous sodium halide solutions on conformational properties of trialanine [Fedorov, 2009]. The main conclusions of that work are the following: (a) NaCl was the most effective at stabilising extended conformation of the trialanine molecule over compact conformations. NaF stabilises compact over extended conformations at low concentrations. NaBr and NaI have lesser effects. (b) The behaviour of trialanine in NaF solutions was significantly different from that in other solutions as well as from that in bulk water. The main reason for this where the strong interactions of the small fluoride ions with counterions, water and with charged groups on the trialanine [Fedorov, 2006; Fedorov, 2007]. (c) The conformational features of the two main cluster of observed conformation in NaCl, NaBr and NaI solutions did not differ significantly from the corresponding clusters in pure water. However, the third cluster had large differences in hydrophilic and hydrophobic SAS areas compared to pure water, as a result of different exposure of the backbone groups to the solvent. This is in agreement with many studies of biomolecule solvation [Avbelj, 2000; Garcia and Sanbonmatsu, 2002; Luo and Baldwin, 1999; Avbelj, 2003; Martinek, 2006]. (d) The effects of ions are different on different polypeptide groups. The net effect of ions on the macromolecular conformation thus depends on the chemical composition of the macromolecule. This conclusion agrees again with findings of Imai et al. and Kinoshita et al. [Imai, 2000; Kinoshita, 2005], who reported a big difference in salt effects on hydrophobic and hydrophilic polypeptide groups.

The recent papers by Dzubiella [Dzubiella, 2008; Dzubiella, 2009] represent the most thorough examination of salt effects on α-helix formation to date, and will be discussed below in detail. Dzubiella investigated the structure and (helix) stability of a shorter version of the salt-bridge forming "EK(i + 4)" peptide with 12 residues and sequence Ace–AEAAAKEAAAKA–Nme by employing standard all-atom MD simulations. He examined the (de)stabilizing action of four different salts (NaCl, NaI, KCl, KF) at large concentrations ($c \geq 3M$) and analyzed the molecular and structural details of these systems for long (μs) simulation runs.

Peptide helicity vs simulation time t is plotted in Figure 3.5 for (a) the salt-free case, (b) 3.7M NaCl, and (c) 3.5 M KCl. In the absence of salt the helicity can be considerable (~80% - 90%) in this system, but two large-scale unfolding transitions were observed at t = 130 and 900 ns, which lead to unfolding of the peptide (helicity < 50%) for ~50 ns. The total helicity averaged over the whole trajectory was found to be 71%, in satisfactory agreement with the experimental value of about 80% of the 17 residue long analogue [Marqusee and Baldwin, 1987]. A large concentration of NaCl clearly destabilizes the helical structure as shown in Figure 3.5b. States with more than 50% helicity are rarely found in the presence of NaCl. The average helicity decreases even further to 30% for 3.7 M NaCl. The destabilizing trend of NaCl is in agreement with experimental measurements of the longer analogue, where it was found that the helicity decreases systematically with increasing NaCl concentrations (e.g., a value of 57% at *c* = 3 M was measured) [Marqusee and Baldwin, 1987]. In contrast to NaCl, KCl has only a slight destabilizing action, as shown in Figure 3.5c. The average helicity (63%) even at the large concentration of 3.5 M KCl is close to the salt-free case. The average helicities are summarized in Table 3.6.

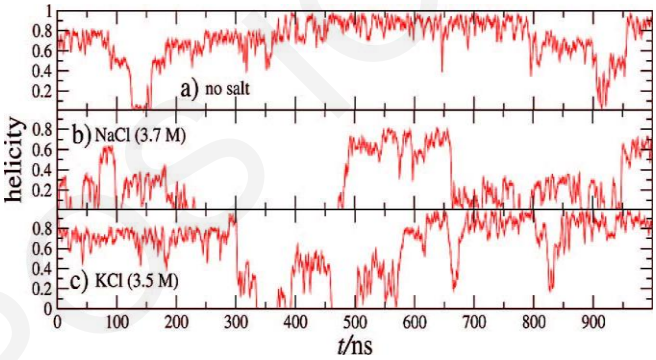

Figure 3.5: *Peptide helicity vs time t for (a) no salt, (b) c = 3.7 M NaCl, and (c) c= 3.5 KCl [Dzubiella, 2008].*

Table 3.6: *Helicity and salt bridge probabilities of the peptide for different salt type and concentration [a] [Dzubiella, 2008].*

Salt	c/M	helicity	P_{sb1}(4.3 Å)	P_{sb1}(7.0Å)	P_{sb2}(4.3 Å)	P_{sb2}(7.0 Å)
	0.0	0.71	0.10	0.27	0.11	0.43
NaCl	3.7	0.30	0.03	0.07	0.06	0.18
KCl	3.5	0.63	0.02	0.11	0.10	0.33
NaI	3.3	0.23	0.04	0.10	0.09	0.24
KF	4.0	0.58	0.03	0.16	0.09	0.31

[a] *The terms $p_{sb1}(r)$ and $p_{sb2}(r)$ correspond to the probability of finding the Glu2-Lys6 and Glu7-Lys11 head groups within a distance r, where r is equal to 4.3 Å and 7.0 Å for direct and indirect salt bridges, respectively [Dzubiella, 2008].*

In order to test the influence of the anion, Dzubiella replaced NaCl by NaI and KCl by KF. He observed only small changes in the helicity for the potassium salts, but a noticeably larger destabilizing action when chloride was replaced by iodide (Table 3.6). In fact, NaI is known to be a strong denaturant [Baldwin, 1996]. It seems, however, that for the particular peptide and ions, which were studied, the cation charge density is the crucial parameter which determines the denaturation capability of the salt. Although comparable in size and often observed to have similar salting-in and salting-out actions on proteins (Baldwin, 1996; Nandi and Robinson, 1972), Na^+ and K^+ exhibit even qualitatively different influence on the solubility of amino acids [Khoshkbarchi and Vera, 1997], and on the activity and stability of halophilic proteins [Madern et al., 2000]. They also have a striking difference in binding to protein carboxylates and carbonyls [Vrbka et al., 2006; Uejio et al., 2008].

The conformations of the investigated peptide in solution and the effects of salts on their distribution were studied by means of the probability *P* of the root-mean-square deviations (rmsd) of a configuration from the fully helical reference structure. The reference was chosen randomly from configurations with 100% helicity. The corresponding free energy $\Delta G(\text{rmsd}) = -k_B T \ln(P)$ vs. the rmsd reaction coordinate without salt, NaCl, and KCl is shown in Figure 3.6. At zero salt concentration and for 3.5 M KCl, there are two distinct minima. In one of them the peptide is in the fully helical state with three helical turns (rmsd = 1.6 Å, Figure 3.6a), and in the other it features two neighboring helical turns (rmsd = 3.1 Å, Figure 3.6b)]. The free energy barrier between these two states is only about 1.5 $k_B T$. Qualitatively different behaviour is observed for 3.7 M NaCl. The minimum corresponding to the full helical state disappears and a broad minimum occurs at larger rmsd values ~5-7 Å. This broad minimum is occupied by mainly two distinct configurations. At rmsd = 5.5 Å, long-lived configurations were observed that feature two helical turns at both ends of the peptide with an intermediate loop (see the snapshot in Figure 3.6c), while a rmsd 6.5 - 7 Å corresponds to the coil state where helicity completely vanishes (see Figure 3.6d). The "loop" states (Figure 3.6c) in NaCl had long lifetimes and were stabilized by specific sodium and water binding to the peptide backbone. In most cases it was found that the middle section of the peptide loops around a single sodium ion, thereby binding it with 3-4 backbone carbonyls, while a partly helical structure can still be maintained, cf. Figure 3.7a. Sometimes an additional water molecule is captured by this backbone-ion comple as illustrated in Figure 3.7b and c. These states were quite stable

over a long (10-20 ns) time scale. Such long-lived states were not observed in the case of potassium; they are of course impossible for anions, which do not bind to the backbone.

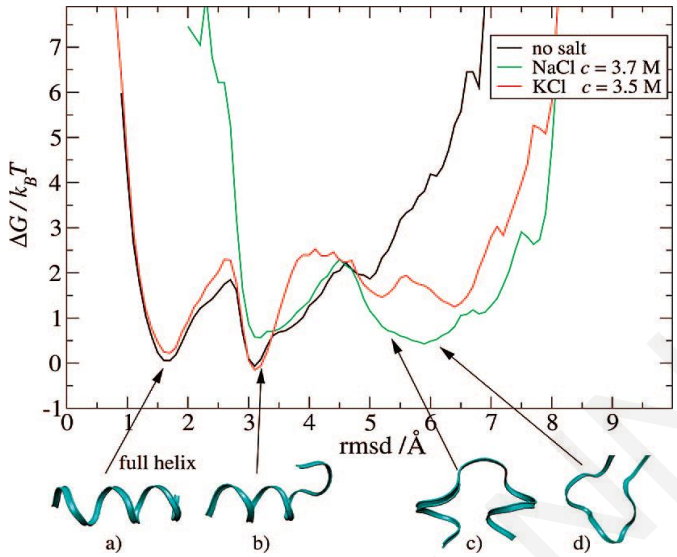

Figure 3.6: *Free energy along the rmsd (root-mean-square deviation from a "perfect" helix formed by this peptide) reaction coordinate. The MD snapshots of the peptide backbone at the bottom are examples of configurations with high probability (low free energy) with an rmsd location indicated by the arrows [Dzubiella, 2008].*

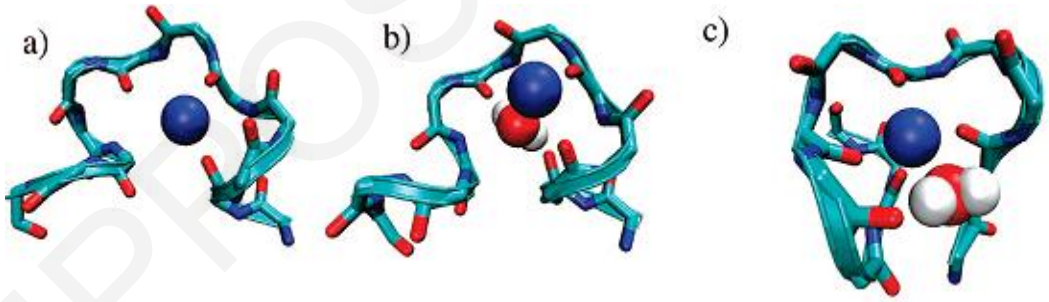

Figure 3.7: *MD simulation snapshots of long-lived (~10-20 ns) peptide configurations observed in NaCl or NaI solutions at large concentrations, where (a) one Na^+ ion (blue sphere) or (b and c) Na^+ and one water molecule (red and white spheres) are permanently hydrogen bonded and immobilized by the peptide backbone. Only backbone atoms of the peptide are shown [Dzubiella, 2008].*

As we discussed before, the charged residues $Glu2^-$ and $Lys6^+$, and residues $Glu7^-$ and $Lys11^+$, are potentially able to form EK-type salt bridges, which may directly stabilize the helix by shifting the equilibrium to the helical state [Marqusee and Baldwin, 1987] or additionally, may contribute to helix stability through backbone desolvation and shielding

from water [Vila et al., 2000; Garcia and Sanbonmatsu, 2002; Ghosh et al., 2003] To elucidate these mechanisms, Dzubiella calculated the (normalized) probability distribution $P(r)$, where r is the distance between the carboxylate carbon atoms on Glu and the amine nitrogen on Lys for the first (Glu2-Lys6) and second (Glu7-Lys11) salt bridge, averaged over the whole MD trajectory. Examples for the salt-free case and large NaCl and KCl concentrations are shown in Figure 3.8 for the Glu7-Lys11 pair. The first peak for distances $r < r_d \approx 4.3$ Å corresponds to a direct salt bridge while the second peak $r_d < r < r_{id} \approx 7.0$ Å corresponds to water - separated salt bridge. With the help of these distributions Dzubiella estimated the probabilities $p(r_i)$ (i = d, id) of finding a direct or both direct and indirect salt bridges. In the absence of electrolytes, a direct salt bridge is formed by one of the Glu-Lys pairs only 11% of the time. This value is in accordance with the results of Ghosh et al. [Ghosh et al., 2003] on a similar EK(i + 3) peptide, who found that possible EK salt bridges spend only 10 - 20% in contact configuration. A higher probability exsists however to find either a direct or an indirect ion-pair for the Glu2-Lys6 pair $\{P(r_{id}) = 27\%\}$ and for the Glu7-Lys11 pair $\{P(r_{id}) = 43\%\}$. The unequal stability of the two salt bridges derives from the interaction of Glu2 with the N-terminal. It is known experimentally that "N-capping" by specific side chains strongly influences the helix distribution along a given peptide [Vasquez et al., 1987; Serrano and Fersht, 1989]. The probability values for forming direct and both direct and indirect salt bridges for all investigated systems are summarized in Table 3.6.

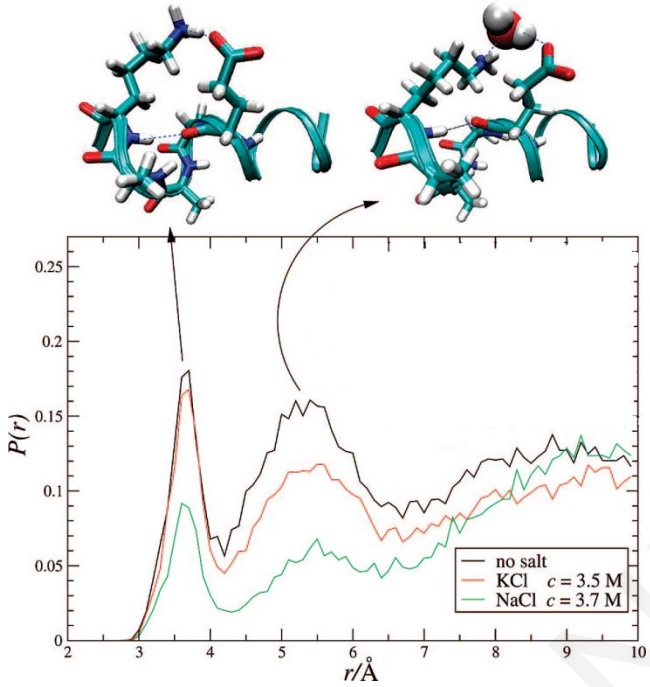

Figure 3.8: *Probability distribution of distances between the carboxylate carbon atom of the Glu7 side chain and the amine nitrogen of the Lys11 side chain. The MD snapshots on the top exemplify direct and indirect (separated by one water molecule) salt-bridge configurations corresponding to the first and second peak of p(r), respectively. Only side chains of amino acids 7-11 are shown [Dzubiella, 2008].*

The distribution function for the Glu7 – Lys11 ion pair depends on salt type and concentration as is also illustrated in Figure 3.8. For NaCl, the salt-bridge formation probability is decreased by more than 50% with respect to pure water. Obviously this behaviour is related to the reduced average helicity, in the system, in this case as in a nonhelical state the charged side chains are too far apart to form a contact ion-pair. KCl affects the distribution much less when compared to NaCl.

The radial distribution functions (rdf) of water and cations around the Glu carboxylate carbon are plotted in Figure 3.9. There is considerably stronger affinity of sodium over potassium to the carboxylates as has been found in other experimental studies and quantum mechanical calculations [Vrbka et al., 2006; Uejio et al., 2008]. The rdf for the potassium – glutamate pair on the other hand is comparable in magnitude to that of the water oxygen – glutamate pair. Estimating the coordination number of species X in the first carboxylate solvation shell of the Glu carboxylate carbon reveals that, while in the salt-free case 8-9 water molecules directly solvate the carboxylate, ~2 of them are replaced on average by sodium ions in the NaCl solution, indicating a strong specific binding of sodium. For this

reason a decreased contact value of the water-carboxylate rdf is observed in the NaCl solution in Figure 3.9. In KCl, on average only ~0.5 ions were found to replace water molecules. It is thus seen that sodium directly competes with water and Lys-nitrogen atoms for binding to the carboxylates and therefore has a strong impact on salt bridge formation.

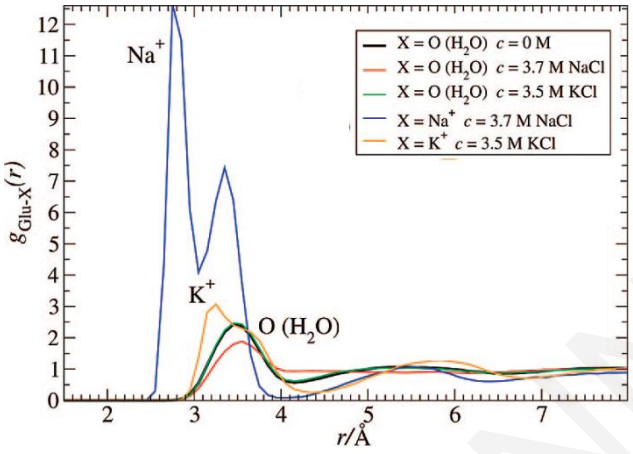

Figure 3.9: *Radial distribution function (rdf) $g_{Glu\text{-}X}(r)$ between the carboxylate carbon of the Glu side chains and X, where X = O (water oxygen), Na^+, or K^+, plotted for no salt (c = 0) and NaCl and KCl at concentrations of c = 3-4 M [Dzubiella, 2008].*

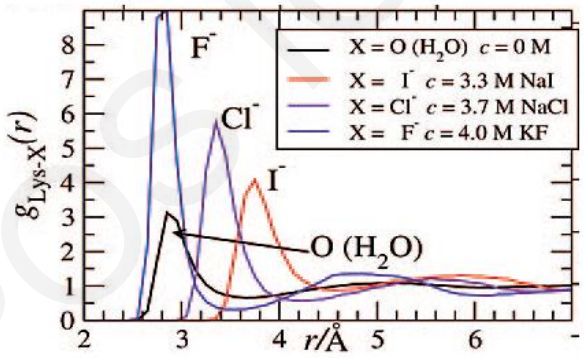

Figure 3.10: *Radial distribution function rdf $g_{Lys\text{-}X}(r)$ between the nitrogen of the Lys side chain and X, where X = O (water oxygen), F^-, Cl^-, or I^- [Dzubiella, 2008].*

The distributions of water and anions around the Lys nitrogen are plotted in Figure 3.10. F^- > Cl^- > I^- is the preferred sequence of interaction as may be expected from electrostatic considerations, i.e., there is a stronger attraction with larger ion charge density. Calculating the coordination numbers however, revealed that on average only ~0.5 fluoride ions are able to replace a water molecule in the water solvation shell of the Lys nitrogen, so fluoride is much less effective in solvating amide groups than sodium in replacing water around the carboxylates.

In order to check whether similar specific binding can be detected for other parts of the peptide, Dzubiella also calculated the rdfs between ions and the backbone amide oxygens and nitrogen atoms. Examples for the cations and anions are plotted in Figure 3.11a and b, respectively. Analogous to the results presented in Figure 3.10, a strong attraction of sodium to all carbonyl oxygens was observed, in striking contrast to a weak affinity of potassium. The anions, however, interacted with the backbone even more weakly than potassium (cf. Figure 3.11b). Interestingly, iodide has the highest first interaction peak compared to the other anions ($I^- > Cl^- > F^-$) whereas for the interaction with the Lys headgroup (see Figure 3.10), the sequence is, $F^- > Cl^- > I^-$. The strong affinity of sodium to the backbone is enhanced in the presence of iodide, which can be understood as a demonstration for rough local electroneutrality.

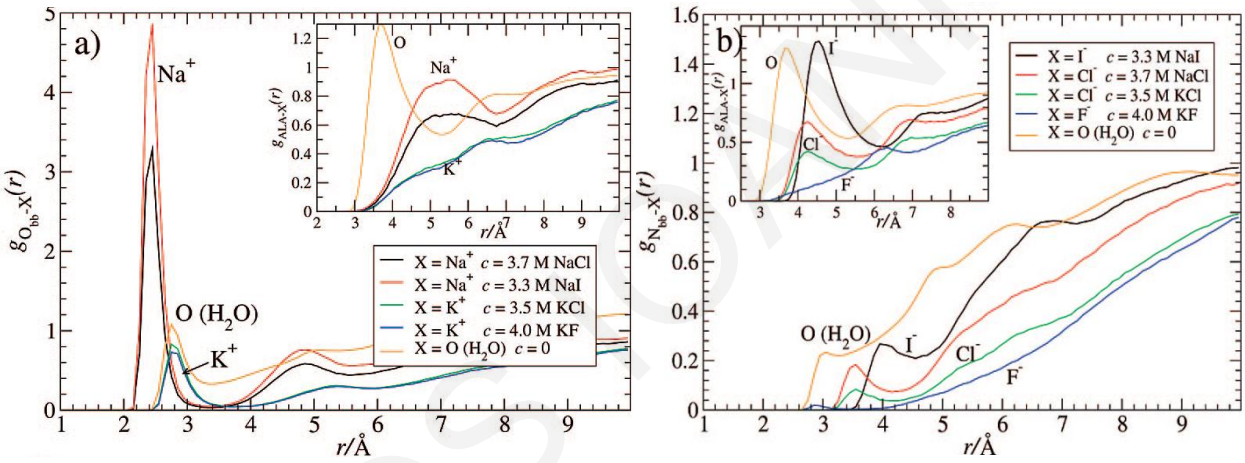

Figure 3.11: *(a) Radial distribution function (rdf) $g_{Obb\text{-}X}(r)$ between the backbone oxygen and X, where X = Na^+, K^+, or water oxygen (O) plotted for different salts - see the legend. (inset) rdf $g_{ALA\text{-}X}(r)$ between alanine side chains and X. (b) rdf $g_{Nbb\text{-}X}(r)$ between the backbone nitrogen and X, where X) F^-, Cl^-, I^-, or water oxygen (O) for different salts, see the legend. (inset) rdf $g_{ALA\text{-}X}(r)$ between alanine side chains and X [Dzubiella, 2008].*

Additionally, Dzubiella calculated the rdf between the carbon atom in the alanine side chain and cations or anions, to investigate the hypothesis that the relatively large anions have an affinity for nonpolar surfaces [Jungwirth and Tobias, 2006] or hydrophobic solutes [Kalra et al., 2001]. Insets in Figure 3.11a and b show that iodide does indeed have the strongest affinity to the nonpolar side chains from all considered ions. These findings are in line with MD of a toy model of a heterogeneous biomolecule, where it was demonstrated that fluoride and iodide binding strongly depends on the local surface characteristics [Lund et al., 2008]. They also support the perspective that the iodide

propensity to nonpolar surfaces may be the reason for its significant effect on protein stability [Jungwirth and Tobias, 2006; Kunz, 2006].

Overall, the simulations in high electrolyte concentrations (3 – 4 M) suggested a small destabilization of the α-helix in the presence of NaCl, and a larger destabilization in the presence of NaI [Dzubiella, 2008]. This destabilization was attributed to a combined effect, due to screening of the salt-bridge interactions by the salt, and enhanced sodium-carbonyl interactions in the presence of iodide.

In the case of the negatively charged alanine-based peptide Ac-$(AE)_6$-NMe, examined with the Amber ff03 force-field, a significant reduction in α-helix content in the presence of NaI and a slight increase in other solutions (NaCl, KCl, KI) were reported, as seen in Table 3.7 [Dzubiella, 2009]. This behavior was again attributed chiefly to enhanced sodium interactions with the peptide carbonyl groups in the presence of iodide, which adsorbs on the hydrophobic Ala side chains [Figures 3.12 and 3.13]. In the case of the positively charged peptide [Ac-$(AK)_6$-NMe], NaI had no effect on the helix, whereas the chloride salts NaCl and KCl stabilized it [Dzubiella, 2009].

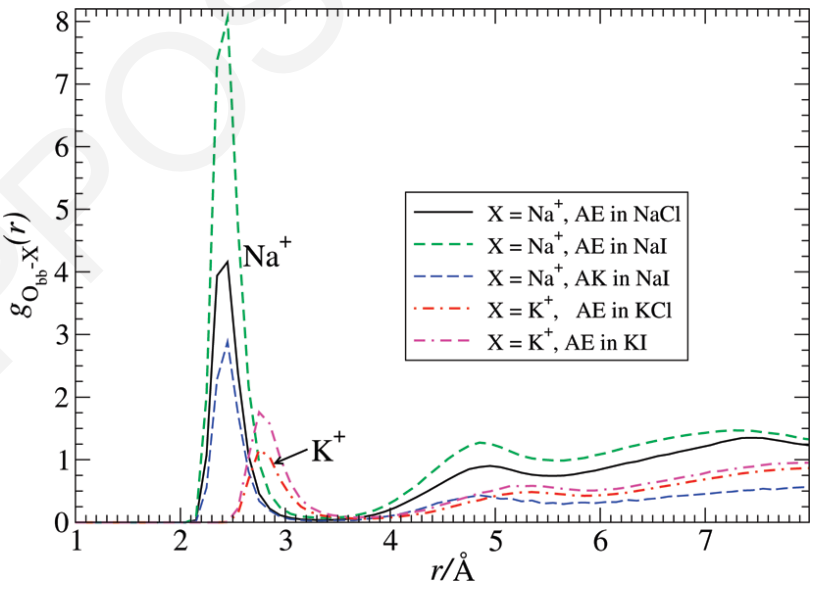

Figure 3.12:*Radial distribution function (rdf) gObb-X(r) between the backbone (carbonyl) oxygen and X, where X) Na+ or K+ plotted for different salts; see legend [Dzubiella, 2009].*

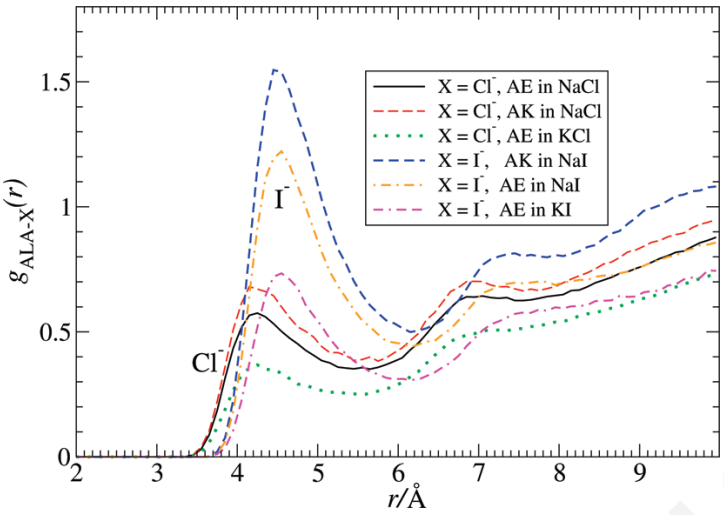

Figure 3.13: *Radial distribution function (rdf) gALA-X(r) between the methyl group in the alanine side chains and anion X) Cl- or I- for different salts; see legend [Dzubiella, 2009].*

Table 3.7: *Average Helicity of the "AE" and "AK" peptides for different types of salt as concentration c [Dzubiella, 2009].*

Salt	*c* (M)	Helicity (%) "AE"	Helicity (%) "AE"
	0.0	0.40 ± 0.13	0.46 ± 0.10
NaCl	2.7	0.44 ± 0.13	0.62 ± 0.04
KCl	2.6	0.54 ± 0.09	0.63 ± 0.11
NaI	2.5	0.18 ± 0.08	0.47 ± 0.08
KI	2.5	0.42 ± 0.08	

In a different study by Asciutto et al. with the Amber ffSB99 force-field, the helicity of a charged alanine based 21-residue peptide, $AAAAA(AAARA)_3A$, containing three arginine residues (R) was shown to increase in the presence of $NaClO_4$ [Asciutto, 2010]. It was stated that the strong stabilization found for $NaClO_4$ was because the ClO_4^- ions compete with water molecules to solvate the peptide. Water is more strongly drawn to the ionic solvation shells than to the peptide surface, hence the latter becomes dehydrated. A less hydrated peptide promotes more intrapeptide hydrogen bonding, which leads to greater helical stability.

The affinities of alkali cations and halide anions for the peptide group were quantified using molecular dynamics simulations of aqueous solutions of the model compound *N*-methylacetamide using both nonpolarizable and polarizable force fields by Heyda et al. [Heyda et al., 2010]. The radial distribution functions revealed that potassium and, more strongly, sodium exhibit an affinity for the carbonyl oxygen of the amide group, while none of the halide anions show any appreciable attraction for the amide hydrogen. Heavier

halides, however, interact with the hydrophobic methyl groups of the *N*-methylacetamide. Based on these results, Heyda et al. concluded that the destabilizing effect of weakly hydrated Hofmeister ions, such as bromide or iodide, is not due to direct interactions with the backbone, but rather due to attraction to hydrophobic regions of the protein. Algaer et al. have also recently examined interactions of sodium salts with N-isopropylacrylamide (NiPAM) and N-methylacetamide (NMA) [Algaer et al., 2011]. They also found a strong affinity of sodium for the carbonyl oxygen and an affinity of iodide towards the hydrophobic groups. They also found that the affinity of anions towards the amide group depends on its environment, with considerable differences observed in the cases of NiPAM (no interactions) and NMA (definite H-bonding of anions with the amide hydrogen). Algaer et al. also concluded that the force field used plays an important role for the quantitation of the interactions.

4. Specific Interactions of Sodium Salts with Alanine Dipeptide and Tetrapeptide in Water

4.1 Introduction

To investigate the ionic effects on the stability of the conformation of the protein backbone we have conducted simulations of the model system alanine dipeptide and tetrapeptide in aqueous salt solutions. The alanine dipeptide has the essential features of the protein backbone and is a starting point in the derivation of all modern protein simulation force fields [Mackerell, 2004]. It has a single pair of backbone dihedral angles (φ, ψ) and two peptide groups, which can form an intramolecular hydrogen bond. It allows checking the specific ion effects on the Ramachandran plot and the relative interaction of the ions with the backbone peptide groups and the methyl side chain and blocking groups [Rossky et al., 1979; Mezei et al., 1985; Tobias and Brooks, 1992; Ishizuka et al., 2010]. Importantly, this molecule contains both polar groups (the peptide bonds) and non-polar groups (the methyl-group side-chain and the two methyl-blocking groups at the N- and C- terminal ends, which model the adjacent C_a atoms in a longer backbone).

The tretrapeptide introduces additional dimensions [Tobias and Brooks, 1991]. With the present choice of N- terminal and C- terminal blocking groups, it has three complete pairs of backbone torsional angles (φ_i, ψ_j) and four peptide groups. Thus, it can form a variety of hydrogen-bonding interactions, including two i, i+3 hydrogen bonds encountered in the β-turns (C_YO_Y-N_3H_{N3}, C_1O_1-N_TH_{NT}) and one i, i +4 hydrogen bond encountered in α-helices (C_YO_Y-N_TH_{NT}). Thus, closed, "quasi-helical" conformations are possible for this model, and the conformational space is greatly extended with respect to the dipeptide. Even though no large scale secondary structure can be formed by the tetrapeptide, an increase of "closed" conformations would immediately signify that the presence of salts stabilizes the initial helix-formation step in this type of oligopeptides.

To keep the systems simple, we have only used sodium chloride (NaCl) and sodium iodide (NaI) as electrolytes. NaCl is generally expected not to give strong specific salt effects in most systems [Collins and Washabaugh, 1985; Cacace et al., 1997; Kunz, 2010; Leontidis

and Aroti, 2009] while iodide is definitely a chaotropic anion and can be used to illustrate potential side-chain or backbone interactions of the more hydrophobic ions [Fedorov et al., 2007; Fedorov et al., 2009; Dzubiella, 2008; Dzubiella, 2009]. We have used a range of electrolyte concentration (0 – 3 M) to investigate concentration effects on the oligopeptide structures.

4.2 Methods

4.2.1 Investigated Systems

The peptides studied have the sequences Ac-Ala-NMe and Ac-Ala_3-NMe (Scheme 4.1), with $C_LH_3C_{LP}O_L$- (Ac) and -$N_RH_RC_RH_3$ (NMe), respectively, as the N- and C- terminal blocking groups. Each simulation system consisted of a single dipeptide or tetrapeptide molecule in a cubic box of 1000 water molecules and an appropriate number of ions, chosen to model the desired salt concentration. Table 4.1 lists the total number of ions and water-box sizes for the various dipeptide and tetrapeptide simulations. Although the actual salt concentrations are those listed in the Table, for simplicity we will designate them as "1 M", "2 M" or "3 M" concentrations in the ensuing discussion.

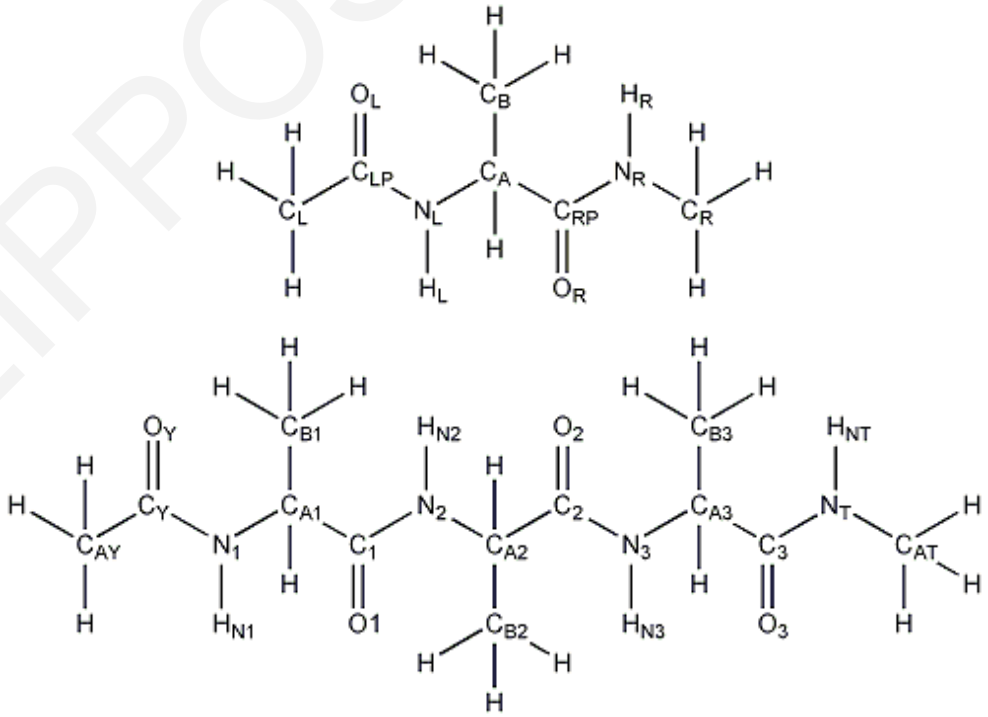

Scheme 4.1: *Terminally Blocked Alanine Dipeptide (Ac-Ala-NMe) and Tetrapeptide (Ac-*Ala_3*-NMe) Used in the Present Investigation*

4.2.2. Force Field and Simulation Protocol

The peptide atomic charges, van der Waals, and stereochemical parameters were taken from the CHARMM22 all-atom force field [Mackerrell et al., 1988], including a recent grid-based torsional (CMAP) correction [Mackerrell et al., 2004]. The water was represented by a modified TIP3P model [Jorgensen et al., 1983; Neria et al., 1996]. Ion parameters, recently optimized for high-concentration simulations, were taken from Joung and Cheatham [Joung and Cheatham, 2008].

Table 4.1: *Numbers of Ions and Water Box Sizes Employed in the Simulations*

solution	# waters	# cations	# anions	box length
Alanine Dipeptide				
0 M	1000	0	0	31.05
1.2 M NaCl	1000	22	22	31.33
2.3 M NaCl	1000	44	44	31.55
1.2 M NaI	1000	22	22	31.33
2.3 M NaI	1000	44	44	31.55
Alanine Tetrapeptide				
0 M	1000	0	0	31.05
1.2 M NaCl	1000	22	22	31.33
2.3 M NaCl	1000	44	44	31.55
3.1 M NaCl	1000	60	60	31.80
1.2 M NaI	1000	22	22	31.33
2.3 M NaI	1000	44	44	31.55
3.1 M NaI	1000	60	60	31.80

Simulations with short alanine-based peptides and comparisons with available experimental data suggest that several of the current biomolecular force fields, including the CHARMM22/CMAP force field employed here, tend to overestimate the α-helical section of the Ramachandran map, at the expense of extended (β-sheet and PPII) conformations [Graf et al., 2007; Mu et al., 2003; Best et al., 2008; Best and Hummer, 2009; Verbaro et al., 2010; Hegefeld et al., 2010]. This overstabilization is likely to have a smaller impact on the conformational preferences of the very short peptides considered here. Furthermore, the main goal of the present work is to monitor the dependence of conformational properties on salt type and concentration. Even if the helical propensities are systematically overestimated, the errors are likely to partially cancel in the propensity changes (among solutions). To check the force-field dependence of our observations, we also simulated the same alanine tetrapeptide, a nonapeptide (Ac-Ala_8-NMe), and a hexadecapeptide (Ac-$(AQAAA)_3$-NMe) in pure water and a 3.0 M NaI aqueous solution,

using AMBER11 [Case et al., 2010] and the all-atom AMBER force field, with recent optimizations (ff03*) improving peptide helicity at 300 K [Best and Hummer, 2009]. The main conclusions of the simulations with these two peptides and their relevance to the present work are presented in the Results section; details of these simulations are described in the following chapters.

All simulations were conducted with the CHARMM program [Brooks et al., 2009], version c35b3. The simulation system was replicated by cubic periodic conditions, using the CRYSTAL facility of CHARMM. Electrostatic interactions were calculated by the particle-mesh Ewald method [Darden et al., 1993], with a parameter k = 0.55555 for the charge screening and sixth-order splines for the mesh interpolations. Lennard-Jones interactions between atom pairs were switched to zero for distances larger than 9 Å [Joung and Cheatham, 2008]. The lengths of covalent bonds involving hydrogen atoms and the internal water molecule geometries were constrained to standard values via the SHAKE algorithm [Ryckaert et al., 1977] implemented in CHARMM.

All solutions were studied by the replica-exchange molecular dynamics method [Garcia and Sanbonmatsu, 2002; Buchete and Hummer, 2008]. Simulations were performed in the canonical ensemble (N,V,T), with all atoms explicitly represented. Nose-Hoover dynamics [Nose, 1984; Hoover, 1985] was conducted, using a 50.0 kcal/mol sec^2 thermal inertia parameter (QREF) and a 2 fs time step. For each solution, we used 18 replicas with temperatures 290, 295, 300, 305, 310, 315, 321, 327, 333, 339, 345, 351, 358, 365, 372, 379, 386, and 393 K. The NaCl solutions were initially equilibrated by constant pressure simulations at 300 K. Subsequently, the box sizes were fixed to the average size of the constant-pressure runs; identical box sizes were used for NaCl and NaI solutions of the same concentration. The replica temperatures were then optimized by serial, constant volume simulations, targeting an exchange acceptance probability between adjacent replicas of ~20%. The obtained exchange probabilities were between 16 and 21%. All replicas performed random walks in the temperature space, spanning several times the entire range of temperatures; for example, in a typical tetrapeptide solution, the temperature space was traversed ~26 times during a 25 ns simulation. The total simulation length at each temperature was 20 ns for the dipeptide (360 ns for each solution) and 25 ns for the tetrapeptide (450 ns for each solution). Exchanges between adjacent replicas were

attempted every 500 steps (1 ps). The last 19 ns (dipeptide) or 20 ns (tetrapeptide) were employed in the analysis.

4.2.3 Secondary Structure Calculations and Conformational Analysis

We computed the tetrapeptide "helicity" (the fraction of α-helical conformations), using the Lifson-Roig (LR) model [Lifson and Roig, 1961]. In the LR definition, a residue *i* is considered α-helical if and only if its backbone torsional angles (φ_i, ψ_i), and the pairs (φ_{i-1}, ψ_{i-1}) and (φ_{i+1}, ψ_{i+1}) of the adjacent residues fall in the α-helical region of the Ramachandran map (φ = -65 ± 35^o, ψ = -37 ± 30^o). Since the tetrapeptide has three torsional angle pairs, a conformation was classified as α-helical if and only if all three torsional angle pairs were simultaneously in the α-helical region.

The alanine tetrapeptide can also form two *β*-turns, respectively involving the atom pairs C_YO_Y-N_3HN_3 and C_1O_1-N_TH_{NT} (see Scheme 1). A *β*-turn was considered present if the following criteria of Wilmot and Thornton [Wilmot and Thomton, 1990] applied: (i) the distance $C_{\alpha,i}$-$C_{\alpha,i+3}$ was smaller than 7 Å, (ii) the torsional angles of residues *i*+1 and *i*+2 were not in the helical region of the Ramachandran map, and (iii) the torsional angles of residues *i*+1,and *i*+2 were within ±30^o of the ideal turn values [Wilmot and Thomton, 1990], with one dihedral allowed to deviate by ±45^o. For the first and second *β*-turn, we used, respectively, the *N*-terminal methyl carbon (C_{AY}) or the *C*-terminal methyl carbon (C_{AT}) in criterion (i). Note that criterion (ii) implies that a *β*-turn cannot coexist with the α-helical state. Main-chain hydrogen bonds were considered present if the distance between the carbonyl oxygen and the amino hydrogen was less than 2.5 Å, without considering any additional angle restrictions.

We classified the tetrapeptide conformations into families, using conformational clustering of the six backbone torsional angles [Carpenter and Grossberg, 1987; Karpen, 1993; Tamamis et al., 2007]. The clustering method is presented in detail in the Karpen study [Karpen, 1993]. Briefly, a trajectory snapshot j is described by a set of *K* predetermined properties (here backbone torsional angles), arranged into a *K*-dimensional vector $x_j = (x_{1j}, x_{2j}, ..., x_{Kj})$. The center of a cluster l containing $M(l)$ snapshots is defined by the arithmetic mean $c_l = (c_{1l}, c_{2l}, ..., c_{Kl})\_1/M_l\Sigma_{j\in M(l)}x_j$. Each of the $M(l)$ snapshots comprising

cluster l is within a certain predefined threshold (radius) d_0 from the cluster center c_l (i.e., $[\Sigma_{i=1}(x_{il} - c_{il})^2]^{1/2} \leq d_0$) . The maximum cluster radius was set to 50^o, corresponding to average structural fluctuations of approximately 20^o for each of the six torsional angles.

4.3 Results

4.3.1 Alanine Dipeptide Simulations

Figure 4.1a displays the joint probability distribution of the dipeptide main-chain torsional angles from the no-salt simulations at 300 K. The preferred backbone conformations (yellow to green areas) fall mainly into the extended-β region (φ= -160 ± 10^o, ψ = 170 ± 10^o), the PPII region (φ = -75 ± 15^o, ψ = 160 ± 20^o), and a broad, right handed α-helical basin with two subregions (φ = -70 ± 20^o, ψ = -60 ± 20^o and φ = -115 ± 30^o, ψ = 0 ± 20^o) [Yu et al., 2010]. A small fraction of left-handed α-helical conformations is also observed (φ = 65 ± 15^o, ψ = 50 ± 10^o). The distribution agrees very well with the map in the study of Buchete and Hummer [Buchete and Hummer, 2008], which was also obtained with the CHARMM22 [Mackerell et al., 1988] force-field and the grid-based correction (CMAP) [Mackerell et al., 2004]. As shown in that work, this distribution reproduces reasonably well the statistics from Protein Data Bank (PDB)-deposited protein conformations, as well as quantum mechanics/molecular mechanics (QM/MM) calculations [Hu et al., 2003]. However, compared to available spectroscopic data for the alanine dipeptide in solution, which report a propensity of the peptide for the PP-II conformation [Poon et al., 2000; Weise and Weisshaar, 2003; Grdadolnik et al., 2008], the present force field clearly favors the α-helical region.

The addition of 2 M NaCl or 2 M NaI to the system does not lead to dramatic changes of the main chain torsional angle probability distribution, as shown in the difference plots (electrolyte solution vs pure water) of Figure 4.1b, c. A slight stabilization of polyproline II conformations is observed for both salts, more so for the chaotropic NaI. Nevertheless, we can state that the dipeptide conformations are weakly affected by electrolytes, at least within the confines of the force field that we used [Mackerell et al., 2004]. A related observation was made by Feig, who investigated effects of sequences on backbone torsional preferences, by simulations with several dipeptides and proteins [Feig, 2008]. Such effects were not apparent in the dipeptide models, but required longer-range

interactions, encountered in the context of larger polypeptide chains and protein structures. As we show below, electrolytes have a much more significant impact on the conformational properties of the tetrapeptide.

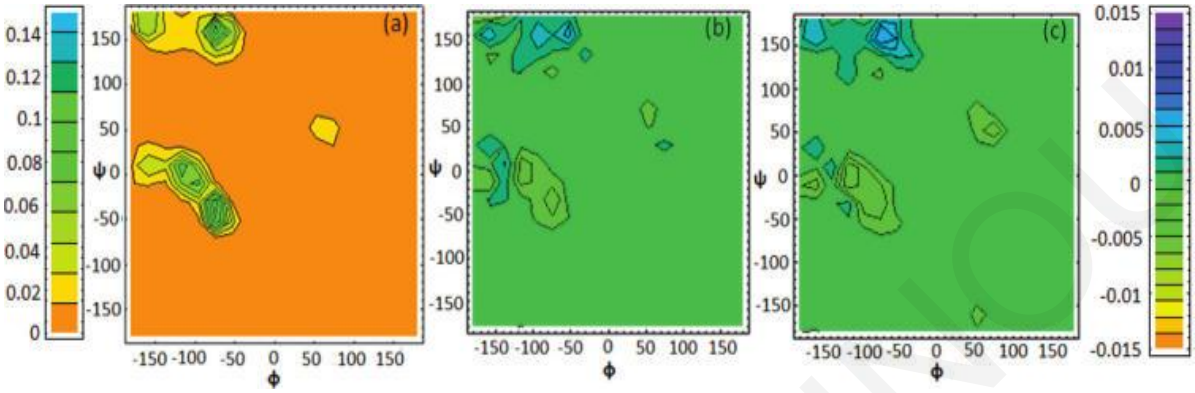

Figure 4.1: *(a) Joint probability density map of the dipeptide torsional angle pair (j, ψ) in pure water; the associated color-code is on the leftmost panel. (b,c) Change in probability when pure water is replaced by a 2 M NaCl solution or a 2 M NaI solution, respectively. The rightmost color-code refers to the last two plots. All maps correspond to 300 K*

In the ensuing discussion, we refer to the "left" (L) side of the dipeptide as the one closer to the *N*-terminal end, and to the "right" (R) side as the one closer to the *C*-terminal end. The rdf's between selected pairs of electrolyte ions and peptide atoms are shown in Figure 4.2; they correspond to simulations at 300 K. In this work we have opted to compare relative strenghts of interactions by looking at the relative heights of the first maxima of the radial distribution functions. In reality this is not necessarily the best choice. It would be better to compute the areas of the first interaction peaks and compare them to each other. The Na^+ - $O_{L/R}$ rdf curves (Figure 4.2a) have a pronounced first contact peak (~4), reflecting the strong sodium interactions with the peptide carbonyl groups. Contrary to this, the larger anion (I^-) has a stronger affinity for the dipeptide amide groups relative to the smaller anion (Cl^-), as reflected by the first contact peaks of the corresponding rdf's with the amide hydrogens $H_{L/R}$ (Figure 4.2b). Both first-contact peaks are, however, below unity, reflecting the lack of preference for the bulkier anions to interact directly with the peptide groups. This behavior of cations and anions is well documented in simulations of model peptides in salt solutions [Dzubiella, 2008; Heyda et al., 2010].

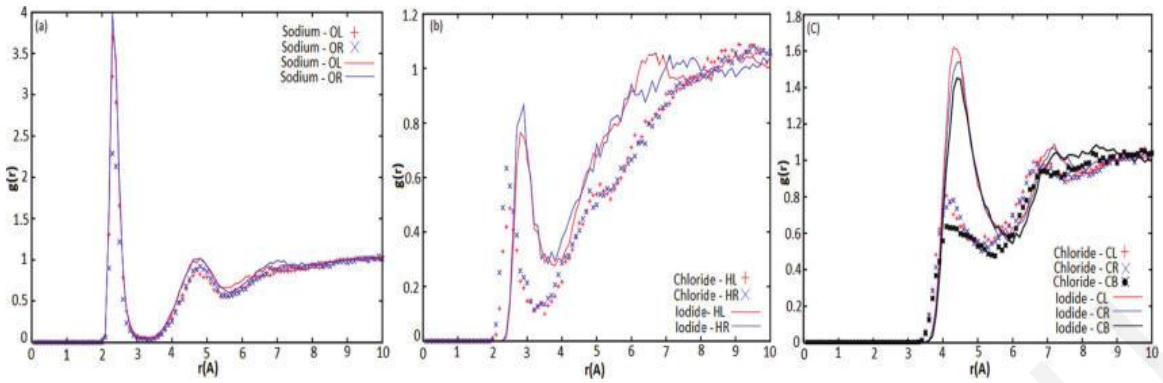

Figure 4.2: *Radial distribution functions (rdf's) between selected ion-dipeptide atom pairs (at 300 K). (a) sodium-carbonyl oxygen; (b) anion-aminogroup hydrogen; (c) anion-methyl carbon. "L" and "R" denote atoms in the "left" (N-terminal) and "right" (C-terminal) groups; "CB" is the side chain atom (Scheme 1). In all plots, lines correspond to the 2 M NaI solution, and symbols correspond to the 2 M NaCl solution.*

Anions in both NaCl and NaI solutions interact more strongly with H_R (Figure 4.2b). This preference might be related to the significant difference of solvent accessible areas of the two amide groups (11.1 $Å^2$ for N_R vs 6.3 $Å^2$ for N_L). By contrast, Na^+ ions in NaCl solutions appear to interact more weakly with the C-terminal peptide oxygen (O_R), compared to the *N*-terminal peptide oxygen (O_L) (Figure 4.2a); this is probably within the simulation uncertainty, since the two groups have comparable solvent accessible areas (33.1 $Å^2$ for O_R vs 35.9 $Å^2$ for O_L).

I^- has a stronger propensity than Cl^- to approach the nonpolar side-chain and blocking methyl groups (Figure 4.2c). The first solvation peaks of the rdf's between iodide ions and nonpolar methyl groups (Figure 4.2c) are actually larger than unity, illustrating a preferential interaction, while the corresponding chloride-C peaks are much smaller than unity, showing that chloride ions avoid the hydrophobic methyl groups. This behavior of iodide has been observed in other simulations of oligopeptide electrolyte solutions [Fedorov et al., 2007; Fedorov et al., 2009; Dzubiella, 2008]; it is partly due to the larger radius of the iodide first hydration shell, which facilitates the loss of hydration water around iodide, relative to chloride. Overall, the dipeptide results show that ions affect to a small extent the intrinsic conformation tendencies of the backbone, and that larger anions interact more strongly with the hydrophobic regions of the chain, in accordance with previous investigations of similar systems [Fedorov et al., 2007; Fedorov et al., 2009; Dzubiella, 2008].

4.3.2 Tetrapeptide Simulations

As explained in the Methods section, the employed tetrapeptide model can form an elementary α-helix, one *i*/*i*+4 hydrogen bond, and two *i*/*i*+3 hydrogen bonds. In the classification of α-helical conformations, we used the LR convention [Lifson and Roig, 1961], which requires all three main-chain torsional angle pairs to fall in the α-helical region of the Ramachandran map (Methods).

Figure 4.3 displays cumulative averages of the resulting "helicities" (fractions of α-helical conformations), at 300 K, with respect to simulation length. The helicities converge slowly toward time-independent averages, because they are proportional to the joint probabilities of all three angle pairs; nevertheless, the limiting values demonstrate certain consistent trends: The helical conformations are stabilized in all electrolyte solutions, relative to pure water. Even in the least well-equilibrated samples (2 M NaCl and 2 M NaI solutions) the limiting helicity values are much higher than the corresponding value of the pure water case, strongly supporting the conclusion that salts enhance helicity. Such differences are unlikely to disappear by prolonging the simulation.

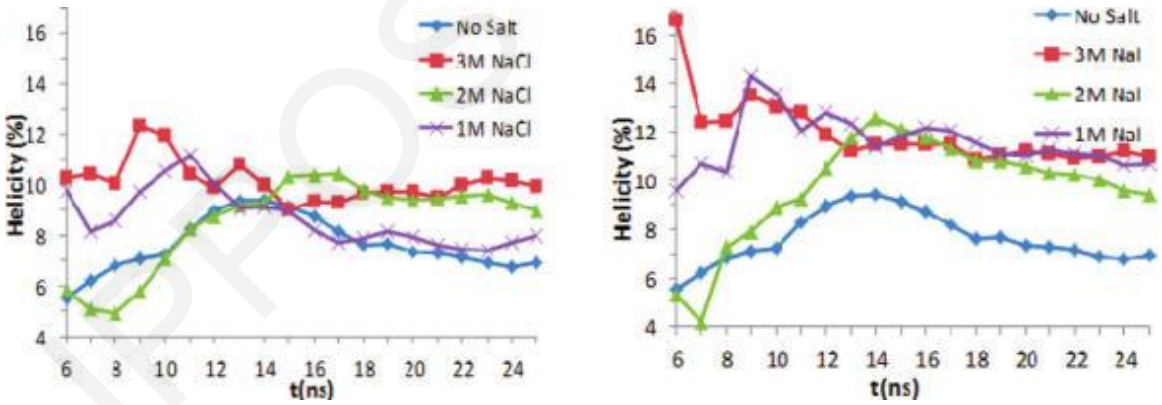

Figure 4.3: *Cumulative average helicity of the alanine tetrapeptide, plotted versus simulation time in (a) NaCl and (b) NaI solutions of various concentrations; pure-water results are also included.*

The cumulative average helicity in pure water was found roughly equal to 7%. This is reasonable, given our definition of average helicity, which requires all three residues to be in a helical conformation simultaneously. In the literature, experimental values of 20% for the second from the N-terminal alanine residue and 10% for the third from the N-terminal residue of tetraalanine have been measured, using a combination of spectroscopic methods [Woutersen et al., 2002; Schweitzer-Stenner et al., 2007]. Older simulation work has also

concluded that the helical conformation of the trialanine may be less than 10% [Gnanakaran and Garcia, 2003], although experiment suggests values closer to 20% [Schweitzer-Stenner et al., 2007].

Even though the average helicities decrease (almost linearly) with temperature, this stabilization persists in the entire temperature range (290 - 390 K) of the simulations. This is shown in Figure 4.4, where the temperature dependence of the average helicities is displayed. Near 300 K, the helicities increase with salt concentration; beyond ~320 K, they become independent of electrolyte type and concentration.

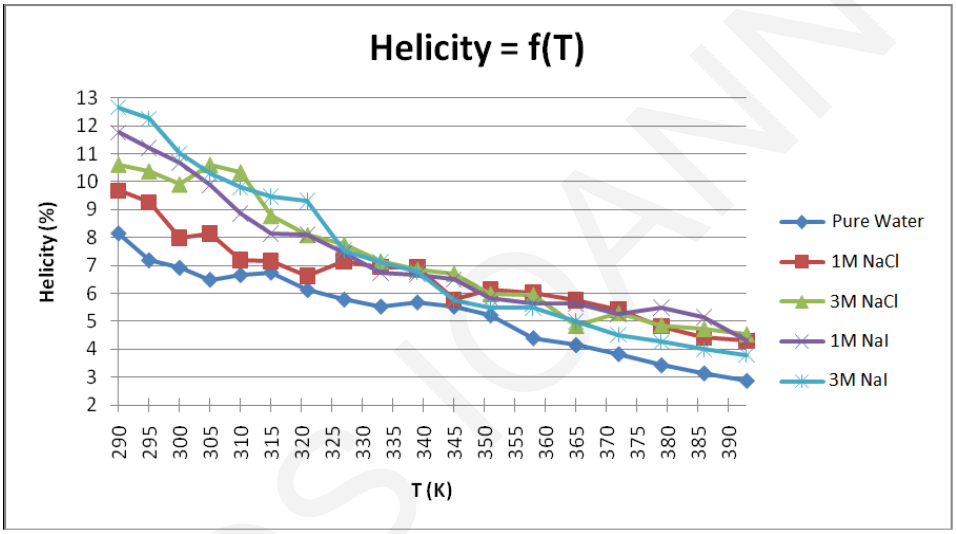

***Figure 4.4**: Percent of helical conformations of the alanine tetrapeptide as a function of temperature for pure water and 1 M and 3 M NaCl and NaI*

Recent studies [Dzubiella, 2008; Dzubiella, 2009; Asciutto et al., 2010] and the present work suggest that the peptide conformational stability is determined by a complex balance of energetic and entropic factors, which depend on the solution (salt type and concentration), the peptide composition, and its length. The peptides of our study have simpler sequences and significantly shorter lengths, compared to the systems studied by Dzubiella and Asciutto [Dzubiella, 2008; Dzubiella, 2009; Asciutto et al., 2010]. We also observe enhanced iodide affinities for the side chain and terminal blocking methyl groups, and pronounced sodium-carbonyl interactions in the presence of iodide, both in the dipeptide (Figure 4.2a) and the tetrapeptide (below) solutions.

These interactions have only a small impact on the dipeptide conformation, as demonstrated by the small changes in the torsional angle probability maps (Figure 4.2),

presumably due to the small size of this system. In the case of the tetrapeptide, the enhanced interactions are accompanied by an increase in the α-helix population. Thus, the above-mentioned ion-peptide interactions alone cannot determine the conformational preferences of these model peptides.

Apart from the sequence and the composition of the solution, the simulation conformational properties of a peptide depend on the employed force fields. The CHARMM force field employed here is known to overstabilize helical conformations in peptides [Graf et al., 2007; Mu et al., 2003; Best et al., 2008; Best and Hummer, 2009; Verbaro et al., 2010; Hegefeld et al., 2010]. To investigate the extent of force-field dependencies in our results, we performed additional simulations with a recently modified version of the Amber all-atom force field (ff03*) [Best and Hummer, 2009], which reproduces the experimentally observed helical population of short, alanine-based peptides at 300 K. The water TIP3P model [Jorgensen et al., 1983; Neria et al., 1996] and ion parameters [Joung and Cheatham, 2008] were the same as in the CHARMM calculations. The resulting tetrapeptide helicities in pure water and a 3 M NaI solution were too low (~ 2-3%), to draw conclusions. We therefore studied the longer peptides Ace-Ala_8-NMe (Alanine nonapeptide) and Ace-$(AAQAA)_3$-NMe (hexadecapeptide). A detailed presentation of the results will appear in the next chapter, which examines salt effects on the conformational preferences of longer peptides. It suffices to state here that the nonapeptide helicity was increased in a 3 M NaI solution, relative to pure water (12.5% at 297 K, compared to 8.8%). This is in agreement with the prediction of the CHARMM22/CMAP [Fedorov et al., 2007; Mackerrell et al., 2004] force field for the (shorter) alanine tetrapeptide; by contrast, for the hexadecapeptide, the helicity was significantly decreased in a 3 M NaI solution, relative to pure water (11.6% and 18.7%, respectively, at 300 K). These results suggest that the helical stabilization by NaI is a more general phenomenon for short peptides, unrelated to the CHARMM force field. However, the same salt apparently destabilizes the helical conformation in longer peptides; additional comparisons of peptides with various lengths are needed to explain this result.

To obtain more insights on the helical stabilization observed here, we summarize in Table 4.2 the average peptide helicities and hydrogen-bond occupancies at 300 K, for all solutions. As expected, the helicities are correlated with the probabilities of the α-helical (*i*/*i*+4) hydrogen-bond. Interestingly, the ions also cause a notable increase in the

occupancies of other hydrogen-bonds. As with the helicity, this increase is monotonic with salt concentration in the NaCl solutions. Thus, the salts seem to promote the general stabilization of folded conformations for the tetrapeptide, via the strengthening of hydrogen-bonding interactions.

Table 4.2: *Average Helicities and Hydrogen-Bond Probabilities (%) for the Ala Tetrapeptide Solutions*[a]

		Hydrogen bond (%)			
System	**Helicity (%)**	***i,i*+4**	***i,i*+3**	***i,i*+2**	**Total hydrogen bond probability (%)**
Pure Water	6.9 ± 3.1	7.8 ± 3.4	6.8 ± 2.2	5.2 ± 1.2	19.8 ± 5.5
1 M NaCl	8.0 ± 2.0	9.3 ± 1.8	7.2 ± 1.6	5.8 ± 0.7	22.3 ± 5.5
2 M NaCl	9.0 ± 3.1	10.0 ± 2.9	9.0 ± 1.6	6.9 ± 1.5	25.9 ± 5.8
3 M NaCl	9.9 ± 2.6	11.7 ± 3.3	9.3 ± 1.9	7.1 ± 0.5	28.1 ± 5.1
1 M NaI	10.7 ± 2.0	11.3 ± 1.6	8.6 ± 0.5	6.9 ± 0.2	26.8 ± 2.8
2 M NaI	9.4 ± 4.1	10.7 ± 3.4	9.3 ± 1.9	5.5 ± 0.8	25.5 ± 6.8
3 M NaI	11.0 ± 1.4	12.1 ± 1.7	9.5 ± 1.5	5.6 ± 0.8	27.2 ± 3.7

[a] *The results are averaged over the last 20 ns of the simulations; standard deviations are computed by separating the trajectories into four blocks of 5 ns.*

This is also shown in Figure 4.5, which displays distance histograms of the *i*/*i*+4 hydrogen-bonding atom pair O_Y - H_{NT}. There are four distinguishable peaks at 2.2, 6.2, 8.5, and 10 Å. The conformations corresponding to these four peaks are similar across all solutions studied; in other words, we can state that in all solutions, peak 1 is mostly helical with some C_YO_Y - N_3H_{N3} β- turns, peak 2 has both β-turns, with C_YO_Y - N_3H_{N3} dominant, and so forth. Cluster analysis showed that the short-distance peak contains mainly helical conformations, or type-I β-turns involving the pair C_YO_Y - N_3H_{N3} (the respective probabilities are 77.5% and 15.4% in the 1 M NaCl solution). The peak at 6.2 Å contains mostly conformations with either type I β-turn, between C_YO_Y and N_3H_{N3} or C_1O_1 and N_TH_{NT} (respectively, 37.7% and 22.8% in 1 M NaCl). The broad peak around 8.5 Å and the peak at 10 Å contain extended conformations, without hydrogen bonds. In a fraction of the conformations contributing to these last two peaks, the main-chain dihedral angles adopt values near the PPII helix region. Table 4.3 contains the detailed results of the cluster analysis of the peaks of Figure 4.5. The presence of salt causes an increase in the first two peaks and a decrease in the last two peaks, in agreement with the increase in hydrogen-bonded structures, reported in Table 4.2.

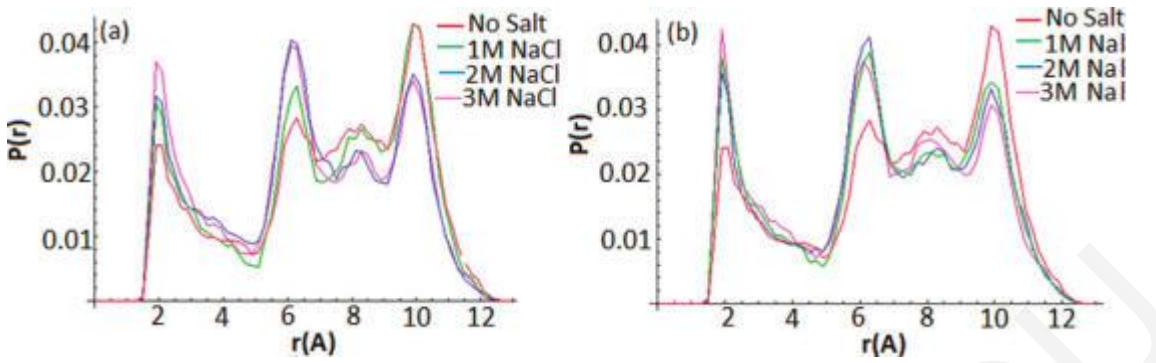

Figure 4.5: *Histograms of the tetrapeptide terminal atom pair distance O_Y - H_{NT} for (a) NaCl solutions, and (b) NaI solutions. The pure-water histogram is also included in both diagrams as a reference.*

Table 4.3: *Cluster analysis for the first and second peak of the rdf between OY and HNT for all simulated systems. Regions for cluster analysis: First peak 1.5-2.5 Å, second peak 5-7 Å.*

Solution	Peak	φ_1^o	ψ_1^o	φ_2^o	ψ_2^o	φ_3^o	ψ_3^o	%	Type
Pure Water	1	-65,3	-39,4	-77,0	-33,1	-71,9	-38,7	74,6	Helical
		-63,7	-37,5	-91,4	-16,0	-122,1	-4,4	16,6	β-turn Type I, CYOY-N3HN3
	2	-70,1	-33,2	-106,8	3,2	-88,1	147,3	28,4	β-turn Type I, CYOY-N3HN3
		-67,3	142,0	-66,6	-38,3	-106,9	4,8	9,0	β-turn Type I, C1O1-NTHNT
1 M NaCl	1	-65,5	-39,7	-76,2	-34,1	-71,2	-37,9	77,6	Helical
		-64,2	-36,5	-90,7	-16,9	-127,3	-4,6	16,1	β-turn Type I, CYOY-N3HN3
	2	-72,4	-32,3	-101,8	-2,5	-94,7	148,1	42,6	β-turn Type I, CYOY-N3HN3
		-101,1	145,0	-66,1	-39,6	-107,1	5,8	21,9	β-turn Type I, C1O1-NTHNT
2 M NaCl	1	-65,6	-40,2	-76,5	-33,7	-70,9	-38,6	76,6	Helical
		-63,6	-37,5	-93,1	-13,8	-117,2	-8,0	17,7	β-turn Type I, CYOY-N3HN3
	2	-71,1	-33,1	-102,1	-2,2	-93,4	148,6	40,7	β-turn Type I, CYOY-N3HN3
		-70,8	150,8	-69,2	-41,3	-107,2	-0,1	19,5	β-turn Type I, C1O1-NTHNT
3 M NaCl	1	-64,4	-40,1	-76,5	-33,8	-70,9	-38,7	73,8	Helical
		-63,5	-38,0	-92,4	-14,2	-119,6	-6,1	15,6	β-turn Type I, CYOY-N3HN3
	2	-69,2	-34,0	-107,0	4,3	-87,6	147,3	22,5	β-turn Type I, CYOY-N3HN3
		-65,4	127,3	-69,2	-37,0	-101,8	-2,5	33,8	β-turn Type I, C1O1-NTHNT
1 M NaI	1	-65,4	-39,8	-75,6	-34,0	-71,1	-38,8	81,8	Helical
		-62,6	-38,3	-92,4	-14,0	-121,2	-5,9	15,3	β-turn Type I, CYOY-N3HN3
	2	-71,3	-32,9	-102,5	-2,0	-92,6	149,9	37,5	β-turn Type I, CYOY-N3HN3
		-93,2	144,5	-67,8	-38,2	-102,6	-0,3	32,8	β-turn Type I, C1O1-NTHNT
2 M NaI	1	-65,8	-39,6	-75,3	-34,3	-70,6	-38,6	78,6	Helical
		-64,0	-37,0	-89.0	-19,3	-125,2	-1,5	11,9	β-turn Type I, CYOY-N3HN3
	2	-70,8	-33,1	-101,4	-2,7	-93,8	149,3	46,0	β-turn Type I, CYOY-N3HN3
		-85,0	144,7	-65,8	-39,4	-107,1	1,9	17,6	β-turn Type I, C1O1-NTHNT
3 M NaI	1	-65,4	-40,0	-74,9	-35,1	-69,8	-39,2	79,7	Helical
		-62,9	-38,0	-88,9	-17,7	-119,0	-5,9	14,6	β-turn Type I, CYOY-N3HN3
	2	-69,5	-34,6	-101,4	-3,0	-90,8	148,1	46,0	β-turn Type I, CYOY-N3HN3
		-86,3	144,2	-40,6	-20,2	-102,3	-3,3	25,0	β-turn Type I, C1O1-NTHNT

Figure 4.6 shows the joint probability distribution of the tetrapeptide backbone torsional angles in pure water, averaged over the three torsional angle pairs. The preferred conformations are found in five different regions of the Ramachandran plot, as in the case

of the dipeptide (Figure 4.1a): regions A ($\varphi = -160 \pm 10^{o}$, $\psi = 170 \pm 10^{o}$), B ($\varphi = -75 \pm 15^{o}$, $\psi = 160 \pm 15^{o}$), C ($\varphi = -75 \pm 15^{o}$, $\psi = -45 \pm 15^{o}$), D ($\varphi = -110 \pm 15^{o}$, $\psi = 0 \pm 15^{o}$), and a less-occupied region E ($\varphi = 65 \pm 15^{o}$, $\psi = 50 \pm 15^{o}$). While regions A and B correspond to extended peptide conformations (respectively, β-sheets and polyproline II in a protein), and C and D correspond to compact, folded peptide conformations (in a protein these would be right-handed α-helices), the less frequently occupied region E corresponds to left-handed helical conformations [Yu et al., 2010].

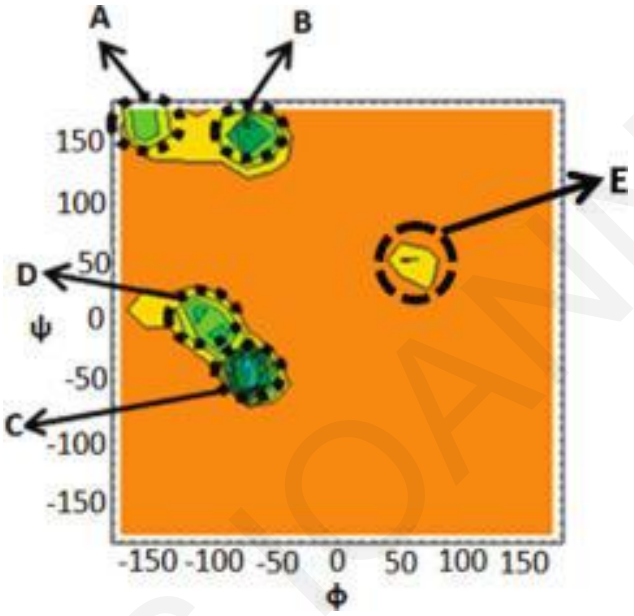

Figure 4.6: *Ramachandran map, displaying the probability distribution of the tetrapeptide main-chain torsional angles φ,ψ in pure water at 300 K; the probability is averaged over the three torsional pairs. Color code is as in Figure 4.1a.*

Figure 4.7 plots the corresponding probability differences (3 M electrolyte solution vs pure water), averaged over the three torsional angle pairs. The addition of NaCl causes a decrease of the probabilities in the extended conformation regions A and B, and an increase in the α-helical regions C and D. This behavior is in agreement with the increased tetrapeptide helicity in electrolyte solutions reported in Table 4.2. In the case of NaI, the increase of the probability maxima in regions C and D is more pronounced, in line with the larger observed helicity.

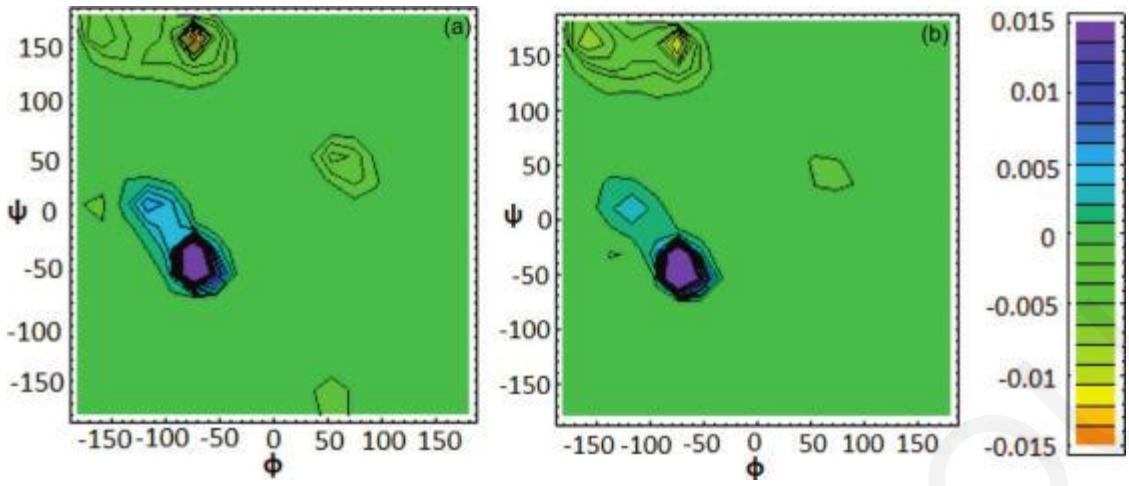

Figure 4.7: *Difference (salt vs pure water) maps of the two-dimensional probabilities for the tetrapeptide main-chain torsional angles; the probabilities are averaged over the three torsional angle pairs: (a) 3 M NaCl solution; (b) 3 M NaI solution. A color code is provided.*

There appears to be a difference in the salt effects on internal dipeptide (increasing PP-II) and tetrapeptide (decreasing PP-II, increasing helical) conformations. This could be partly explained by the fact that the tetrapeptide can form three internal hydrogen bonds (*i*/*i*+2, *i*/*i*+3, *i*/*i*+4), compared to a single hydrogen bond (*i*/*i*+2) for the dipeptide; the occupancies of these bonds are increased by salt, promoting the helical conformations in the larger peptide (see Table 4.2).

To obtain microscopic insights about the observed helicity changes, we analyzed the various rdf's; selected functions are discussed below. The rdf curves of the anion (Cl^- or I^-) - amide pairs are displayed in Figure 4.8, averaged over the tetrapeptide amide groups. The contact peak of the chloride rdf is not sensitive to concentration and is in fact much lower than unity, showing that this anion is excluded from the vicinity of the amide group; this was also observed in the dipeptide simulations. In the case of iodide, the contact peaks are higher. Furthermore, all of the rdf curves (up to 10 Å) increase considerably with concentration. Thus, iodide interacts more strongly with the peptide group, and this interaction increases with salt concentration.

Sodium has a strong affinity for the peptide carbonyl groups as shown by the pronounced first solvation peaks of the corresponding rdf in Figure 4.9. This affinity is enhanced in NaI, relative to NaCl solutions. We believe that this is related to the higher simultaneous affinity of iodide for the peptide methyl groups, as also observed in the dipeptide simulations (Figure 4.2) and elsewhere [Dzubiella, 2008; Dzubiella, 2009; Heyda al.,

2010]. Nevertheless, it is accompanied by an increase in helicity for the tetrapeptide vs no effects for the dipeptide, reflecting the insufficiency of these interactions to account entirely for the conformational preferences of the peptide. This is further analyzed below.

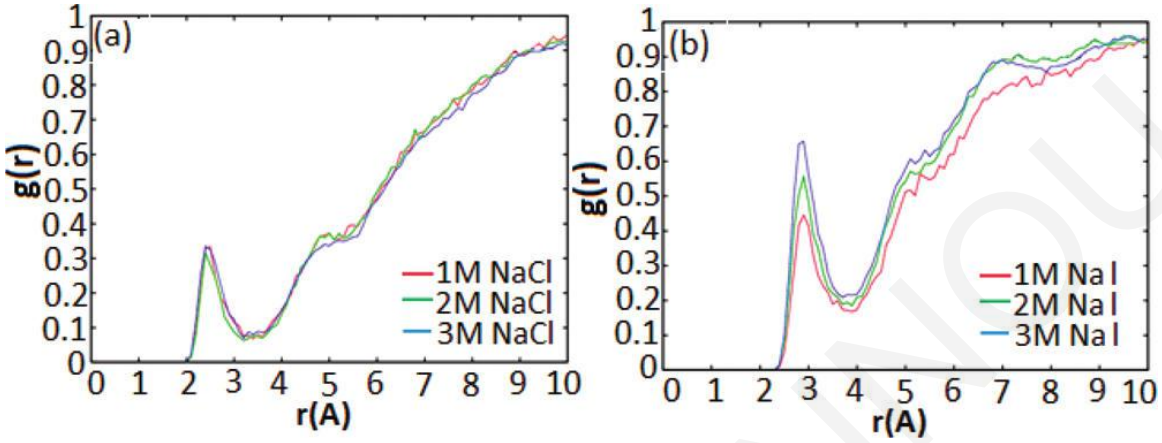

Figure 4.8: *Anion-amide hydrogen rdf's for (a) NaCl solutions of various concentrations, and (b) NaI solutions of various concentrations.*

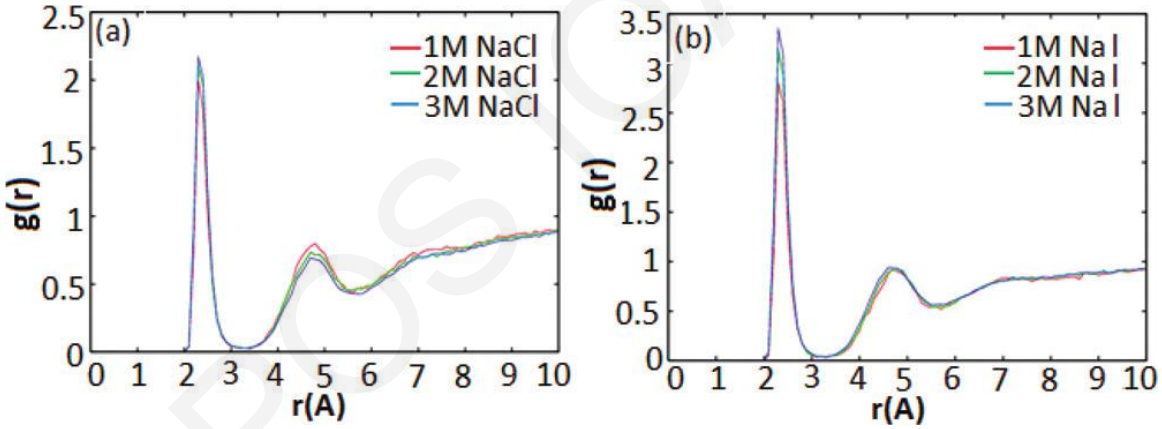

Figure 4.9: *Sodium-carbonyl oxygen rdf's for (a) NaCl solutions and (b) NaI solutions.*

Figure 4.10 displays the rdf functions between the anions and the side-chain methyl groups. As in the case of the dipeptide (Figure 4.2c), Cl^- actually avoids the methyl groups, and an increase in NaCl concentration does not enhance the weak interaction between Cl^- and the side chain carbon; I^-, in contrast, has a stronger interaction with the methyl carbons, which increases with NaI concentration (the first rdf peaks are actually a little larger than unity, indicating a preference for the side group region by 0.1-0.2 kcal/mol). These findings are in agreement with the behavior of the anions toward the hydrophobic groups of the dipeptide (Figure 4.2c) and other works [Fedorov et al., 2007; Dzubiella, 2008, Dzubiella, 2009]. Table 4.4 contains pair interaction energies between the ions,

water, and various peptide groups. The calculated H-bond energy between water molecues is smaller than the generally expected value of about 5.0 kcal/mol.

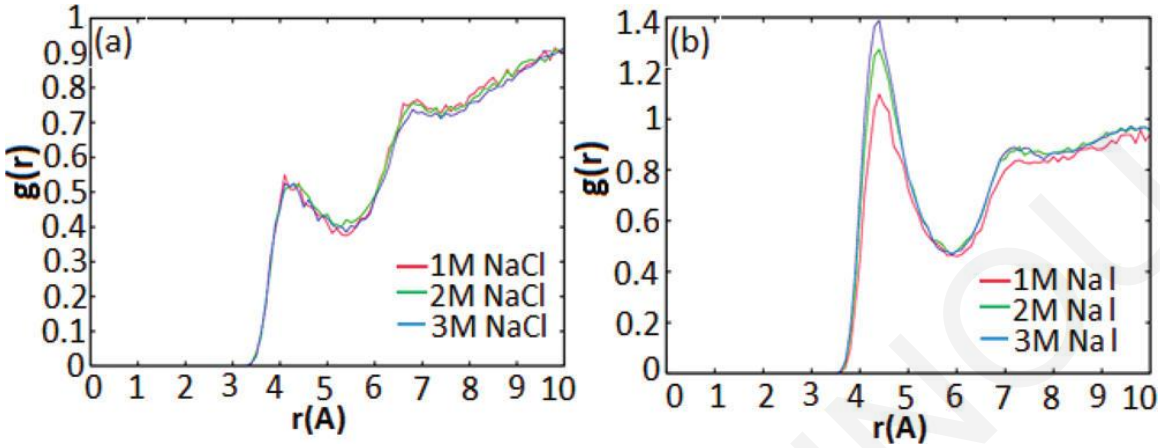

Figure 4.10: *Anion-peptide side-chain methyl rdf's for (a) NaCl solutions and (b) NaI solutions.*

Table 4.4: *Average pair interaction energies (in kcal/mol) between ions, water and various peptide groups.*

	water-water	Na-water	Anion-water	Anion-NH	Anion-CB	Na-CO	Water-NH	Water-CO
0 M	-1.19						-2.29	-3.90
1 M NaCl	-0.95	-22.73	-12.78	-6.64	-0.81	-24.08	-2.27	-3.84
3 M NaCl	-0.73	-22.29	-12.55	-6.72	-0.80	-24.09	-2.25	-3.80
1 M NaI	-0.95	-22.85	-9.75	-4.91	-0.73	-23.97	-2.25	-3.78
3 M NaI	-0.65	-22.65	-9.50	-4.91	-0.67	-23.91	-2.21	-3.66

An interesting question is whether the ions lead to dehydration of the peptide. This has been proposed as a plausible reason for the enhanced helicities in related systems [Asciutto, 2010]. To examine this question, in Figure 4.11 we compare the rdf's between water and the amide or carbonyl groups in the presence of electrolytes. In all curves, the contact peaks are insensitive to the presence of ions. A small increase of the second solvation peak with salt concentration is observed (more clearly for NaI solutions), suggesting that the density of water at some distance from the peptide increases slightly when salt is present. We speculate that this result is related to the enhanced ion-water interaction in the region beyond the first solvation shell, discussed with reference to Table 4.6 below.

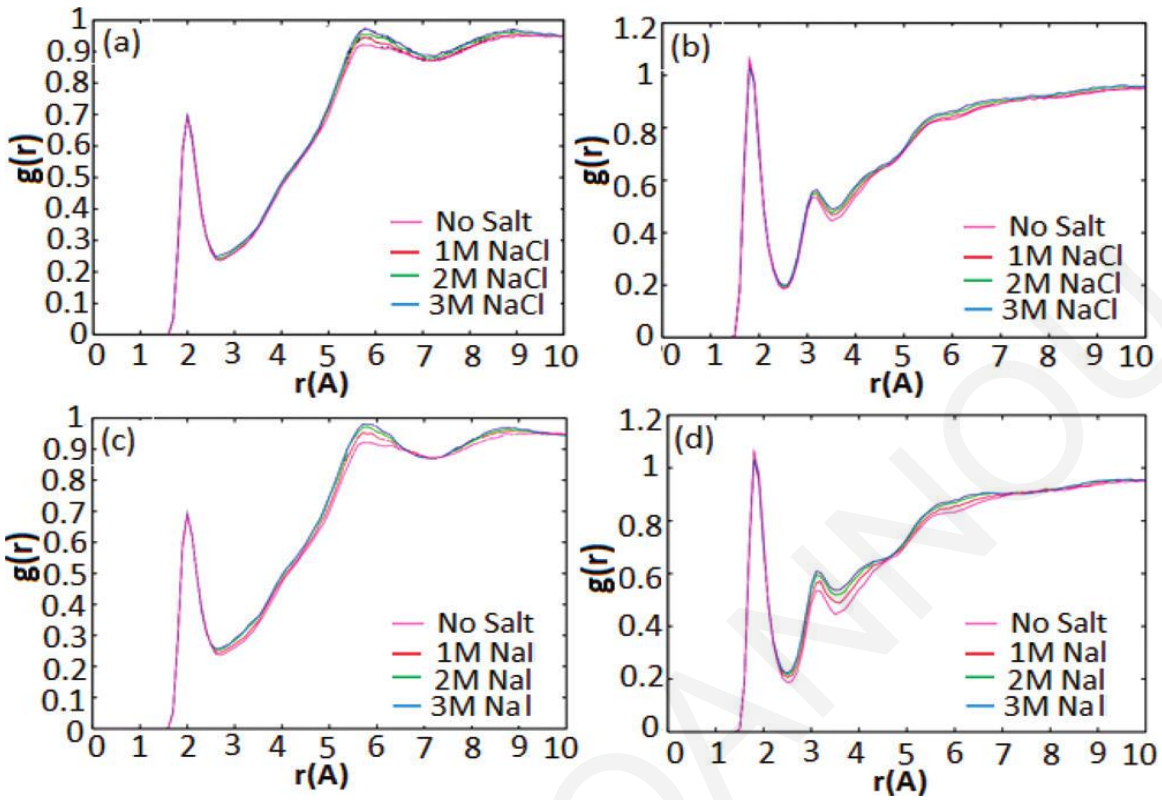

Figure 4.11: *Peptide-water rdf's. (a,c) Water oxygen-amide hydrogens and (b,d) water hydrogen-carbonyl oxygens. Top plots: NaCl solutions. Bottom plots: NaI solutions.*

The ion-water rdf's are shown in Figure 4.12. The water oxygen-sodium ion rdf and the water hydrogen-anion rdf are largely insensitive to salt concentration and type. The important feature of these plots is that the contact peak is much higher than unity, in contrast to the results of Figure 4.11. It is clear therefore that water prefers to interact with the ions rather than with the peptide groups.

To obtain further insights on the factors contributing to the tetrapeptide conformational preferences, we split the simulation system into peptide ("P"), ion ("I"), and water ("W") components. We computed total interaction energies among all possible combinations of component pairs. These energies were averaged separately for (a) "closed" peptide conformations (with an i/i+4 hydrogen bond), and (b) completely extended conformations (without any intramolecular hydrogen bonds). Selected terms are reported in Table 4.5.

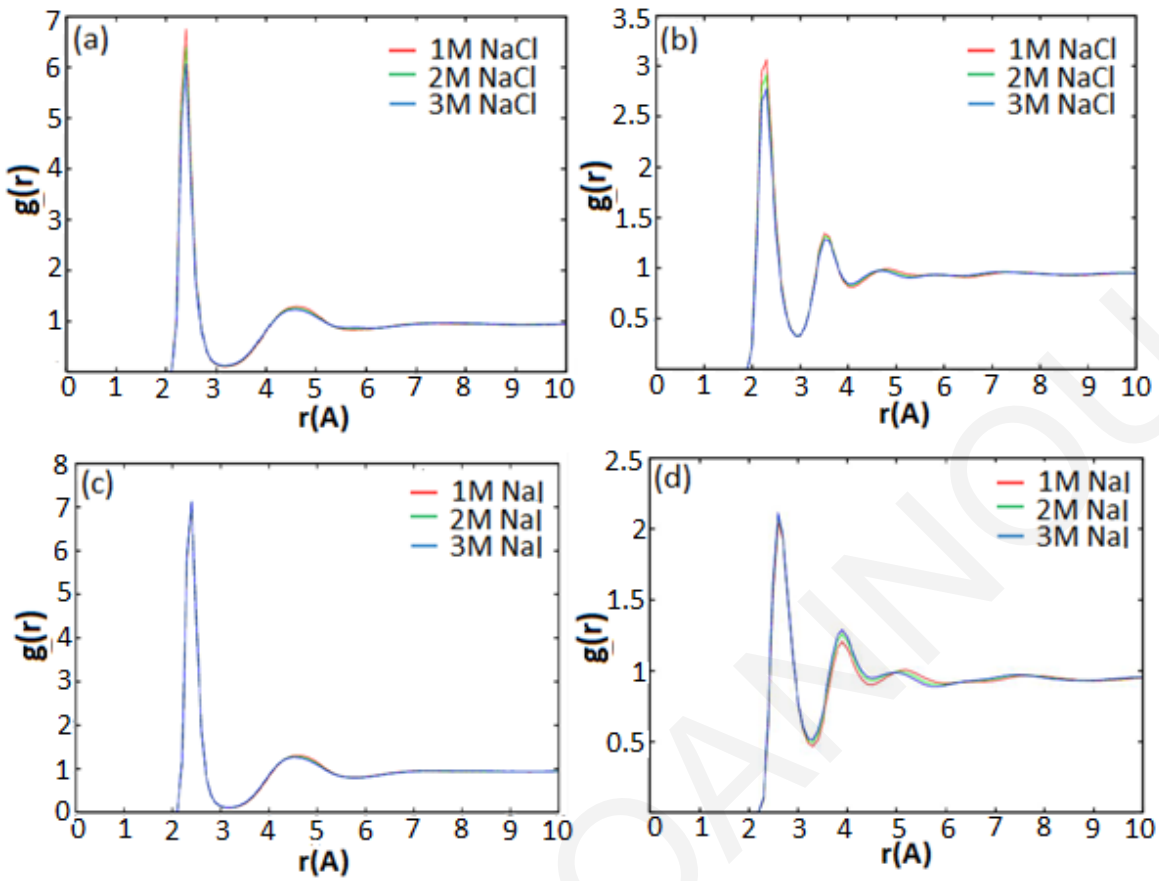

***Figure 4.12**: Water-Ion rdf's. (a,c) Water oxygen - sodium and (b,d) water hydrogen - anion. Top plots: NaCl solutions. Bottom plots: NaI solutions.*

The present analysis aims to investigate whether certain energy terms decrease with salt concentration, in the presence of helical conformations, in accordance with the observed increase in the tetrapeptide helicity (Table 4.2). It should be noted that the observed impact of salt on helicity is small, corresponding to a sub-kcal/mol decrease in the free energy of the helical conformations. On the other hand, the changes in various energetic averages [among helical ("closed") and extended conformations], reported in Table 4.5, are on the order of 10^1 - 10^2 kcal/mol. Thus, it is difficult to attribute the helicity enhancement to a specific energy term. Furthermore, this analysis strongly emphasizes energy, while it can be argued that entropy considerations are equally important. As we explain below, our results suggest that entropic contributions are also important, even though they are not analyzed here in detail.

Table 4.5: *Average Intermolecular Energies (in kcal/mol) between All Important Components of the Tetrapeptide Salt Solutions, for Closed and Extended Conformations*

Energy components[a]												
solution	total	E_{PP}	E_{PW}	E_{PI}	E_{IW}	E_{II}	E_{WW}	$E_{PP}+E_{PW}+E_{PI}$	$E_{PI}+E_{IW}+E_{II}$	$E_{WW}+E_{WI}$	$E_{WI}+E_{II}$	$E_{WW}+E_{WI}+E_{II}$
Pure water												
closed[b]	-10385	45					-10335	-50		-10335		
extended[b]	-10391	50					-10341	-50		-10441		
difference	-6	-5					-6	0		-6		
1 M NaI												
closed[b]	-14070	45	-82	-16	-6021	-432	-7564	-53	-6469	-13585	-6453	-14017
extended[b]	-14066	50	-87	-16	-6028	-428	-7557	-53	-6972	-13585	-6456	-14013
difference	+4	+5	-5	0	-7	+4	+7	0	-3	0	-3	+4
1 M NaCl												
closed[b]	-14422	45	-85	-12	-5956	-773	-7641	-52	-6741	-13597	-6729	-14370
extended[b]	-14418	50	-90	-11	-5934	-783	-7650	-51	-6728	-13584	-6717	-14367
difference	+4	+5	-5	+1	+18	-10	-9	+1	+13	+13	+12	+3
2 M NaI												
closed[b]	-17677	45	-69	-31	-10554	-1627	-5441	-55	-12212	-15995	-12181	-17722
extended[b]	-17684	50	-75	-30	-10578	-1618	-5433	-55	-12226	-16011	-12196	-17629
difference	-7	+5	-6	+1	-24	+9	+8	0	-14	-16	-15	-7
2 M NaCl												
closed[b]	-18381	45	-77	-21	-9678	-2693	-5957	-53	-12392	-15635	-12371	-18328
extended[b]	-18384	50	-82	-21	-9680	-2695	-5957	-53	-12395	-15637	-12374	-18331
difference	-3	+5	-5	0	-2	-2	0	0	-3	-2	-3	-3
3 M NaI												
closed[b]	-20278	45	-60	-42	-12985	-2940	-4296	-57	-15967	-17281	-15925	-20221
extended[b]	-20282	51	-65	-43	-13038	-2915	-4272	-57	-15996	-17310	-15953	-20225
difference	-4	+6	-5	-1	-53	+25	+24	0	-29	-29	-28	-4
3 M NaCl												
closed[b]	-21219	45	-74	-25	-11291	-4651	-5223	-54	-15967	-16514	-15942	-21165
extended[b]	-21234	50	-77	-27	-11358	-4623	-5199	-54	-16008	-16557	-15981	-21180
difference	-15	+5	-3	-2	-67	+28	+24	0	-41	-43	-39	-15

[a] *"P", "I" and "W" denote, respectively, peptide, ion, and water terms; for example, EPP is the total intramolecular peptide energy; EIP is the total ion_peptide energy. b Entries "closed" and "extended" denote tetrapeptide conformations with an i/i+4 hydrogen bond, or without any intramolecular hydrogen bond.*

For each solution, the Table separately reports component energies, averaged over snapshots with "closed" (helical) conformations of the peptide, and "extended" conformations. The difference in averages (extended vs closed) is also included. Column 2 contains the total energy of the solution. Columns 3-8 contain the interactions for the various combinations of component pairs. For example, column "E_{PP}" contains peptide intramolecular interactions; column "E_{II}" contains the sum of all anion-anion, anion-cation, and cation-cation interactions. In the next several columns, we further group the

interactions together. For example, the column marked "$E_{PP}+E_{PI}+E_{PW}$" contains all the interactions that involve peptide groups, and the one marked "$E_{PI}+E_{IW}+E_{II}$" contains all interactions involving ions. The purpose of the above groupings is to identify consistent trends in the energy differences (values near zero, negative or positive) between extended and helical conformations, which might help interpret the peptide preferences toward the former or the latter.

The total energies are reported in the second column. In pure water, they are slightly more negative (by 6 kcal/mol) when the tetrapeptide conformation is extended, due to the E_{WW} term (see below). At low salt concentrations (1 M NaI and 1 M NaCl), they become more negative with helical conformations. This change correlates nicely with the helix stabilization due to salt, but is not consistently observed at higher concentrations: at 2 M NaI and 3 M NaCl, the energies are more negative for extended conformations (respectively, by -7 and -15 kcal/mol).

It can be argued that these energy differences are results of subtractions of large numbers, and therefore they are not statistically significant. It turns out that the standard deviations of energy terms, such as E_{WW}, E_{IW}, or E_{II} (as calculated from block-averaging of trajectories every 5 ns) are surprisingly small (e.g., in the 3 M NaCl system we find that E_{WW} = -5223 ± 10 kcal/mol and E_{II} = -4651 ± 12 kcal/mol). Some of the total energy differences between extended and helical conformations reported above are comparable to these standard deviations and therefore cannot be used to establish energetic trends; however, other energy differences are meaningful. As analyzed below, individual energy components change more consistently across solutions.

Intramolecular peptide-peptide interactions (E_{PP}) are constant across solutions, reflecting the insensitivity of helical (closed) and extended conformations to the composition of the solution. These terms stabilize the helical conformations by ∼5 kcal/mol, due to the approach of the N-terminal carbonyl and C-terminal amide groups and the formation of the *i*/*i*+4 hydrogen bond. Peptide-water interactions (E_{PW}) become less favorable (less negative) with an increase in salt concentration and anion size. This can be attributed to a competition between peptide-water and peptide-ion interactions, which is indicated by the approximately constant value of the combined term $E_{PW}+E_{PI}$ (ca. -100 kcal/mol); despite their dependence on electrolyte type and concentration, the terms E_{PW} are consistently

more negative by ~5 kcal/mol in extended conformations, due to increased exposure of the peptide groups to solvent; thus, the contributions from E_{PW} and E_{PP} cancel almost exactly in the energy difference (extended vs closed).

Ion-peptide interactions (E_{PI}) become more negative with salt concentration and anion size, in accordance with the more pronounced iodide affinities for the alanine methyl groups and sodium affinities for the peptide carbonyl group. Interestingly, these terms are not sensitive to the peptide conformation! As a result, the total sum of peptide-related energy terms ($E_{PP}+E_{PW}+E_{PI}$) is fairly constant. The remaining sum, $E_{WW}+E_{WI}+E_{II}$, is more negative for extended peptide conformations in the 2 and 3 M salt solutions. The change in this sum (extended vs closed) is dominated by the contribution from the ion-water term (E_{IW}), which is anticorrelated with the contributions from the two other terms (E_{WW} and E_{II}), and approximately twice as large in absolute value.

The above analysis shows that the total sum of peptide-related energy components ($E_{PP}+E_{PW}+E_{PI}$ sum in the ninth column) is not the determining factor for the peptide conformational properties. This somewhat surprising result further supports our earlier conclusion, that the enhanced sodium-carbonyl interactions are not solely responsible for the changes in oligopeptide helical stabilities. In most solutions, the total energy is more negative for extended peptide conformations, mainly due to the E_{IW} term. These observations do not explain our salt-induced stabilization of helical conformations, but together suggest that entropic contributions (due to solvent, salt, and peptide) are also important determining factors; accurate computation of entropic contributions is a difficult task [Kuffel and Zielkiewicz, 2008] and will not be attempted in this thesis.

To probe more deeply the origin of the more negative E_{IW} values with extended peptide conformations, we partitioned the simulation box into two subregions: one region (A) containing ions and water within 5.5 Å from any peptide group, and a second region (B) containing the rest of the solution. In Table 4.6 we decompose the total E_{IW} term into four contributions $E_{IA\text{-}WA}$, $E_{IA\text{-}WB}$, $E_{IB\text{-}WA}$, and $E_{IB\text{-}WB}$; each term $E_{IX\text{-}WY}$ corresponds to the interactions between ions in region X and water in region Y (X, Y = A or B). For each simulation snapshot, we divided the total values by the total number of ion-water pairs; the resulting normalized values were averaged over the simulation trajectories; the final values are reported in the Table.

Table 4.6: *Average Ion-Water Pair Interaction Energies (in kcal/mol) between Ions and Water in Two Regions near and Away from the Peptide*

Solution							
Interaction[a]	Peptide conformation[b]	3 M NaI	2 M NaI	1 M NaI	3 M NaCl	2 M NaCl	1 M NaCl
E_{IA-WA}	closed	-0.8846	-0.8969	-0.8946	-0.8596	-0.9112	-0.9139
	extended	-0.8171	-0.8369	-0.8601	-0.8010	-0.8378	-0.8749
E_{IA-WB}	closed	-0.0421	-0.0497	-0.0595	-0.0419	-0.0477	-0.0582
	extended	-0.0424	-0.0493	-0.0587	-0.0408	-0.0480	-0.0575
E_{IB-WB}	closed	-0.1148	-0.1273	-0.1453	-0.0993	-0.1164	-0.1434
	extended	-0.1158	-0.1283	-0.1463	-0.1003	-0.1170	-0.1438
E_{IB-WA}	closed	-0.0329	-0.0399	-0.0488	-0.0283	-0.0349	-0.0475
	extended	-0.0336	-0.0393	-0.0479	-0.0287	-0.0347	-0.0462

[a] *EIX⁻WY denotes pair interactions between ions in region X and water in region Y (X, Y = A, B); regions A and B are defined in the text.* [b] *Entries "closed" and "extended" denote tetrapeptide conformations with an i/i+4 hydrogen bond, or without any intramolecular hydrogen bond.*

The strongest average ion-water pair interactions are observed in region A, due to the smaller volume of this region and the reduced ion-water distances. Ion-water interactions in this region are stronger when the peptide assumes hydrogen-bonded conformations, presumably due to a reduction in the solvent and ion accessibility of the peptide groups. On the contrary, in region B the ion-water pairwise interactions are slightly more negative for extended peptide conformations. Since the number of ion-water pairs in region B is orders of magnitude higher than that in region A, the total energy term E_{IW} slightly favors the extended conformations (as is indeed observed in the simulations), but less so in the presence of salts. In conclusion, the more negative E_{IW} values of Table 4.5 are due to improved ion-water interactions outside the peptide first hydration shell.

4.4 Conclusions and Perspective

In our investigation of salt effects on the conformations of an alanine dipeptide, we found that the "intrinsic" conformational states of the backbone, as described by Ramachandran maps, are not greatly affected even by large concentrations of NaCl and NaI. Apparently, the intrinsic tendencies of the backbone in such a small molecule are too strong to be affected by environmental factors, a fact also mentioned by Feig [Feig, 2008]. In the case of an alanine tetrapeptide, however, the Ramachandran maps show an increased tendency for more compact conformations in the presence of salts. Cl^- ions prefer to stay away from the peptides, while I^- ions have a preferential interaction with the hydrophobic methyl groups. This preference is not a result of enhanced pairwise methyl-iodide with respect to

water-iodide interactions, as is revealed in Table 4.4, hence it must be of entropic origin. Na^+ ions on the other hand have a significant affinity for the carbonyl groups with a strong enthalpic component (Table 4.4), a fact observed in several other recent investigations as well [Fedorov et al., 2007; Asciutto et al., 2010].

The tetrapeptide simulations were quite insightful, since they allowed the examination of the salt effect on the tendency for adoption of compact conformations. The helicity is enhanced in the presence of salts, with NaI being more effective. This tendency decreases with increasing temperature, as found experimentally [Shalongo et al., 1994] and computationally [Best et al., 2008] in related systems. Our finding that helicity is enhanced by salts was associated here with a concomitant increase in the formation probabilities of the α-helical hydrogen bond (*i*/*i*+4), and other hydrogen bonds (*i*/*i*+3, *i*/*i*+2). It was corroborated by examining slightly longer peptides with the AMBER force-field [Best and Hummer, 2009]. It is thus not a force-field artifact. At first glance, this finding appears to disagree with the results of Dzubiella [Dzubiella, 2008], who found that salts lead to a significant decrease of helicity of a dodecapeptide. However, it must be stressed that helicity is defined in a very narrow way for a short tetrapeptide, since there is only the possibility for a single "turn" and the formation of a terminal H-bond. In addition, Dzubiella used oligopeptides containing charged residues. In the following chapters by using the AMBER force-field [Best and Hummer, 2009], we were able to show that much longer peptides, comparable to those of Dzubiella [Dzubiella, 2008; Dzubiella, 2009], or of Asciutto et al. [Asciutto et al., 2010] do in fact behave in an opposite way: they show decreased helicity in the presence of electrolytes. We were able to show that the enhanced helicity is not due to stronger ion-peptide interaction, or to a difference in the hydration of the peptide in the presence of ions. The detailed analysis in Tables 4.5 and 4.6 points out that the stabilization of helical conformations coexists with enhanced ion-water interactions outside the first hydration shell of the peptide. This intriguing finding in turn suggests that the stabilization may have a significant entropic component. It is interesting to examine whether this tendency of stabilization of the primary helical fold in the presence of electrolytes still holds for larger peptides. This is the focus of the work which is presented in the next chapter.

5. Impact of Sodium Salts on the Helix-Coil Equilibrium of the model peptide $(AAQAA)_3$

5.1 Introduction

To investigate ionic effects on the stability of the α-helix secondary-structural motif and the helix/coil equilibrium, we have conducted simulations of the model neutral peptide Ac–$(AAQAA)_3$–NMe in pure water and a range of aqueous NaCl and NaI solutions. Experimental studies have shown that a related peptide adopts an α-helical conformation in NaCl solutions, with stability (average helicity) that depends on the ionic strength of the solution [Scholtz et al., 1991; Shalongo et al., 1994; Smith and Scholz, 1998]. The peptide has been employed in several computational studies of the helix/coil equilibrium in implicit and explicit solvent, but not in the presence of salts [Shirley and Brooks, 1997; Ferrara et al., 2000; Gnanakaran and Garcia, 2005; Best and Hummer, 2009; Best and Mittal, 2010]. With the use of this neutral peptide it was possible to remove charge-charge electrostatic effects on the helix stability, and focus on the salting-in and salting–out interactions of the solution ions with the peptide polar and nonpolar groups.

5.2 Methods

5.2.1 Investigated Systems

The peptide studied has the sequence Ac-$(AAQAA)_3$-NMe (Scheme 5.1), with Ac ($C_LH_3C_{LP}O_L$) and NMe ($N_RH_RC_RH_3$), respectively, denoting the N- and C- terminal blocking groups, and A, Q denoting alanine and glutamine. Each simulation system consisted of a single model peptide placed in an octahedral box of water molecules and an appropriate number of ions, chosen to model the desired salt concentration. Table 5.1 lists the total number of ions, water molecules and water-box sizes for the various peptide simulations. Although the actual salt concentrations are those listed in the Table, for simplicity we will designate them as “1 M” or “3 M” concentrations in the ensuing discussion.

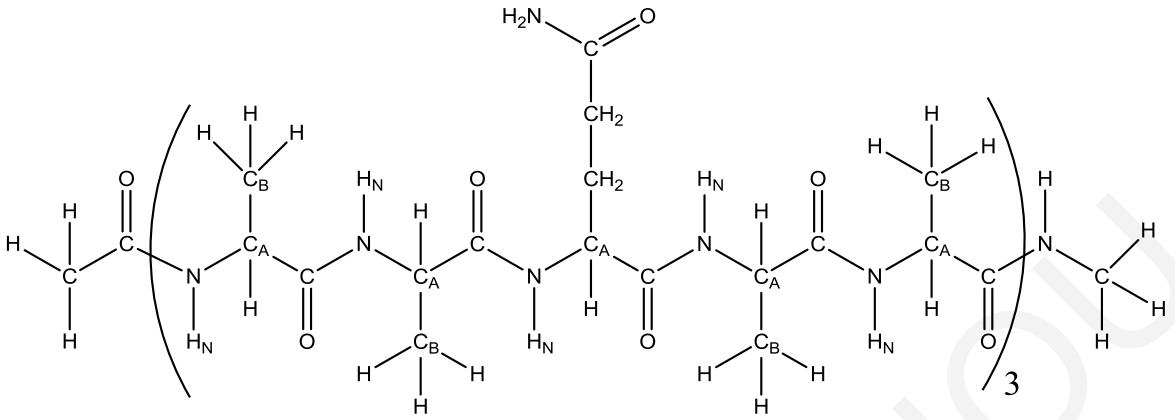

Scheme 5.1: *The peptide used in the Present Investigation Ac-(AAQAA)$_3$-NMe.*

5.2.2 Force Field and Simulation Protocol

The peptide atomic charges, van der Waals, and stereochemical parameters were taken from the AMBER 11 all-atom force field [Case et al., 2010]. The water was represented by a modified TIP3P model [Jorgensen et al., 1983; Neria et al., 1996]. Ion parameters, recently optimized for high-concentration simulations, were taken from Joung and Cheatham [Joung and Cheatham, 2008].

Table 5.1: *Water box sizes and numbers of ions and water molecules employed in the Simulations*

solution	# waters	# cations	# anions	box length / Å
		$(AAQAA)_3$		
0 M	2623	0	0	47.32
1.1 M NaCl	2524	54	54	46.92
3.2 M NaCl	2491	160	160	47.38
1.1 M NaI	2557	54	54	47.60
3.0 M NaI	2556	160	160	49.04

All simulations were conducted with the AMBER 11 simulation package [Case et al., 2010], and the ff03* force field [Best and Hummer, 2009]. Starting from a helical conformation, the peptide was first minimized, heated up gradually from 0 to 300 K six 30-ps stages (every 50 K) and then subjected to a 50-ns production simulation at 300 K in vacuum. From the 50 ns MD simulation we identified the structure with the lowest energy and solvated it in a truncated octahedron simulation cell with the appropriate number of

TIP3P water molecules and ions, chosen to model the desired salt concentration. We minimized the system in two stages. In the first stage we kept the peptide fixed and just minimized the positions of the water molecules and ions. In the second stage we minimized the entire system. Next, we heated up the entire system from 0 to 300 K by a 20-ps MD run at constant volume with weak restraints on the peptide; we then switched off the restraints, and ran a 1 ns equilibration at 300 K under constant-pressure conditions. Using the average cell size of the previous run, we conducted 0.5 ns simulation runs at constant volume for temperatures in the range T = 280 – 520 K, with 20 K intervals. We used the mean potential energies and temperatures of these simulations and the method of Sugita and Okamoto [Sugita and Okamoto, 1999] to calculate optimal temperatures for replica-exchange runs, targeting an exchange probability between neighboring replicas of ~18 %. Finally, we employed 48 replicas, spanning a temperature range T = 293.2 – 520.6 K.

The REMD runs were done at constant-volume conditions with a 2-fs time step, and had a total length of 1.44 μs (30 ns per replica). The initial conformation used for the replica runs was unfolded (taken from the 520 K run). Replica exchange attempts were made every 1 ps; the obtained exchange probabilities were 16 - 18 %. All replicas performed random walks in the temperature space, spanning several times the entire range of temperatures. Long-range electrostatics were calculated using particle-mesh Ewald method, with a 0.99 Å grid spacing and a 9-Å cutoff. Chirality restraints were used on the peptide bond, to ensure that no trans – cis conformational changes at the highest temperatures of the REMD runs.

5.2.3 Secondary Structure Calculations and Conformational Analysis

We computed the Ac-$(AAQAA)_3$-NMe peptide "helicity" (the fraction of α-helical conformations), using the Lifson-Roig (LR) model [Lifson and Roig, 1961], as in the previous analysis of the alanine dipeptide and tetrapeptide (chapter 4). In the LR definition, a residue *i* is considered α-helical if and only if its backbone torsional angles (φ_i, ψ_i), and the pairs (φ_{i-1}, ψ_{i-1}) and (φ_{i+1}, ψ_{i+1}) of the adjacent residues fall in the α-helical region of the Ramachandran map ($\varphi = -65 \pm 35^o$, $\psi = -37 \pm 30^o$). A helical segment is defined to contain at least two successive residues in helical conformation. A single residue in helical

conformation between residues in coil conformation is not counted as a helical segment. The average number of helical hydrogen bonds $<n_H>$ and helical segments $<n_S>$ was computed from the analysis of the simulation data. By fitting these values to equation (Eq. 5.1) below we deduced the LR parameters w and u [see section 2.5].

$$< n_H >= \frac{1}{n-2}\frac{w}{Z}.\frac{dZ}{dw} \qquad (b)\ < n_S >= \frac{v}{Z}.\frac{dZ}{dv_{12}} \qquad \text{(Eq. 5.1)}$$

with the partition function Z given by the following expression:

$$Z = (001)M^n \begin{pmatrix} 0 \\ 1 \\ 1 \end{pmatrix} \text{ with } M = \begin{pmatrix} w & v & 0 \\ 0 & 0 & 1 \\ v & v & 1 \end{pmatrix} \qquad \text{(E.q. 5.2)}$$

The free energy change associated with the propagation of a long helix by one residue was obtained from the Zimm-Bragg parameter s [Zimm and Bragg, 1959] via the equation [Best and Hummer, 2009; Garcia and Sanbonmatsu, 2002]:

$$\Delta G(T) = -k_B T \ln s(T) \qquad \text{(Eq. 5.3)}$$

The temperature dependence of the parameter s was obtained from the replica-exchange simulations. Equation (5.3) was fitted to the thermodynamic expression (Eq. 5.4) [Best and Hummer, 2009; Garcia and Sanbonmatsu, 2002], to obtain the associated helix-propagation enthalpy ΔH, entropy ΔS (both at the reference temperature T_0) and heat-capacity ΔC_p.

$$-k_B T \ln s(T) = \Delta H(T_0) - T\Delta S(T_0) + \Delta C_p[T - T_0] - T\Delta C_p \ln[T/T_0] \qquad \text{(Eq. 5.4)}$$

Equation 5.4 assumes that the heat capacity ΔC_p does not depend on temperature. It can be re-arranged into the form:

$$\Delta G(T) = a + bT + cT\ln(T/T_0), \text{ where } a = \Delta H_0 - T_0\Delta C_p\ , b = \Delta C_p - \Delta S_0, c = -\Delta C_p.$$

In our calculations, T_0 was set to 293.2 K, the lowest temperature of the REMD runs.

5.3 Results

5.3.1 Impact of salt on helicity

Figure 5.1 displays the temperature dependence of the average peptide helicity for the various solutions considered. As expected, the helicity decreases monotonically with temperature, reflecting the destabilization of folded conformations at higher temperatures. In the temperature range 290 – 380 K, the helicity depends on the salt type and concentration. Salt effects are less prominent at the lower concentration (1 M); however, at 3 M the two salts have opposite effects: NaCl stabilizes the helical population, whereas NaI decreases the probability of helix formation. Here, it is worth noting that this behavior has also been seen in computational studies of the peptide $(AE)_6$ by Dzubiella [Dzubiella, 2009].

The destabilization of helical populations by NaI is in contrast to our simulation results with the Ala tetrapeptide Ac-Ala_3-NMe (Chapter 4), as well the Ala nonapeptide Ac-Ala_8-NMe (see below). As discussed below, the impact of NaI on helical stability depends on the peptide length, and is stabilizing for short peptides and destabilizing for long peptides.

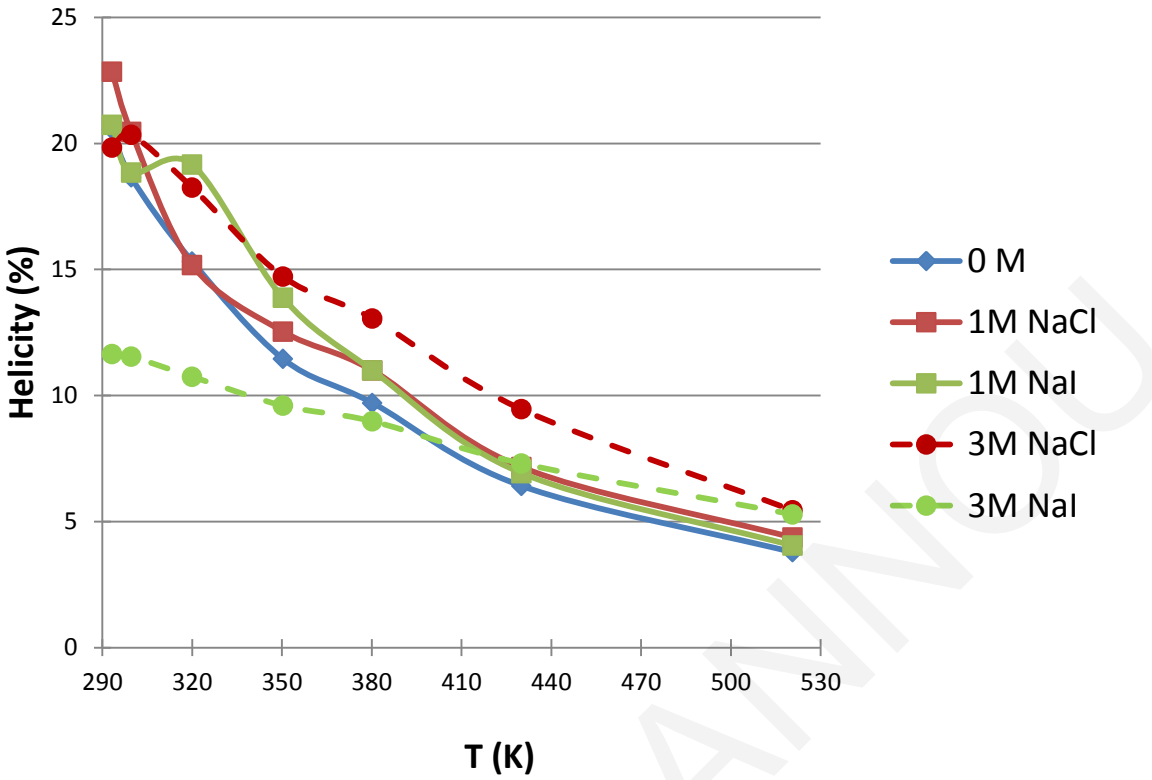

Figure 5.1: *Average helicity of the neutral model peptide Ac-(AAQAA)$_3$-NMe as a function of temperature, for the various solutions considered in this work.*

Only the results for the pure water system will be compared to other studies because, as stated before, this is the first MD study of the effects of ions on the $(AAQAA)_3$ peptide. The average helicity in the pure water solution (18.7%), near room temperature (299.6 K), is in agreement with other computational studies [Best and Hummer, 2009]. The reduction of helicity with temperature is more gradual than the experimental observation, which indicates the total loss of helical populations above ~ 350 K [Shalongo et al., 1994]. An analogous weaker dependence of helical population on temperature was also observed in recent simulation studies by Huang et al. [Huang et al., 2008], and by Best and Hummer [Best and Hummer, 2009]. The latter study attributed this weaker temperature dependence to inaccuracies in the peptide force field, rather than other uncertainties (statistical sampling, pressure effects, the water model, the definition of "helix", or the simulation protocol). This conclusion was supported by the observation that the computed enthalpic and entropic contributions to helix propagation were ~50 % of the corresponding experimental values. A similar observation holds in our study, as discussed below.

5.3.2 Impact of salt on the helix LR propagation and nucleation parameters

We can obtain insights on the salt and temperature impact on helicity by analyzing the Lifson-Roig parameters of helix propagation (w) and nucleation (v) [Lifson and Roig, 1961]. Figure 5.2 displays the temperature dependence of the propagation parameter (w) for the different solutions considered. The obtained curves are very similar to the curves of average helicity (Figure 5.1), reflecting the strong dependence of helical probability on the propagation parameter. The value in pure water at 299.6 K (1.08) is in good agreement with the computational estimate of Best and Hummer (1.10) for the same peptide [Best and Hummer, 2009]. Experimental estimates for related peptides are somewhat larger. For example, Scholtz *et al.* [Scholtz *et al.,* 1992] obtained an average value of 1.35 for the sequence Ac-Y$(AEAAKA)_n$–FNH_2 (n=2-6) at 273 K; Rohl and Baldwin obtained a value of ~1.28 for peptide Ac-(AAKAA)n-GY-NH_2 at 300 K (n =2-4) [Rohl and Baldwin, 1997]. We note that Vitalis and Caflisch have argued in recent work that the values of LR parameters from computational and experimental studies are not directly comparable, due to different assumptions employed in their estimation [Vitalis and Caflisch, 2012].

The addition of a 3 M NaI salt causes a significant reduction in the propagation parameter throughout the temperature range of the simulations. The other salt solutions have a very weak effect on the propagation parameter.

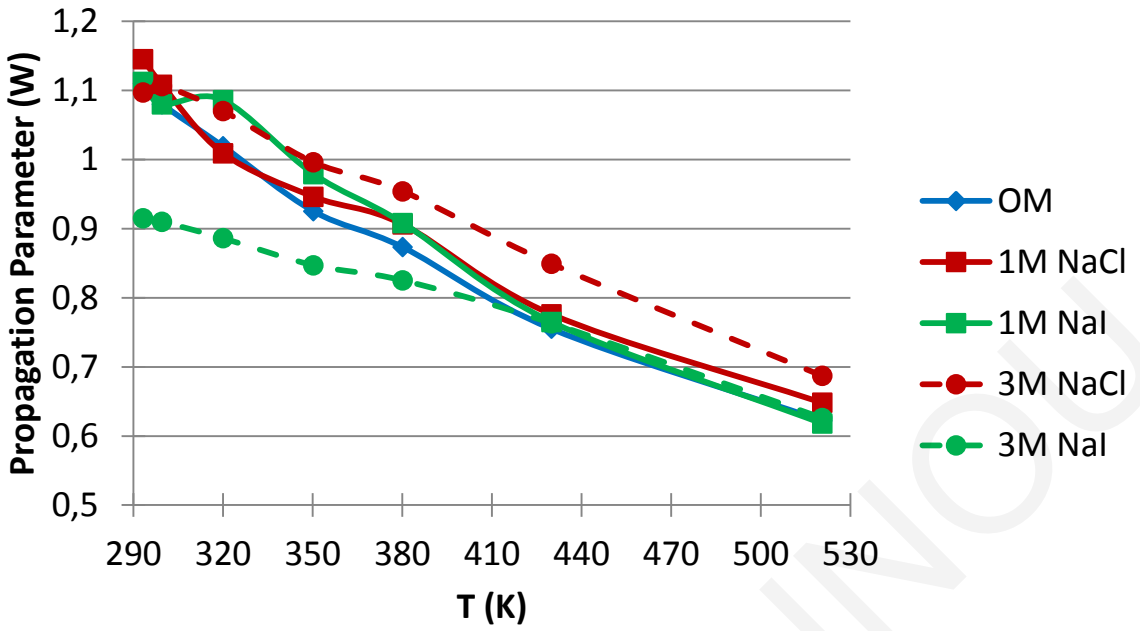

Figure 5.2: *Propagation Parameter of the neutral peptide Ac-(AAQAA)$_3$-NMe for the different systems as a function of temperature.*

The temperature dependence of the nucleation parameter (v) of the Ac-(AAQAA)$_3$-NMe peptide is displayed in Figure 5.3. The value in pure water at 299.6 K is 0.214, in good agreement with the values 0.18-0.21 obtained by Best and coworkers for the same peptide [Best and Hummer, 2009; Best and Mittal, 2010]. As in other computational applications of the LR model, the v values are an order of magnitude larger than the experimental estimates of 0.03 – 0.05 at 0 C [Rohl et al., 1996; Rohl and Baldwin, 1997], due to limitations in the LR model [Vitalis and Caflisch, 2012].

Table 5.2 displays the calculated values of the peptide helicity, the Lifson-Roig parameters and Zimm-Bragg parameters of the pure water system at various temperatures, for an easier comparison with other bibliography.

Table 5.2: *The calculated helicity (%), LR parameters (v and w) [Lifson and Roig, 1961], ZB parameters (σ and s) [Zimm and Bragg, 1959].*

Temp (K)	Helicity (%)	v	w	σ	s
293.2	20.56	0,213	1,11	0,0210	0,915
299.6	18.66	0,214	1,08	0,0211	0,890
320.0	15.32	0,227	1,02	0,0227	0,830
350.3	11.46	0,257	0,93	0,0265	0,736
380.2	9.71	0,264	0,87	0,0273	0,691
430.0	6.42	0,258	0,76	0,0266	0,600
520.6	3.79	0,238	0,62	0,0240	0,503

Figures 5.2 and 5.3 imply that temperature and salt-type have markedly different impact on the nucleation parameter, and on the propagation parameter / overall helicity. Even though the helicity and propagation parameter decrease monotonically with temperature, the nucleation parameter increases up to ~ 380 K (with the exception of the 3 M NaI solution where it maintains an approximately constant large value), and decreases slowly afterwards.

The addition of salt also causes an increase in the nucleation parameter. This increase can be understood as follows: The nucleation of an α-helical conformation requires the parallel orientation of three peptide groups before the formation of the first α-helical bond (i/i+4). This orientation is disfavored electrostatically, and should therefore be facilitated by salt due to screening of electrostatic interactions (Figure 5.3). This behavior is consistent with a theory developed by Kirkwood, which supported the stabilization of α-helical conformations by salt due to an interaction between the electrolyte and the helix macrodipole [Kirkwood, 1943]. The prediction of Kirkwood was verified by Baldwin and coworkers [Scholtz et al., 1991], in the first reported use of the peptide Ac-(AAQAA)$_3$Y-NH$_2$.

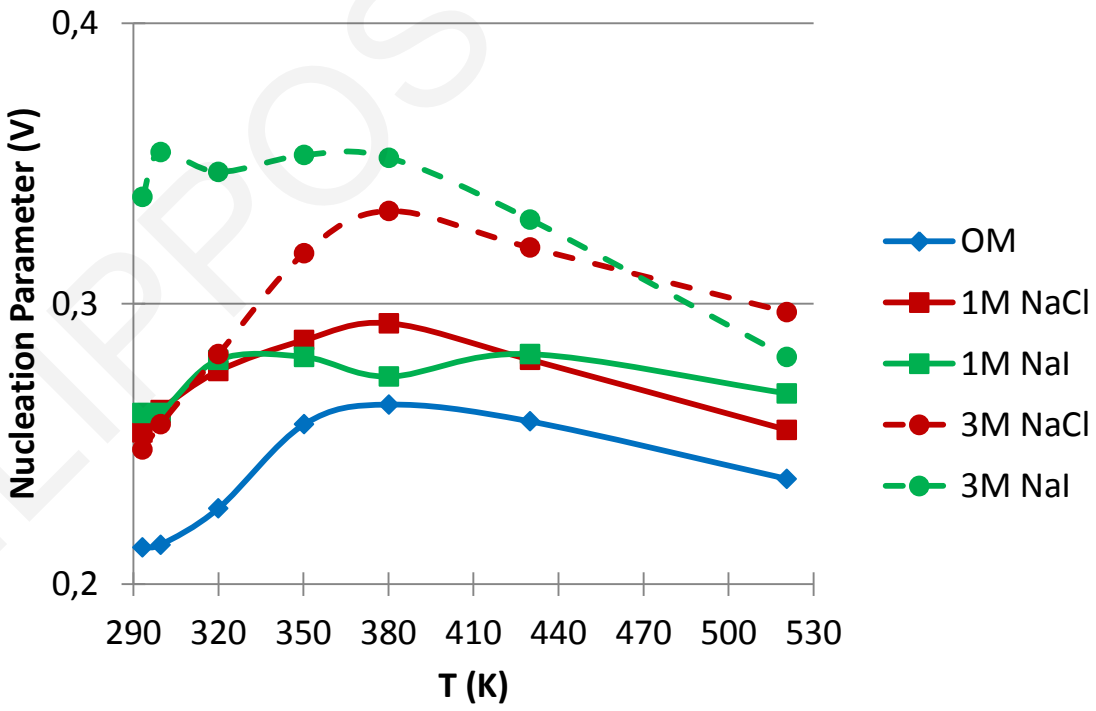

Figure 5.3: *Nucleation Parameter of the neutral peptide Ac-(AAQAA)$_3$-NMe for the different systems as a function of temperature of various solutions.*

A close inspection of Figures 5.1 – 5.3 shows that the peptide helicity depends on the interplay of both nucleation and propagation parameters. In the case of 3 M NaI, the significant reduction in the propagation parameter is responsible for the destabilization of helical conformations, despite the concomitant increase of the nucleation parameter (at lower temperatures). In the presence of 3 M NaCl and 1 M NaI both parameters are increased (with respect to pure water), in accord with the overall stabilization of helical conformations (Figure 5.1); this is especially apparent for 3 M NaCl, in the entire temperature range. Finally, in the presence of 1 M NaCl the propagation parameter remains unaltered, yielding a similar helicity as in pure water.

A potential explanation of the salt impact on the propagation parameter w can be offered by analysis of the interactions between the various solution components. For this purpose, we next discuss selected radial distributions functions (rdf).

The water – peptide group radial distribution functions (rdf) are displayed in Figures 5.4 and 5.5. The addition of ions causes a slight decrease of the rdf curves, reflecting the competition between water molecules and ions for the peptide groups; the decrease of the first peak is somewhat greater for the water hydrogen – carbonyl oxygen rdf curves, compared to the water oxygen – amino hydrogen.

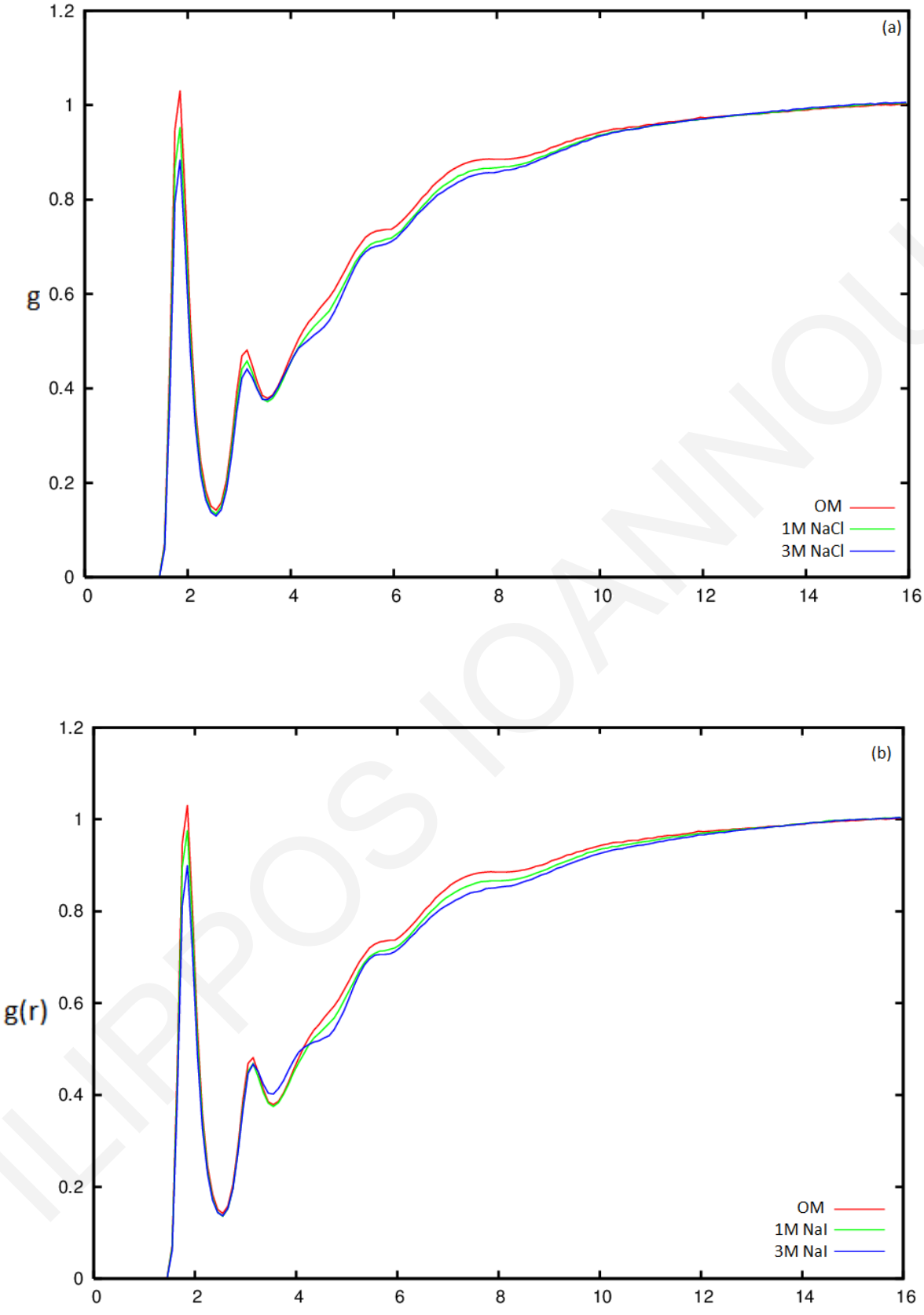

Figure 5.4: *Radial distribution function between water hydrogen and carbonyl oxygen for the NaCl (a) and NaI (b) solutions.*

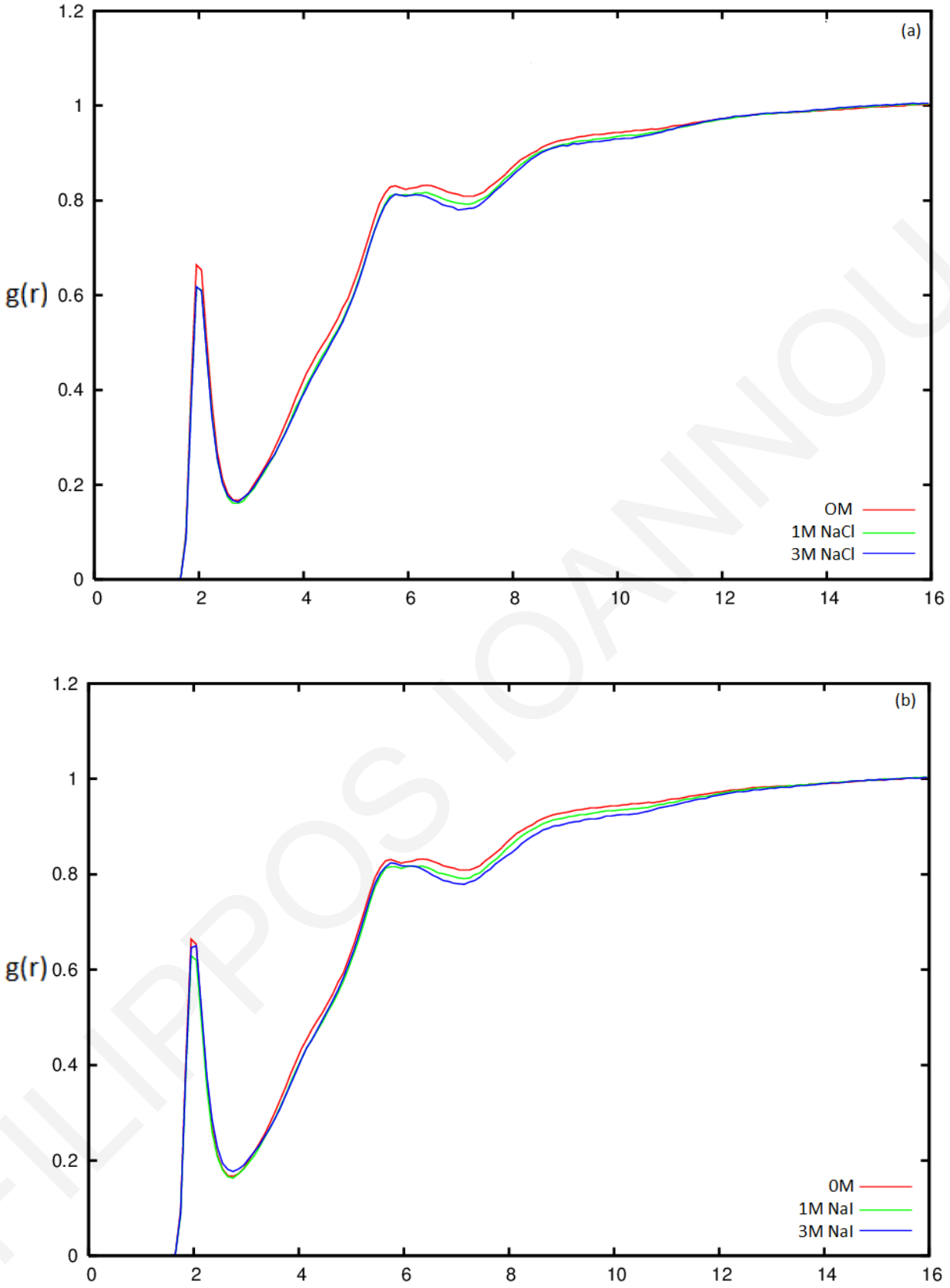

Figure 5.5: *Radial distribution function between water oxygen and amino-group hydrogen for the NaCl (a) and NaI (b) solutions.*

Sodium has a strong affinity for the peptide carbonyl groups, as shown by the prominent first peaks of the corresponding rdf in Figure 5.7. These contact peaks are much more pronounced in the NaI solutions, reflecting a stronger sodium affinity for the peptide group in the presence of iodide. This behavior has also been observed in our earlier alanine dipeptide and tetrapeptide simulations [Ioannou et al., 2011], as well as other studies [Heyda et al., 2010; Dzubiella, 2008; Dzubiella, 2009]. It has been related to the stronger iodide affinity, relative to chloride, for the side-chain methyl groups and the peptide amide group (see below and [Ioannou et al., 2011; Dzubiella, 2008; Dzubiella, 2009; Heyda et al., 2010; Algaer et al., 2011]).

The higher sodium affinity for the amide peptide groups in the presence of iodide is in line with the stronger reduction of the helix propagation parameter at 3 M NaI, relative to 3 M NaCl (and other solutions), and has been used to explain the destabilization of helical conformations in the presence of NaI [Dzubiella, 2009]. In the case of alanine tetrapeptide, the presence of NaI increased the population of helical conformations [Ioannou et al., 2011] (Chapter 4). As we show below, we expect a stabilization of helical conformations, due to NaI, in short alanine-based peptides and a destabilization in longer peptides, due to a competition between the helix nucleation and propagation parameters. This complex behavior reflects the insufficiency of sodium-peptide interactions to account entirely for the conformational preferences of the peptides. In fact, a more complicated picture emerges from the present study, which necessitates the separate consideration of ion impact on the helix initiation (nucleation) and propagation:

(i) The increase in the nucleation parameter (Figure 5.3) suggests that salts promote the initiation of helices. This seems to be a general effect; it can be attributed to the screening of electrostatic interactions, which facilitates the alignment of peptide-bond dipoles during helix initiation. Equivalently, the salt interaction with the helix dipole stabilizes the helical conformations, as advocated by Kirkwood [Kirkwood, 1943] and first demonstrated by Baldwin and coworkers [Scholtz et al, 1991].

(ii) The helix propagation parameter (Figure 5.2) is largely decreased in 3 M NaI, and is slightly altered in the other electrolyte solutions. In the LR formalism [Lifson and Roig, 1961], this propagation parameter is related to the free-energy change due to the addition of a helical hydrogen bond in a long, pre-existing helix. In our case, the length of the

observed helices is limited by the peptide size (average length of helices ≈ 6.2 residues at 299.6 K), and the overall helicity is mostly determined by internal hydrogen bonds, which depend on both nucleation and propagation parameters. Figure 5.6 displays the probability of the various main-chain CO groups to participate in *internal* α-helical bonds. Since the observed helices are not very long, the formation of these bonds is affected not only by the propagation but also the nucleation parameter. We observe a uniform suppression of hydrogen bonds in the presence of 3 M NaI (in line with the reduction of the propagation parameter w), and an increase in the presence of NaCl, except in the central peptide region (CO groups of residues 5-6). The NaCl-induced stabilization of helical conformations has also been observed in simulations of similar model peptides [Dzubiella, 2009, Fedorov et al., 2007]. Thus, the addition of salt may hinder or promote the formation of *internal* α-helical hydrogen bonds in relatively short model peptides, such as the one of the present study. This more complex, salt-dependent behavior is due to the competition between salt-water, salt-peptide, and peptide-peptide interactions. The net salt result on helix stability is a combination of the impact on helix initiation and propagation.

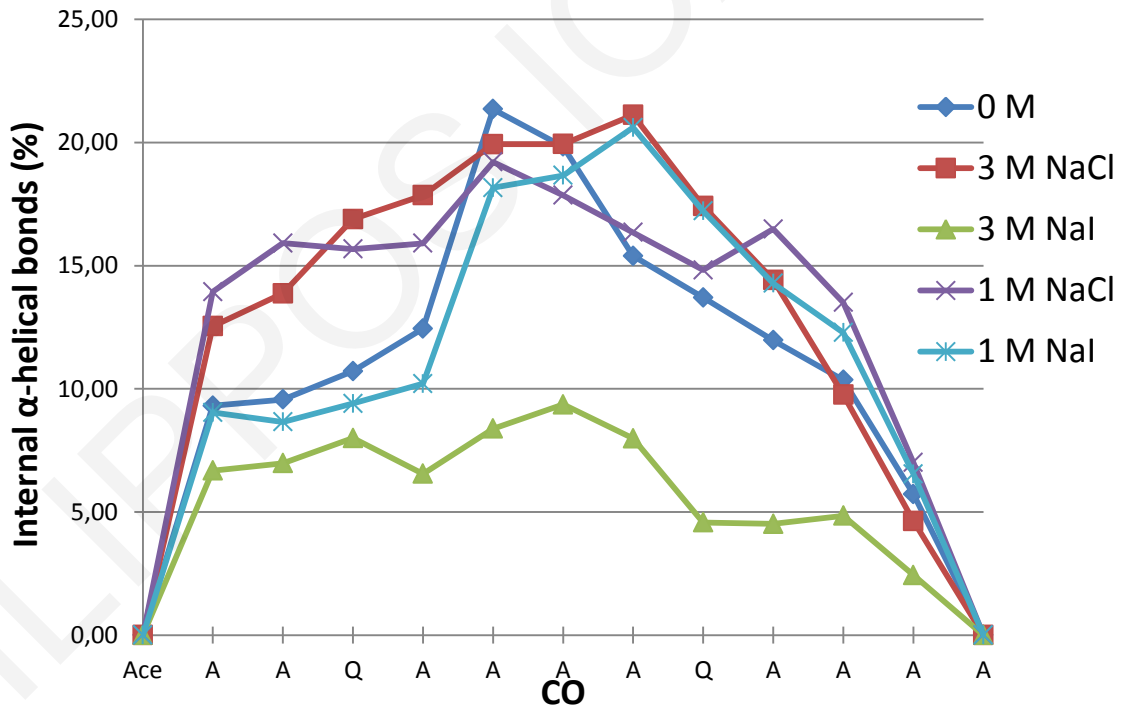

Figure 5.6: *Probability profile of the peptide main-chain CO groups to participate in internal a-helical bonds.*

The destabilization of helical conformations by NaI has been partly attributed to the strong sodium affinity for the main-chain CO groups [Ioannou et al, 2011; Dzubiella, 2009]. Since sodium manifests also a strong affinity for CO in the presence of chloride (see

Figure 5.7a), a question poses itself naturally: Why does the addition of NaCl have a stabilizing effect on helical conformations of the present peptide? This behavior should result from a combined contribution of salt-peptide, salt-water and peptide-peptide interactions, as discussed below.

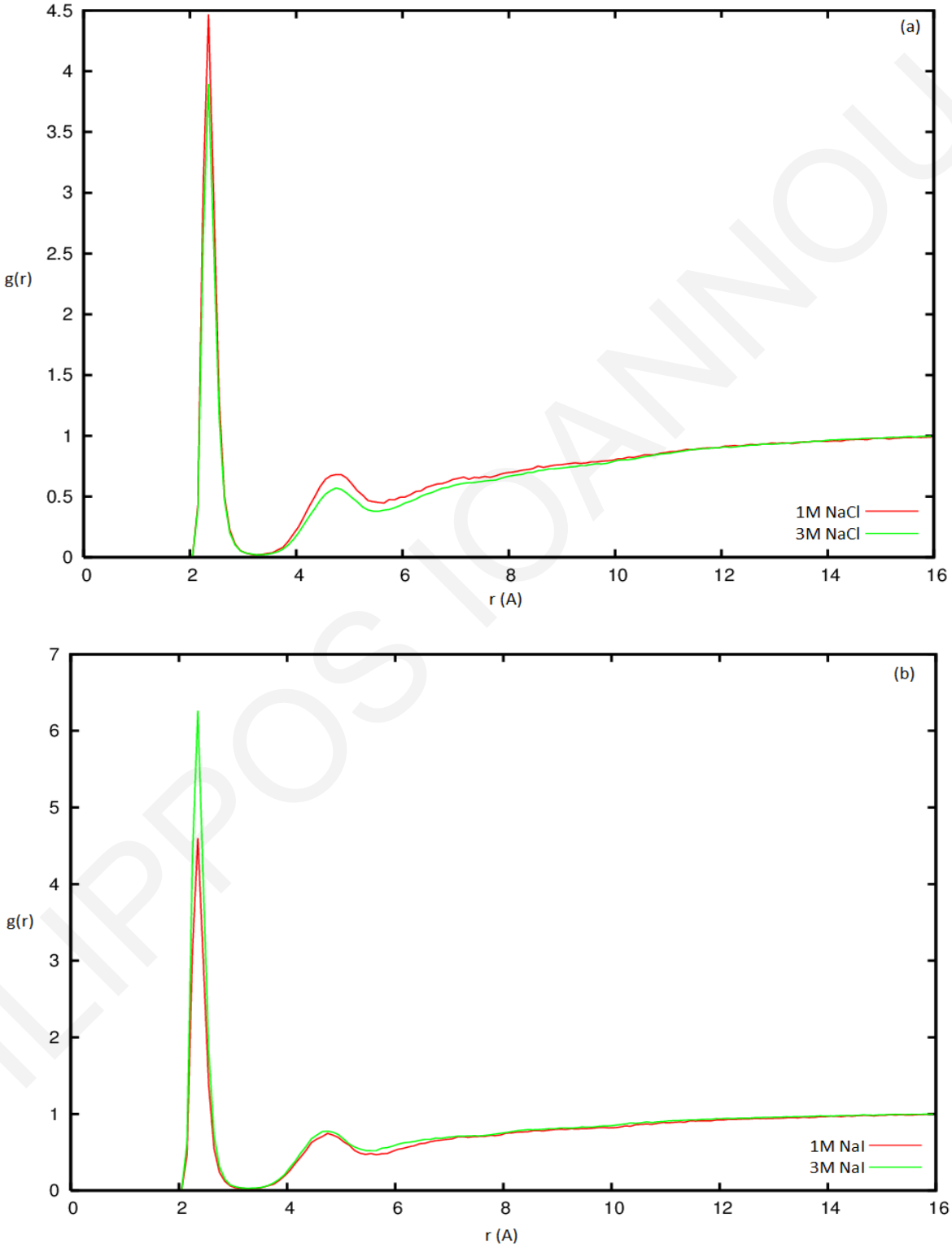

Figure 5.7: *Radial distribution function between sodium and carbonyl oxygen for the NaCl (a) and NaI (b) solutions.*

The rdf curves of the anion (Cl^- or I^-) – amide pairs are displayed in Figure 5.8. Both contact peaks are much smaller than unity, showing that both anions are excluded from the vicinity of the amide group; the more pronounced iodide contact peak reflects the stronger tendency of this anion to be near the peptide. This tendency is enhanced with concentration, as shown by the increment of the I – amide rdf curve at 3 M NaI.

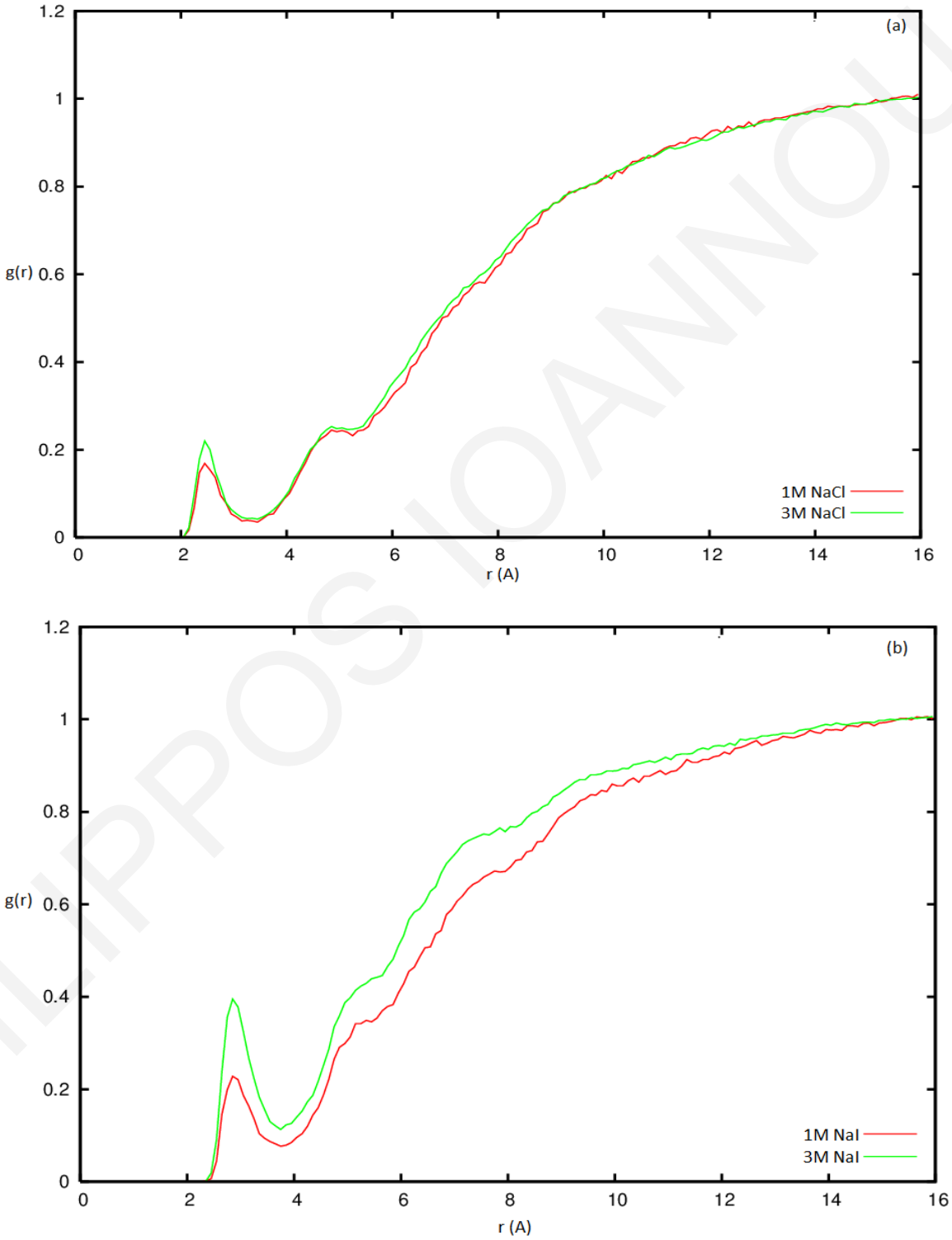

Figure 5.8: *Radial distribution function between anion and amino-group hydrogen for the NaCl (a) and NaI (b) solutions.*

Figure 5.9 displays the rdf function of the anion – alanine side-chain methyl group pairs. As for the alanine dipeptide and tetrapeptide studied in the previous chapter, Cl^- actually avoids the methyl groups, and an increase in NaCl concentration does not enhance the weak interaction between Cl^- and the side chain carbon; I^- on the contrary, has a stronger interaction with the methyl carbons, which increases with NaI concentration. These findings are in agreement with the behavior of the anions toward the hydrophobic groups observed in other works [Fedorov et al., 2007; Dzubiella, 2008, Dzubiella, 2009], and explain the stronger sodium affinity for the peptide in the NaI solutions (Figure 5.6.b).

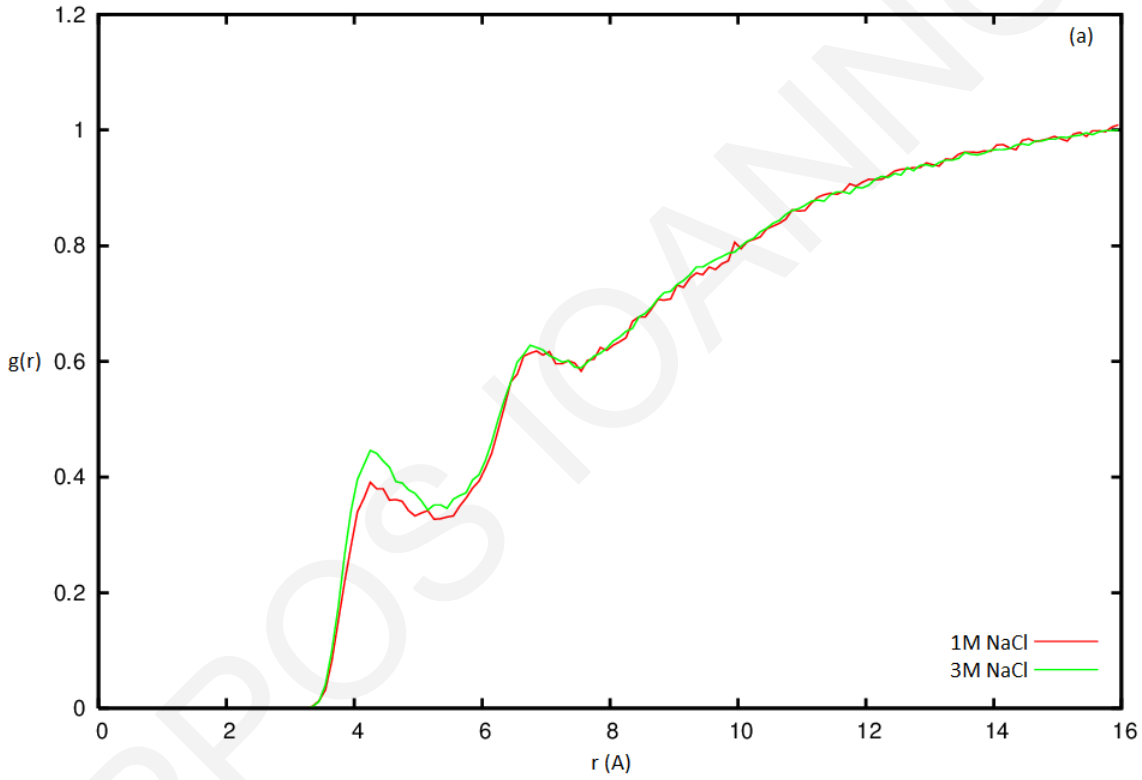

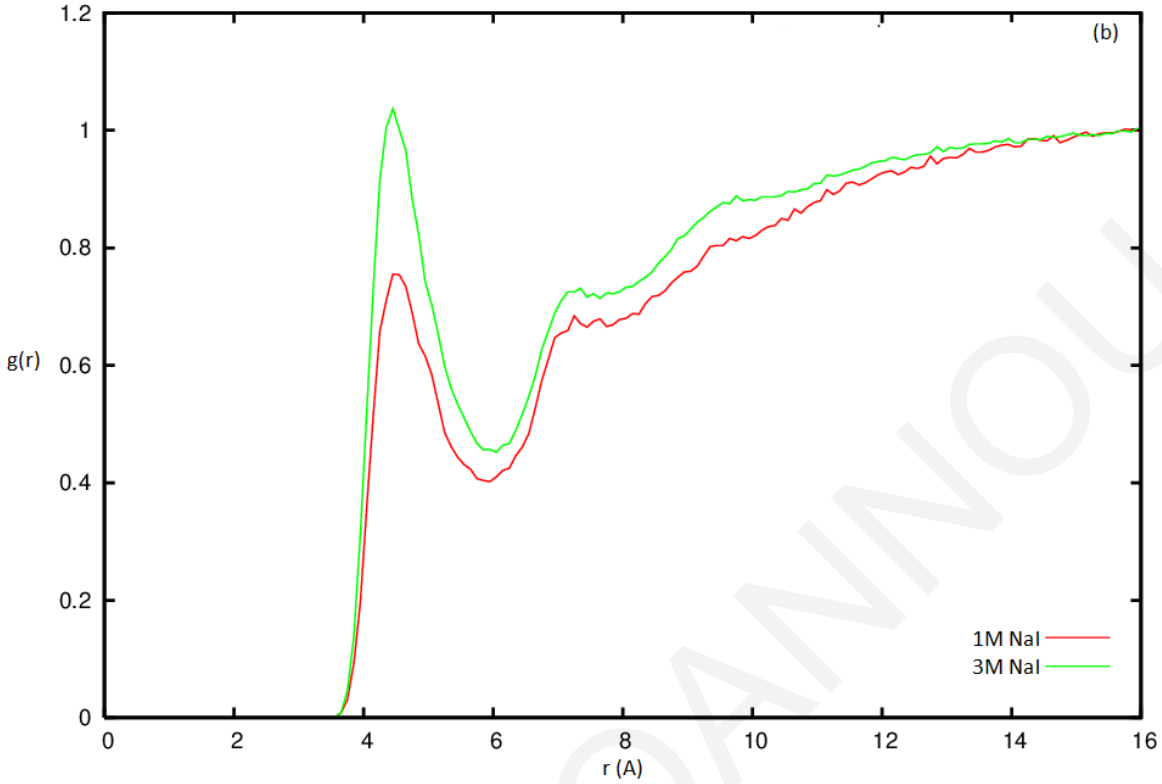

Figure 5.9: *Radial distribution function between anion and peptide side-chain methyl group for the NaCl (a) and NaI (b) solutions.*

In summary, chloride has a very weak affinity for the peptide, as shown in Figures 5.8-5.9. At the same time, it manifests a much stronger affinity for water (Figure 5.10) and sodium (Figure 5.11). Presumably, the much stronger chloride affinity for water and sodium, relative to the peptide groups, facilitates the formation of intra-peptide interactions and stabilizes helical structures. On the other hand, the iodide affinity for water and sodium is significantly weaker (Figures 5.10 – 5.11), in line with the lack of a similar enhancement of helical conformations in the NaI solutions.

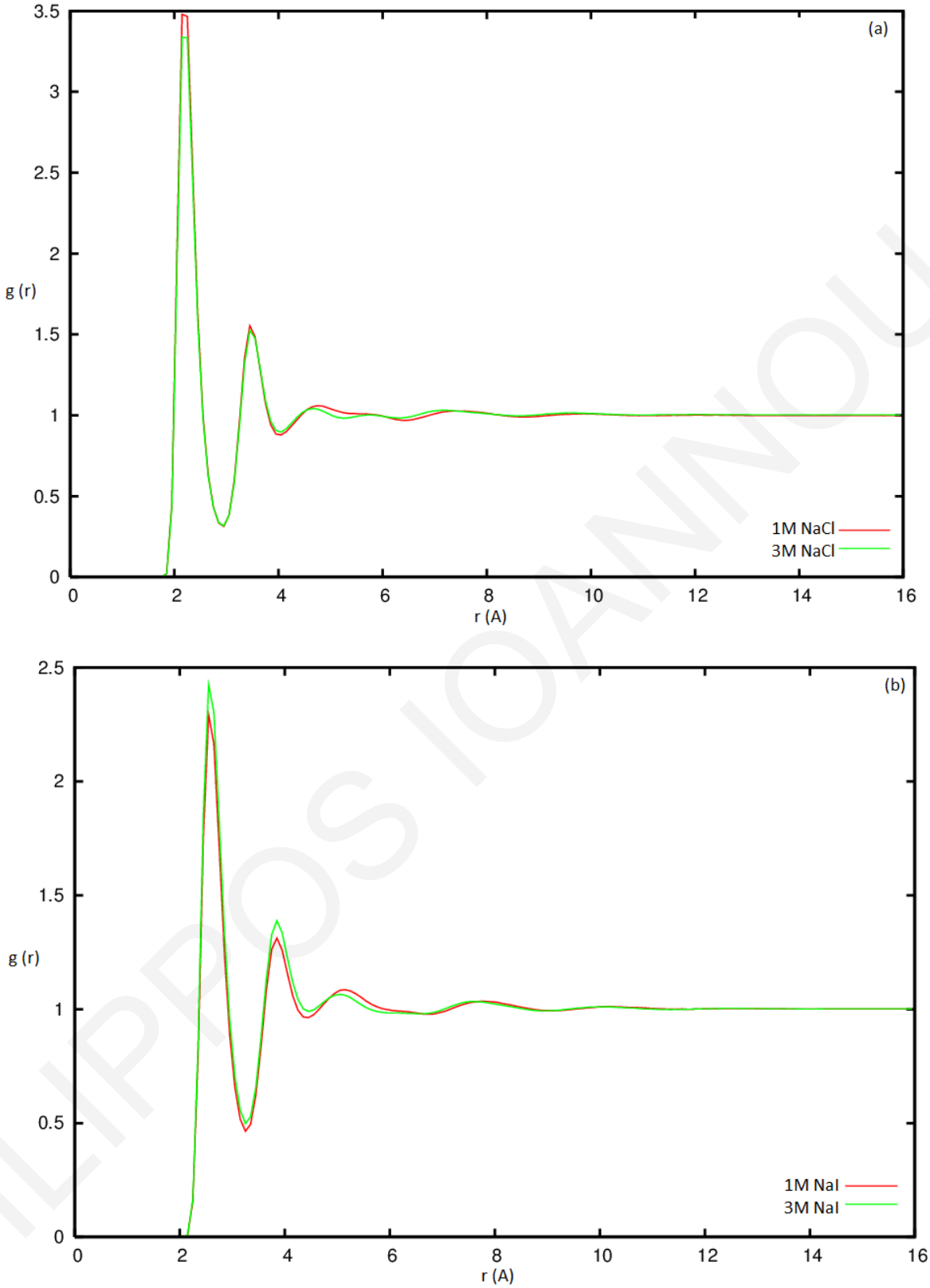

Figure 5.10: *Radial distribution function between anion and water hydrogen for the NaCl (a) and NaI (b) solutions.*

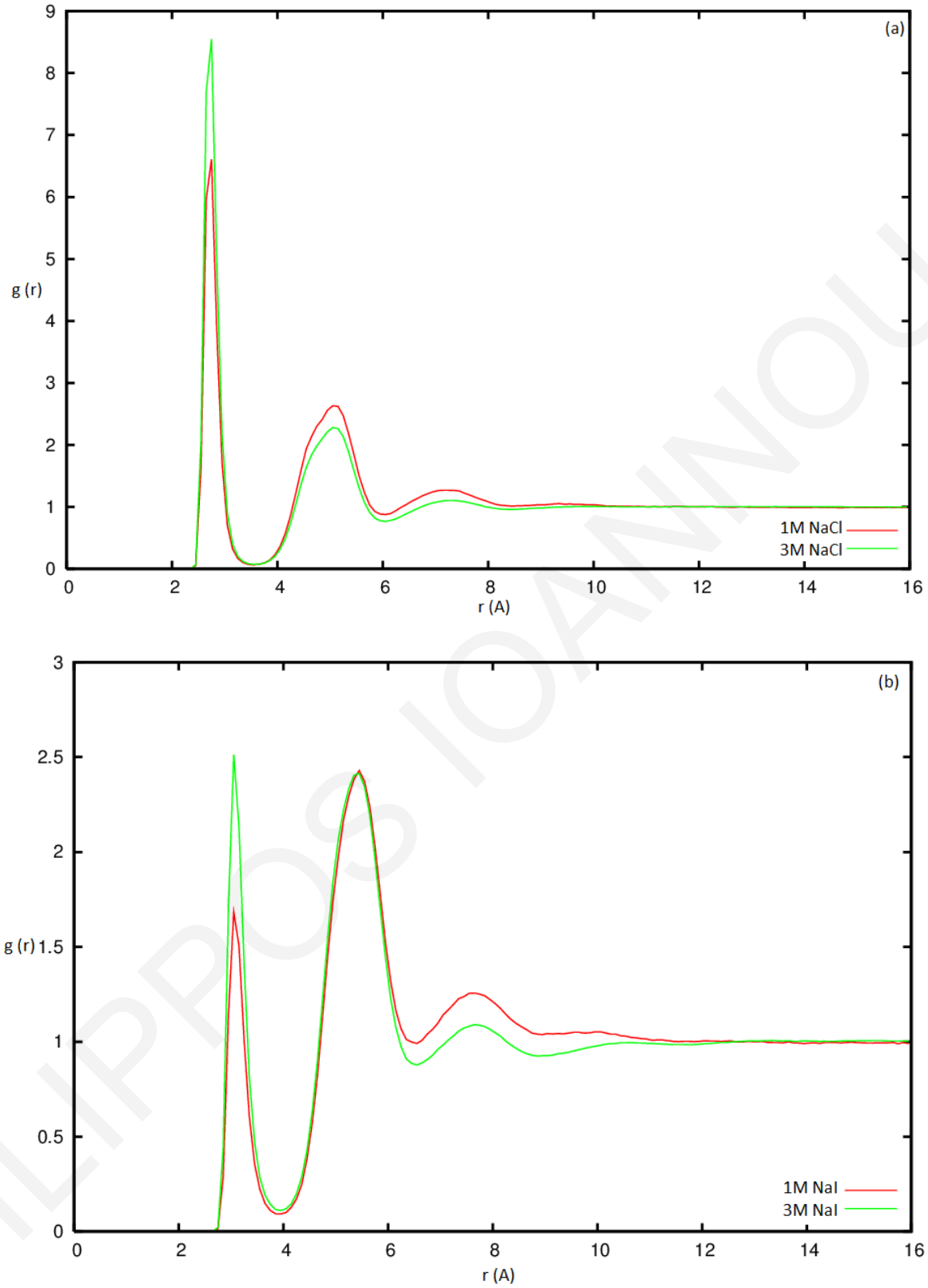

Figure 5.11: *Radial distribution function between sodium and anion for the NaCl (a) and NaI (b) solutions*

5.3.3 Impact of salt on thermodynamics of helix formation

Using Eq. (5.3) and the Zimm-Bragg propagation parameter s(T) (eq. 5.2), we can compute the free energy change, ΔG, due to the conversion of a coil residue to a helical one, at the end of a long helix with the characteristics of the Ac-$(AAQAA)_3$-NMe peptide. This free energy can be decomposed into enthalpic and entropic contributions via Eq. 5.4, using the assumption of a temperature-independent heat capacity ΔC_p and a reference temperature T_0 [Gnanakaran and Garcia, 1995; Best and Hummer, 2009].

We fitted the free energy ΔG to Eq. 5.4, using as reference temperature the lowest value of the REMD runs, T_0 = 293.2 K, and the assumption of a temperature-independent heat capacity ΔC_p. The resulting temperature dependence of the free energy, enthalpy and entropy is displayed in Figures 5.12 – 5.14. In Figure 5.12 the fitted free energy is displayed with solid lines and the calculated free energy with points. The standard deviation between the fitted and computed free energies is small (0.005 – 0.01 kcal/mol).

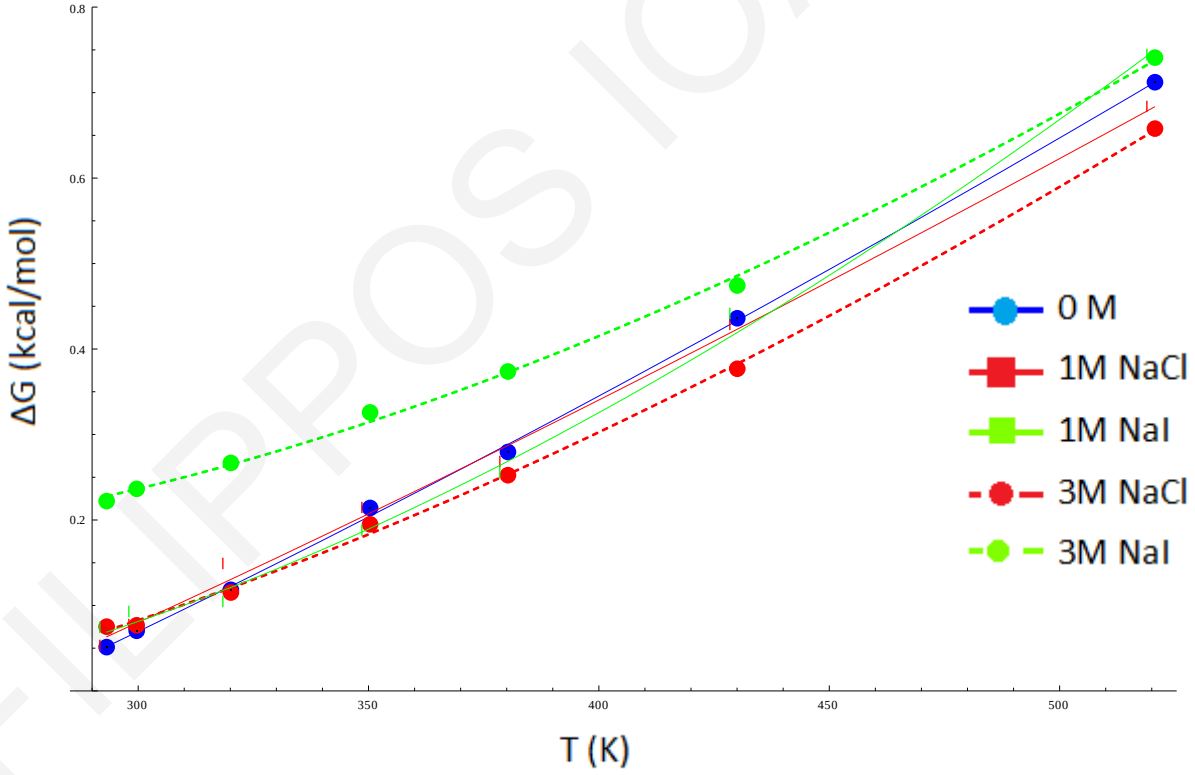

Figure 5.12: *Temperature dependence of the helix-propagation free energy (ΔG) for the neutral peptide Ac-$(AAQAA)_3$-NMe. The fitted free energies [Eq. (5.2)] are shown as solid lines.*

Table 5.3: *The free energy, enthalpy, entropy and heat-capacity change associated with the conversion of a coil residue to a helical one at the end of a long a-helix. The results correspond to T = 293.2 K, and arise from the simulations of the peptide Ac-(AAQAA)$_3$-NMe in the various solutions considered.*

	Pure water	**1 M NaCl**	**3 M NaCl**	**1 M NaI**	**3 M NaI**
ΔG(kcal/mol)	0.052	0.053	0.075	0.073	0.228
ΔH_0 (kcal/mol)	-0.70	-0.65	-0.44	-0.45	-0.13
ΔS_0 (cal/mol/K)	-2.57	-2.45	-1.74	-1.77	-1.23
ΔC_P (cal/mol/K)	-1.04	-0.88	-2.65	-3.90	-3.22

Table 5.3 lists various thermodynamic quantities, evaluated at 293.2 K. The value obtained for the free energy ΔG in pure water (0.052 kcal/mol) is comparable to values from MD studies (ΔG = 0.085 kcal/mol at 300 K) [Gnanakaran and Garcia, 2005]. As expected, the helix extension is enthalpically favored (ΔH = -0.70 kcal/mol), and entropically opposed (ΔS = -2.57 cal/mol/K). Best and Hummer obtained a similar enthalpy value in their MD study (ΔH = -0.61 kcal/mol at 300 K) [Best and Hummer, 2009]. Experimental measurements by CD [Scholtz et al., 1991] and calorimetry [Richardson and Makhatadze, 2004; Scholtz et al., 1991] place the enthalpy change in the range -0.9 to -1.3 kcal/mol. Given the difficulty in obtaining accurate estimates of enthalpy and entropy changes, the agreement with the experimental values is satisfactory. Still, the obtained enthalpic and entropic contributions are ~50 % of the experimental values. Best and Hummer attributed the weaker destabilization of the helical conformations with temperature dependence, compared to experiment, to this deviation [Best and Hummer, 2009].

Helix elongation becomes slightly less favored enthalpically and slightly less opposed entropically in the presence of salt; the enthalpic contribution prevails, yielding a net destabilization of helix elongation by salt. These trends are more apparent in the NaI solutions. The considerable increase of the free energy for helix elongation in the presence of 3 M NaI (Figure 5.12) reflects the reduced helicity in the presence of this salt; furthermore, the smaller entropic penalty of helix elongation by NaI could be due to the more effective screening of electrostatic interactions by this salt, as also manifested in the stronger impact to the nucleation parameter.

The obtained heat capacity values lie within the estimated range of values for helix formation, -8 to +8 cal/mol/K [Lopez MM, 2002]. Differential scanning calorimetry

measurements have reported a value of -7.6 cal/mol/K [Richardson and Makhatadze, 2004]. Best and Hummer estimated a negative heat capacity (≈-0.4 cal/mol/K).

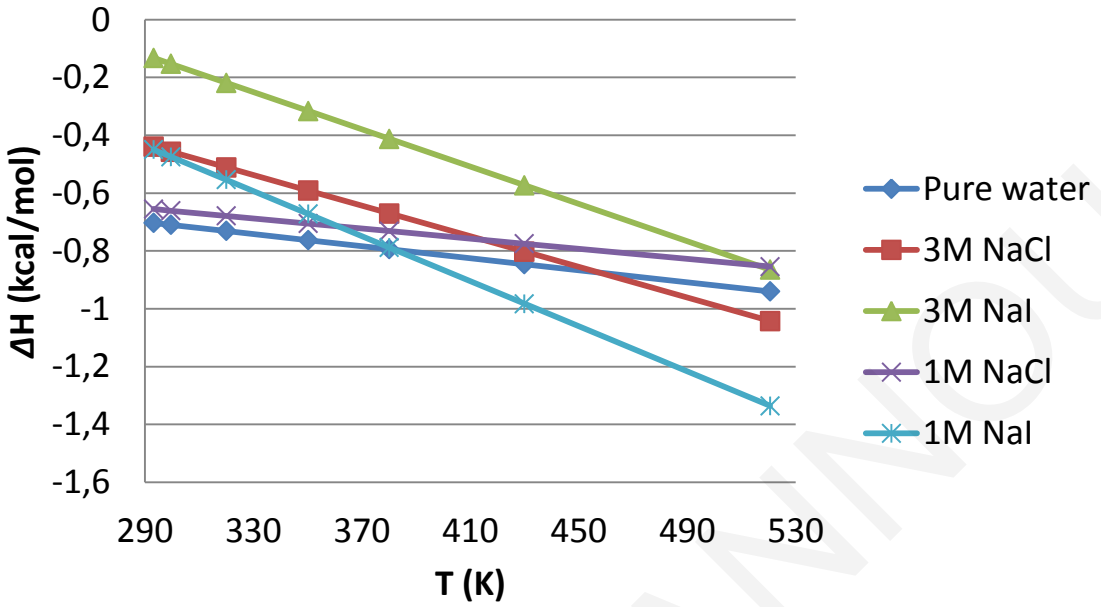

Figure 5.13: *Temperature dependence of the enthalpy (ΔH) for the neutral peptide Ac-(AAQAA)$_3$-NMe in the various solutions. The lines are drawn as an aid to the eye using Excel's chart type "Scatter with Straight Lines and Markers".*

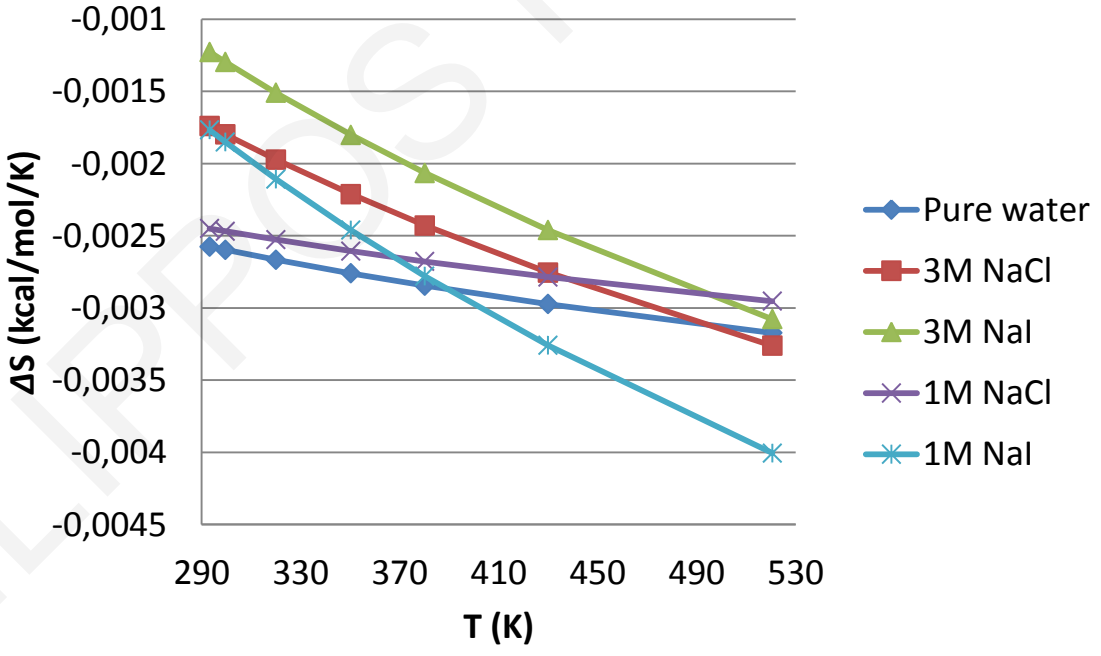

Figure 5.14: *Temperature dependence of the entropy (ΔS) for the neutral peptide Ac-(AAQAA)$_3$-NMe in the various solutions. The lines are drawn as an aid to the eye.*

The slopes of ΔH and ΔS with temperature have a systematic variation with salt type and concentration. The slope decreases for higher salt concentrations and decreases from NaCl to NaI.

5.3.4 Dependence of helix stability on peptide length

As explained above, in the LR formalism the average number of helical hydrogen bonds (fraction of peptide in helix) depends on the nucleation and propagation parameters, and on the peptide length (see Eq. (5.1)). Using the average nucleation and propagation parameters from the T=299.6 K simulations in pure water (w = 1.08 and v = 0.21) and in 3M NaI (w = 0.91, and v = 0.35), we computed a theoretical helicity as a function of peptide length (n) using eq. (5.1). This estimate ignores the actual dependence of w and v on the peptide length, and is a qualitative indicator of the helicity fraction vs length for a peptide with the average characteristics of the simulated sequence $(AAQAA)_3$.

The resulting graph (Figure 5.15) shows that the addition of 3 M NaI is mildly stabilizing helical conformations in "short" peptides (due to its effect on helix nucleation), whereas it destabilizes helical conformation in "long" peptides due to the salt impact on propagation. For a 15-residue peptide, the helicities are, respectively, ~20 % and ~ 12 % in 0 M and 3 M NaI, in agreement with the simulation estimate. With the employed LR parameters, the crossover between destabilization and stabilization by 3 M NaI occurs at a peptide length of ~6-7 residues. This results suggests that the increase in helicity of the alanine tetrapeptide (Chapter 4) in the presence of 3 M NaI was correct, rather than an artifact of the CHARMM force field.

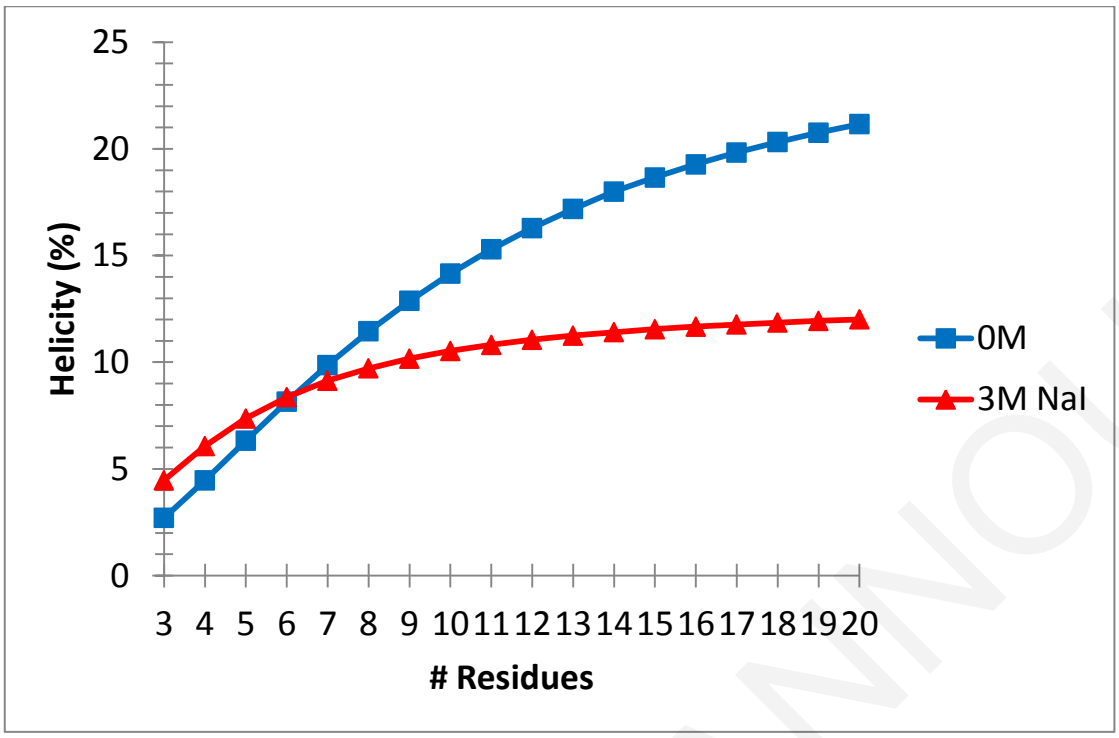

Figure 5.15: *Dependence of helicity on peptide length, computed by (Eq. 5.1) and the LR parameters for the Ace-(AAQAA)$_3$-NMe peptide.*

To check the prediction of Figure 5.15, we conducted simulations with the Alanine peptide Ace-Ala$_8$-NMe in pure water and a 3 M NaI solution, using the same computational method as for the Ace-(AAQAA)$_3$–NMe peptide. We employed 24 replicas spanning the temperature range 292.5 – 428.4 K. The simulation length was 30 ns/replica. The calculated helicity is displayed in Figure 5.16 as a function of temperature. Indeed, the addition of 3 M NaI salt causes a helicity increase in Ace-Ala$_8$-NMe. The actual helicities and the crossover value n=6 do not agree with Fig. 5.15. This could be partly due to the pure-alanine content of this peptide; in contrast, Figure 5.15 uses average v and w values from the 15-residue peptide, which has a 20 % glutamine content.

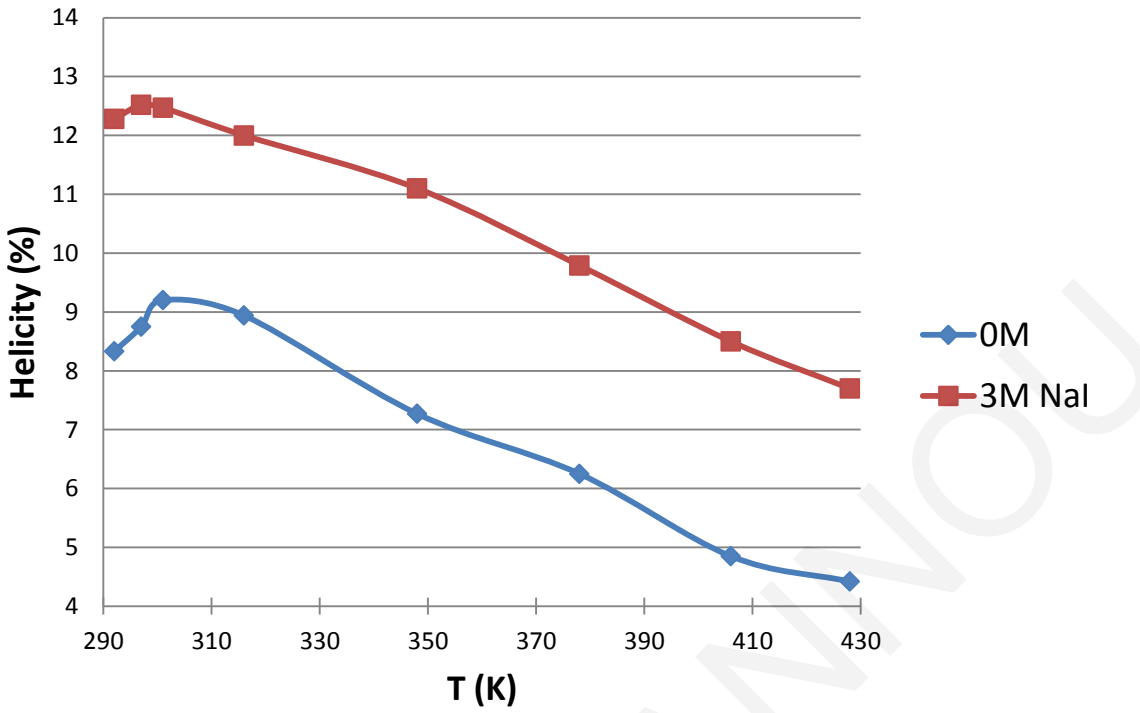

Figure 5.16: *Helicity of the alanine nonapeptide Ace-Ala$_8$-NMe as a function of temperature in pure water and a 3 M NaI solution.*

5.4 Conclusions and Perspective

In this work, we have examined the conformational stability of the 15-residue model peptide Ac-(AAQAA)$_3$-NMe in pure water and various electrolyte solutions. Our simulations show a net stabilization of α-helical structures in the presence of high concentration NaCl, and a net destabilization in the presence of high-concentration NaI.

Analysis of the corresponding LR parameters shows a general enhancement of the helix nucleation step by salts. This observation is in line with the increase in helicity of the Alanine tetrapeptide (Chapter 4) by both NaCl and NaI. It is possibly due to the screening of electrostatic interactions by salt, which reduce the free-energy penalty associated with the ordering of peptide groups upon the initiation of an α-helix.

The same LR analysis suggests that salts hinder the propagation of helices in a salt-specific manner: the LR propagation parameter of Ac-(AAQAA)$_3$-NMe is significantly reduced (relative to pure water) in the presence of 3 M NaI, and slightly reduced in all other salt environments studied here. An important conclusion of the present analysis is that the net impact of salt on the stability of helical conformations is best understood by considering

separately its influence on the nucleation and propagation steps. In shorter peptides, the facilitation of the nucleation step may lead to a net stabilization of helical conformations by salt, as shown explicitly by our simulations with the Ala tetrapeptide (Chapter 5) and Ala nonapeptide (this Chapter) in a 3 M NaI environment. The same salt environment can destabilize helical conformations in longer peptides, as shown here for Ace-$(AAQAA)_3$-NMe. Furthermore, in a peptide of *given length*, the addition of different salts stabilize or destabilize helical conformations, depending on their effects on nucleation and propagation. This is manifested here by the 3 M NaCl and 3 M NaI simulations of Ace-$(AAQAA)_3$-NMe.

The helix destabilization by NaI (relative to NaCl) can be understood in terms of the larger anion (iodide) size. Indeed, examination of the solution structures reveals much stronger affinities of both cation and anion for the peptide in the NaI solution. The larger iodide size renders it less polar (more hydrophobic). As a result, its affinity for sodium is decreased, and its affinity for the peptide non-polar side-chains and main-chain peptide groups is increased. Overall, ion-peptide non-polar and polar interactions are enhanced in the NaI solution (relative to the NaCl solution) and destabilize the formation of α-helical conformations, which require the formation of extensive intra-peptide polar interactions at the expense of salt-peptide interactions.

The helix stabilization by NaCl (relative to pure water), also documented in other studies [Fedorov et al., 2009; Dzubiella, 2009], might be also understood in terms of the small anion size: Chloride has a large affinity for sodium and water, and small affinity for the peptide. Helical conformations may be enhanced in the presence of NaCl, because the engagement of peptide groups in intra-peptide interactions facilitate the formation of anion-cation and salt-water interactions.

6. Impact of Solvent - Exposed Salt Bridges on the Helix-Coil Equilibrium of the Model Peptides, in Conditions of Variable Ionic Concentration and Temperature

6.1 Introduction

To investigate (a) the strength of interactions between solvent – exposed charged side-chains in a helix-forming peptide and (b) the impact of solvent – exposed salt-bridge formation on the α-helix/coil equilibrium, in the presence of salts we have conducted simulations of the model peptides Ac-AAQAA-EAQKA-AAQAA-NMe (referred to hereafter as EK+3), Ac-AAQAA-EAQAK-AAQAA-NMe (EK+4) and Ac-AAQAA-EAQAA-KAQAA-NMe (EK+5), in aqueous salt solutions. These model peptides differ from the peptide Ac-$(AAQAA)_3$-NMe of Chapter 5, in that they contain two oppositely charged amino acids, Glutamic acid (E), and Lysine (K) in positions *i*/*i*+3, *i*/*i*+4, or *i*/*i*+5. Due to the geometry of the α-helix (3.6 residues per turn), the interactions between the charged side chains are expected to be stronger in the first two peptides.

Studies have postulated the stabilization of helical structure in alanine-based peptides resulting from interactions of charged side chains (such as Lys, Glu, or Arg) through formation of salt bridges [Masqusee and Baldwin, 1987; Mayne et al., 1998], interactions of charged residues with the helix dipole [Huyghues-Despointes et al., 1993; Lockhart and Kim, 1993; Shoemaker et al., 1995], or the favorable free energy gained by hydration of charged residues [Vila et al., 1992; Williams et al., 1998]. Peptides EK+3, EK+4 and EK+5 are analogous, respectively, to peptides E6K9 and E6K10 studied in Ref. [Scholtz et al., 1993] and 3EK, 4EK 5EK studied in Ref. [Smith and Scholtz, 1998]. They differ from those peptides at their C-terminal end, where they lack a tyrosine residue and are blocked by a N-CH_3 group instead of an amide group. Experimental studies with E6K9 and E6K10 have shown that a strong, singly charged hydrogen bond between Glu and Lys is found. The strength of this singly-charged hydrogen bond does not depend upon the ionic strength of the solution up to 2.5 M NaCl [Scholtz et al., 1993]. Smith and Scholtz suggest in their

study that hydrogen bonding is a major factor in the interaction between these side chains and that the interaction of the ion pairs observed at high salt is not just a simple electrostatic interaction.

6.2 Methods

6.2.1 Investigated Systems

Each simulation system consisted of a single model peptide molecule in an octahedral box of water molecules and an appropriate number of ions, chosen to model the desired salt concentration. Table 6.1 lists the total number of ions and water molecules as well as the water-box sizes for the various peptide simulations. Although the actual salt concentrations are those listed in this Table, we will designate them for simplicity as "1 M" or "3 M" concentrations in the ensuing discussion. The original (control) peptide Ace-$(AAQAA)_3$-NMe is referred to as AQ.

6.2.2 Force Field and Simulation Protocol

The peptide atomic charges, van der Waals, and stereochemical parameters were taken from the AMBER 11 all-atom force field [Case et al., 2010]. The water was represented by a modified TIP3P model [Jorgensen et al., 1983; Neria et al., 1996]. Ion parameters, recently optimized for high-concentration simulations, were taken from Joung and Cheatham [Joung and Cheatham, 2008].

Table 6.1: *Water box sizes and numbers of ions and water molecules employed in the simulations*

solution	# waters	# cations	# anions	box length
		EK+3		
0 M	2316	0	0	45.43
1.1 M NaCl	2225	48	48	45.04
3.3 M NaCl	2209	144	144	45.62
1.1 M NaI	2262	48	48	45.73
3.0 M NaI	2264	144	144	47.27

solution	# waters	# cations	# anions	box length
		EK+4		
0 M	2318	0	0	45.49
1.1 M NaCl	2230	48	48	45.18
3.3 M NaCl	2227	144	144	45.73
1.1 M NaI	2237	48	48	45.62
3.0 M NaI	2284	144	144	47.32
		EK+5		
0 M	2314	0	0	45.44
1.1 M NaCl	2227	48	48	45.10
3.3 M NaCl	2200	144	144	45.54
1.1 M NaI	2239	48	48	45.60
3.0 M NaI	2271	144	144	47.27

All simulations were conducted with the AMBER 11 simulation package [Case et al., 2010] and the ff03* force field [Best and Hummer, 2009]. Starting from a helical conformation, the peptide was first minimized, heated up gradually from 0 to 300 K six 30-ps stages (every 50 K) and then subjected to a 50-ns production simulation at 300 K in vacuum. From the 50 ns MD simulation we identified the structure with the lowest energy and solvated it in a truncated octahedron simulation cell with the appropriate number of TIP3P water molecules and ions, chosen to model the desired salt concentration. We minimized the system in two stages. In the first stage we kept the peptide fixed and just minimized the positions of the water molecules and ions. In the second stage we minimized the entire system. Next, we allowed the entire system to heat up from 0 to 300 K by a 20-ps MD run at constant volume with weak restraints on the peptide; we then switched off the restraints, and run a 1 ns equilibration at 300 K under constant-pressure conditions. Using the average cell size of the previous run, we conducted 0.5 ns simulation runs at constant volume for temperatures in the range T = 280 – 520 K, with 20 K intervals. Following the method of Sugita and Okamoto [Sugita and Okamoto, 1999], we used the mean potential energies and temperatures of these simulations to calculate the optimal temperatures for replica-exchange runs, targeting an exchange probability between neighboring replicas of ~18 %. Finally, we employed 48 replicas, spanning a temperature range T = 292.6 – 523.3 K.

The initial conformation used for the replica runs was unfolded (taken from the 520 K run). Starting from this conformation, we conducted 300-ps runs at the replica temperatures as an equilibration stage, prior to the actual REMD runs. The REMD runs were done at constant-volume conditions with a 2-fs time step, and had a total length of 1.44 μs (30 ns

per replica). Replica exchange attempts were made every 1 ps. The obtained exchange probabilities were 16 - 18 %. All replicas performed random walks in the temperature space, spanning several times the entire range of temperatures. Chirality restraints were used on the peptide bond, to ensure no trans – cis conformational changes at the highest temperatures of the REMD runs. Long-range electrostatics were calculated using PME, with a 0.99 Å grid spacing and a 9-Å cutoff.

6.2.3 Secondary Structure Calculations and Conformational Analysis

We computed the peptide "helicity" (the fraction of α-helical conformations), using the Lifson-Roig (LR) model [Lifson and Roig, 1961], as in the previous analysis of the alanine dipeptide and tetrapeptide [chapter 4]. In the LR definition, a residue *i* is considered α-helical if and only if its backbone torsional angles (φ_i, ψ_i), and the pairs (φ_{i-1}, ψ_{i-1}) and (φ_{i+1}, ψ_{i+1}) of the adjacent residues fall in the α-helical region of the Ramachandran map ($\varphi = -65 \pm 35^o$, $\psi = -37 \pm 30^o$). For the calculation of the Lifson-Roig parameters we also calculated the average number of "helical segments" in the peptide. A helical segment is defined to contain at least two successive residues in helical conformation. A single residue in helical conformation between residues in coil conformation is not counted as a helical segment (while ….chhc…. is a helical segment). The average number of helical hydrogen bonds $<n_H>$ and helical segments $<n_S>$ was computed from the analysis of the simulation data. By fitting these values to the equations (Eq. 5.1) we deduced the LR parameters w and u (see section 2.5).

6.3 Results

6.3.1 Pure water simulations

Figure 6.1 displays the average helicities of the four peptides in pure water, as a function of temperature. The corresponding helicities are also listed in table 6.2. Peptides EK+3 and EK+5 have, respectively, larger and smaller helicities than AQ in the entire temperature range of the simulations. Peptide EK+4 has a mixed behavior: its helicity lies between the EK+3 and EK+5 helicities up to 470 K; it is also smaller than the helicity of AQ up to

~350 K. Thus, the two charged-residue substitutions and the relative spacing of the charged residues affect the stability of helical conformations.

Table 6.2: *Average peptide helicity for the various peptides in pure water*

T(K)	AQ	EK+3	EK+4	EK+5	E6	K10
292,6	20.56	23.85	14.62	12.42	15	14.4
299,4	18.66	23.7	14.9	11.67	13.7	14.7
320,9	15.32	21.58	13.52	10.51	12.56	12.74
348,8	11.46	16.93	11.91	9.06	9.68	11.34
380,2	9.71	12.73	9.47	7.53	8.05	9.22
427,4	6.42	8.53	7	5.88	6	6.75
523,3	3.79	4.52	5.46	3.16	3.53	3.82

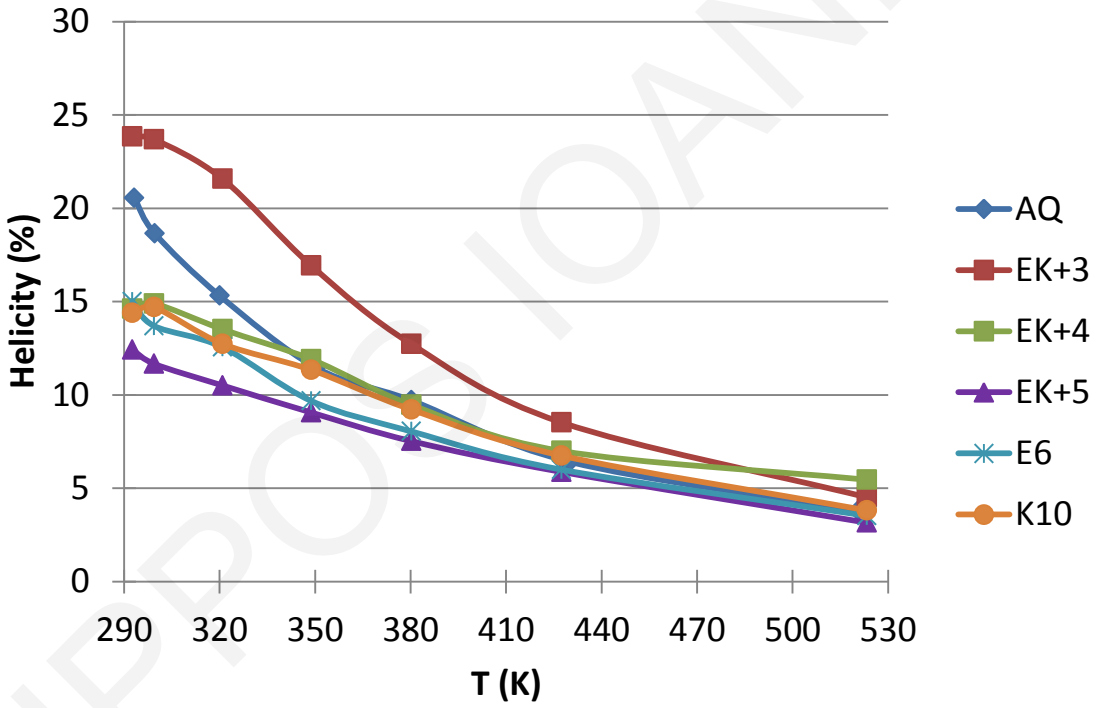

Figure 6.1: *Temperature dependence of the average peptide helicity in pure water.*

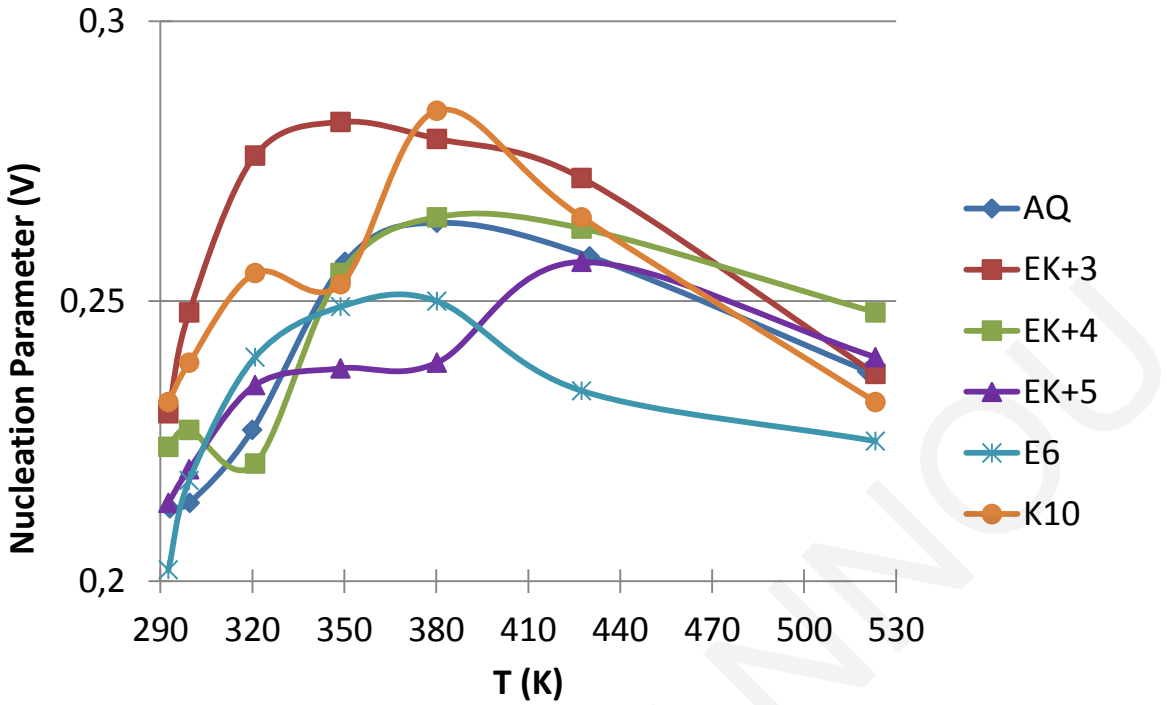

Figure 6.2: *Temperature dependence of the LR helix nucleation parameter (v) for the various peptides in pure water.*

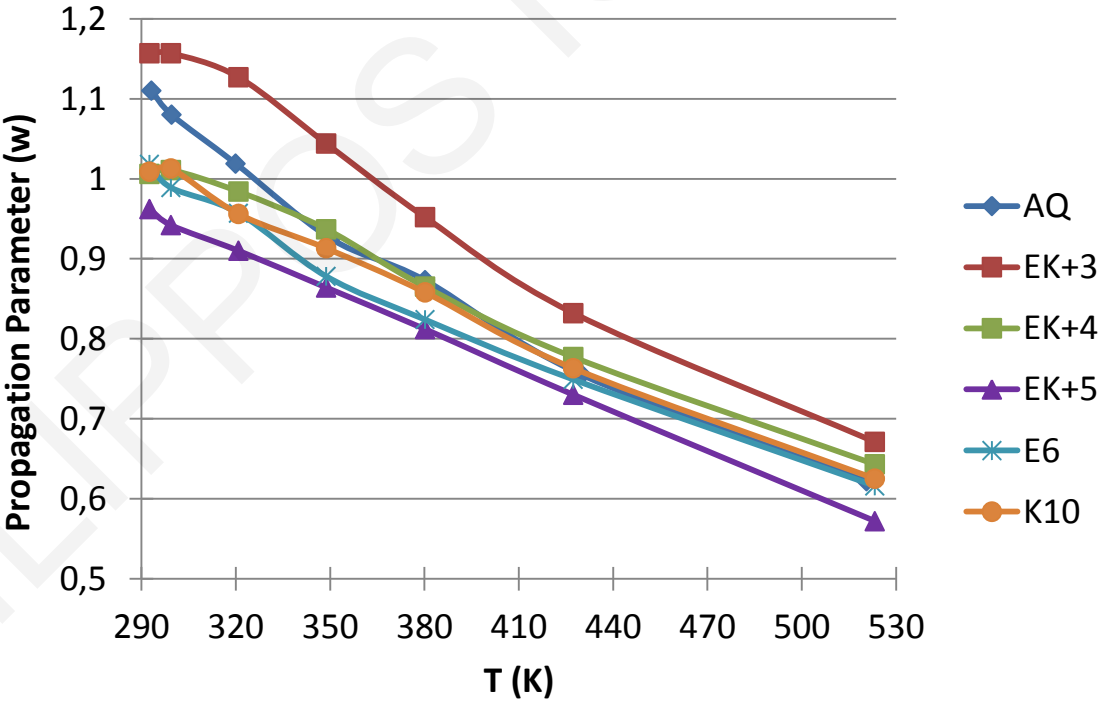

Figure 6.3: *Temperature dependence of the LR helix propagation parameter (w) for the various peptides in pure water.*

We can obtain insights on the origin of helicity differences among the four peptides by analysis of the corresponding LR nucleation (v) and propagation (w) parameters. These parameters were obtained from Eq. (5.1) and reflect average values, as we made no effort to distinguish between the four residue types of the simulated sequences (alanine, glutamine, glutamic acid and lysine). The temperature dependence of the parameters v and w is displayed, respectively, in Figures. 6.2 and 6.3. The profiles of peptide AQ (from chapter 5) are also included for comparison.

The nucleation parameter of peptide AQ (Figure 6.2 and Chapter 5) increases fast at lower temperatures (up to ~350 K), and decreases slowly at higher temperatures. The profiles for the three EK-containing peptides follow a similar temperature dependence; the behavior of EK+5 is somewhat more complex, with the corresponding curve reaching a plateau in the region 320 – 380 K. This could partly arise from a different response of the four residues (A, Q, E, K) to temperature.

The propagation parameter decreases with temperature and with the E – K spacing (i.e., from EK+3 to EK+5). The average helicities of the various EK sequences are mostly determined by this parameter (see Figures 6.3 and 6.1), as was also concluded for peptide AQ (Chapter 5). Indeed, as discussed elsewhere [Scholtz et al., 1993; Chakrabartty and Baldwin, 1995; Smith and Scholtz, 1998], the helicities of the EK-containing sequences are expected to depend on the positions of E and K along the sequence and the E – K spacing, through interactions of the charged E, K side-chains with (i) each other, (ii) the helix macrodipole, and (iii) the glutamine side-chains of the AQ template sequence.

The degree of intermolecular E – K interaction for the various peptides and solutions can be appreciated with the aid of Figure 6.4, which displays histograms of the C – N distance between the carbon atom (C) of the glutamic acid side-chain carboxylate and the nitrogen (N) atom of the lysine side-chain. The sharply defined peak near 3.5 Å corresponds to contact configurations of the E and K residues, whereas the broader peaks correspond to water-separated configurations. A salt bridge between the E and K side chains is frequently observed in sequence EK+3, less so in EK+4 and very infrequently in EK+5. This behavior suggests that the increased helicity of the EK+3 sequence (relative to EK+4 and EK+5) is partly due to electrostatic interactions between the E and K side chains. This is also supported by the fact that the formation of a E6 – K9 salt bridge is strongly correlated with

the appearance of helices: the average C – N distance between the E side-chain carboxylate carbon and the lysine side-chain nitrogen nitrogen is 5.9 Å in EK+3 conformations with a 100% α-helix, compared to 9.4 Å for non-helical conformations. The salt simulations also support this conclusion, as discussed below.

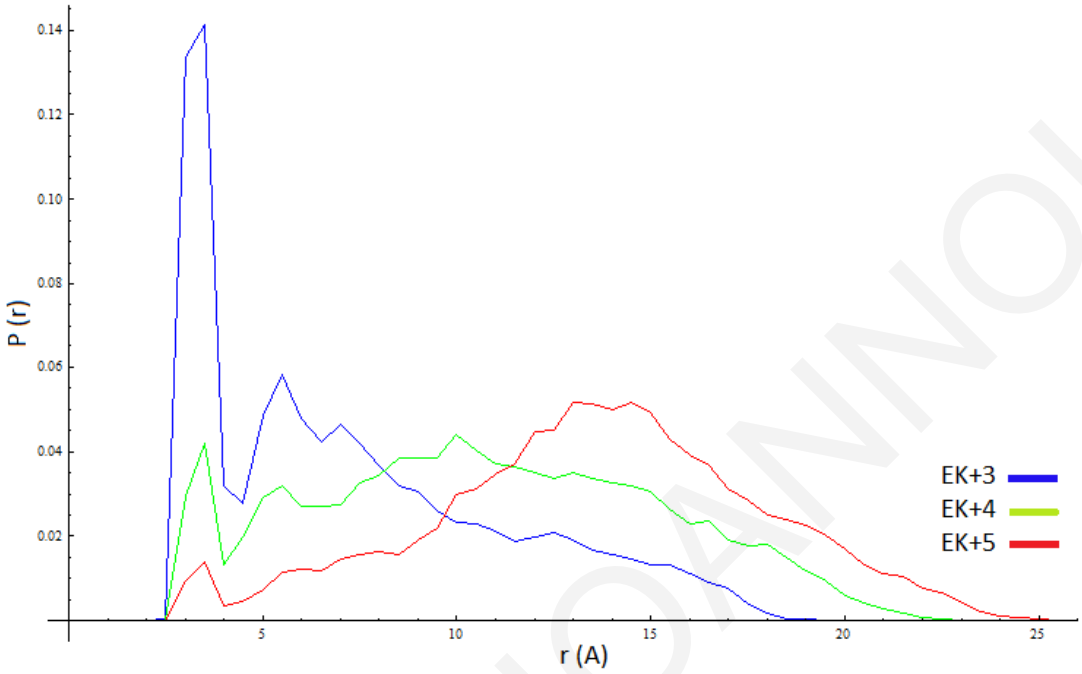

Figure 6.4: *Histogram of the distance C – N between the carbon atom (C) of the glutamic acid side chain carboxylate and the nitrogen atom (N) of the lysine side chain, observed in the pure water simulations of the three EK peptides.*

The helicities of sequences EK+4 and EK+5 are reduced not only relative to EK+3, but also relative to AQ. To obtain some insight on this observation, we simulated two AQ variants, respectively with a single E substitution at position 6 (peptide E6), or a single K substitution at position 10 (K10). The resulting helicities were very similar to the EK+4 and EK+5 helicities (Figure 6.1). Thus, the E and K substitutions lower the helicity of the parent sequence AQ, and are mainly responsible for the smaller helicities of EK+4 and EK+5. This reduction has also been seen in experimental measurements with analogous peptides [Scholtz et al., 1993]. On the other hand, the formation of an E-K salt bridge in sequence EK+3 counteracts this reduction, yielding a helicity that is higher relative to the parent AQ sequence.

The computed helicities range from ~23.9 % for EK+3 to ~12.4 % for EK+5 at the lowest simulated temperature (292.6 K); these values are smaller than the experimental values of analogous peptides at 273 K (48 % for AQ, 34 % for E6K9, and 37% for E6K10 [Scholtz

et al., 1993]), but in agreement with the experimental and theoretical helicity of AQ near 300 K [Best and Hummer, 2009]. The EK+3 peptide is more helical than AQ, in contrast to the experimental result [Scholtz et al, 1993; Smith and Scholtz, 1998]. This discrepancy could be partly due to the much lower temperature of the experiments (273 K): Inspection of Figure 6.1 shows that the AQ helicity increases at a much faster rate at lower temperatures, compared to EK+3; it is likely that simulations at 0 ^{o}C would give similar helicities for the two peptides. Our replica-exchange simulations (292.6 – 523.3 K) did not include the experimental temperature due to insufficient computational resources; instead, we opted for simulations at high temperatures (which increased sampling efficiency) and made sure that the chosen temperature range included the room-temperature region (~298 K).

Figure 6.5 displays the participation probability of the various main-chain CO groups in α-helical (*i, i+4)* bonds. Peptides AQ and EK+3 have a noticeably increased probability for the CO groups of residues 3-6, suggesting that the majority of helices are formed in the central region 3-10. In EK+3 the probability is increased across the whole peptide, and has a pronounced maximum for the CO group of glutamate. For the EK+4 and EK+5 peptides we observe a decrease of hydrogen-bond formation, relative to AQ, across the whole sequence.

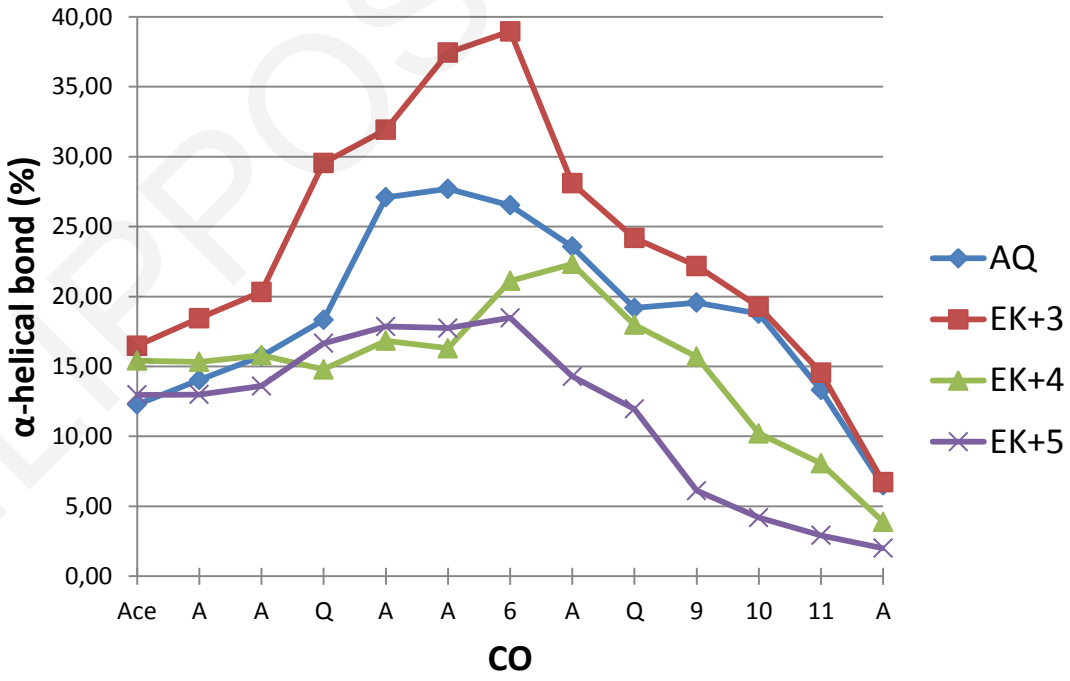

Figure 6.5: *The participation probability of the various main-chain CO groups in a-helical bonds, in pure water.*

Figure 6.6 displays the average number of water molecules in the first hydration shell of the main-chain peptide groups, determined from the first minimum in the corresponding rdf's in the pure water simulations. The amide groups of residues with bulky side chains (Gln, Glu, Lys) have reduced exposure to water (Figure 6.6a). The reduction is particularly noticeable in the central region of EK+3 (residues 6 – 10), presumably due to an additional contribution from the E6 – K9 salt bridge and the increased helicity of this peptide. The different solvent accessibilities at the C-terminal region (residues 13 – 15) are due to differences in helicity (see Figure 6.5). Similarly, the CO solvent accessibility (Figure 6.6b) is reduced for the CO groups of Lys residues, and (to a smaller extent) for Ala4 (adjacent to Gln3), Ala7 (adjacent to Glu6). Overall, CO groups are more solvent-exposed in EK+4, EK+5, in line with the reduced helicity of these peptides.

This behavior indicates that the Lys, Gln and Glu side chains shield the backbone from solvent. A combination of this shielding and the E6 – K9 salt bridge contribute to the increase in helicity of EK+3. Ghosh and coworkers [Ghosh et al., 2003] conducted simulations of the peptide EK (sequence Ac-YAEAAKAAEAAKAAEAAKAF-Nme) in pure water, and observed a similar solvent-exclusion of the backbone by lysine side-chains, and a small probability for formation of E(i) - K(i+4) salt bridges (as in sequence EK+4 of the present study). Based on these results, they attributed the increased helicity of EK to the shielding of the α-helical hydrogen bonds by the Lys side chains. It is not straightforward to compare our results with theirs, since our sequences contain only one (E, K) pair. Nevertheless, in our sequences the reduction in backbone solvent-accessibility does not suffice to increase helicity (sequences EK+4, EK+5); together with a stable E6 – K9 salt bridge, it yields a markedly increased helicity (sequence EK+3).

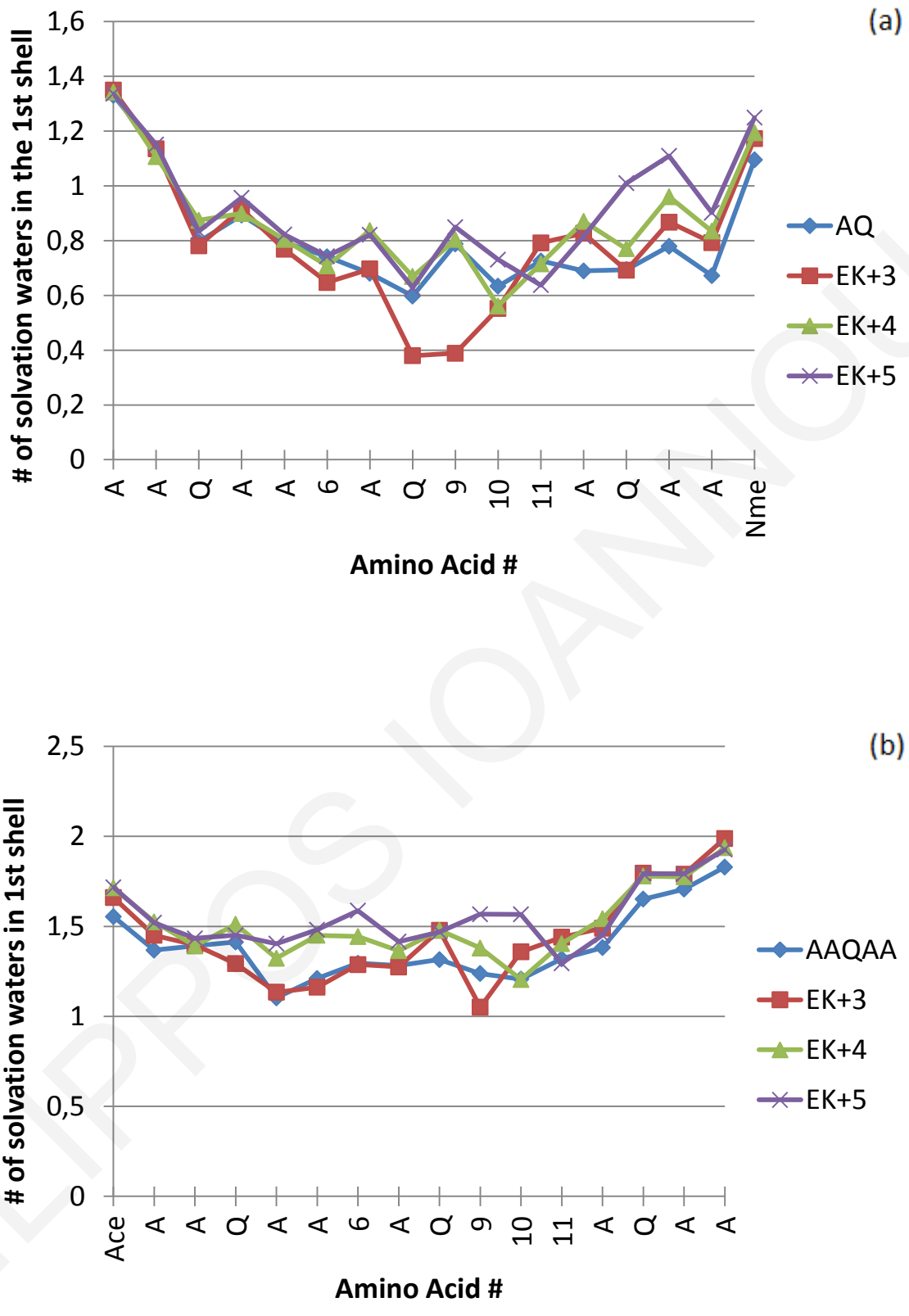

Figure 6.6: *Average number of water molecules within the first hydration shell for (a) amide hydrogen of each residue and (b) carbonyl oxygen. Residue number 6, 9, 10 and 11 depends on the peptide. Example: for the EK+3 peptide residue 6 is E, 9 is K, 10 is A,11 is A and for the EK+5 peptide residue 6 is E, 9 is A, 10 is A,11 is K.*

6.3.2 Salt simulations

Figure 6.7 displays the temperature dependence of the average EK+3, EK+4 and EK+5 helicities in the different electrolyte solutions. The helicity of peptide EK+3 varies in the order 0 M > 3 M NaCl > 1 M NaI > 1 M NaCl > 3 M NaI (Figure 6.7a). We can understand this result by considering separately the impact of salt on the helix-stabilizing E – K salt bridge (which is frequently formed in peptide EK+3), and on the general peptide propensity for helix formation (as manifested by the salt effects on the AQ sequence).

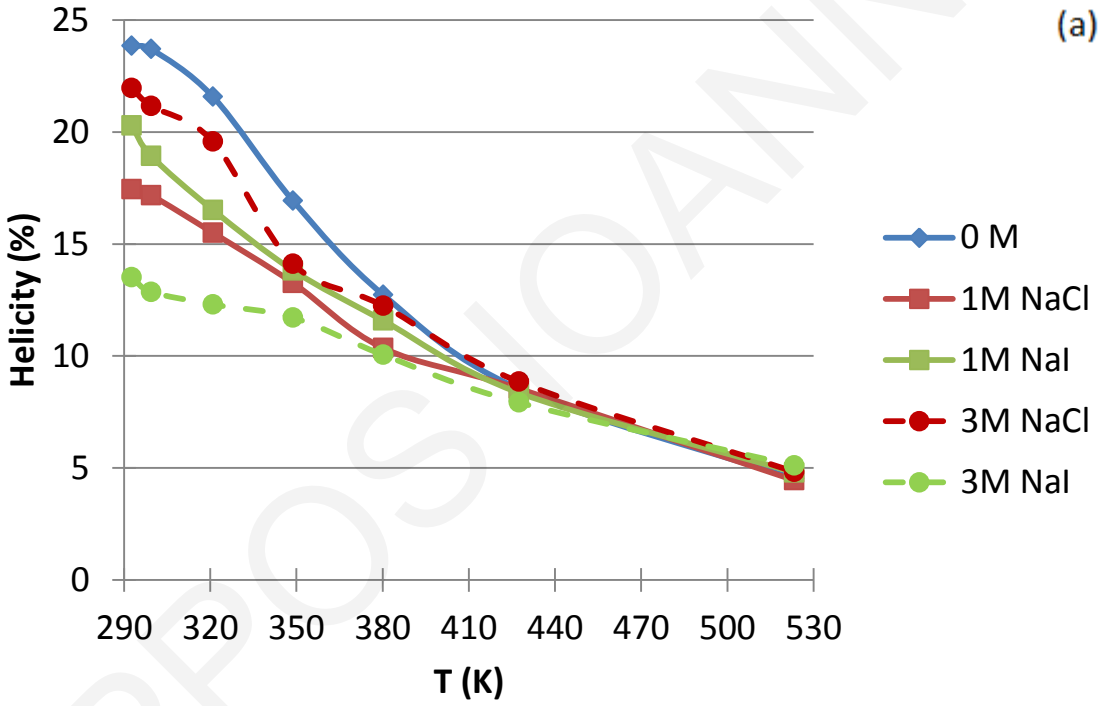

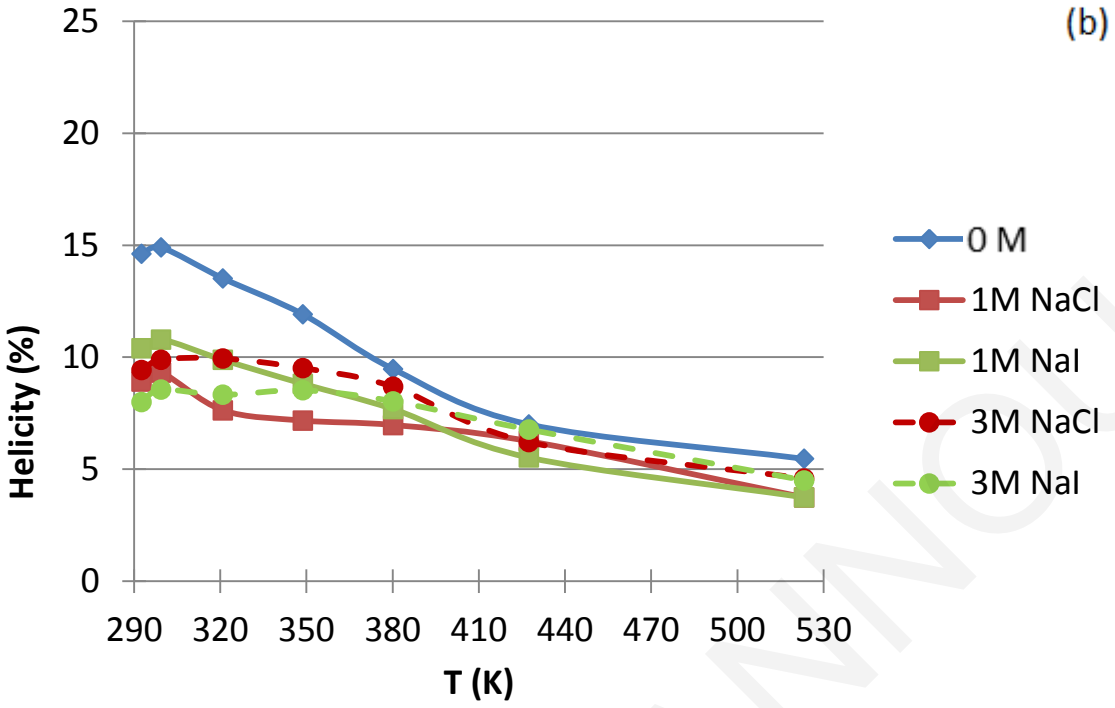

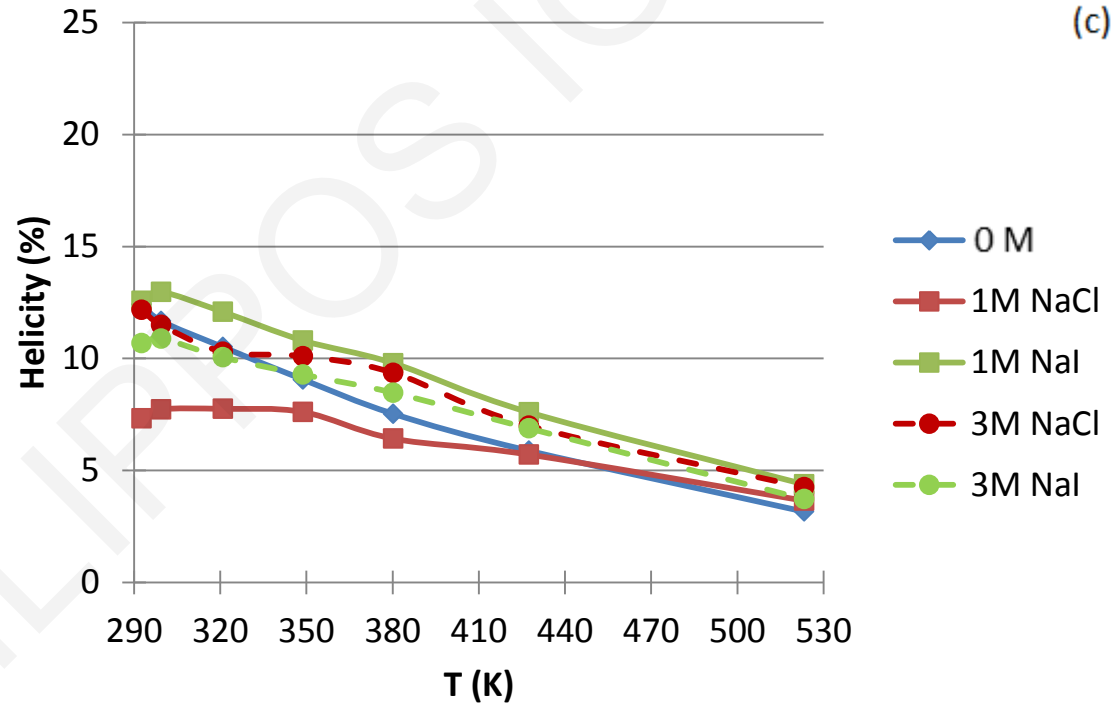

Figure 6.7: *Temperature dependence of helicity for the various peptides in the electrolyte solutions considered in this work: (a) EK+3, (b) EK+4 and (c) EK+5.*

As shown above (Figure 6.1), the helicity of EK+3 in pure water is increased relative to AQ, due to the stabilizing salt-bridge interaction E – K. Figure 6.8 displays histograms of

the distance C – N, between the carbon (C) atom of the E side chain carboxylate and the nitrogen (N) atom of the lysine side chain. The contact peak is more prominent in peptide EK+3 (Figure 6.7a), indicating the frequent formation of the salt bridge. The presence of ions causes a decrease of this first peak, which depends on solution. Based on the magnitude of this peak, we conclude that the salt screening of the salt-bridge follows the order 3 M NaI > 1 M NaI > 3 M NaCl ~ 1 M NaCl. The more effective screening by NaI is in accord with the higher peptide affinities of I and Na ions in the NaI solutions. This higher affinity was also established in Chapter 5 for the AQ sequence (see Figure 5.7 and 5.8 of Chapter 5), and in the case of shorter peptides (Figure 4.8 and 4.9 of Chapter 4).

In addition to its impact on the E – K interaction, salt also affects the general helical propensities of the peptides via interactions with the helix macrodipole or absorption on hydrophobic parts of the peptide surface or on specific groups [Scholtz et al., 1991; Kirkwood, 1943]. This general impact depends in a complex manner on the salt type and concentration. Nevertheless, we can obtain useful insights by considering the parent sequence AQ, as discussed next.

As shown in Chapter 5 (see Figure 5.1), salt changes the AQ helicity (below ~350 K) in the sequence 3 M NaCl > 1 M NaI > 1 M NaCl ~ 0 M >> 3 M NaI. Thus, the EK+3 helicity should be mostly reduced in the 3 M NaI solution, due to both the general destabilization of helical conformations in this solution (as for the AQ peptide), and the more effective screening of the helix-promoting E – K interaction by this salt (Figure 6.8a); a much smaller reduction in helicity would be expected in 3 M NaCl, because the two effects are partly cancelling each other (this salt increases helical propensity, as in AQ, and screens the E – K interaction, but to a much smaller extent, relative to 3 M NaI). The observed helicity variation (0 M > 3 M NaCl > 3 M NaI) is in line with these remarks. The presence of 1 M NaI promotes helicity to a similar extent as in the 3 M NaCl solution, up to 350 K (Figure 5.1), but also screens more effectively the E – K interaction (Figure 6.8a); thus helicity should be reduced in 1 M NaI, relative to 3M NaCl, as shown in Figure 6.7a. Finally, the addition of 1 M NaCl destabilizes less the helix-promoting E – K interaction, relative to 1 M NaI, but also augments to a smaller extent the general propensity of helical conformations (see Figure 5.1). The net result is a slightly smaller helicity in 1 M NaCl, compared to 1 M NaI (Figure 6.7a).

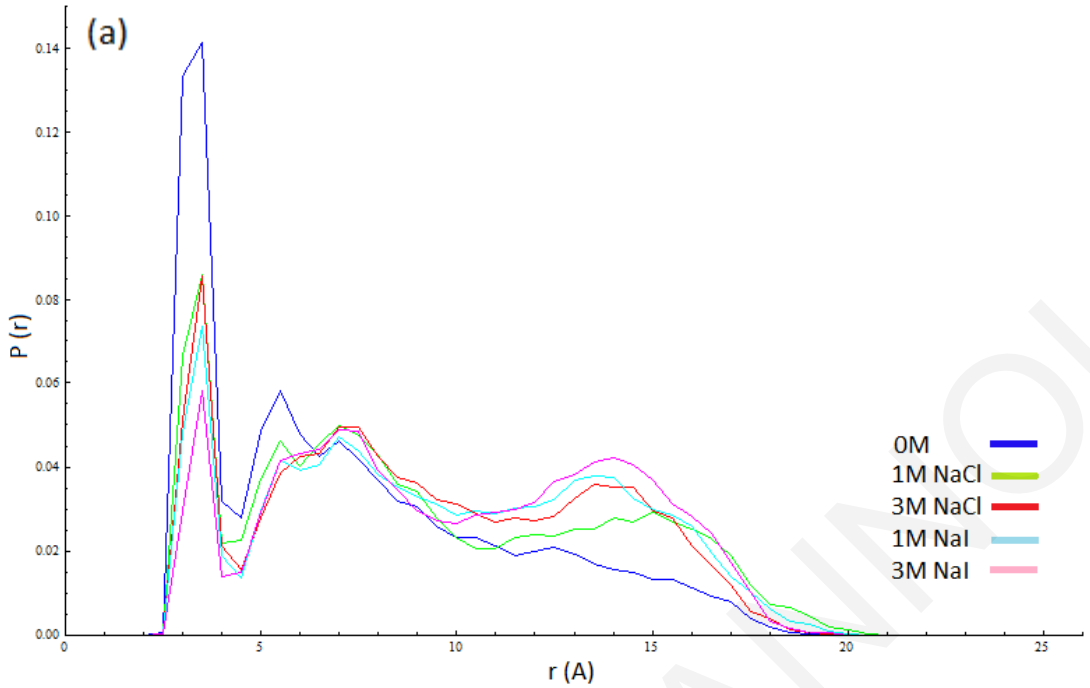

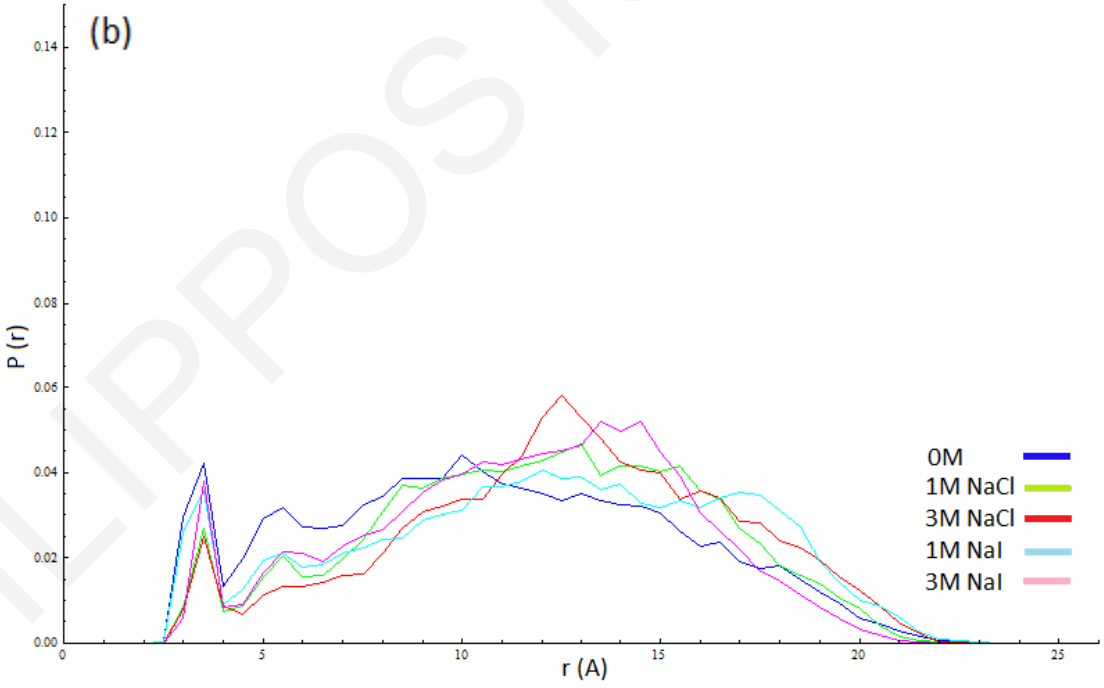

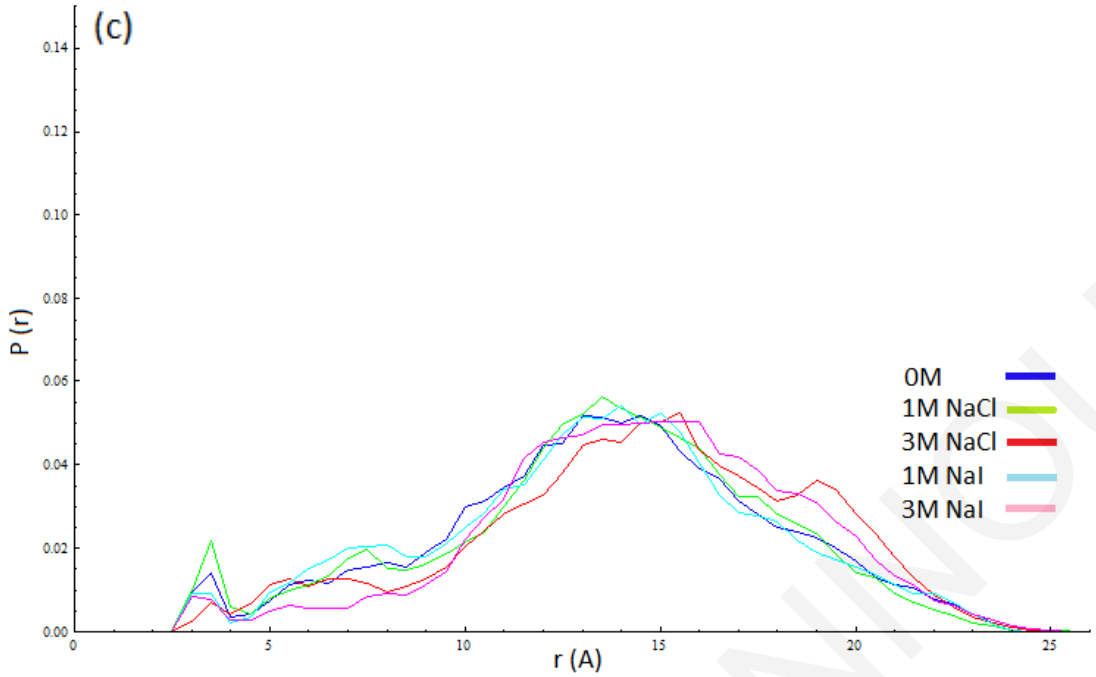

Figure 6.8: *Histogram of the distance C – N between the carbon atom (C) of the glutamic acid side chain carboxylate and the nitrogen atom (N) of the lysine side chain, observed in the various solutions for peptide EK+3 (a), EK+4 (b), and EK+5 (c).*

We next turn to the EK+4 peptide (Figure 6.7b). The helicity of this peptide is maximal at 0 M salt, and is reduced to 8-10 % in the various salt solutions. To interpret this result, we note that the inherent helical propensity of sequence AQ is similar in pure water and salt (~20 % at 290 K), with the exception of 3 M NaI where it is reduced to ~12 % (see Figure 5.1). The substitutions E and K at positions 6 and 10 of the AQ sequence reduce the helical propensity from ~20 % (for AQ) to ~15 % at 0 M (see Figure 6.7b), and to ~8-10 % in the presence of salt (with the exception of 3 M NaI), presumably due to screening of E-K interactions and other factors.

In the case of peptide EK+5, the helicity is reduced to ~13 % at 0 M solution, compared to ~20 % for AQ, due to the E and K substitutions at positions 6 and 11 (see Figures 6.6c and 5.1). A similar reduction is observed at conditions of 1 M NaI, 3 M NaCl, presumably due to the lack of E – K stabilizing interaction (see Figures 6.7c and 5.1). The 3 M NaI solution does not affect the (already small) helicity (~12 %). In contrast, in the presence of 1 M NaCl the resulting helicity is noticeably small (~7 %); the origin of this effect is not clear.

The LR nucleation and propagation parameters are displayed in Figures 6.9 and 6.10. The salt solutions cause the nucleation parameter to increase and the propagation parameter to decrease, compared always to the pure water system; a similar effect was seen for the AQ peptide (Figures 5.2 and 5.3). An exception occurs for the propagation parameter of the EK+5 peptide for the 1 M NaI solution, which as can be seen form Figure 6.10.c is slightly larger than the propagation parameter in pure water. The larger nucleation and propagation (Figure 6.9c) values for 1 M NaI give an overall higher peptide helicity which is shown in Figure 6.7.c.

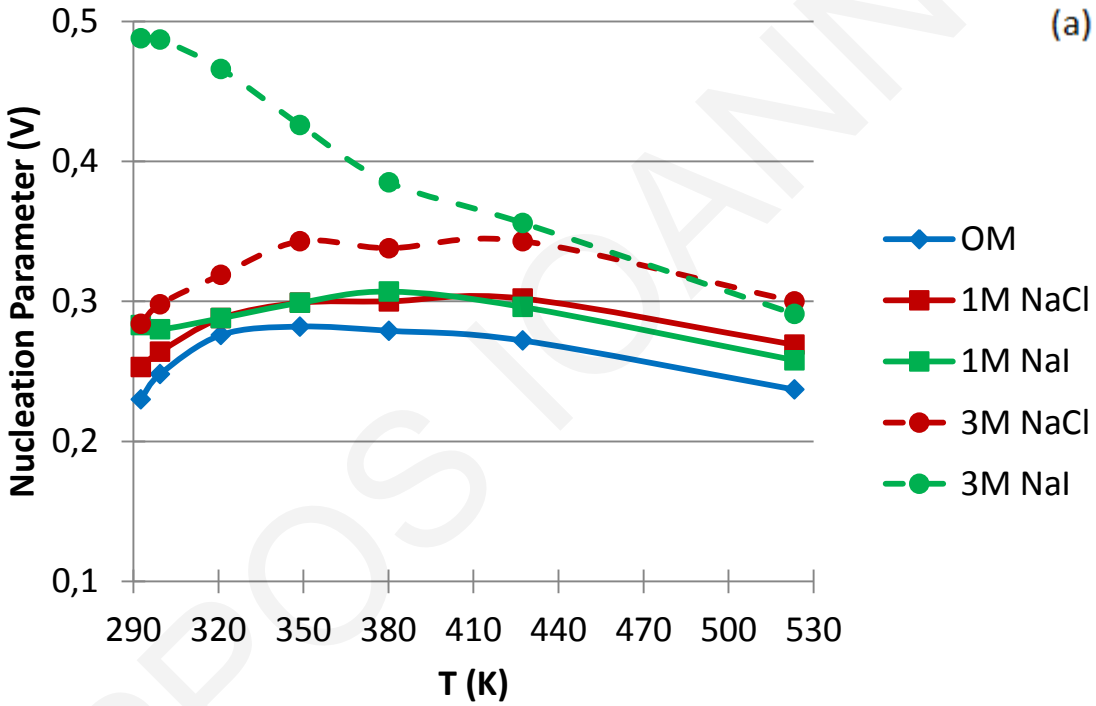

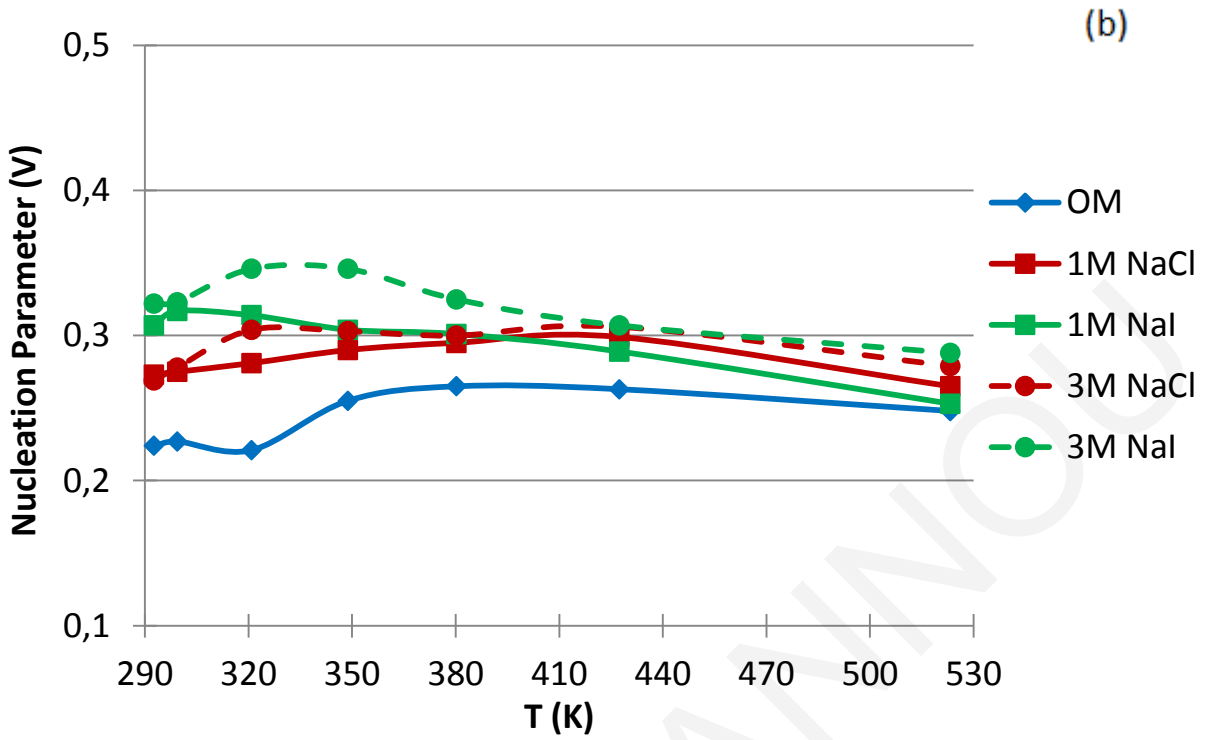

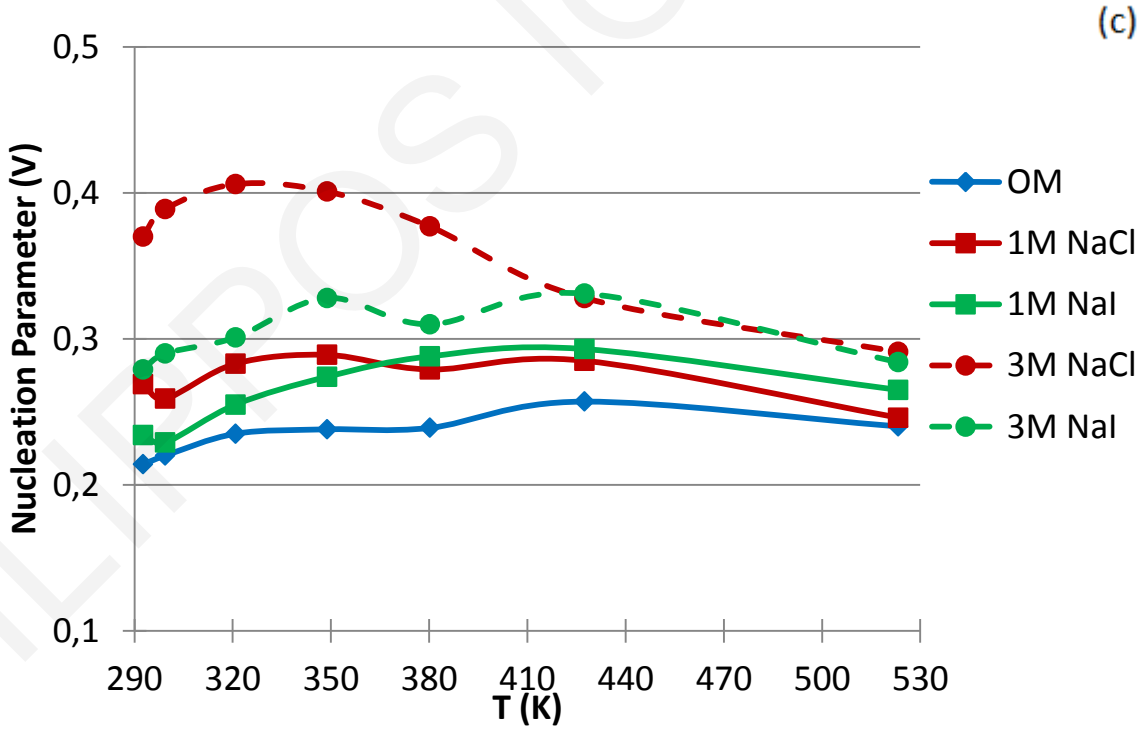

Figure 6.9: *Temperature dependence of the LR nucleation parameter for the peptides EK+3 (a), EK+4 (b), and EK+5 (c) in the various solutions.*

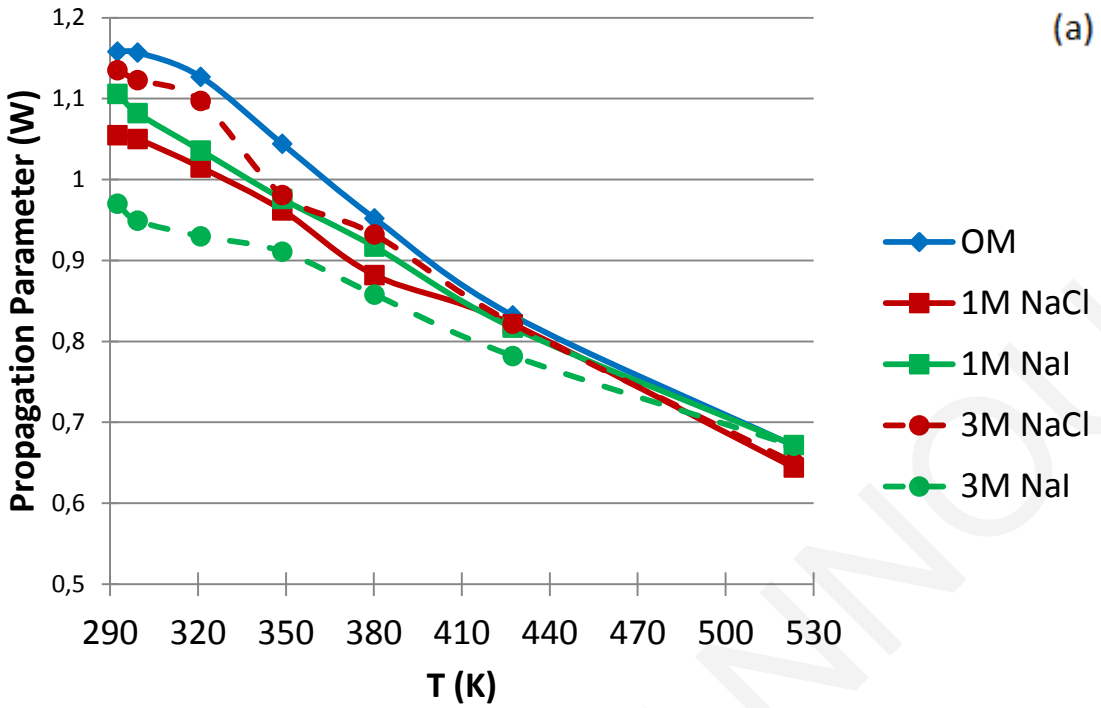

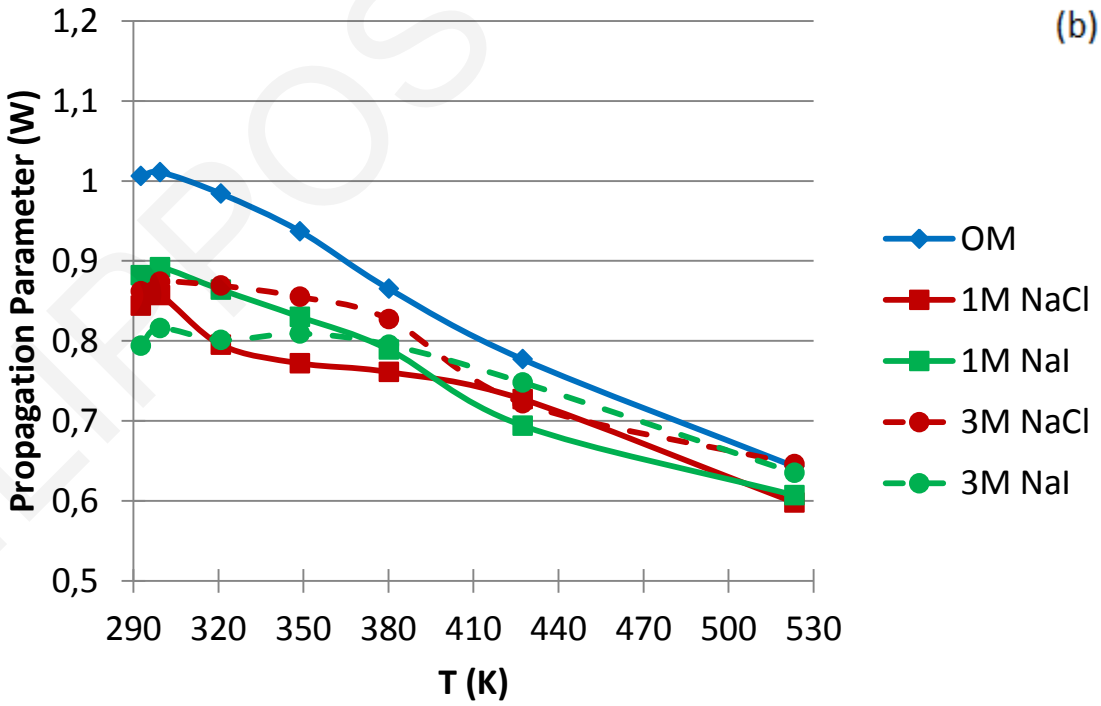

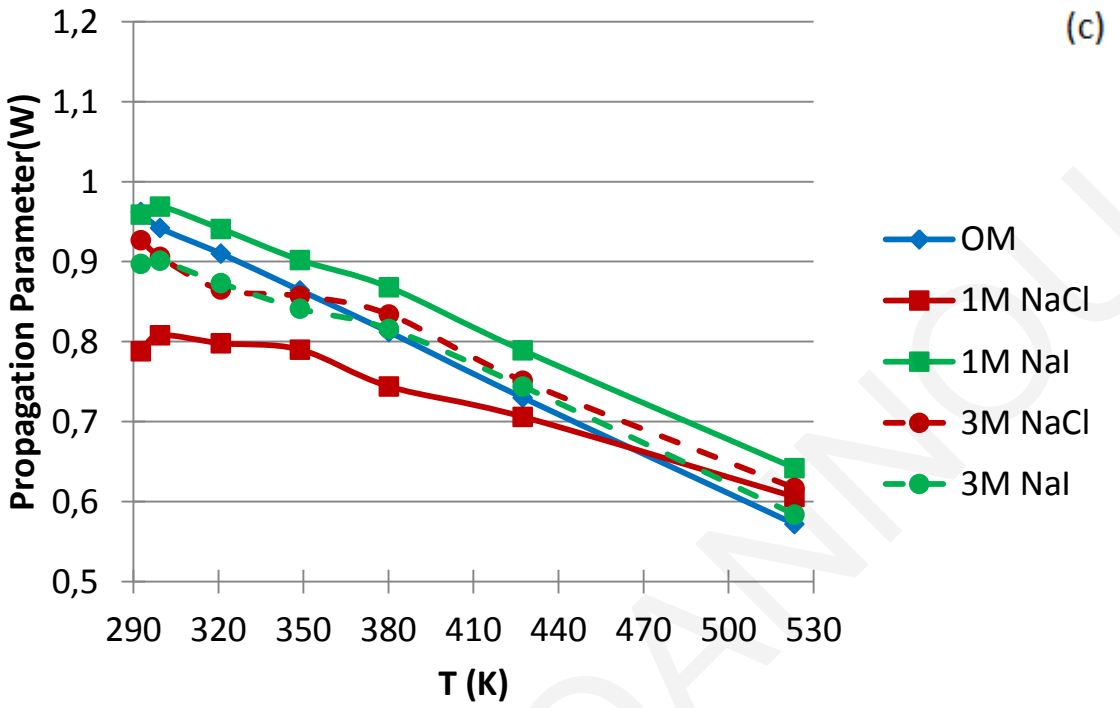

Figure 6.10: *Temperature dependence of the LR propagation parameter for the peptides EK+3 (a), EK+4 (b), and EK+5 (c) in the various solutions.*

6.4 Conclusions and Perspective

In this Chapter, we have studied by MD simulations a series of related model peptides, derived from the parent 15-residue peptide Ace-$(AAQAA)_3$-NMe (AQ) of Chapter 5. Two of the peptides contain a single E or K substitution at position 6 (sequence E6) or 10 (sequence K10) of the parent sequence. Both peptides have markedly reduced helicities relative to AQ in pure water, suggesting that the E and K substitutions destabilize helical conformations. Three peptides (EK+3, EK+4, EK+5) contain both substitutions, respectively at positions (6, 9), (6, 10) and (6, 11). Sequences EK+4 and EK+5 have also reduced helicities relative to AQ; however, sequence EK+3 has increased helicity, which is highly correlated with the formation of the intramolecular salt bridge E – K. Thus, in pure water the helical conformations of these model peptides can be significantly stabilized by direct electrostatic interactions between suitably positioned, oppositely charged residues. For all peptides in pure water the helicity trend with temperature closely follows the variation of the helix propagation parameter.

Additional simulations were conducted in a range of electrolyte solutions (1 M and 3 M NaCl and NaI). As for the AQ sequence (Chapter 5), salt increased the helix nucleation parameter, and decreased the propagation parameter of the various peptides. At the same time, it screened out the electrostatic interactions between E and K, reducing the formation probability of the E – K salt bridge. All these factors affected the observed average helicities of the three sequences. The present study shows that the addition of salt affects the helix/coil equilibrium of model peptides in several different ways; separate consideration of each factor can assist in the understanding of the net salt impact on helicity.

7. Overall Conclusions

In this Thesis, we have investigated systematically and quantified the salt effects on the helix-coil equilibrium of several model peptides with sequences of increasing complexity, by analyzing geometrical and energetic features of the peptide solutions (peptide Ramachandran maps, radial-distribution functions, energy components) and by computing the associated Lifson-Roig and Zimm-Bragg helix-coil transition parameters as a function of salt type and concentration. Such a computation has never been attempted before in the presence of salts and constitutes the major innovation in the present project. In order to increase sampling efficiency, we have conducted simulations with the replica-exchange method, which provided information on the behavior of all solutions in a large range of temperatures.

For the first time a very systematic sequential work on model peptides has been carried out, in which we add new interactions with each new model we simulated, using the information learned from the previous models.

In our investigation of salt effects on the conformations of alanine oligopeptides we found that:

- For the alanine dipeptide the "intrinsic" conformational states of the backbone, as described by Ramachandran maps, are not greatly affected even by large concentrations of NaCl and NaI. Thus, the salt effects observed on longer peptides are not due to changes in the intrinsic conformational preferences of the backbone, but arise from more complex interactions, not present in the very short dipeptide.

- The alanine tetrapeptide exhibits an increased tendency for more compact conformations and an increased population of the characteristic α-helical hydrogen bond (i/i+4) in the presence of salts, with NaI being more effective than NaCl.

- Cl^- ions prefer to stay away from the peptides, while I^- ions have a preferential interaction with the hydrophobic methyl groups. Na^+ ions on the other hand have a significant affinity for the carbonyl groups that is enhanced in the presence of I^-.

- Detailed energetic analysis of the alanine tetrapeptide simulations shows that ion-peptide interactions are fairly constant in helical and extended conformations. At the

same time, the stabilization of helical conformations coexists with enhanced ion-water interactions outside the first hydration shell of the peptide. This intriguing finding suggests that the stabilization of helices by salt cannot be interpreted on the basis of energetic interactions alone (especially ion-peptide interactions), and may have a significant entropic component.

- Simulations of the Alanine nona-peptide (Ac-Ala_8-NMe) show a similar stabilization of helical conformations by both NaCl and NaI. However, in the case of the longer, 15-residue model peptide Ac-$(AAQAA)_3$-NMe we observe a net stabilization of α-helical structures by high concentrations of NaCl, and a net destabilization by high concentrations of NaI. These results show that a *given salt* can stabilize or destabilize a peptide, depending on its length. On the other hand, for a peptide of *given length*, the effect of salt on helical stability can depend on the salt type and concentration. These effects can be understood by considering the salt impact on helix nucleation and propagation.

- Sequences EK+4 and EK+5, as well as E6 and K10 have reduced helicities relative to AQ in pure water, suggesting that substitutions of A by E and K tend to destabilize helical conformations; however, sequence EK+3 has increased helicity relative to AQ, which is highly correlated with the formation of an intramolecular E – K salt bridge. Salts screen out the electrostatic interactions between E and K, reducing the formation probability of the E – K salt bridge.

The present study shows that salt can affect the helix/coil equilibrium of model peptides in several different ways. In the case of the A oligopeptides and the AQ sequence, we were able to interpret changes in helicity through the influence of salt on the helix nucleation and propagation step. For the EK sequences, we needed to also consider the helix-stabilization due to the E-K salt bridge, and due to solvent-exclusion of backbone by the E and K side-chains. An important conclusion of the present analysis is that salt can affect in different, often competing ways the backbone and side-chain interactions. Separate consideration of each factor can assist in the better understanding of the net salt impact on helicity.

How many of our findings have a direct relevance for the protein folding-unfolding problem is not entirely obvious at this point. Secondary structure elements that are buried within compact protein structures may not be easily affected by salts in the ways

demonstrated here for special short oligopeptides. However, our findings should have a bearing on the behavior of structural elements that are in contact with the solvent. In particular, our finding that chaotropic anions have a strong affinity for hydrophobic protein groups is general enough and has been observed before. Our significant finding that salts (especially chaotropic salts) enhance the helix nucleation step, but tend to disfavor the helix propagation, also appears to be general and to suggest mechanistic steps for the salting in / unfolding of proteins by chaotropic ions.

8. Future Perspectives

As future work I propose the following:

(a) To perform simulations of the same peptides with a sodium salt of a very chaotropic anion, (on the right of iodide in the Hofmeister series). Such salts are for example $NaPF_6$ (sodium hexafluorophosphate) and $NaB(C_6H_5)_4$ (sodium tetraphenyl borate). These anions have very strong interactions with the hydrophobic groups and we expect that they will have a strong effect on the peptide configurations. It is in fact interesting to check if the helicity is considerably decreased in the presence of these salts even for short-chain peptides, in contrast to what was observed in the present work.

(b) The peptides used in this study, especially the longer peptides are extremely hydrophobic and so it will be difficult to use them in experiments due to solubility problems. Thus the experimental verification of the results of the present work will be difficult. Related peptides must be chosen, perhaps with charged blocking ends, which will be more soluble and will have a significant helix percentage at 298K. With these it will be possible to perform simple experiments to compare to the simulations.

I APPENDIX: Potential Energy Function

The development of approximate energy functions for biomolecular simulations has been the subject of intense computational efforts in the last 40 years, as the choice of an appropriate energy function is critical to a successful biomolecular simulation [Karplus and McCammon 2002]. These functions are approximate, but if properly parameterized they can produce structural and thermodynamic properties with satisfactory accuracy. Furthermore, they are completely under the control of the user (i.e. the removal or alteration of particular contributions can identify the role of specific interactions in determining specific properties) [Karplus and McCammon 2002].

A variety of force fields have been developed specifically for simulations of proteins, featuring energy functions consisting of a large number of parameterized terms. These parameters are predominantly obtained from experimental and/or quantum-mechanical studies of small molecules or fragments. In all cases, it is assumed that such parameters may be transferred to the larger molecule of interest [Adcock and McCammon, 2006]. CHARMM, AMBER, GROMOS and OPLS are the most commonly used biomolecular force fields (reviewed in [Mackerell et al., 2004]).

In conventional MD simulations, the energy function contains "bonded energy terms", that retain the molecular stereochemistry, and "non-bonded energy terms" describing the interatomic steric-repulsion, dispersion and Coulombic interactions. The bonded-energy terms contain two-, three- and four-body interactions, describing the dependence of energy on covalent bonds, bond-angles and torsional angles. The non-bonded terms are represented by simple, pairwise-additive functions of nuclear coordinates.

The general form of the potential energy function used in our work is the *Chemistry at Harvard Molecular Mechanics* (CHARMM) all-atom function, shown in eq. I.1 [Brooks et al., 2009].

$$U(\overrightarrow{R}) = \sum_{bonds} K_b(b - b_0)^2 + \sum_{angles} K_\theta(\theta - \theta_0)^2 + \sum_{Urey-Bradley} K_{UB}(S - S_0)^2 +$$

$$\sum_{dihedrals} K_\varphi(1 - \cos(n\varphi - \delta)) + \sum_{impropers} K_\omega(\omega - \omega_0)^2 +$$

$$\sum_{\substack{non-bonded \\ pairs}} \left\{ \varepsilon_{ij}^{min} \left[\left(\frac{R_{ij}^{min}}{r_{ij}} \right)^{12} - 2 \left(\frac{R_{ij}^{min}}{r_{ij}} \right)^{6} \right] + \frac{q_i q_j}{4\pi\varepsilon_0\varepsilon_1 r_{ij}} \right\} + \sum_{residues} U_{CMAP}(\varphi, \psi)$$

(Eq. I.1)

The potential energy *U*(R), is a sum over individual terms, representing the bonded and non-bonded contributions as a function of the atomic coordinates. The first four terms on the right-hand side of eq. I.1 correspond to the bonded contributions and depend, respectively, on the covalent bonds (*b*), valence-angles (θ), distances S between the extreme atoms A, C of a valence angle A-B-C [Urey-Bradley (*UB*) terms], dihedral angles (φ) and improper angles (ω). The parameters K_b, K_θ, K_{UB} K_φ and K_ω are the respective force constants, and the variables with the subscript *0* are the respective equilibrium values. The bond, angle, *UB* and improper dihedral terms are approximated in quadratic function. The dihedral angle term is a sinusoidal expression, in which *n* expresses the periodicity of the dihedral angle and δ is the phase shift determining the position of the energetic minima/maxima. The improper dihedral angle term is used at branch points; that is, for atoms A, B and D bonded to a central atom, C, the term is a quadratic function of the (pseudo)-dihedral angle defined by A-B-C-D. in addition, for the protein backbone, a numerical correction cross term, called CMAP, has recently been implemented [last term on the r.h.s of eq. I.1]. The CMAP backbone torsional energetics inclusion, which is based on certain small systematic errors in the description of the protein backbone by the all-atom CHARMM force field, improves the structural and dynamic results obtained with MD simulations of proteins in crystalline and solution environments [Brooks et al. 2009 and references therein].

The first two terms on the last line of eq. I.1 are the non-bonded interactions. They include Coulombic interactions between point charges (q_i and q_j) and the Lennard-Jones (LJ) term, which is used for the treatment of the core-core repulsion and the attractive van der Waals

dispersion interaction. For atoms in covalently-bonded atom pairs and atom-pairs separated by two covalent bonds, the corresponding non-bonded interactions are absorbed in the bonded-energy terms. For other atom-pairs, nonbonded interactions are calculated if the distance between atoms in the pair is within a user-specified interatomic cutoff distance. The parameter ε_{ij} is the Lennard-Jones well depth, R_{ij}^{min} is the distance at which the slope of the Lennard-Jones potential is zero. In the Coulombic terms, q_i is the partial atomic charge of atom *i*, ε_1 is the effective dielectric constant, and r_{ij} is the distance between atoms *i* and *j*. Values for the atomic partial charges, q_i, are determined from a template-based scheme; the charges are suitably chosen (often modified) to reproduce dielectric shielding effects (i.e. to mimic some of the effects of shielding from a high dielectric constant solvent); ε_1 is set to unity for explicit-solvent simulations [Adcock and McCammon, 2006; Brooks et al., 2009 and references therein].

II APPENDIX: CPU Time

Table I: CPU time for each model peptide

Model Peptide	# of different systems	# of replicas ≈ # of processors	Days needed/system	CPU time (days)/Model Peptide
Dipeptide	5	18	20	1800
Tetrapeptide	7	18	22	2772
AQ	5	48	25	6000
EK+3	5	48	25	6000
EK+4	5	48	25	6000
EK+5	5	48	25	6000

A total of **78.3 years** (28572 days) of CPU time was needed to simulate the peptides used in this thesis.

BIBLIOGRAPHY

Adcock, S. A.; McCammon, J. A. Molecular dynamics: survey of methods for simulating the activity of proteins. *Chem. Rev.* **2006**, 106, 1589-1615.

Algaer, E. A.; van der Vegt, N. F. A. Hofmeister Ion Interactions with Model Amide Compounds. *J. Phys. Chem. B* **2011**, 115, 13781-13787.

Anisimov, V. M.; Lamoureux, G.; Vorobyov, I. V.; Huang, N.; Roux, B.; Mackerell, A. D. Determination of Electrostatic Parameters for a Polarizable Force Field Based on the Classical Drude Oscillator. *J. Chem. Theory Comput.* **2005**, 1, 153-168.

Archontis, G.; Leontidis, E. Dissecting the stabilization of iodide at the air-water interface into components: A free energy analysis. *Chem. Phys. Lett.* **2006**, 420, 199-203.

Archontis, G.; Leontidis, E.; Andreou, G. Attraction of iodide ions by the free water surface, revealed by simulations with a polarizable force field, based on Drude oscillators. *J. Phys. Chem. B* **2005**, 109, 17957-17966.

Argos, P.; Palau, J. Amino acid distribution in protein secondary structures. *J. Peptide Protein Res.* **1982**, 19, 380-393.

Asciutto, E. K.; General, I. J.; Xiong, K.; Asher, S. A.; Madura, J. D. Sodium Perchlorate Effects on the Helical Stability of a Mainly Alanine Peptide. *Biophys. J.* **2010**, 98, 186-196.

Avbelj, F.; Baldwin, R. L. Role of backbone solvation in determining thermodynamic propensities of the amino acids. *Proc. Natl. Acad. Sci.* USA **2002**, 99, 1309-1313.

Avbelj, F.; Baldwin. R. L. Role of backbone solvation and electrostatics in generating preferred peptide backbone conformations: distributions of phi. *Proc. Natl. Acad. Sci. USA* **2003**, 100, 5742-5747.

Avbelj, F.; Luo, P.; Baldwin, R. L. Energetics of the interaction between water and the helical peptide group and its role in determining helix propensities. *Proc. Natl. Acad. Sci. USA* **2000**, 97, 10786-10791.

Baldwin, R. L. Relation between peptide backbone solvation and the energetics of peptide hydrogen bonds. *Biophys Chem.* **2002**, 101, 203-210.

Baldwin, R. L. How Hofmeister ion interactions affect protein stability. *Biophys. J.* **1996**, 71, 2056-2063.

Barlow, D. J.; Thorton, J. M. Helix geometry in proteins. *J. Mol. Biol.* **1988**, 201, 601-619.

Bernal, J. D.; Fowler, R.H. A theory of water and ionic solution, with particular reference to hydrogen and hydroxyl ions. *J. Chem. Phys.* **1933**, 1, 515-548.

Best R. B.; Mittal, J. Protein Simulations with an Optimized Water Model: Cooperative Helix Formation and Temperature-Induced Unfolded State Collapse. *J. Phys. Chem. B* **2010**, 114, 14916-14923.

Best, R. B.; Buchete, N.-V.; Hummer, G. Are current molecular dynamics force fields too helical? *Biophys. J.* **2008**, 95, L07-09.

Best, R. B.; Hummer, G. Optimized Molecular Dynamics Force Fields Applied to the Helix-Coil Transition of Polypeptides. *J. Phys. Chem. B* **2009**, 113, 9004-9015.

Bjerrum, N. Untersungen Uber Ionenassoziation. *Kgl. Danske Vid. Selsk. Mat.-fys. Medd.* **1926**, 7, 1-48.

Blaber, M.; Zhang, X. J.; Lindstrom, J. D.; Pepiot, S. D.; Baase, W. A.; Matthews, B. W. Determination of α-Helix Propensity within the Context of a Folded Protein: Sites 44 and 131 in Bacteriophage T4 Lysozyme. *J. Mol. Biol.* 1994, 235, 600-624.

Borodin, O. Polarizable force field development and molecular dynamics simulations of ionic liquids. *J. Phys. Chem. B* **2009**, 113, 11463-11478.

Boström, M.; Graig, V. S. J.; Albion, R., Williams, D. R. M.; Ninham, B. W. Hofmeister Effects and the Role of Coions in pH Measurements. *J. Phys. Chem. B* **2003**, 107, 2875-2877.

Boström, M.; Tavares, F. W.; Finet, S.;Skouri-Panet, F.; Tardieu, A.; Ninham, B. W. Why forces between proteins follow different Hofmeister series for pH above and below pI. *Biophys. Chem.* **2005**, 117, 217-224.

Boström, M.; Tavares, F. W.; Ninham, B. W.; Prausnitz, J. M. Effect of salt identity on the phase diagram for globular protein in aqueous electrolyte solution. *J. Phys. Chem. B* **2006**, 110, 24757-24760.

Boström, M.; Williams, D. R. M.; Ninham, B. W. Surface Tension of Electrolytes: Specific Ion Effects Explained by Dispersion Forces. *Langmuir* **2001**, 17, 4475-4478.

Brant, D. A.; Miller, W. G.; Flory, P. J. Conformational energy estimates for statistically coiling polypeptide chains. *J. Mol. Biol.* **1967**, 23, 47-65.

Brant, D. E.; Flory, P. J. The configuration of random polypeptide chains. *J. Amer. Chem. Soc.* **1965**, 87, 2791-2800.

Brodsky, A. Is there predictive value in water computer simulations? *Chem. Phys. Lett.* **1996**, 261, 563-568.

Brooks B. R.; Brooks, C. L. III; Mackerell, A. D.; Nilsson, L; Petrella, R. J.; Roux, B.; Won, Y; Archontis, G; Bartels, C; Boresch, S; Caflisch, A; Caves, L; Cui, Q; Dinner, A. R.; Feig, M.; Fischer, S.; Gao, J.; Hodoscek, M.; Im, W.; Kuczera, K.; Lazaridis, T.; Ma, J.; Ovchinnikov, V.; Paci, E.; Pastor, R. W.; Post, C. B.; Pu, J. Z.; Schaefer, M.; Tidor, B.; Venable, R. M.; Woodcock, H. L.; Wu, X.; Yang, W.; York, D. M.; Karplus, M. CHARMM: the biomolecular simulation program. *J. Comput. Chem.* **2009**, 30, 1545-1614.

Buchete, N.-V.; Hummer, G. Peptide folding kinetics from replica exchange molecular dynamics. *Phys. Rev. E* **2008**, 77, 030903.

Cacace, M. G. ; Landau, E. M. ; Ramsden, J. The Hofmeister series. *J. Quart. Rev. Biophys.* **1997**, 30, 241-277.

Camões, M. F.; Lito, M. J. G.; Ferra, M. I. A.; Covington, A. K. Consistency of pH standard values with the corresponding thermodynamic and dissociation constants. *Pure Appl.Chem.* **1997**, 69, 1325-1333.

Cantor, C. R.; Schimmel, P. R. Biophysical Chemistry, Part I; W. H. Freeman: San Francisco, **1980.**

Carpenter G. A.; Grossberg, S. ART 2: Stable self-organization of pattern recognition codes for analog input patterns. *Appl. Optics* **1987**, 26, 4919-4930.

Case, D. A.; Darden, T. A.; Cheatham, T. E. III; Simmerling, C. L.; Wang, J.; Duke, R. E.; Luo, R.; Walker, R. C.; Zhang, W.; Merz, K. M.; Roberts, B.; Wang, B.; Hayik, S.; Roitberg, A.; Seabra, G.; Kolossvari, I.; Wong, K. F.; Paesani, F.; Vanicek, J.; Liu, J.; Wu,

X.; Brozell, S. R.; Steinbrecher, T.; Gohlke, H.; Cai, Q.; Ye, X.; Wang, J.; Hsieh, M-J.; Cui, G.; Roe, D. R.; Mathews, D. H.; Seetin, M. G.; Sagui, C.; Babin, V.; Luchko, T.; Gusarov, S.; Kovalenko A.; Kollman, P.A. **2010**. AMBER 11, University of California, San Francisco.

Chakrabartty, A.; Baldwin, R. L. Stability of alpha-helices. *Adv Protein Chem.* **1995**, 46, 141-176.

Chakrabartty, A.; Kortemme, T.; Baldwin, R. L. Helix propensities of the amino acids measured in alanine-based peptides without helix-stabilizing side-chain interactions. *Protein Sci.* **1994**, 3, 843-852.

Chaplin, M. F. A proposal for the structuring of water. *Biophys. Chem.* **1999**, 83, 211-221.

Clarke, R. J.; Lüpfert, C. Influence of anions and cations on the dipole potential of phosphatidylcholine vesicles: a basis for the Hofmeister effect. *Biophysical J.* **1999**, 76, 2614-2624.

Clough, S. A.; Beers, Y.; Klein, G. P.; Rothman, L. S. Dipole moment of water from Stark measurements of H_2O, HDO, and D_2O. *J. Chem. Phys.* **1973**, 59, 2254-2260.

Collins, K. D. and Washabaugh, M. W. The Hoffmeister effects and the behavior of water at interfaces. *Quart. Rev. Biophys*. **1985**, 18, 323-422.

Collins, K. D. Charge density-dependent strength of hydration and biological structures. *Biophys. J.* **1997**, 72, 65-76.

Collins, K. D. Ions from the Hofmeister series and osmolytes: effects on proteins in solution and in the crystallization process. *Methods* **2004**, 34, 300-311.

Creamer, T. P.; Rose, G. D. Side-Chain Entropy Opposes Alpha-Helix Formation but Rationalizes Experimentally Determined Helix-Forming Propensities. *Proc. Natl. Acad. Sci.* USA **1992**, 89, 5937-5941.

Creamer, T. P.; Rose, G. D. Alpha-Helix-Forming Propensities in Peptides and Proteins. *Proteins* **1994**, 19, 85-97.

Dang, L. X.; Chang, T.-M. Molecular mechanism of ion binding to the liquid/vapor interface of water. *J. Phys. Chem. B* **2002**, 106, 235-238.

Darden, T.; York, D.; Petersen, L. Particle mesh Ewald: An Nlog(N) method for Ewald sums in large systems. *J. Chem. Phys.* **1993**, 98, 10089-10092.

Dill, K.A.B., S., *Molecular Driving Forces: Statistical Thermodynamics in Chemistry & Biology* **2002**, London: Taylor & Francis.

Doig, A. J.; Chakrabartty, A.; Klingler, T. M.; Baldwin, R. L. Determination of free energies of N-capping in alpha-helices by modification of the Lifson-Roig helix-coil therapy to include N- and C-capping. *Biochemistry* **1994**, 33, 3396-3403.

Doty, P.; Yang, J. T. Polypeptides. VII. Poly-γ-Benzyl-L-Glutamate: The Helix-Coil Transition in Solution. *J. Am. Chem. Soc.* **1956**, 78, 498-500.

Dumetz A. C.; Snellinger-O'Brien, A. M.; Kaler, E. W.; Lenhoff, A. M. Patterns of protein protein interactions in salt solutions and implications for protein crystallization. *Protein Sci.* **2007**, 16, 1867-1877.

Dyer, W. J. Protein denaturation in frozen and stored fish. *J. Food Science* **1951**, 16, 522-552.

Dzubiella, J. Salt-specific stability and denaturation of a short salt-bridge forming alpha-helix. *J. Am. Chem. Soc*. **2008**, 130, 14000-14007.

Dzubiella, J. Salt-specific stability of short and charged alanine-based alpha-helices. *J. Phys. Chem. B* **2009**, 113, 16689-16694.

Edsall, J. T.; Flory, P. J.; Kendrew, J. C.; Liquori, A. M.; Némethy, G.; Ramachandran, G. N.; Scheraga, H. A. A proposal of standard conventions and nomenclature for the description of polypeptide conformations. *J. Mol. Biol.* **1966**, 15, 339-407.

Fedorov, M. V.; Goodman, J. M.; Kolombet, V. V.; Schumm, S.; Socorro, I. M. Conformational changes of trialanine in sodium halide solutions: An in silico study. *J. Molec. Liq.* **2009**, 147, 117-123.

Fedorov, M. V.; Goodman, J. M.; Schumm, S. Solvent effects and hydration of a tripeptide in sodium halide aqueous solutions: an in silico study. *Phys. Chem. Chem. Phys.* **2007**, 9, 5423-5435.

Fedorov, M. V.; Schumm, S; Goodman, J. M. Solvent effects and conformational stability of a tripeptide. *Computational life sciences II. Berthold, M., Glen, R. & Fischer, I. (eds.) Berlin* **2006**, 141-149.

Feig, M. Is alanine dipeptide a good model for representing the torsional preferences of protein backbones? *J. Chem. Theory Comput.* **2008**, 4, 1555-1564.

Ferrara, Ph.; Apostolakis, J.; Catflisch, A. Thermodynamics and Kinetics of Folding of Two Model Peptides Investigated by Molecular Dynamics Simulations. *J. Phys. Chem. B* **2000**, 104, 5000-5010.

Finet, S.; Skouri-Panet, F.; Casselyn, M.; Bonnet, F.; Tardieu, A. The Hofmeister effect as seen by SAXS in protein solutions. *Current Opinion in Colloid & Interface Science* **2004**, 9, 112-116.

Flory, P. J. *Statistical Mechanics of Chain Molecules; John Wiley & Sons; New York,* **1969.**

Franks, G. V. Zeta Potentials and Yield Stresses of Silica Suspensions in Concentrated Monovalent Electrolytes: Isoelectric Point Shift and Additional Attraction. *J. Colloid Interface Sci.* **2002**, 249, 44-51.

Frumkin, A. Z. Phase-boundary forces and adsorption at the interface air: Solutions of inorganic salts. *Phys. Chem.* **1924**, 109, 34-48.

García, A. E. and Sanbonmatsu, K. Y. Alpha helical stabilization by side chain shielding of backbone hydrogen bonds. *Proc. Nat. Acad. Sci.* **2002**, 99, 2782-2787.

Ghosh, T.; Garde, S.; Garcia, A. E. Role of backbone hydration and salt-bridge formation in stability of α-helix in solution. *Biophys. J.* **2003**, 85, 3187-3193.

Gibbs, J. H.; DiMarzio, E. A. Statistical Mechanics of Helix-Coil Transitions in Biological Macromolecules. *J. Chem. Phys.* **1959**, 30, 271-283.

Gnanakaran, S.; Garcia, A. E. Validation of an All-Atom Protein Force Field: From Dipeptides to Larger Peptides. *J. Phys. Chem. B* **2003**, 107, 12555-12557.

Gnanakaran, S.; Garcia, A. E. Helix-coil transition of alanine peptides in water: Force field dependence on the folded and unfolded structures. *Proteins, Struct. Funct. and Bioinf.* **2005**, 59, 773-782.

Gnanakaran, S.; Nymeyer, H.; Portman, J. J.; Sanbonmatsu, K. Y.; Garcia, A. E. Peptide folding simulations. *Curr. Apenture. Struct. Biol.* **2003**, 13, 168-174.

Goch, G.; Maciejczyk M.; Oleszczuk, M; Stachowiak, D.; Malicka, J.; Bierzynski, A. Experimental investigation of initial steps of helix propagation in model peptides. *Biochemistry* **2003**, 42, 6840-6847.

Gopalakrishnan, S.; Liu, D.; Allen, H. C.; Kuo, M.; Shultz, M. Vibrational Spectroscopic Studies of Aqueous Interfaces: Salts, Acids, and Nanodrops. *J. Chem. Rev.* **2006**, 106, 1155-1175.

Graf, J.; Nguyen, P. H.; Stock, G.; Schwalbe, H. Structure and dynamics of the homologous series of alanine peptides: a joint molecular dynamics/NMR study. *J. Am. Chem. Soc.* **2007**, 129, 1179-1189.

Grdadolnik, J.; Grdadolnik-Golic, S.; Avbelj, F. Populations of the three major backbone conformations in 19 amino acid dipeptides. *J. Phys Chem B* **2008**, 112, 2712-2718.

Grossfield, A. Dependence of ion hydration on the sign of the ion's charge. *J. Chem. Phys.* **2005**, 122, 024506.

Hall, D. L.; Darke, P. L. Activation of the herpes simplex virus type 1 protease. *J. Biol. Chem.* **1995**, 270, 22697-22700.

Hamada, H.; Arakawa, T; Shiraki, K. Effect of additives on protein aggregation. *Current Pharmaceutical Biotechnology* **2009**, 10, 400-407.

Handbook of Chemistry and Physics, 56 ed., edited by R.C Weast CRC Press; USA. **1975.**

Hegefeld, W. A.; Chen, S. E.; DeLeon, K. Y.; Kuczera, K.; Jas, G. S. Helix formation in a pentapeptide: experiment and force-field dependent dynamics. *J. Phys. Chem. B* **2010**, 114, 12391-12402.

Heuft, J. M., An ab initio study of ion solvation in water. Ph.D. diss., University of Amsterdam, **2006**

Heyda, J.; Vincent, J. C.; Tobias, D. J. ; Dzubiella, J. ; Jungwirth, P. Ion specificity at the peptide bond: molecular dynamics simulations of N-methylacetamide in aqueous salt solutions. *J. Phys. Chem. B* **2010**, 114, 1213-1220.

Hiraoka, K.; Mizuse, S.; Yamabe, S. Solvation of halide ions with water and acetonitrile in the gas phase. *J. Phys. Chem.* **1988**, 92, 3943-3952.

Hochachka, P. W.; Somero, G. N. *Princeton, NJ: Princeton University Press,* **1984.**
Hofmeister, F. About the science of the effect of salts. *Arch. Exp. Pathol. Pharmacol* **1888**, 24, 247-260.

Hoover, W. G. Canonical dynamics: Equilibrium phase-space distributions. *Phys. Rev. A* **1985**, 31, 1695-1697.

Horinek, D.; Herz, A.; Vrbka, L.; Sedlmeier, F.; Mamatkulov, S. I., Netz, R. R. Specifc ion adsorption at the air/water interface: The role of hydrophobic solvation. *Chem. Phys. Lett.* **2009**, 479, 173-183.

Hribar, B.; Southall, N.T.; Vlachy, V.; Dill, K. A. How Ions Affect the Structure of Water. *J. Am. Chem. Soc.* **2002**, 124, 12302-12311.

Hu, H.; Elstner, M.; Hermans, J. Comparison of a QM/MM force field and molecular mechanics force fields in simulations of alanine and glycine "dipeptides" (Ace-Ala-Nme and Ace-Gly-Nme) in water in relation to the problem of modeling the unfolded peptide backbone in solution. *Proteins: Struct., Funct., Genet.* **2003**, 50, 451-463.

Huang, C. Y.; Getahum, Z.; Zhu, Y. J.; Klemke, J. W.; Degrado, W. F.; Gai, F. Helix formation via conformation diffusion search. *Proc. Natl. Acad. Sci. USA* **2002**, 99, 2788-2793.

Huang, X; Browman, G. R.; Pande, V. S. Convergence of folding free energy landscapes via application of enhanced sampling methods in a distributed computing environment. *J. Chem. Phys.* **2008**, 128, 205106.

Hummer, G.; Garcia A.; Garde S. Conformational Diffusion and helix formation kinetics. *Phys. Rev. Lett.* **2000**, 85, 2637-2640.

Hummer, G.; Garcia, A.; Garde, S. Helix nucleation kinetics using molecular simulations in explicit solvent. *Proteins **2001,*** 42, 77-84.

Huyghues-Despointes, B. M.; Scholtz, J. M.; Baldwin, R. L. Helical peptides with three pairs of Asp-Arg and Glu-Arg residues in different orientations and spacings. *Protein Sci.* **1993**, 2, 80-85.

Imai, T.; Kinoshita, M.; Hirata, F.; Bull. Salt Effect on Stability and Solvation Structure of Peptide. *Chem, Soc. Jpn.* **2000**, 73, 1113-1122.

Ingwall, R. T.; Scheraga, H. A.; Lotan, N.; Berger, A.; Katchalski, E. Conformational studies of poly-L-alanine in water. *Biopolymers* **1968**, 6, 331-368.

Ioannou, F.; Archontis, G.; Leontidis, E. Specific Interactions of Sodium Salts with Alanine Dipeptide and Tetrapeptide in Water: Insights from Molecular Dynamics. *J. Phys. Chem. B* **2011**, 115, 13389-13400.

Ishizuka, R.; Huber, G. A.; McCammon, J. A. Solvation Effect on the Conformations of Alanine Di peptide: Integral Equation Approach. *J. Phys. Chem. Lett.* 2**010**, 1, 2279-2283.

Jagoda-Cwiklik, B; Vacha, R.; Lund, M.; Srebro, M.; Jungwirth, P. Ion pairing as a possible clue for discriminating between sodium and potassium in biological and other complex environments. *J. Phys. Chem. B* **2007**, 111, 14077-14080.

Jarvis, N. L.; Scheiman, M. A. Surface Potentials of Aqueous. Electrolyte Solutions. *J. Phys. Chem*. **1968**, 72, 74-77.

Jorgensen, L. W.; Chandrasekhar, J.; Madura, D. J.; Impey, W. R.; Klein, L. M. Comparison of Simple Potential Functions for Simulating Liquid Water. *J. Chem. Phys.* **1983**, 79, 926-935.

Joung S., Cheatham E. Determination of alkali and halide monovalent ion parameters for use in explicitly solvated biomolecular simulations. *J. Phys. Chem. B* **2008**, 112, 9020-9041.

Jungwirth, P.; Tobias, D. Specific Ion Effects at the Air/Water Interface. *J. Chem. Rev.* **2006**, 106, 1259-1281.

Jungwirth, P.; Tobias, D. J. Surface effects on aqueous ionic solvation: A molecular dynamics simulation study of NaCl at the air/water interface from infinite dilution to saturation. *J. Phys. Chem. B* **2000**, 104, 7702-7706.

Jungwirth, P.; Tobias, D. J. Ions at the Air/Water Interface. *J. Phys. Chem. B* **2002**, 106, 6361-6373.

Jungwirth, P.; D. J. Tobias, D. J. The Molecular Structure of Salt Solutions: A New View of the Interface with Implications for Heterogeneous Atmospheric Chemistry. *J. Phys. Chem. B* **2001,** 105, 10468-10472.

Kalra, A.; Tugcu, N.; Cramer, S.; Garde, S. Salting-in and Salting-out of Hydrophobic Solutes in Aqueous Salt Solutions. *J. Phys. Chem. B* **2001**, 105, 6380-6386.

Karlström, G.; Hagberg, D. Toward an understanding of the hofmeister effect: A computer game with dipoles and an ion. *J. Phys. Chem.* **2002**, 106, 11585-11592.

Karpen, M. E.; Tobias, D. T.; Brooks C. L. Statistical clustering techniques for analysis of long molecular dynamics trajectories. I: Analysis of 2.2 ns trajectories of YPGDV. *Biochemistry* **1993**, 32, 412-420.

Karplus, M.; McCammon, J. A. Molecular dynamics simulations of biomolecules. *Nat. Struct. Biol.* **2002**, 9, 646-652.

Kendrew, J. C., Dickerson, R. E., Strandberg, B. E., Hart, R. G., Davies, D. R., Phillips, D. C., and Shore, V. C. Structure of myoglobin: A three-dimensional Fourier synthesis at 2 A. resolution. *Nature* **1960**, 185, 422-427.

Kinoshita, M.; Harano, Y.; Bull. Potential of mean force between solute atoms in salt solution: effects due to salt species and relevance to conformational transition of biomolecules. *Chem. Soc. Jpn* **2005**, 78, 1431-1441.

Kirkwood, J. G. *In Proteins, Amino Acids and peptides: Cohn, E. J.; Edsall, J. T.; Eds: Reinhold Publishing, New York*, **1943**, p 275.

Klement K.; Wieligmann, K.; Meinhardt, J.; Hortschansky, P.; Richter, W.; Fändrich, M. Effect of different salt ions on the propensity of aggregation and on the structure of Alzheimer's abeta(1-40) amyloid fibrils. *Journal of Molecular Biology* **2007**, 373, 1321-1333.

Khoshkbarchi, M. K.; Vera, J. H. Effect of NaCl and KCl on the Solubility of Amino Acids in Aqueous Solutions at 298.2 K: Measurements and Modeling. *Ind. Eng. Chem. Res.* **1997**, 36, 2445-2451.

Kropman, M. F.; Bakker, H. J. Femtosecond mid-infrared spectroscopy of aqueous solvation shells. *J. Chem. Phys.* **2001**, 115, 8942-8948.

Kuffel, A.; Zielkiewicz, J. Structural and Dynamic properties of Water within the Solvation Layer around Various Conformations of the Glycine-based Polypeptide. *J. Phys. Chem. B* **2008**, 112, 15503-15512.

Kumar, A. Aqueous guanidinium salts - Part II. Isopiestic osmotic coefficients of guanidinium sulphate and viscosity and surface tension of guanidinium chloride, bromide, acetate, perchlorate and sulphate solutions at 298.15 K. *Fluid Phase Equilib.* **2001**, 180, 195-204.

Kunz, W. (ed) *Specific Ion Effects; World Scientific: Singapore*, **2010.**

Kunz, W. Specific ion effects in liquids, in biological systems, and at interfaces. *Pure Appl. Chem.* 2006, 78, 1611-1617.

Kunz, W.; LoNostro, P. L.; Ninham, B. W. The Present State of Affairs with Hofmeister Effects. *Curr. Opin. Colloid Interface Sci.* **2004**, 9, 1-18.

Laasonen, K.; Sprik, M.; Parrinello, M.; Car, R. AB-INITIO LIQUID WATER. *J. Chem. Phys.* **1993**, 99, 9080-9089.

Lanyi J. K. Salt-dependent properties of proteins from extremely halophilic bacteria. *Bacteriological Rev.* **1974**, 38, 272-290.

Leontidis, E. Hofmeister Anion Effects on Surfactant Self-Assembly and the Formation of Porous Solids. *Curr. Opin. Colloid Int. Sci.* **2002**, 7, 81-91.

Leontidis, E.; Aroti, A. DPPC liquid-expanded monolayers as model systems to understand the anionic Hofmeister series.2. Ion partitioning is mostly a matter of size. *J. Phys. Chem. B* **2009**, 113, 1460-1467.

Levinthal, C. Molecular Model-building by Computer. Scientific American. *Scientific American* **1966**, 214, 42-52.

Lewith, S. Zur Lehre von der Wirkung der Salze *Arch. Exp. Path. Pharm.* **1888,** 24, 1-16.

Lifson, S.; Oppenheim, I. Neighbor Interactions and Internal Rotations in Polymer Molecules. IV. Solvent Effect on Internal Rotations. *J. Chem. Phys.* **1960**, 33, 109-115.

Lifson, S.; Roig, A. On the theory of helix-coil transition in polypeptides. *J. Chem Phys.* **1961**, 34, 1963-1974.

Lockhart, D. J.; Kim, P. S. Electrostatic screening of charge and dipole interactions with the helix backbone. *Science* **1993**, 260, 198-202.

Loladze, V. V.; Ermolenko, D. N.; Makhatadze, G. Thermodynamic consequences of burial of polar and non-polar amino acid residues in the protein interior. *J. Mol. Biol.* **2002**, 320, 343-357.

Lopez, M. M.; Chin, D. H.; Baldwin, R. L.; Makhatadze, G. I. The enthalpy of the alanine peptide helix measured by isothermal titration calorimetry using metal-binding to induce helix formation. *Proc. Natl. Acad. Sci. USA* **2002**, 99, 1298-1302.

Lund, M.; Vacha, R.; Jungwirth, P. Specific ion binding to macromolecules: effects of hydrophobicity and ion pairing. *Langmuir* **2008**, 24, 3387-3391.

Lund, M.; Vrbka, L.; Jungwirth, P. Specific ion binding to non-polar surface patches of proteins. *J. Am. Chem. Soc.* **2008**, 130, 11582-11583.

Luo, P.; Baldwin, R. L. Interaction between water and polar groups of the helix backbone: an important determinant of helix propensities. *Proc. Natl. Acad. Sci. USA* **1999**, 96, 4930-4935.

Lynden-Bell, R. M.; Rasaiah, J. C. From hydrophobic to hydrophilic behaviour: A simulation study of solvation entropy and free energy of simple solutes. *J. Chem. Phys.* **1997**, 107, 1981-1991.

Mackerell, A. D. Empirical force fields for biological macromolecules: overview and issues. *J. Comp. Chem.* **2004**, 25, 1584-1604.

Mackerell, A. D.; Feig, M.; Brooks, C. L. III. Improved treatment of the protein backbone in empirical force fields. *J. Am. Chem. Soc.* **2004**, 126, 698-699.

MacKerell, A. D. Jr.; Bashford, D.; Bellott, M.; R. L. Dunbrack, R. L.; J. D. Evanseck, J. D.; M. J. Field, M. J.; Fischer, S.; Gao, J.; H. Guo, H.; Ha, S.; Joseph-McCarthy, D.; Kuchnir, L.; Kuczera, K.; Lau, F. K. T.; Mattos, C.; Michnick, S.; Ngo, T.; Nguyen, D. T.; Prodhom, B.; Reiher, W. E.; Roux, B.; Schlenkrich, M., Smith, J. C.; Stote, R.; Straub, J.; Watanabe, M.; Wiorkewicz-Kuczera, J.; Yin D.; Karplus, M. All-atom empirical potential for molecular modeling and dynamics Studies of proteins. *J. Phys. Chem. B* **1988**, 102, 3586-3616.

Madern, D.; Ebel, C.; Zaccai, G. Halophilic adaptation of enzymes. *Extremophiles* **2000**, 4, 91-98.

Madison, V.; Schellman, Optical activity of polypeptides and proteins. *J. Biopolymers* **1972**, 11, 1041-1076.

Maison, W.; Kennedy, R. J.; Kemp, D. S. Angew. Chaotropic Anions Strongly Stabilize Short, N-Capped Uncharged Peptide Helicies: A New Look at the Perchlorate Effect. *Chem. Int. Ed.* **2001**, 40, 3819-3821.

Makhatadze, G. I.; Privalov, P. L. Energetics of protein structure. *Adv. Protein Chem.* **1995**, 47, 307-425.

Marcus, Y. Ion Properties*; Marcel Dekker: New York*, **1997**.

Marqusee, S. and Baldwin R. L. Helix stabilization by Glu-...Lys+ salt bridges in short peptides of de novo design. *Biochemistry* **1987**, 84, 8898-8902.

Marqusee, S.; Robbins, V. H.; Baldwin, R. L. Unusually stable helix formation in short alanine-based peptides. *Proc. Natl. Acad. Sci. USA* **1989**, 86, 5286-5290.

Martinek, T. A.; Mandity, I. M.; Fulop, L.; Toth, G. K.; Vass, E.; Hollosi, M.; Forro, E.; Fulop, F. Effects of the alternating backbone configuration on the secondary structure and self-assembly of beta-peptides. *J. Am. Chem. Soc.* **2006**, 128, 13539-13544.

Mason, P. E.; Brady, J. W.; Neilson, G. W.; Dempsey, C. E. The interaction of guanidinium ions with a model peptide. *Biophys. J.* **2007**, 93, L04-06.

Mayne, L.; Englander, S. W.; Qui, R.; Yang, J. X.; Gong, Y. X.; Spek, E. J.; Kallenbach, N. R. Stabilizing effect of a multiple salt bridge in a prenucleated peptide. *J. Am. Chem. Soc.* **1998**, 120, 10643-10645.

McLaughlin, S., Bruder, A.; Chen, S.; Moser, C. Chaotropic anions and the surface potential of bilayer membranes. *Biochim. Biophys. Acta* ***1975,*** 394, 304-313.

Mezei, M.; Mehrotra, P. K.; Beveridge, D. L. Monte Carlo determination of the free energy and internal energy of hydration for the Ala dipeptide at 25.degree.C. *J. Am. Chem. Soc.* **1985**, 107, 2239-2245.

Miller, J. S; Kennedy, R. J.; Kemp, D. P. Solubilized, Spaced Polyalanines: A Context-Free System for Determining Amino Acid α-Helix Propensities. *J. Am. Chem. Soc.* **2002**, 124, 945-962.

Monticelli L.; Tieleman D. P.;Colombo G. Mechanism of Helix Nucleation and Propagation: Microscopic View from Microsecond Time Scale MD Simulations. *J. Phys. Chem. B* **2005**, 109, 20064-20067.

Mu, Y.; Kosov, D. S.; Stock, G. Conformational Dynamics of Trialanine in Water II: Comparison of AMBER, CHARMM, GROMOS, and OPLS Force Fields to NMR and Infrared Experiments. *J. Phys. Chem. B* **2003**, 107, 5064-5073.

Nagai, K. Configuration change of polypeptide molecules. *J. Phys. Soc. Jpn.* **1960**, 15, 407-416.

Neria, E.; Fischer, S.; Karplus, M. Simulation of activation free energies in molecular systems. *J. Chem. Phys.* **1996**, 105, 1902-1921.

Ninham , B. W.; Yaminski, V. Ion binding and ion specificity – The Hofmeister effect, Onsager and Lifschitz theories. *Langmuir* **1997**, 13, 2097-2108.

Nose, S. A unified formulation of the constant temperature molecular-dynamics methods. *J. Chem. Phys.* **1984**, 81, 511-519.

Nymeyer, H.; Gnanakaran, S.; Garcia, A. E. Atomic simulations of protein folding, using the replica exchange algorithm. *Methods in Enzymology* **2004**, 383,119-149.

O'Neil, K. T.; Degrado, W. F. A thermodynamic scale for the helix-forming tendencies of the commonly occurring amino acids. *Science,* **1990**, 250, 646-651.

Ohkubo, Y.Z.; Brooks, C. L. III. Exploring Flory's isolated-pair hypothesis: statistical mechanics of helix-coil transitions in polyalanine and the C-peptide from RNase A. *Proc. Nat. Acad. Sci.* **2003**, 100, 13916-13921.

Omta, A. W.; Kropman, M. F.; Woutersen, S.; Bakker, H. J. Negligible effect of ions on the hydrogen-bond structure in liquid water. *Science* **2003**, 301, 347-349.

Onsager, L.; Samaras, N. N. T. The surface tension of Debye-Hückel electrolytes. *J. Chem. Phys.* **1934**, 2, 528-536.

Pace, C. N.; Scholtz, J. M. A helix propensity scale based on experimental studies of peptides and proteins. *Biophys. J.* **1998**, 75, 422-427.

Padmanabhan, S.; Marqusee, S.; Ridgeway, T.; Laue, T. M.; Baldwin, R. L. Relative helix-forming tendencies of nonpolar amino acids. *Nature* **1990**, 344, 268-270.

Pauling, L.; Corey, R. B.; Branson, H. R. The Structure of Proteins: Two Hydrogen-Bonded Helical Configurations of the Polypeptide Chain. *Proc. Natl. Acad. Sci. USA* **1951**, 37, 205-211.

Pegram, L. M.; Record, M. T. Hofmeister Salt Effects on Surface Tension Arise from Partitioning of Anions and Cations Between Bulk Water and the Water/Vapor Interface. *J. Phys. Chem. B* **2007**, 111, 5411-5417.

Pegram, L. M.; Record, M. T. Thermodynamic Origin of Hofmeister Ion Effects. *J. Phys. Chem. B* **2008**, 112, 9428-9436.

Pegram, L. M.; Record, M. T. Partitioning of Atmospherically Relevant Ions Between Bulk Water and the Water/Vapor Interface. *Jr. PNAS* **2006**, 103, 14278-14281.

Peller, L. On a Model for Helix-Random Coil Transition in Polypeptides I. The Model and its Thermal Behavior. *J. Phys. Chem.* **1959**, 63, 1194-1199.

Perutz, M. F. New x-ray evidence on the configuration of polypeptide chains. *Nature* **1951**, 167, 1053-1054.

Petersen, P. B.; Saykally, R. On the Nature of Ions at the Liquid Water Surface. *J. Annu. Rev. Phys. Chem.* **2006**, 57, 333-364.

Piazza, R.; Pierno, M. Protein interactions near crystallization: A microscopic approach to the Hofmeister series. *J. Phys.: Condens. Matter* **2000**, 12, A443-A449.

Platzer, K. E. B.; Anathanarayanan, R. H. A. V. S.; Scheraga, H. A. Helix-Coil Stability Constants for the Naturally Occurring Amino Acids in Water. IV. Alanine Parameters from Random Poly(hydroxypropylglutamine-co-L-alanine) *Macromolecules* **1972**, 5, 177-187.

Poland, D.; Scheraga, H. A. Comparison of theories of the helix-coil transition in polypeptides. *J. Chem. Phys.* **1965**, 43, 2071-2074.

Poland, D.;Scheraga, H. A. Theory of Helix-Coil Transition in Biopolymers; Statistical Mechanical Theory of Order-Disorder Transitions in Biological Macromolecules. Academic Press; New York, **1970.**

Poon, C. D; Samulski, E. T; Weise, C. F; Weisshaar, J. C. Do bridging water molecules dictate the structure of a model dipeptide in aqueous solution? *J. Am. Chem. Soc.* **2000**, 122, 5642-5643.

Qian, H.; Schellman, J. A. Helix-coil theories: A comparative study for finite length preferences. *J. Phys. Chem.* **1992**, 96, 3987-3994.

Raman, B; Chatani, E; Kihara, M.; Ban, T.;Sakai, M.;Hasegawa, K.; Naiki, H.; Rao, C.; Goto,Y. Critical balance of electrostatic and hydrophobic interactions is required for beta 2-microglobulin amyloid fibril growth and stability. *Biochem.* **2005**, 44, 1288-1299.

Randles, J. E. B. Ionic hydration and the surface potential of aqueous electrolytes. *Discuss Faraday Soc.* **1957**, 24, 194-199.

Raugei, S.; Klein, M. L. An ab initio study of water molecules in the bromide ion solvation shell. *J. Chem. Phys.* **2002**, 116, 196-202.

Ray, A.; Nemethy, G. Effects of ionic protein denaturants on micelle formation by nonionic detergents. *J. Am. Chem. Soc.* **1971**, 93, 6787-6793.

Richardson, J. M.; Lopez, M. M.; Makhatadze, G. I. Enthalpy of helix-coil transition: missing link in rationalizing the thermodynamics of helix-forming propensities of the amino acid residues. *Proc. Natl. Acad. Sci.* **2005**, 102, 1413-1418.

Richardson, J. M.; Makhatadze, G. I. Temperature dependence of the thermodynamics of helix-coil transition. *J. Mol. Biol.* **2004**, 335, 1029-1037.

Rohl, C. A.; Baldwin, R. L. Deciphering rules of helix stability in peptides. *Methods Enzymol* **1998**, 295, 1-26.

Rohl, C. A.; Chakrabartty, A; Baldwin, R. L. Helix propensities of basic amino acids increase with the length of the side-chain. *Protein Sci.* **1996**, 5, 2623-2637.

Rohl, C. A; Baldwin, R. L. Comparison of NH exchange and circular dichroism as techniques for measuring the parameters of the helix-coil transition in peptides. *Biochemistry* **1997**, 36, 8435-8442.

Rossky, P. J.; Karplus, M. Solvation. A Molecular Dynamics Study of a Dipeptide in Water. *J. Am. Chem. Soc.* **1979**, 101, 1913-1937.

Ryckaert, J. P.; Ciccotti, G.; Berendsen, H. J. C. Numerical Integration of the Cartesian Equations of Motion of a System with Constraints: Molecular Dynamics of n-Alkanes. *J. Comput. Phys.* **1977**, 23, 327-341.

Sanbonmatsu, K.Y.; Garcia, A. E. Structure of Met-enkephalin in explicit aqueous solution using replica exchange molecular dynamics. *Proteins* **2002**, 46, 225-234.

Schellman J. A. The stability of hydrogen-bonded peptide structure in aqueous solution. *Trav. Lab. Carlsberg Ser. Chim.* **1955**, 29, 230-259.

Schimmel, P. R.; Flory, P. J. Conformational energies and configurational statistics of copolypeptides containing L-proline. *J. Mol. Biol.* **1968**, 34, 105-120.

Scholtz J. M.; Baldwin R.L. The mechanism of α-helix formation by peptides. *Annu. Rev. Biophys. Biomol. Struct.* **1992**, 21, 95-118.

Scholtz J. M.; Barrick, D.; York, E. J.; Stewart, J. M.; Baldwin, R. L. Urea unfolding of peptide helices as a model for interpreting protein unfolding. *Proc. Natl. Acad. Sci. USA* **1995**, 92, 185-189.

Scholtz, J. M., York, E. J., Stewart, J. M.; Baldwin, R. L. A Neutral water-soluble, α-helical peptide: The effect of ionic strength on the helix-coil equilibrium. *J. Am. Chem. Soc.* **1991**, 113, 5102-5104.

Scholtz, J. M.; Qian, H.; Robbins, V. H.; Baldwin, R. L. The energetics of ion-pair and hydrogen-bonding interactions in a helical peptide. *Biochemistry* **1993**, 32, 9668-9676.

Schott, H.; Royce, A. E.; Han, S. K. Effect of inorganic additives on solutions of non ionic surfactants VII. Cloud point shift values of individual ions. *J. Colloid Int. Sci.* **1984**, 98, 196-201.

Schweitzer-Stenner, R.; Measey, T.; Kakalis, L.; Jordan, F.; Pizzanelli, S.; Forte, C.; Griebenow, K Conformations of alanine based peptides in water probed by FTIR, Raman, vibrational circular dichroism, electronic circular dichroism, and NMR spectroscopy. *Biochemistry* **2007**, 46, 1587-1596.

Schwierz, N.; Horinek D.; Netz, R. R. Reversed anionic Hofmeister series: the interplay of surface charge and surface polarity. *Langmuir* **2010**, 26, 7370-7379.

Serrano, L.; Fersht, A. R. Capping and alpha-helix stability. *Nature*, **1989**, 342, 296-299.

Shalongo, W.; Dugad, L.; Stellwagen, E. Distribution of helicity within the model peptide Acetyl$(AAQAA)_3$amid. *J. Am. Chem. Soc.* **1994**, 116, 8288-8293.

Shimizu, S.; McLaren, W. L.; Matubayasi, N. The Hofmeister series and protein-salt interactions. *J. Chem. Phys.* **2004,** 124, 234905.

Shirley, W. A.; Brooks, C. L. 3rd**.** Curious structure in "canonical" alanine-based peptides. *Proteins* **1997**, 28, 59-71.

Shoemaker, E. M.; Hassig, P. J.; Roddy, D. Numerical simulations of the Shoemaker–Levy 9 impact plumes and clouds: A progress report. *J. Geophys. Res. Lett.* **1995,** 22, 1825-1828.

Shoemaker, K. R.; Kim, P. S.; Brems, D. N.; Marqusee, S.; York, E. J.; Chaikenthe I.; M.; Steward, J. M.; Baldwin, R. L. Nature of the charged-group effect on the stability of the C-peptide helix. *Proc. Natl. Acad. Sci. USA* **1985**, 82, 2349-2353.

Shulgin, I. L.; Ruckenstein, E. Relationship between preferential interaction of a protein in an aqueous mixed solvent and its solubility. *Biophys. Chem.* **2005**, 118, 128-134.

Siedlecka, M.; Goch, G.; Ejchart, A.; Sticht, H.; Bierzynski, A. α-Helix nucleation by a calcium-binding peptide loop. *Proc. Natl. Acad. Sci. USA* **1999**, 96, 903-908.

Silvestrelli, P. L.; Parrinello, M. Water Molecule Dipole in the Gas and in the Liquid Phase. *Phys. Rev. Lett.* **1999**, 82, 3308-3311.

Smith, J. S.; Scholtz, J. M. Energetics of Polar Side-Chain Interactions in Helical Peptides: Salt Effects on Ion Pairs and Hydrogen Bonds. *Biochemistry* **1998**, 37, 33-40.

Spek, E. J.; Olson, C. A.; Shi, Z. S.; Kallenbach, N. R. Alanine Is an Intrinsic α-Helix Stabilizing Amino Acid. *J. Am. Chem. Soc.* **1999**, 121, 5571-5572.

Stryer, L. Βιοχημεία, Πανεπιστημιακές εκδόσεις Κρήτης, Τρίτη ‘Εκδοση, **1997.**

Stuart, S. J.; Berne, B. J. Effects of Polarizability on the Hydration of the Chloride Ion. *J. Phys. Chem.* **1996**, 100, 11934-11943.

Sugita, Y.; Okamoto, Y. Replica-exchange molecular dynamics method for protein folding**.** *Chem. Phys. Lett.* **1999**, 314, 141-151.

Suresh, S. J.; Nik, V. M. Hydrogen bond thermodynamic properties of water from dielectric constant data. *J. Chem. Phys.* **2000**, 113, 9727-9732

Tamamis, P.; Skourtis, S.; Lambris, J. D.; Morikis, D.; Archontis, G. Conformational analysis of compstatin analogues with molecular dynamics simulations in explicit water. *J. Mol. Graphics Model.* **2007**, 26, 571-580.

Tatulian, S. A. Effect of lipid phase transition on the binding of anions to dimyristoylphosphatidylcholine liposomes. *Biochim. Biophys. Acta* **1983**, 736, 189-195.

Tobias, D. J.; Brooks, C. L. Thermodynamics and mechanism of alpha- helix initiation in alanine and valine peptides. *Biochemistry* **1991**, 30, 6059-6070.

Tobias, D. J.; Brooks, C. L. Conformational equilibrium in the alanine dipeptide in the gas phase and aqueous solution: a comparison of theoretical results. *J. Phys. Chem.* **1992**, 96, 3864-3870.

Tobias, D. J.; Hemminger, J. C. Getting specific about specific ion effects. *Science* **2008**, 319, 1197-1198.

Uejio, J. S.; Schwartz, C. P.; Duffin, A. M.; Drisdell, W. S.; Cohen, R. C.; Saykally, R. J. Characterization of selective binding of alkali cations with carboxylate by x-ray absorption spectroscopy of liquid microjets. *Proc. Natl. Acad. Sci.* **2008**, 105, 6809-6812.

Vácha, R.; Jurkiewicz, P.; Petrov, M.; Berkowitz, M. L.; Böckmann, R. A.; Barucha-Kraszewska, J.; Hof, M.; Jungwirth, P. Mechanism of Interaction of Monovalent Ions with Phosphatidylcholine Lipid Membranes. *J. Phys. Chem. B* **2010**, 114, 9504-9509.

Vasquez, M.; Pincus, M. R.; Scheraga, H. A. Helix–coil transition theory including long-range electrostatic interactions: Application to globular proteins. *Biopolymers* **1987**, 26, 351-371.

Verbaro, D.; Ghosh, I.; Nau, W. M.; Schweitzer-Stenner, R. Discrepancies between conformational distributions of a polyalanine peptide in solution obtained from molecular dynamics force fields and amide I′ band profiles. *J. Phys. Chem. B* **2010**, 114, 17201-17208.

Vila J., Ripoll D. R., and Scheraga H. A. Physical reasons for the unusual α-helix stabilization afforded by charged or neutral polar residues in alanine-rich peptides. *Proc. Natl. Acad. Sci. USA* **2000**, 97, 13075-13079.

Vila, J.; Williams, R. L.; Grant, J. A.; Wojcik, J.; Scheraga, H. A. The intrinsic helix-forming tendency of L-alanine. *Proc. Natl. Acad. Sci. USA* **1992**, 89, 7821-7825.

Vitalis, A.; Caflisch, A. 50 Years of Lifson–Roig Models: Application to Molecular Simulation Data. *J. Chem. Theory and Computation.* **2012,** 8, 363-373.

Vlachy, N.; Jagoda-Cwiklik, B.; Vacha, R.; Touraud, D, Jungwirth, P. Kunz, W. Hofmeister series and specific interactions of charged headgroups with aqueous ions. *Adv. Colloid and Interface Sci.* **2009**, 146, 42-47.

von Hansen, Y.; Kalcher, I., Dzubiella, J. Ion Specificity in α-Helical Folding Kinetics. *J. Phys. Chem. B* **2010**, 114, 13815-13822.

von Hippel, P. H.; Wong, K. Y. Neutral salts: the generality of their effects on the stability of macromolecular conformation. *Science* **1969**, 145, 577-580.

von Hippel, P. H.; Felsenfeld, G. Micrococcal Nuclease as a Probe of DNA Conformation. *Biochemistry*. **1964**, 3, 27-39.

Vrbka, L.; Jungwirth, P.; Bauduin, P. Specific Ion Effects at Protein Surfaces: A Molecular Dynamics Study of Bovine Pancreatic Trypsin Inhibitor and Horseradish Peroxidase in Selected Salt Solutions. *J. Phys. Chem. B* **2006**, 110, 7036-7043.

Vrbka, L.; Vondrasek, J.; Jagoda-Cwiklik, B.; Vacha, R.; Jungwirth, P. Quantification and rationalization of the higher affinity of sodium over potassium to protein surfaces. *Proc. Natl. Acad. Sci. USA.* **2006**, 103, 15440-15444.

Washburn, E. W. Ed. In International Critical Tables of Numerical Data, Physics, Chemistry, and Technology, 1st electronic ed.; Knovel: Norwich, NY, **2003**, 463.

Weis, P.; Kemper, P. R.; Bowers, M. T.; Xantheas, S. S. A new determination of the fluoride ion-water bond energy. *J. Am. Chem. Soc.* **1999**, 121, 3531-3532.

Weise, C. F.; Weisshaar, J. C. Conformational Analysis of Alanine Dipeptide from Dipolar Couplings in a Water-Based Liquid Crystal. *J. Phys. Chem. B* **2003**, 107, 3265-3277.

Weissenborn, P. K.; Pugh, R. J. Surface tension of aqueous solutions of electrolytes: relationship with ion hydration, oxygen solubility, and bubble coalescence. *J. Colloid Interface Sci.* **1996**, 184, 550-563.

Williams, L.; Kather, K.; Kemp, D. S. High Helicities of Lys-Containing, Ala-Rich Peptides Are Primarily Attributable to a Large, Context-Dependent Lys Stabilization. *J. Am. Chem. Soc.* **1998**, 120, 11033-11043.

Williams, S.; Causgrove, T. P.; Gilmanshin, R.; Fang, K. P., Callender, R. H.; Woodruff, W. H.; Dyer, R. B. Fast Events in Protein Folding: Helix Melting and Formation in a Small Peptide. *Biochemistry* **1996**, 35, 691-697.

Wilmot, C. M.; Thornton, J. M.β-Turns and their distortions: a proposed new nomenclature. *Protein Eng.* **1990**, 3, 479-493.

Woutersen, S.; Pfister, R.; Hamm, P.; Mu, Y.; Kosov, D. S.; Stock, G. Peptide conformational heterogeneity revealed from nonlinear vibrational spectroscopy and molecular-dynamics simulations. *J. Chem. Phys.* **2002**, 117, 6833-6840.

Wright, ER. M.; Diamond, J. M. Anion selectivity in biological systems. *Physiol. Rev.* **1977**, 57, 109-156.

Xiong, K.; Asciutto, E. K.; Madura, J. D.; Asher, S. A. Salt Dependence of an α-Helical Peptide Folding Energy Landscapes. *Biochemistry* **2009**, 48, 10818-10826.

Yang, J.; Zhao, K.; Gong, Y.; Vologodskii, A.; Kallenbach, N. R. α-Helix Nucleation Constant in Copolypeptides of Alanine and Ornithine or Lysine. *J. Am. Chem. Soc.* **1998**, 120, 10646-10652.

Yu, H.; Mazzanti, C. L.; Whitfield, T. W.; Koeppe II, R. E.; Andersen, O. S; Roux, B. A Combined Experimental and Theoretical Study of Ion Solvation in Liquid N-Methylacetamide. *J. Am. Chem. Soc.* **2010**, 132, 10847-10856.

Zhang, L.; Somasundaran, P.; Maltesh, C. Electrolyte Effects on the Surface Tension and Micellization of n-Dodecyl β-d-Maltoside Solutions. *Langmuir* **199**6, 12, 2371-2373.

Zhang, Y.; Cremer, P. Interactions between macromolecules and ions: the Hofmeister series**.** *Model system/Biopolymers* **2006**, 10, 658-663.

Zimm, B. H.; Bragg, J. K. Theory of the Phase Transition between Helix and Random Coil in Polypeptide Chains. *J. Chem. Phys.* **1959**, 31, 526-535.

References from the Internet

I_1: www.dynamicscience.com.au/tester/solutions/chemistry/watr.html